The biochemical basis for genetically inherited Frontotemporal Dementia with TDP-43 pathology

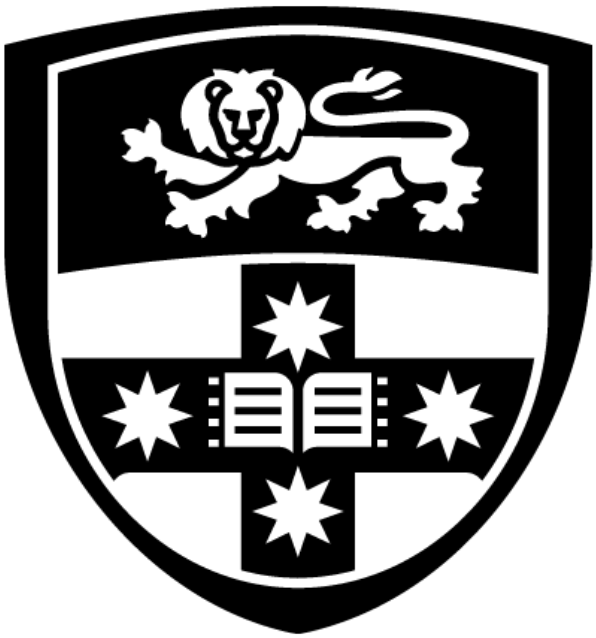

Oana Claudia Marian

A thesis submitted to fulfil requirements for the degree of
Doctor of Philosophy

Faculty of Medicine and Health

The University of Sydney

2024

Originality Statement

This is to certify that to the best of my knowledge, the content of this thesis is my own work. This thesis has not been submitted for any degree or other purposes.

I certify that the intellectual content of this thesis is the product of my own work and that all the assistance received in preparing this thesis and sources have been acknowledged.

Oana Claudia Marian

June 2023

Abstract

Frontotemporal Dementia (FTD) is a highly heritable form of younger-onset dementia and a majority of inherited cases can be attributed to heterozygous loss of *GRN* or hexanucleotide repeat expansions in the *C9orf72* gene. The pathogenic basis for FTD caused by either of these gene mutations is still under investigation, however current evidence suggests that neurodegeneration in FTD caused by *GRN* mutations (FTD-*GRN*) ensues from disrupted lysosomal lipid catabolism, whereas the neurodegenerative trigger in FTD-*C9orf72* cases remains indeterminate.

This thesis investigates the biochemical basis for FTD caused by *GRN* and *C9orf72* mutations in post-mortem tissue from heavily affected frontal lobe and less affected parietal lobe, and the potential of peripheral myelin lipids as FTD biomarkers through the development of an isomer separation method to quantify the myelin lipid galactosylceramide in plasma.

Lipidomic analysis demonstrated pronounced myelin-enriched sphingolipid loss in the frontal white matter of FTD-*GRN* cases, with a similar, but less-pronounced loss observed in FTD-*C9orf72* cases. FTD-*GRN* cases were distinguished from FTD-*C9orf72* cases by marked cholesterol ester accumulation in white matter and acylcarnitine accumulation in the grey matter, suggestive of mitochondrial dysregulation. Evidence of phagocytic microglia were identified in both FTD groups while increased activity of sphingolipid catabolic enzymes was observed in FTD-*GRN* cases alone.

Proteomic analysis confirmed mitochondrial dysfunction and identified increased abundance of phagosome maturation and decreased abundance of synaptic signalling and mevalonate pathway proteins in both FTD groups, although these changes were more pronounced in FTD-*GRN* cases.

Finally, we demonstrate that the myelin galactosphingolipids are significantly lower in plasma of FTD cases, establishing the potential for these lipids to serve as diagnostic and prognostic plasma biomarkers in FTD.

Publications and Presentations

Publications:

• **Marian, O.C.,** Teo, J.D., Lee, J.Y. Song, H., Kwok, J.B., Landin-Romero, R., Halliday, G & Don, A.S (2023) "Disrupted myelin lipid metabolism differentiates frontotemporal dementia caused by GRN and C9orf72 gene mutations." Acta Neuropathologica Communications 11, 52.

• Teo, J. D., **Marian, O. C**., Spiteri, A. G., Nicholson, M., Song, H., Khor, J. X. Y., McEwen, H. P., Ge, A., Sen, M. K., Piccio, L., Fletcher, J. L., King, N. J. C., Murray, S. S., Brüning, J. C., & Don, A. S. (2023). "Early microglial response, myelin deterioration and lethality in mice deficient for very long chain ceramide synthesis in oligodendrocytes". Glia, 71(4), 1120–1141.

• Lee, J.Y., **Marian, O.C**. & Don, A.S. (2021), "Defective Lysosomal Lipid Catabolism as a Common Pathogenic Mechanism for Dementia" Neuromolecular Medicine, vol. 23, pp. 1–24.

• **Marian, O.C.** Tran, C. & Don, A.S (2020) "Chapter 23: Altered lipid metabolic homeostasis in the pathogenesis of Alzheimer's disease" Lipid Signaling and Metabolism, ch. 23, pp. 469-504.

Presentations:

• Alzheimer's disease and Parkinson's disease Conference -Oral Presentation (2023)
• Australian Lipid Meeting- Poster Presentation (2022)
• International Society for Neurochemistry Flagship School- Poster Presentation (2022)
• International Society for Neurochemistry Conference Young Scientists Symposium- Oral Presentation (2022)
• Sydney Mass Spectrometry Roadmapping Day Symposium- Oral Presentation (2022)
• Agilent Early Career Researchers Competition Rapid Fire Presentation- Oral Presentation (2021)

Acknowledgements

I extend my deepest gratitude to the following individuals without whom this thesis would not have been possible:

To my primary supervisor Anthony, to whom I am infinitely grateful, for your encouragement, your willing and enthusiastic mentorship, your support and dedication to your students and for your role in making this journey one of the most rewarding in my life so far.

To my auxiliary supervisor Melanie, for your warmth, your willingness to teach and dedication to your students, and to the other members of the Cordwell-White lab, to Stuart, Ashleigh and Molly, for your guidance and friendship.

To my auxiliary supervisor John, for your enthusiasm and assistance in this project from the start.

To my former supervisor Claire, for inspiring me with your strength and dedication, and for your encouragement throughout.

To the Sydney Mass Spectrometry team for all your assistance.

To past and present members of the Don lab, to Collin, Jon, Holly, Tim, Jun, Lisa, Jasmine, India and Dagny, and to CPC members Dylan, Stewart, Michael, Caine, Mark, Natalia and Aster for your care and friendship, and for making this experience valuable beyond the science.

To my parents Monica and Romeo, for being my greatest inspirations, for your resilience, your unwavering encouragement and excitement for my work, and to Adrian and Paul for your support. To my grandparents, Maria, Ilie, Adela and Viorel for giving me strength along the way and reminding me of what I am capable of.

To the friends who colour my life and have uplifted and encouraged me throughout.

And to everyone who has unknowingly contributed in large or small ways to this endeavour,

Thank you.

Table of Contents

List of Figures

List of Tables

List of Abbreviations

AcCa	Acylcarnitine
ALS	Amyotrophic Lateral Sclerosis
AD	Alzheimer's Disease
ASPA	Aspartoacylase
BMP	Bis(Monoacylglycero)Phosphate
BSA	Bovine Serum Albumin
bvFTD	Behavioural Variant FTD
C9orf72	Chromosome 9 open reading frame 72
Cer	Ceramide
CerS	Ceramide Synthase
Chol	Cholesterol
CholE	Cholesterol Ester
CL	Cardiolipin
CNP	2',3'-Cyclic Nucleotide 3'-Phosphodiesterase
CSF	Cerebrospinal Fluid
CTSD	Cathepsin D
DAB	3,3'-Diaminobenzidine
DAG	Diacylglyerol
DAPI	Diamidino-2-Phenylindole Dihydrochloride
FTD	Frontotemporal Dementia
GALC	β-Galactocerebrosidase
GalCer	Galactosylceramide
GCase	β-Glucocerebrosidase
GluCer	Glucosylceramide
GO	Gene Ontology
GPNMB	Glycoprotein nonmetastatic melanoma protein B
GRN	Progranulin
HCD	Higher-energy collisional dissociation
Hex1Cer	Monohexosylceramide
Hex2Cer	Dihexosylceramide
HILIC	Hydrophilic interaction chromatography
HPLC	High performance liquid chromatography
IPA	Ingenuity Pathway Analysis
LC	Liquid chromatography
LC-MS/MS	Liquid chromatography- tandem mass spectrometry
LFB	Luxol Fast Blue
LPA	Lysophosphatidic acid
LPC	Lysophosphatidylcholine
LPC(O)	Alkyl-LPC

LPE	Lysophosphatidylethanolamine
LPE(O)	Alkyl-Lysophosphatidylethanolamine
LPI	Lysophosphatidylinositol
LPS	Lysophosphatidylserine
MAG	Monoacylglycerol
MBP	Myelin Basic Protein
MRI	Magnetic Resonance Imaging
MS	Mass spectrometry
MTBE	Methyl-Tert-Butyl Ether
mTOR	mammalian target of rapamycin
mTORC1	mammalian target of rapamycin complex 1
NCL	Neuronal Ceroid Lipofuscinosis
PC	Phosphatidylcholine
PE	Phosphatidylethanolamine
PE(O)	Alkyl-PE
PE(P)	Alkenyl-PE(PE plasmalogen)
PG	Phosphatidylglycerol
PI	Phosphatidylinositol
PD	Parkinson's Disease
PLP	Myelin Proteolipid Protein
PLS-DA	Partial Least Squares-Discriminant Analysis
PMI	Post-Mortem Interval
PS	Phosphatidylserine
PSM	Peptide Spectral Match
S1P	Sphingosine-1-Phosphate
SCMAS	Subunit C of mitochondrial ATP synthase
SM	Sphingomyelin
Sph	Sphingosine
SREBP	Sterol regulatory element binding protein
ST	Sulfatide
TAG	Triacylglycerol
TMT	Tandem Mass Tag
TBST	Tris Buffered Saline, 0.1% Tween 20
TDP-43	TAR DNA-binding protein 43

Chapter 1: Literature Review

1.1 Frontotemporal Dementia

Frontotemporal dementia (FTD) is a common cause of younger-onset dementia and encompasses a group of progressive neurological disorders affecting the frontal and temporal lobes of the brain (Olney et al. 2017). FTD is the second leading cause of presenile dementia after young-onset Alzheimer's disease, and patients are commonly diagnosed between 45 and 65 years of age (Snowden et al. 2002, Vieira et al. 2013). Although prevalence estimates vary widely, approximately 2% of dementia cases in individuals older than 65, and 10% of dementia cases under the age of 65 can be attributed to FTD, and males and females appear to be affected equally (Hogan et al. 2016). Patients have relative memory sparing but develop progressive behavioural and/or language changes and cognitive deficits for which there are no disease-modifying therapies (Neary et al. 1998, Coyle-Gilchrist et al. 2016, Greaves et al. 2019).

FTD is a highly heterogeneous form of dementia and is classified into three distinct clinical syndromes. The most common is behavioural variant FTD (bvFTD), accounting for up to 60% of FTD cases, and is characterised by pronounced changes to personality that can include apathy, emotional blunting, inattention, socially inappropriate behaviour such as disinhibition and cognitive deficits (Neary et al. 1998, Johnson et al. 2005). Patients are often misdiagnosed initially with psychiatric disorders such as major depression, bipolar disorder or schizophrenia (Velakoulis et al. 2009, Woolley et al. 2011, Shinagawa et al. 2016). The other two syndromes are forms of primary progressive aphasia; progressive non-fluent aphasia (PNFA), characterised by impaired speech production and difficulty finding words, although word comprehension is preserved; and semantic dementia (SD), characterised by loss of naming and word comprehension, despite intact and effortless speech production (Hodges et al. 1992, Neary et al. 1998, Gorno-Tempini et al. 2011, Olney et al. 2017). These functional deficits are associated with focal atrophy of the frontal or temporal lobes, and as the disease progresses, degeneration of other brain regions is often observed (Kertesz et al. 2005, Seelaar et al. 2011). Co-occurrence of movement disorders such as

motor neuron disease (MND) or parkinsonism may also be observed (Siuda et al. 2014). On average, death occurs within 6-8 years of disease onset (Hodges et al. 2003).

1.2 Diagnosis and Treatment of FTD

Diagnosis of FTD is made on the basis of clinical and behavioural symptoms and neuroimaging. A probable diagnosis bvFTD is given on the presence of behavioural changes including uncharacteristic apathy, disinhibition, and socially inappropriate behaviour, while SD or PNFA may be diagnosed following presentation of progressive language impairment including speech or comprehension. Often, people with FTD present with these symptoms in their mid-life and in some cases, these may be accompanied by symptoms of motor neuron disease or parkinsonism. Clinical assessment may be followed by neuroimaging to confirm atrophy of the frontal or temporal lobes and genetic testing may be undertaken in cases bearing a family history of dementia (Gorno-Tempini et al. 2011, Rascovsky et al. 2011).

Currently, no targeted treatments exist for FTD. Clinical management is limited to treatment of symptoms with antipsychotics and antidepressants, and supportive counselling for caregivers (Tsai et al. 2014, Balachandran et al. 2021).

The heterogeneous clinical presentation and lack of therapeutic options for FTD highlight the need for research into the biochemical basis for this group of neurodegenerative diseases.

1.3 Neuropathology of FTD

FTD is associated with neuronal loss, pronounced atrophy of frontal and/or temporal lobes, and pathological protein inclusions in neurons and glia (Krueger et al. 2010, Mackenzie et al. 2016, Yousef et al. 2017). The majority of FTD cases are characterised by intraneuronal aggregates of hyperphosphorylated tau protein (FTD-Tau), or ubiquitin-positive inclusions most commonly featuring aggregates of hyperphosphorylated and proteolytically cleaved C-terminal fragments of the 43 kilodalton Transactive Response DNA-binding protein (TDP-43) (Figure 1.1) (Spillantini

et al. 1998, Neumann et al. 2006). FTD associated with TDP-43-positive pathological inclusions is the most common subtype (Mackenzie et al. 2016). This thesis will focus on the molecular basis of FTD caused by inherited mutations that lead to TDP-43-positive forms of FTD.

TDP-43 is an RNA/DNA binding protein shown to be involved in RNA splicing, and in FTD, pathological aggregates can be seen in the cytoplasm of neurons and glia and are accompanied by the loss of physiological nuclear TDP-43 (Buratti et al. 2001, Neumann et al. 2007, Valori et al. 2021). The mechanisms by which pathological TDP-43 contributes to neurodegeneration, whether by loss of function or toxic gain-of-function, are still being explored, however, loss of nuclear TDP-43 is thought to occur early in FTD pathogenesis (Nana et al. 2019).

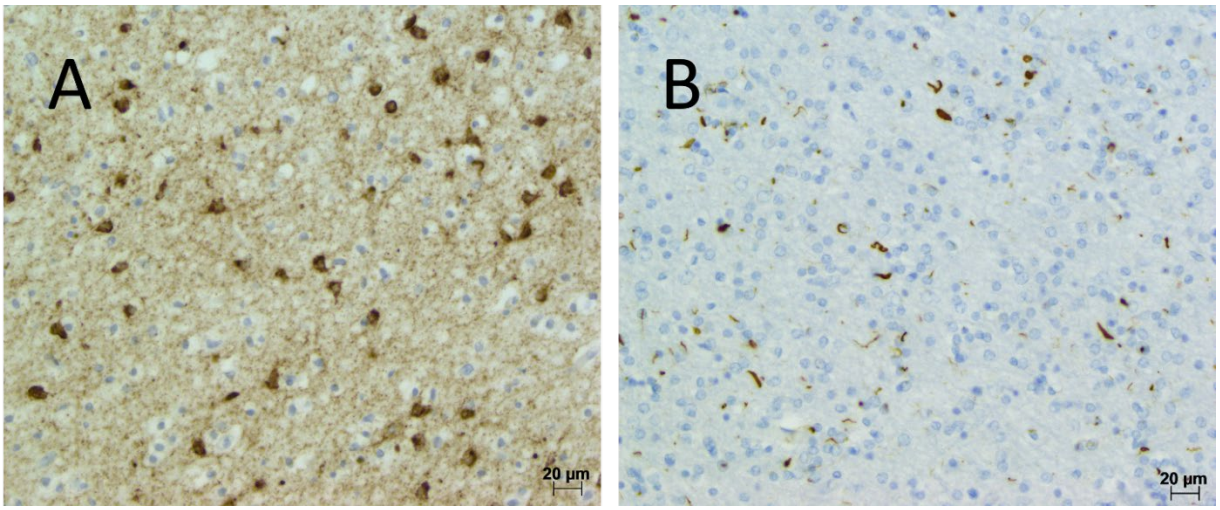

Figure 1.1: TDP-43 pathological aggregates

Representative examples of neuronal and glial TDP-43 positive pathological aggregates stained with anti-phospho TDP-43 antibody and detected by 3,3'-Diaminobenzidine (DAB) reaction (brown staining) in A) frontal grey matter and (B) frontal white matter. Magnification 200x. Scale bar: 20 µm. (Marian et al. 2023).

1.4 Genetics of FTD

Heritability of FTD is high, with an estimated 30-50% of cases having a family history of dementia (Seelaar et al. 2011, Onyike et al. 2013). The remainder of cases are sporadic, arising in the absence of a family history of dementia, but may nonetheless be attributed to genetic mutations that confer risk for FTD (Greaves et al. 2019). Mutations in the *MAPT*, *GRN* and *C9orf72* genes cause the majority of inherited FTD cases (Figure 1.2). Inherited FTD-Tau is caused by heterozygous mutations in the microtubule-associated protein tau (*MAPT* gene) accounting for approximately 6% of familial FTD and 1% of sporadic FTD cases (Cruts et al. 2006, DeJesus-Hernandez et al. 2011). The two most common genetic causes of inherited FTD with TDP-43 pathology are heterozygous mutations in the gene encoding Progranulin (*GRN*), which accounts for 3-20% of familial FTD and 1-5% of sporadic FTD; and hexanucleotide repeat expansions in a non-coding region of the chromosome 9 open reading frame 72 (*C9orf72*) gene, accounting for 11-22% of familial FTD and 3-15% of sporadic cases (Cruts et al. 2006, Gass et al. 2006, Gijselinck et al. 2008, DeJesus-Hernandez et al. 2011, Rademakers et al. 2012). These cases of FTD are hereafter referred to as FTD-*GRN* and FTD-*C9orf72*. *C9orf72* repeat expansions are also the most common genetic cause of motor neuron disease (MND), which is also characterised by TDP-43 protein aggregation. As such, FTD and MND are often considered as diseases along the same clinicopathological spectrum, with approximately 15% of FTD cases going on to develop MND (Burrell et al. 2011, DeJesus-Hernandez et al. 2011, Renton et al. 2011).

TDP-43 pathology is classified into subtypes based on morphology and distribution of neuronal inclusions; FTD-*GRN* cases are commonly classified as type A, characterised by many neuronal cytoplasmic inclusions and many short dystrophic neurites, and FTD-*C9orf72* as type B, characterised by moderate neuronal cytoplasmic inclusions and few dystrophic neurites (Mackenzie et al. 2011, Lee et al. 2017).

The semantic dementia and progressive non-fluent aphasia clinical presentations are often sporadic in nature, but mutations in *MAPT, C9orf72 and GRN* have also been reported to lead to these clinical syndromes, with their corresponding Tau or TDP-43 positive neuropathology (Samra et al. 2023).

A small proportion (less than 5%) of inherited cases can also be attributed to mutations in other genes such as the gene encoding TDP-43 (*TARDBP)*, sequestosome-1/p62 (*SQSTM1*), valosin-containing protein (*VCP)* and Tank Binding Kinase (TBK1), which are all associated with TDP-43 aggregates; charged multivesicular body protein 2B *(CHMP2B)*, associated with TDP-43 negative, ubiquitin-positive inclusions; and fused-in-sarcoma *(FUS),* leading to FUS-immunoreactive inclusions (Greaves et al. 2019). Frequently, these inclusions are also immunoreactive for ubiquitin and/or p62, indicating that they have been targeted for degradation via autophagy or ubiquitin-proteasome pathways (Davidson et al. 2022).

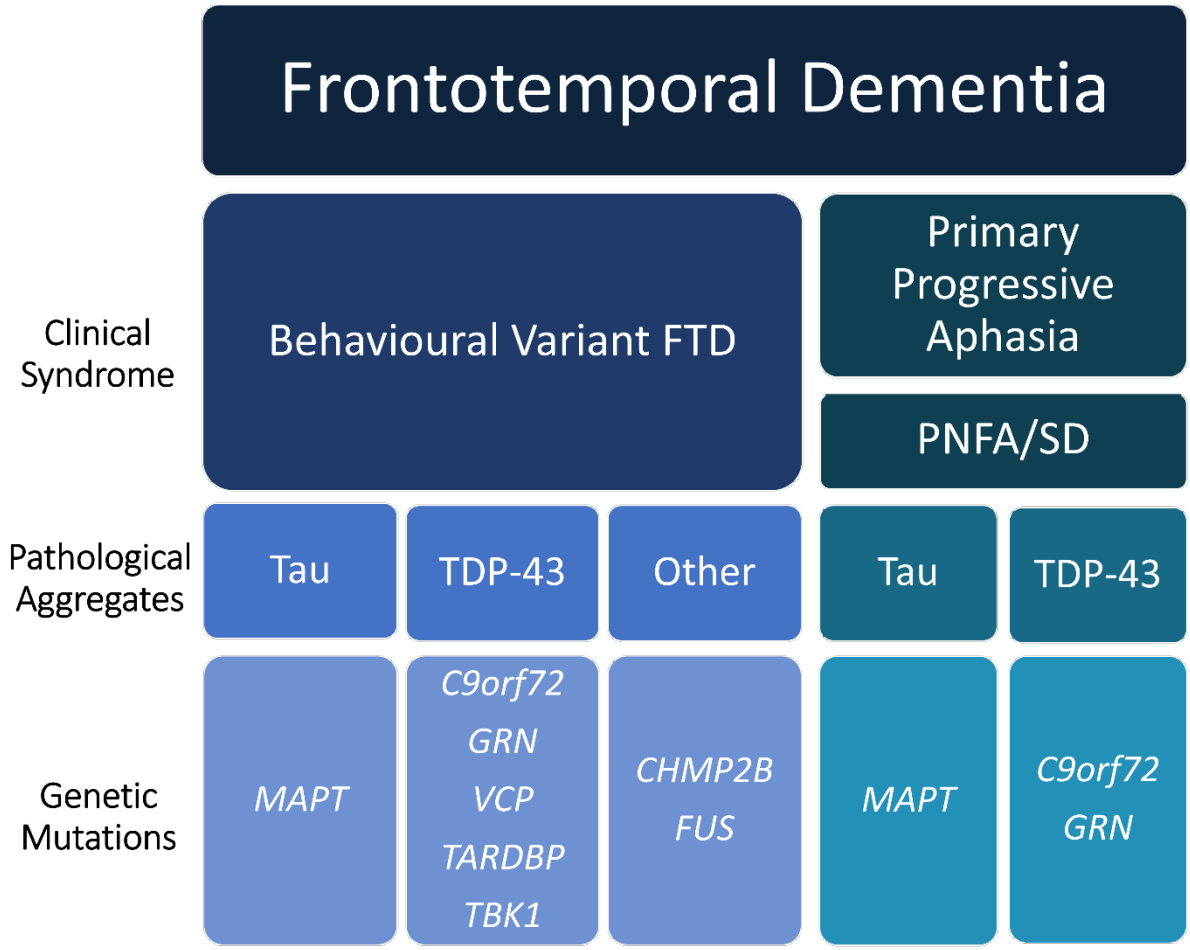

Figure 1.2: Genetics of Familial Frontotemporal Dementia

FTD is a heterogeneous form of dementia and can be classified into several clinical syndromes. Several neuropathological protein aggregates can be seen in FTD, and the vast majority of these can be broadly classified into tau-positive or TDP-43 positive inclusions. FTD is a highly heritable form of dementia, and most inherited cases can be attributed to heterozygous mutations in the MAPT, C9orf72 or GRN genes, which most often lead to FTD with the bvFTD clinical syndrome (Greaves et al. 2019).

1.5 Patterns of neurodegeneration and white matter dysfunction in FTD

People with FTD carrying disease-causing mutations present with distinctive patterns of brain atrophy relating to their clinical symptoms. While both mutations in *GRN* and *C9orf72* cause bvFTD due to their frontotemporal predominance, FTD patients with *GRN* mutations (FTD-*GRN*) present with asymmetric, severe frontal and temporal lobe atrophy, and moderate parietal lobe atrophy whereas those with *C9orf72* repeat expansions (FTD-*C9orf72*) show more diffuse, symmetrical bilateral atrophy, most severely affecting the frontal and temporal lobes along with parietal lobe and cerebellum (Rohrer et al. 2008, Mahoney et al. 2012, Rademakers et al. 2012, Paternico et al. 2016, Cash et al. 2018). Cerebral hypometabolism, indicative of metabolic dysfunction as measured by the rate of [^{18}F] fluorodeoxyglucose uptake by positron emission tomography (FDG-PET), can be seen 10 years prior to symptom onset in in the frontal lobe of both FTD-*GRN* and FTD-*C9orf72* cases (Jacova et al. 2013, Popuri et al. 2021).

MRI studies have widely reported evidence of white matter hyperintensities (WMH) in the brains of FTD patients carrying *GRN* mutations, including in presymptomatic cases (Caroppo et al. 2014, Ameur et al. 2016, Paternico et al. 2016, Sudre et al. 2017, Woollacott et al. 2018, Sudre et al. 2019). In the absence of vascular risk factors, WMH are generally indicative of focal demyelination. Using a combination of MRI and brain histopathology, Woollacott and colleagues confirmed pathological correlates of demyelination, substantial gliosis and cortical atrophy in regions underlying WMH by MRI in a single FTD-*GRN* case study (Woollacott et al. 2018). No other prior studies have demonstrated myelin loss histopathologically in FTD-*GRN* cases.

WMH have been associated with cognitive deficits in FTD (Tartaglia et al. 2012, Huynh et al. 2021) and notably, bvFTD patients have considerably higher WMH burden when compared to Alzheimer's disease patients (Mahoney et al. 2014, Huynh et al. 2021). Although significant WMH were not observed in the brains of FTD patients carrying *C9orf72* repeat expansions (Paternico et al. 2016, Sudre et al. 2017), structural imaging studies employing diffusion tensor imaging have uncovered diffusion changes to white matter tracts in FTD cases carrying *C9orf72*, *GRN* and *MAPT* mutations up to 30 years prior to estimated symptom onset (Mahoney et al. 2015, Jiskoot et al. 2018). It was recently shown that presymptomatic abnormalities to white matter structure in

GRN mutation carriers exhibited an accelerated trajectory compared with *C9orf72* mutation carriers (Lee et al. 2022). WMH and white matter diffusion changes in FTD follow signature patterns within each mutation group corresponding to characteristic patterns of cortical atrophy, but importantly have also been observed extending beyond the zones of grey matter atrophy and may indeed precede grey matter loss (Lam et al. 2014, Mahoney et al. 2014, Agosta et al. 2015, Meeter et al. 2017, Cash et al. 2018, Jiskoot et al. 2018, Huynh et al. 2021).

1.6 Progranulin

Heterozygous *GRN* mutations cause haploinsufficiency and have a disease penetrance of >90% by age 70 (Gass et al. 2006). More than 70 pathogenic mutations have been identified to date; these are typically nonsense mutations or splicing mutations that lead to premature termination of the *GRN* transcript and nonsense-mediated decay of *GRN* mRNA, or missense mutations leading to cytoplasmic mis-sorting or secretion of immature progranulin and its subsequent degradation, resulting in a reduction in progranulin protein levels (Baker et al. 2006, Cruts et al. 2006, Gijselinck et al. 2008, Shankaran et al. 2008, Yu et al. 2010, Chen-Plotkin et al. 2011, Greaves et al. 2019). This can be observed in levels of plasma and CSF progranulin, which are reduced in FTD cases bearing *GRN* mutations compared to FTD non-carriers and normal controls (Ghidoni et al. 2008, Finch et al. 2009). Interestingly, *GRN* mRNA levels are selectively increased in the heavily-affected frontal lobe in FTD-*GRN* cases, however this does not appear to translate into increased levels of progranulin protein (Chen-Plotkin et al. 2009).

Progranulin is an ~88 kDa secreted glycoprotein and comprises 7 tandem peptide repeats, plus a half-repeat of a cysteine-rich motif, that can be cleaved into mature granulin peptides by a number of proteases such as neutrophil elastase and cathepsin L (Zhou et al. 1993, Zhu et al. 2002, Cenik et al. 2012, Lee et al. 2017). Progranulin is synthesised in the endoplasmic reticulum lumen and undergoes post-translational modifications such as glycosylation (Songsrirote et al. 2010, Kao et al. 2017).It is ubiquitously expressed and localises to endolysosomes and the golgi. In the central nervous system (CNS) its expression is highest in microglia but is also expressed in

cerebellar Purkinje and pyramidal neurons of the hippocampus and cerebellum (Ryan et al. 2009, Hu et al. 2010, Zhang et al. 2014).

Full-length progranulin is thought to act as a neuroprotective factor with roles in proliferation, inflammation and wound repair (He et al. 2003, Van Damme et al. 2008, Ryan et al. 2009, Hu et al. 2010). In contrast, cleaved granulins appear to have opposing actions and are involved in promoting neutrophil and monocyte recruitment and inflammation (Bateman et al. 1990, Zhu et al. 2002, Ahmed et al. 2007). Loss of progranulin promotes a disease-associated neurodegenerative phenotype in microglia characterised by increased activation, enhanced phagocytosis and migration, and increased secretion of pro-inflammatory cytokines (Martens et al. 2012, Götzl et al. 2019, Zhang et al. 2020). Abnormally-increased microglial-mediated synaptic pruning via complement pathways is observed in progranulin deficiency, and this is thought to play a causative role in the precipitation of FTD (Lui et al. 2016). Conditioned media from cultured *Grn*-deficient microglia is sufficient to promote aggregation and cytoplasmic mis-localisation of TDP-43 in cultured neurons (Zhang et al. 2020). Indeed, it has been proposed that *GRN* may play an important role in suppressing hyperactive neurodegenerative microglial phenotypes with ageing (Martens et al. 2012, Lui et al. 2016). Progranulin deficiency in mice has been shown to result in brain glucose hypometabolism and may be associated with a requirement for increased brain energy consumption due to the presence of a chronic hyperactive microglial state (Götzl et al. 2019). Microglial pathology demonstrating pronounced activation and increased phagocytosis in FTD-*GRN* has been confirmed in the heavily affected frontal lobe, and shown to correspond with regional severity of WMH by MRI (Woollacott et al. 2018).

1.7 C9orf72

The physiological function of the protein encoded by *C9orf72* is still being investigated, however it is widely expressed in many tissue types, with the highest expression in myeloid cells (O'Rourke et al. 2016). The expanded GGGGCC repeats in the *C9orf72* gene that cause FTD and MND are thought to cause reduced expression of the encoded protein, the formation of neurotoxic nuclear RNA foci containing the repeat expansion, and impaired clearance of toxic dipeptide repeats, generated by repeat-associated non-AUG initiated translation of the repeat expansion (DeJesus-Hernandez et al. 2011, Rademakers et al. 2012, Waite et al. 2014, Mackenzie et al. 2015, Goodier et al. 2020). Whether the repeat expansion causes FTD through a predominant loss of physiological protein function or toxic gain of function is still a topic of research, as models of either have been shown to lead to pathogenic consequences (Pang et al. 2021). Greater than 30 copies of hexanucleotide repeats in the *C9orf72* gene are thought to be pathogenic, however the number of repeats between tissue types may vary within an individual (Renton et al. 2011). Non-repeat expansion carriers usually bear up to 20 copies of the repeat, whereas FTD/MND cases bearing the repeat expansion may harbour in the hundreds to thousands of copies (DeJesus-Hernandez et al. 2011).

C9orf72 is thought to be required for endosomal vesicle trafficking, autophagy and lysosomal biogenesis, and is thought to be essential for the normal function of myeloid cells (Farg et al. 2014, Webster et al. 2016, Shi et al. 2018). *C9orf72* deficient mice and MND patients bearing *C9orf72* repeat expansions display accumulation of CD68-positive microglia, indicative of an activated phagocytic phenotype (Brettschneider et al. 2012, Lall et al. 2021). The loss of C9orf72 in mice leads to marked lysosomal accumulation and promotes a pro-inflammatory neurodegenerative signature in macrophages and microglia, with up-regulation of inflammatory cytokines, abnormally-increased synaptic pruning and increased expression of the lipid-sensing microglial marker *Trem2* (triggering receptor expressed on myeloid cells 2) (O'Rourke et al. 2016, Lall et al. 2021).

Decreased C9orf72 protein levels due to the repeat expansion may also sensitise neurons to excitotoxicity. Induced motor neurons deficient for *C9orf72* display glutamate receptor

accumulation, a resulting increase in levels of the excitatory neurotransmitter glutamate, and neuronal hyperexcitability thought to result from impaired lysosomal degradation of excess glutamate receptors (Shi et al. 2018). Aberrant microglial phenotypes related to lysosomal dysfunction therefore appear to be common to the pathogenesis of FTD-*GRN* and FTD-*C9orf72.*

1.8 Lysosomal dysfunction in genetic FTD

Lysosomes are acidic membrane-bound organelles containing hydrolytic enzymes and are essential for the degradation and recycling of cellular macromolecules (Trivedi et al. 2020). Autophagy is the process by which misfolded proteins, damaged organelles and other cellular components destined for degradation are directed to lysosomes for breakdown. This occurs through the endocytic pathway, either through direct endocytosis of intracellular components with the lysosomal membrane, sequestration of these components into autophagosomes which then fuse with endosomes or lysosomes to release their cargoes, or through chaperone-mediated autophagy, whereby soluble cargoes are transported across the lysosomal membrane through interaction with chaperone proteins such as LAMP2A and HSC70 (Saftig et al. 2009, Trivedi et al. 2020). Lysosomes also play a dynamic role in maintaining cellular homeostasis through recycling of cellular components such as amino acids, and regulation of cholesterol levels to facilitate the metabolic and structural requirements of the cell (de Araujo et al. 2020, Hosios et al. 2022). For example, under nutrient deprivation conditions, the energy-sensing AMP-activated protein kinase (AMPK) becomes activated, while the mammalian Target of Rapamycin Complex 1 (mTORC1) becomes inactivated, and these act in tandem to initiate autophagy through phosphorylation of the Unc-51-like kinase 1 (ULK1) autophagy initiation complex to promote the catabolism and recycling of nutrients (Kim et al. 2011, Trivedi et al. 2020).

Lysosomal dysfunction and defective protein degradation has been widely reported in other forms of dementia and may widely underpin the aetiology of FTD, as a large proportion of genetic risk factors for FTD and/or MND encode proteins involved in protein clearance pathways (Bain et al. 2019, Lee et al. 2021). As both *GRN* and *C9orf72* may be required for normal lysosomal

function, FTD with TDP-43 pathological aggregates may have lysosomal dysfunction as a common upstream disease mechanism. TDP-43 itself appears to be involved in gene expression of autophagosomal and lysosomal biogenesis and autophagosome-lysosome fusion (Iguchi et al. 2013, Xia et al. 2016). As FTD with TDP-43 pathology is accompanied by a loss of physiological nuclear TDP-43, this may contribute to lysosomal dysfunction (Neumann et al. 2006). As stated above, mutations in the gene encoding TDP-43, *TARDBP,* also cause familial MND and less commonly, familial FTD (Moreno et al. 2015). In cell models, TDP-43 loss has been shown to result in an upregulation of genes involved in promoting autophagy and lysosomal biogenesis, thought to be through decreased lysosomal localisation of mTORC1 and its resulting inhibition (Xia et al. 2016). Phosphorylation of the transcription factor EB (TFEB) by mTORC1 at the lysosome is thought to prevent its nuclear translocation, however, under starvation conditions, lysosomal inhibition or TDP-43 depletion, TFEB translocates to the nucleus, where it upregulates lysosomal biogenesis genes (Settembre et al. 2011, Roczniak-Ferguson et al. 2012, Xia et al. 2016). TDP-43-deficient cells and *Drosophila* demonstrate an accumulation of immature autophagic vesicles and impaired autophagic flux (Xia et al. 2016). TDP-43-dependent impairment in the vesicular trafficking machinery is thought to result from decreased levels of the motor protein dynactin 1, leading to reduced autophagosomal-lysosomal fusion and impaired autophagic flux (Xia et al. 2016).

1.8.1 Role of Progranulin in Lysosomal Function

The importance of progranulin (product of the *GRN* gene) in sustaining normal lysosomal function is highlighted by the fact that while heterozygous loss of function *GRN* mutations are a common cause of FTD, homozygous loss of function mutations in *GRN* cause the severe lysosomal storage disease neuronal ceroid lipofuscinosis, characterised by enlarged lysosomes and accumulation of the insoluble auto-fluorescent material lipofuscin in neurons (Smith et al. 2012, Almeida et al. 2016). These hallmarks are similarly observed in induced pluripotent stem cell (iPSC)-derived *GRN* mutant cortical neurons, and the brains of *Grn*-/- mice and FTD-*GRN* cases (Ahmed et al. 2010, Gotzl et al. 2014, Evers et al. 2017, Valdez et al. 2017, Ward et al. 2017). Lipofuscin commonly

accumulates in the lysosomes of post-mitotic cells such as neurons throughout the course of normal ageing, and is associated with oxidative stress (Double et al. 2008). Lipofuscin is composed of undegraded protein debris, lipids, metal cations, and subunit C of mitochondrial ATP synthase (Moreno-García et al. 2018).

Progranulin is thought to be essential in initiating catabolism of complex lipids in lysosomes through a multi-faceted approach including its roles in regulating lysosomal acidification, facilitating lysosomal trafficking and processing of proteins essential for lipid catabolism, and modulating the activity of lysosomal lipases such as glucocerebrosidase (GCase) and hexosaminidase A (HexA) (Jian et al. 2016, Tanaka et al. 2017, Zhou et al. 2017, Chen et al. 2018, Arrant et al. 2019, Valdez et al. 2019). Extracellular progranulin is internalised into endolysosomes through binding to its receptor, sortilin (Hu et al. 2010, Zhou et al. 2017) or through sortilin-independent mechanisms through its association with prosaposin and the cation-independent mannose-6-phosphate receptor and low density lipoprotein receptor-related protein 1 (Zhou et al. 2015, Zhou et al. 2017). In the lysosome, full-length progranulin and granulin E are thought to regulate the function of the major lysosomal protease cathepsin D (Beel et al. 2017, Valdez et al. 2017). In yeast, the homolog of cathepsin D promotes clearance of TDP-43 by maintaining endosomal-lysosomal function (Leibiger et al. 2018). Interestingly, similar to *GRN* deficiency, cathepsin D deficiency causes a congenital form of neuronal ceroid lipofuscinosis (Siintola et al. 2006). Cathepsin D cleaves prosaposin, the precursor to the sphingolipid activator proteins (saposins) A-D into individual saposins (Hiraiwa et al. 1997, Beel et al. 2017, Tanaka et al. 2017, Valdez et al. 2017). Saposins are lipid-binding glycoproteins, and each are essential cofactors for specific lysosomal hydrolases that carry out sphingolipid catabolism by facilitating the interaction between hydrophobic lipid substrates and hydrophilic lysosomal hydrolases (Figure 1.3).

Deficiency of specific lysosomal hydrolases or their corresponding saposin cofactor precipitate lysosomal storage diseases, characterised by accumulation of the undegraded lipid substrates (Kishimoto et al. 1992, Hiraiwa et al. 1997, Sandhoff 2013). For example, heterozygous loss of function in the *GBA* gene, encoding glucocerebrosidase (GCase), is the most common risk factor for Parkinson's disease (Neumann et al. 2009). Homozygous *GBA* loss leads to accumulation of

the GCase substrate glucosylceramide and precipitates the common lysosomal storage disease, Gaucher's disease (Nilsson et al. 1982). Saposin C acts as a cofactor for GCase, and its loss in the presence of the functional enzyme similarly leads to accumulation of glucosylceramide and precipitates atypical Gaucher's disease (Christomanou et al. 1989, Vaccaro et al. 2010). Impaired processing of prosaposin into saposin C has been shown in FTD-*GRN* brain tissue but not in other FTD cases or controls (Valdez et al. 2019). While parkinsonism has been shown to co-occur with all FTD subtypes, it is present in up to 60% of FTD-*GRN* cases (Park et al. 2013, Siuda et al. 2014). The essential role of Progranulin in Prosaposin trafficking and its downstream consequences suggests Progranulin may act as a broad regulator of lysosomal lipid metabolism. In support of this, *Grn* -/- mice display myelination deficits, demyelination and age-dependent microglial dysfunction with accumulation of enlarged lysosomes containing myelin debris (Tanaka et al. 2014, Huang et al. 2020, Wu et al. 2021).

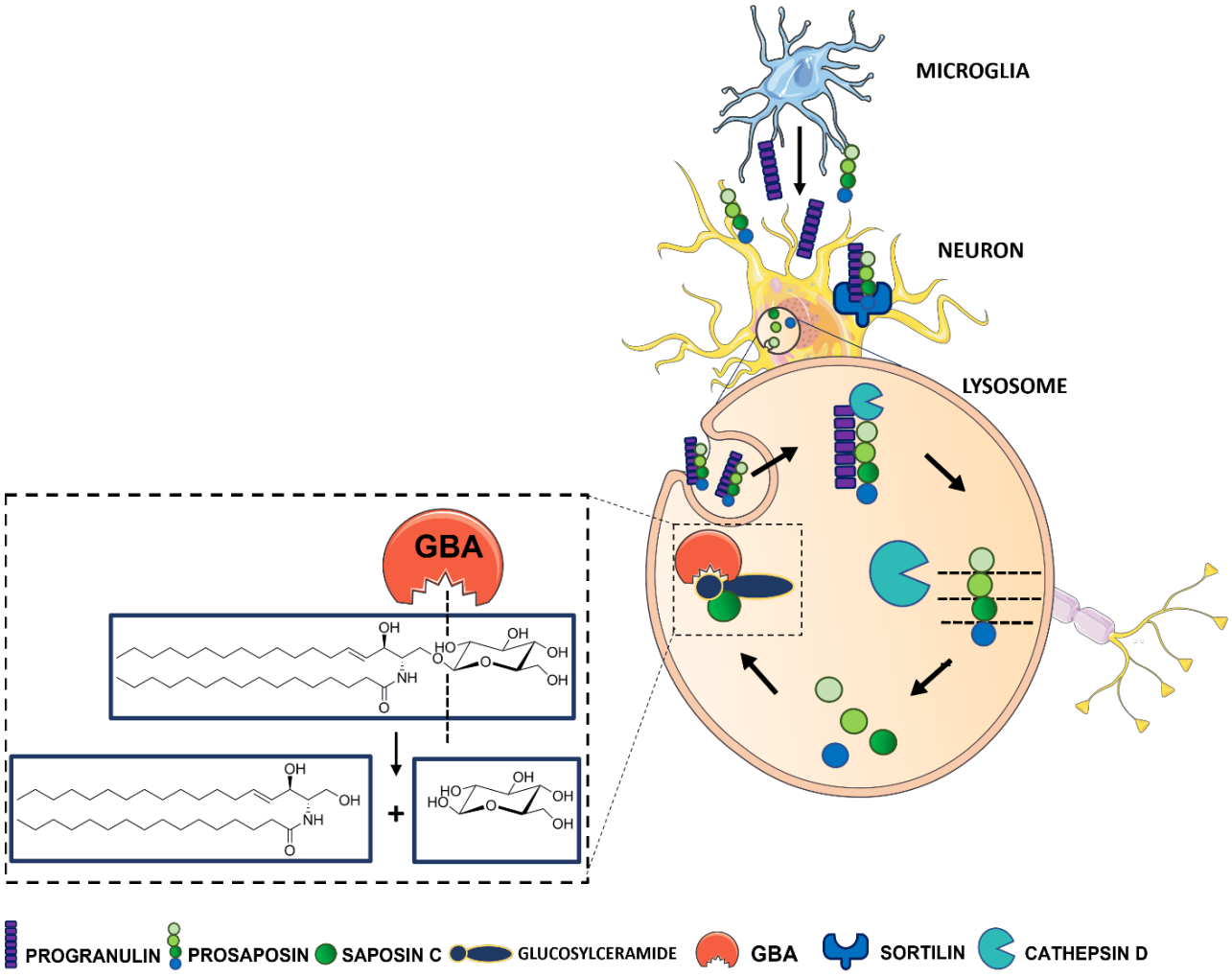

Figure 1.3: Proposed mechanism for regulation of lipid catabolism by Progranulin

Progranulin is highly expressed in microglia. Secreted Progranulin interacts with prosaposin, and this complex in internalised into lysosomes through the sortilin receptor, or through sortilin-independent pathways (Zhou et al. 2015, Zhou et al. 2017). Evidence suggests that Progranulin regulates the Cathepsin D-mediated cleavage of prosaposin into individual saposins (Sphingolipid Activator Proteins) A-D (Tanaka et al. 2017, Valdez et al. 2017). Saposins are essential cofactors for the degradation of complex sphingolipids in lysosomes by facilitating the interaction between hydrophilic lipid catabolic enzymes and their hydrophobic lipid substrates (Matsuda 2008, Sandhoff 2013). For example, saposin C is essential for the hydrolysis of glucosylceramide to glucose and ceramide by glucocerebrosidase (GBA/GCase). (Adapted from (Lee et al. 2021)).

The endosomal/lysosomal enriched phospholipid Bis(monoacylglycerol)phosphate (BMP), also known as lyso-bis-phosphatidic acid (LBPA) has recently gained attention for its potential involvement in FTD with *GRN* mutations. BMP is an isomer of its precursor, phosphatidylglycerol, but possesses a unique structure, allowing it to maintain a negative charge in the acidic lysosomal environment (Hullin-Matsuda et al. 2009, Abdul-Hammed et al. 2017). Due to its negative charge, BMP is thought to electrostatically attract and concentrate positively charged lysosomal hydrolases to stimulate their activity, and progranulin has been proposed to stabilise BMP (Abdul-Hammed et al. 2017, Logan et al. 2021). BMP levels have been shown to accumulate in several lysosomal storage diseases, however decreased levels of several BMP species have been reported in the brains of *Grn* deficient mice and cerebrospinal fluid of FTD cases (Käkelä et al. 2003, Akgoc et al. 2015, Logan et al. 2021, Boland et al. 2022). Accumulation of several gangliosides in the brains of *Grn* deficient mice and FTD-*GRN* frontal cortex was recently reported alongside normal ganglioside catabolic enzyme activity, but decreased levels of some BMP species (Boland et al. 2022). *Grn*-/- HeLa cells also displayed accumulation of gangliosides that could be rescued with BMP supplementation, leading the authors to propose that *GRN* loss leads to impaired lysosomal function via the action of BMP (Boland et al. 2022).

1.8.2 Role of *C9orf72* in Lysosomal function

C9orf72 localises to early endosomes and lysosomes, and is thought to play an important role in regulating autophagy and lysosome function through several mechanisms (Amick et al. 2016, Shi et al. 2018). C9orf72 can exist alone or form a stable complex with SMCR8 (Smith-Magenis Syndrome Chromosome Region, Candidate 8) and WDR41 (WD Repeat domain 41), and this protein complex has been shown to interact with several Rab GTPases involved in endosomal trafficking and autophagy (Farg et al. 2014, Sellier et al. 2016, Sullivan et al. 2016, Shi et al. 2018).

Rabs are a large family of nucleotide exchange factor proteins which carry out exchange between GTP and GDP to coordinate intracellular membrane trafficking events in the endocytic and exocytic pathways, such as vesicular transport and membrane fusion. Individual Rab proteins are

regulators of specific functions within their target organelle and have specific downstream effectors (Banworth et al. 2018). The C9orf72-SMCR8-WDR41 complex interacts with the FIP200/ULK1 complex, an essential regulator of autophagy initiation, through regulation of Rab1a trafficking of the ULK1 complex to the phagophore to initiate autophagosome formation (Sullivan et al. 2016). Pathological *C9orf72* repeat expansions result in an accompanying decrease in C9orf72 protein levels, which would be expected to affect the function of this complex and lead to impaired autophagy initiation (Shi et al. 2018).

Autophagy was reduced in rat primary cortical neurons subject to C9orf72 knockdown and was accompanied by an increase in p62 immunoreactivity (Webster et al. 2016). The p62 protein (encoded by *SQSTM1*, itself an FTD risk gene) is an autophagic substrate that delivers and anchors ubiquitinated proteins to the autophagosome membrane for degradation, and therefore an increase in p62 may indicate impaired autophagic flux (Rubino et al. 2012, Liu et al. 2016, Ma et al. 2019). Further indication of the role of C9orf72 in maintaining autophagic flux is through its colocalisation with Rab5, Rab7 and Rab11, and that C9orf72 deficient cells show enlarged late endosomes and lysosomes that cluster perinuclearly (Farg et al. 2014, Amick et al. 2016). Rab5 and Rab7 are determinants of early and late endosomes, respectively, and Rab11 is involved in endosomal recycling (Rink et al. 2005, Wilke et al. 2017, Banworth et al. 2018). C9orf72 may be required for lysosomal biogenesis with patient *C9orf72* induced motor neurons displaying fewer lysosomes (Shi et al. 2018). Survival of these neurons was rescued by a constitutively active form of Rab5, thought to be through the action of Rab5 recruitment of PI3 kinase to early endosomes, and its subsequent formation of a key promoter of maturation of endosomes to lysosomes, phosphatidylinositol-3-phosphate (PI3P), indicating that the action of C9orf72 on Rab5 and its downstream effectors maintain autophagic flux and prevent neurodegeneration (Shi et al. 2018).

The C9orf72 complex also interacts with autophagic Rab8a and Rab39b, and supplementation of constitutively active Rab39b was able to correct autophagy impairment in a neuronal cell line subjected to C9orf72 depletion (Sellier et al. 2016). Lysosomal acidification is essential to maintain active lysosomal hydrolases and subsequent degradative capability in lysosomes (Trivedi et al. 2020). The C9orf72 complex has also been implicated in regulating lysosome acidification, with *C9orf72-/-* mice displaying increased lysosomal pH and severely reduced levels

of mature cathepsin D in mutant macrophages (Shao et al. 2020). C9orf72 has also been shown to interact with Ubiquilin-2, a key protein involved in the transport of ubiquitinated cargoes to the proteasome and autophagosome for degradation (Farg et al. 2014, Renaud et al. 2019) These findings suggest that impaired endosomal trafficking, maturation, and lysosomal biogenesis may be significant contributors to neurodegeneration in ALS/FTD with *C9orf72* repeat expansions.

1.9 Brain Lipid Metabolism

In humans, the brain is the second-most lipid-rich organ after adipose tissue. This is due to the high proportion of lipid-rich cerebral white matter, which makes up approximately half the brain volume and contains bundles of myelinated axons (Hamilton et al. 2007, Ardesch et al. 2021). In humans, myelination begins in the third trimester, increases substantially in the first two years of life, and continues until the third decade of life (Brody et al. 1987, Lebel et al. 2011). Myelin is essential for movement, learning and cognition and is formed in the CNS by specialised glial cells called oligodendrocytes. Myelin is the multilayered membrane extension of oligodendrocyte plasma membranes that tightly wrap around neuronal axons (Nave 2010). This provides electrical insulation and allows for the fast and efficient conduction of electrochemical signals along neuronal axons in a process known as saltatory conduction. In myelinated axons, the conduction of action potentials is restricted to unsheathed axonal segments known as the nodes of Ranvier, where voltage gated sodium ion channels are concentrated, thereby greatly increasing the speed of conduction of nerve impulses (Pedraza et al. 2001, Sherman et al. 2005). Each oligodendrocyte may myelinate multiple neuronal axons and provide metabolic and trophic support to neurons (Lee et al. 2012).

Myelination is a dynamic process, with myelin lipids constantly being turned over (Ando et al. 2003). The physiological turnover and maintenance of myelin is predicted to require a high level of constitutive lipid catabolism in microglial and oligodendrocyte lysosomes (Gomez-Sanchez et al. 2015, Cignarella et al. 2020). Disruption of autophagic flux in microglia, such as through Rab7

deficiency induces lysosomal dysfunction featuring enlarged lysosomes and accumulation of myelin debris in a mouse model (Safaiyan et al. 2016).

Interestingly, TDP-43 appears to be essential for oligodendrocyte survival and myelination and is thought to play a role in regulating expression of myelin-related genes (Wang et al. 2018, Heo et al. 2022). Mice deficient for TDP-43 in mature oligodendrocytes show progressive demyelination, necroptosis of mature oligodendrocytes and premature death (Wang, 2018).

1.9.1 Lipid Metabolic Dysfunction in FTD

The presence of substantial white matter alterations seen by MRI in genetic forms of FTD may indicate a crucial role for lipid metabolic dysfunction in the precipitation of FTD. Rare variants in genes known to cause the severe demyelinating and hypomyelinating disorders termed leukodystrophies also confer FTD risk, such as *TMEM106B* (hypomyelinating leukodystrophy), *TREM2* (Nasu-Hakola disease), *ARSA* (metachromatic leukodystrophy) and *CYP27A1* (cerebrotendinous xanthomatosis), underscoring the involvement and importance of dysfunctional brain lipid metabolism in the origin of frontotemporal dementia (Gieselmann et al. 2003, Borroni et al. 2014, Simons et al. 2017, Lok et al. 2021). In addition, variants of *TMEM106B*, a transmembrane protein which is mainly localised to late endosomes and lysosomes, increase FTD risk in both *GRN* and *C9orf72* mutation carriers (Van Deerlin et al. 2010, Chen-Plotkin et al. 2012, Gallagher et al. 2014). While the major *TMEM106b* risk allele confers increased risk of developing FTD in either group, in *C9orf72* repeat expansion carriers it also confers a later age at disease onset and later age at death, while in *GRN* mutation carriers it leads to an earlier age of disease onset and has been associated with increased longitudinal accrual of white matter hyperintensities by MRI (Cruchaga et al. 2011, Gallagher et al. 2014, Sudre et al. 2019). While the function of *TMEM106B* is still unknown, it has been shown to regulate intracellular progranulin levels and its overexpression *in vitro* is associated with disrupted endosomal-lysosomal pathways (Chen-Plotkin et al. 2012). TMEM106B may also play an essential role in myelination; the protein was recently shown to locate to oligodendrocyte lysosomes and regulate cathepsin D levels in oligodendrocytes (Feng et al. 2020). *Tmem106b*-/- mice exhibit susceptibity to demyelination and

reduced capacity to remyelinate following treatment with the copper chelating oligodendrocyte toxin cuprizone, thought to be due to impaired trafficking of the major myelin protein PLP from oligodendrocyte lysosomes to the plasma membrane (Zhou et al. 2020, Song et al. 2021). Lysosomal dysfunction and accumulation of myelin debris were recently shown in microglia from *Tmem106b*/*Grn* double knockout mice, highlighting the interplay between lysosomal dysfunction and demyelination (Feng et al. 2020).

1.9.2 CNS Myelin Composition

The unique composition and structure of myelin in the CNS allows for tight membrane packing and efficient insulation of axons. Myelin is composed approximately 70-80% (dry weight) of lipids, primarily comprising cholesterol, phospholipids, ethanolamine plasmalogens and galactosylceramides maintained in a tightly regulated molar composition ratio of 2:2:1:1 of cholesterol, phospholipids, galactolipids and plasmalogens (O'Brien et al. 1965, Norton et al. 1973, Nave et al. 2014). Myelin is arranged in a series of concentric spiralled layers, with up to 100 layers insulating heavily myelinated axonal segments (Figure 1.4) (Hildebrand et al. 1993). The most abundant protein constituents of myelin are the integral membrane protein proteolipid protein (PLP) and the cytoplasmic protein myelin basic protein (MBP), which are constituents of compact myelin, and interact with lipid bilayers to maintain tight membrane packing between apposing myelin sheaths and maintenance of the ordered lamellar structure of myelin (Simons et al. 2000, Jahn et al. 2020, Ruskamo et al. 2022). Protein components of non-compact myelin are primarily located on the innermost and outermost layers of the myelin sheath, and largely comprise 2’,3’-cyclic-nucleotide 3'-phosphodiesterase (CNP), myelin oligodendrocyte glycoprotein (MOG) and myelin-associated glycoprotein (MAG) which are thought to be involved in interactions between the lipid bilayer and cytoplasmic or cytoskeletal structures (Jahn et al. 2009, Simons et al. 2015, Ruskamo et al. 2022). Myelin proteins associate with cholesterol and glycosphingolipid-rich regions in the plasma membrane that self-assemble to form specialised detergent-resistant domains known as lipid rafts, which carry out recruitment and transport of selected proteins and organise assembly of the myelin sheath (Simons et al. 2000). Impairments

to myelin homeostasis are likely to contribute to neurodegeneration and to this end, several recent studies have reported changes to myelin proteins in FTD with *C9orf72* or *GRN* mutations. Huang and colleagues reported age-dependent decreases to lipid metabolic proteins and protein markers of myelin, oligodendrocytes and neurons in the whole-brain proteome from *Grn-/-* deficient mice, and were able to validate these findings in a small cohort of FTD-*GRN* cases (Huang et al. 2020). Decreased levels of MBP, myelin loss and changes to oligodendrocyte gene expression were also reported in the brains of FTD-*C9orf72* cases accompanied by an increase in MBP levels in cerebrospinal fluid (Sirisi et al. 2022).

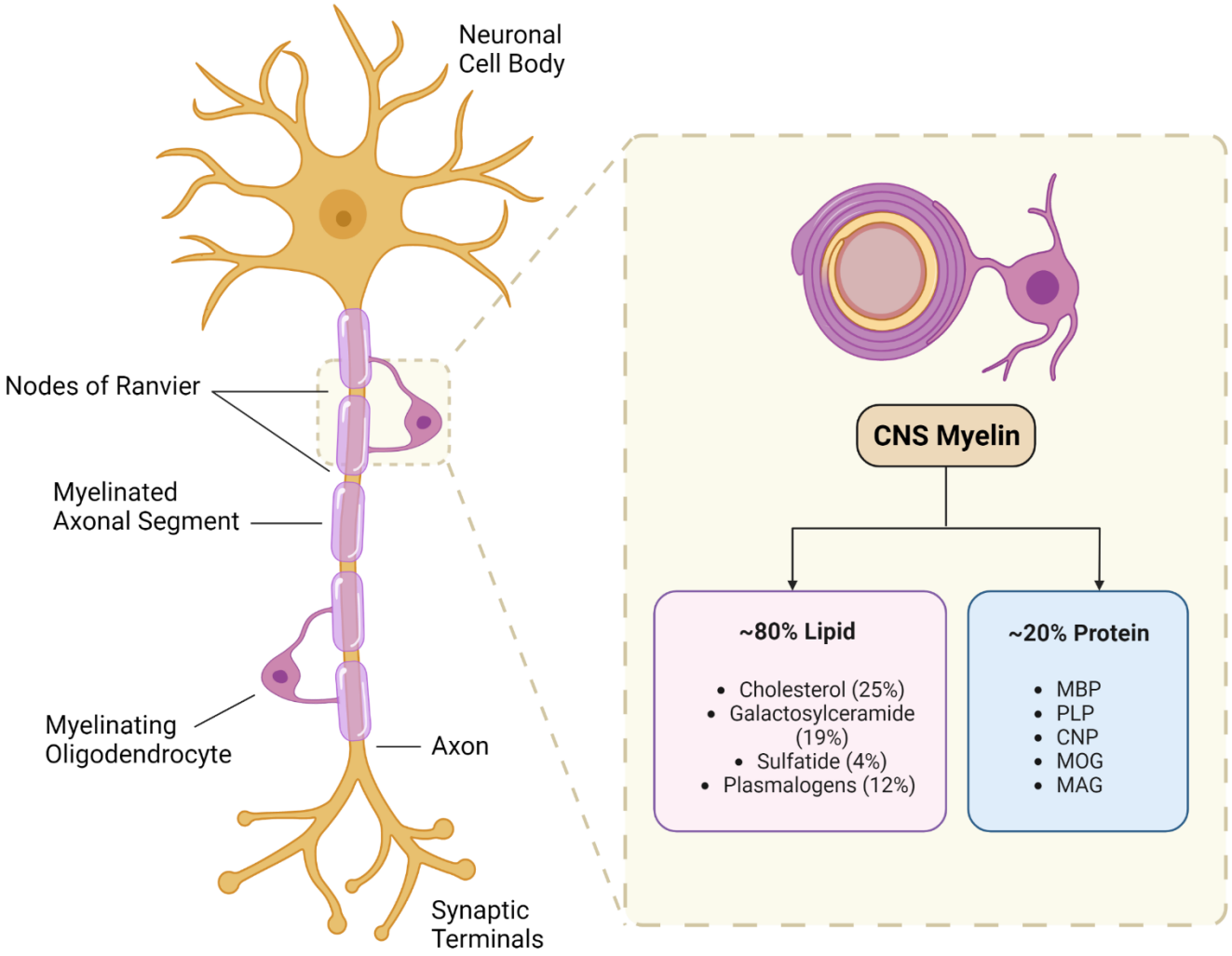

Figure 1.4: Composition of CNS myelin

Myelin is formed by oligodendrocytes in the CNS and is highly lipid rich, comprising 70-80% dry weight of lipid (O'Brien et al. 1965, Norton et al. 1973). Myelin is highly enriched in cholesterol and the unique galactolipids galactosylceramide and sulfatide, as well as ethanolamine plasmalogens. Myelin basic protein (MBP) and proteolipid protein (PLP) are the major myelin proteins and constitute approximately 70% of myelin protein. 2',3'-cyclic-nucleotide 3'-phosphodiesterase (CNP), myelin oligodendrocyte glycoprotein (MOG) and myelin-associated glycoprotein (MAG) are less abundant protein components (Jahn et al. 2020).

1.9.3 Myelin Cholesterol

The brain is the organ most highly enriched in cholesterol, which makes up over 20% of myelin lipid (O'Brien et al. 1965). The pool of cholesterol in the brain is separated from the peripheral pool of cholesterol due to the presence of the blood-brain barrier and is almost exclusively synthesised *de novo* by oligodendrocytes in the CNS (Jurevics et al. 1995). Cholesterol is indispensable for myelin formation and its importance in development is highlighted by the fact that deficiency in mice of either HMG-CoA reductase, the rate-limiting enzyme in the cholesterol biosynthetic pathway, or squalene synthase, which catalyses the first reaction within the pathway committed to sterol biosynthesis, are embryonically lethal (Tozawa et al. 1999, Ohashi et al. 2003). Cholesterol is a limiting component for myelin synthesis, with mice deficient for squalene synthase in oligodendrocytes showing a severely reduced capacity to myelinate. Interestingly, while myelin formed slowly due to the minimal availability of cholesterol from other sources, such as uptake from astrocytes, the ratio between lipid classes described in normal myelin was maintained (Saher et al. 2005).

Almost all cholesterol in the brain is found in the free or unesterified format (O'Brien et al. 1965, Bryleva et al. 2010). Free cholesterol is essential for conferring plasma membrane fluidity and may confer electrical insulating properties (Saher et al. 2005). The pool of cholesterol is tightly regulated by sterol regulatory element binding transcription factors (SREBP) 1 and 2, which activate gene transcription for cholesterol and fatty acid biosynthesis and are in turn activated by mTORC1 signalling (Horton et al. 2003, Düvel et al. 2010). TDP-43 has also been shown bind to SREBP2 mRNA and influence transcription of cholesterol biogenesis genes in oligodendrocytes, resulting in cholesterol reduction and demyelination under TDP-43 depletion (Wang et al. 2018, Ho et al. 2021).

Cholesterol turnover is essential for remyelination, and the major CNS cholesterol transporter, APOE, is required for removal of cholesterol debris following demyelination (Cantuti-Castelvetri et al. 2018). Excess accumulation of myelin cholesterol debris in macrophages promotes lysosomal rupture and NLRP3 inflammasome activation (Cantuti-Castelvetri et al. 2018). Cholesterol cannot be broken down in the CNS, instead, the primary mechanism for removal is

thought to be through excretion following a series of hydroxylation reactions. This occurs largely through the action of the neuronal cytochrome P450 CYP46A1, upon which the resulting 24(S)-hydroxycholesterol is able to cross the blood-brain barrier and enter the circulation (Björkhem et al. 1998, Lund et al. 1999, Chiang et al. 2020). Mice incapable of excreting CNS cholesterol through CYP46A1-dependent mechanisms do not show resulting cholesterol accumulation, but rather downregulated cholesterol synthesis, suggesting that the tight regulation of the CNS cholesterol pool is highly important (Lund et al. 2003).

Another mechanism by which excess levels of cholesterol are regulated is through the formation of cholesterol esters and their intracellular storage in lipid droplets. Cholesterol esters are formed in response to high levels of cholesterol or impaired cholesterol efflux through the addition of a fatty acyl coA to free cholesterol by acyl-coenzyme A:cholesterol acyltransferase 1 (ACAT1) in the endoplasmic reticulum (Petrov et al. 2016). Accumulation of cholesterol esters has been described as a feature in the brains of Alzheimer's disease cases (Chan et al. 2012), motor cortex of ALS cases (Sadler et al. 2022) and frontal lobe from FTD-*GRN* cases (Boland et al. 2022).

1.9.4 Myelin Sphingolipids

Myelin is enriched in the unique glycosphingolipids galactosylceramide (GalCer, also known as cerebroside) and its sulfated form, sulfatide (ST), representing a combined 23% of myelin lipid content (O'Brien et al. 1965). These prototypical myelin lipids are synthesised exclusively by oligodendrocytes in the CNS and are formed from very long-chain ceramides, essential for conferring stability to the myelin membrane (O'Brien et al. 1965, Schmitt et al. 2015, Teo et al. 2023). Structurally, GalCer and ST are composed of a galactose sugar head group (or in the case of ST, a sulfated galactose head group) attached to a sphingosine backbone and very long-chain fatty acid (VLCFA) tail (Figure 1.5) (O'Brien et al. 1964).

In the endoplasmic reticulum, the family of fatty acid elongase enzymes (ELOVL 1-7) extend long chain (C16-C18) fatty acids to VLCFAs (C20-C24), and a significant proportion of these are hydroxylated at the 2-carbon of the fatty acid moiety by fatty acid-2 hydroxylase (FA2H)

(Alderson et al. 2004, Eckhardt et al. 2005, Jakobsson et al. 2006). These VLCFAs are incorporated into ceramides by ceramide synthase 2 (CERS2), primarily in oligodendrocytes, and in the Golgi the UDP-galactose:ceramide galactosyltransferase enzyme (UGT8) is responsible for the addition of galactose to very long chain ceramides to form GalCer and ST (Schaeren-Wiemers et al. 1995, Becker et al. 2008). GalCer can be sulfated by cerebroside sulfotransferase (CST) to form ST (Figure 1.6) (Wattenberg 2019).

These highly hydrophobic lipid fatty acid tails create strong intermolecular forces and interleave into the apposing plasma membrane, acting to hold together the layers of the myelin sheath. Their hydroxylated counterparts are further able to form hydrogen bonds to further strengthen membrane packing, and galactose headgroups of apposing membranes attract each other and are essential for optimal axonal insulation, normal myelin structure and long-term stability (Bosio et al. 1996, Kulkarni et al. 1999). Mice deficient for UGT8 are able to form compact myelin through the incorporation of glucose rather than galactose to form glucosylceramide, an isomer of GalCer traditionally found in minor quantities in the brain into the myelin sheath, however the insulating properties of the myelin sheath are compromised, and mice display impaired nerve conduction, tremors, demyelination and premature death (Bosio et al. 1996, Coetzee et al. 1996).

Unlike most lipids that are turned over in lysosomes, the breakdown of VLCFAs occurs via β-oxidation in peroxisomes (Tolbert 1981). Oligodendrocytes are the CNS cell type shown to be particularly vulnerable to the effects of peroxisomal dysfunction (Hein et al. 2008). Impaired peroxisomal function causes X-linked adrenoleukodystrophy, leading to accumulation of VLCFAs, demyelination and neurodegeneration, and interestingly, a recent study reported elevated levels of several VLCFA-containing lipids in frontal cortex of FTD cases (He et al. 2021).

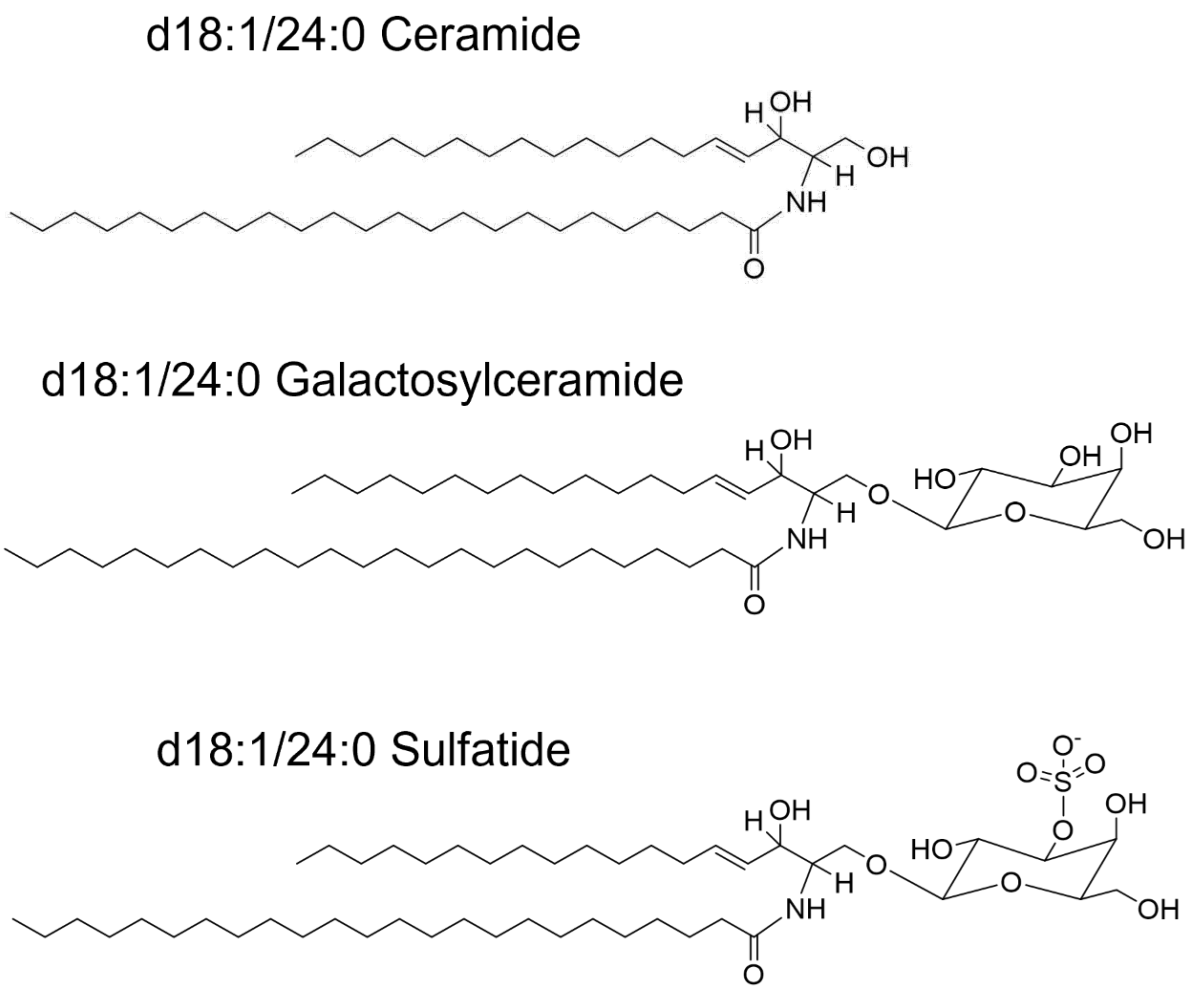

Figure 1.5 Structure of major myelin sphingolipids

Myelin is highly enriched in the sphingolipids galactosylceramide (GalCer) and sulfatide (ST), and these lipids are essential for the structural stability of myelin (Bosio et al. 1996, Coetzee et al. 1996) . GalCer and ST are formed from very long chain ceramides with the addition of a galactose, or sulfated galactose, and these myelin lipids are formed exclusively by oligodendrocytes in the CNS (Becker et al. 2008, Teo et al. 2023).

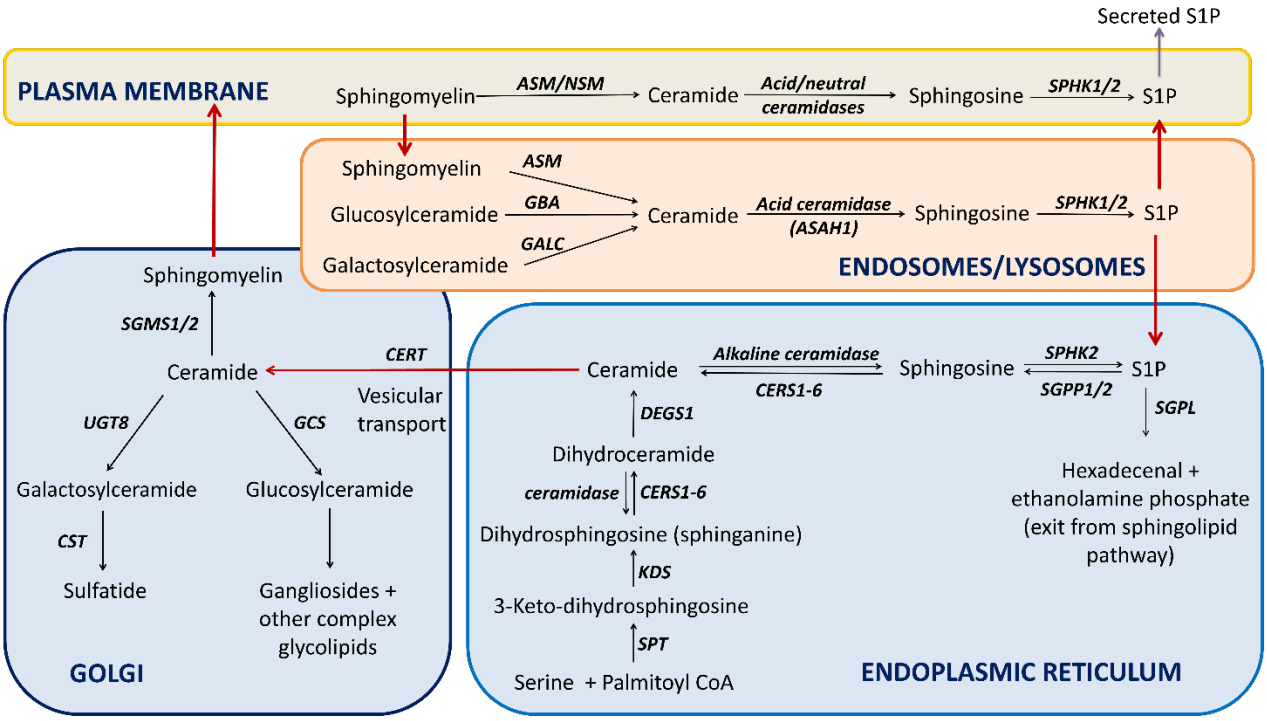

Figure 1.6: Oligodendrocyte sphingolipid metabolism

Myelin-enriched sphingolipids are synthesised and modified in the endoplasmic reticulum and Golgi and transported to the plasma membrane where they carry out their functions. Sphingolipid catabolism takes place in endosomes and lysosomes by the action of lysosomal hydrolases, and dysfunctional lipid catabolic enzymes give rise to lysosomal storage diseases. Red arrows indicate transport; black arrows are biochemical reactions. Enzyme names are shown in italics: ASAH1, acid ceramidase; ASM, acid sphingomyelinase; CERS1-6, ceramide synthases 1-6; CERT, ceramide transfer protein; CST, cerebroside sulfotransferase; DEGS1, dihydroceramide desaturase 1; GALC, galactosylceramidase; GBA, glucocerebrosidase; GCS, glucosylceramide synthase; KDS, 3-ketodihydrosphingosine reductase; NSM, neutral sphingomyelinase; S1P, sphingosine- 1 -phosphate; SGMS1/2, sphingomyelin synthases 1 and 2; SGPL, sphingosine 1-phosphate lyase; SGPP1/2, sphingosine 1-phosphate phosphatases 1 and 2; SPHK1/2, sphingosine kinases 1 and 2; SPT, serine palmitoyltransferase; UGT8, UDP-Galactose Ceramide Galactosyltransferase. (Adapted from (Marian et al. 2020)).

1.9.5 Myelin Phospholipids

Phospholipids are membrane lipids and in myelin, the most abundant are ethanolamine plasmalogens (PE(P)), phosphatidylethanolamines (PE) and phosphatidylcholines (PC) (Norton et al. 1973). Ethanolamine plasmalogens are the most highly abundant, representing approximately 12% of myelin lipid (Norton et al. 1966). PE(P)s are phosphatidylethanolamines comprising an ethanolamine headgroup attached to a glycerophosphate backbone and fatty acid tails through a vinyl ether bond, rather than the ester bond traditionally observed in PE and other phospholipids (Figure 1.7) (Braverman et al. 2012). Unlike other lipids synthesised in the endoplasmic reticulum, PE(P) synthesis is initiated in peroxisomes (Honsho et al. 2017). Their unique structure is thought to allow for dense membrane packing and decreased membrane fluidity as it straightens out the shape of the molecule (Braverman et al. 2012). It has also been suggested that due to their readily oxidisable structure, they may confer antioxidant properties to the myelin membrane (Sindelar et al. 1999, Luoma et al. 2015). Plasmalogens are important for appropriate myelin formation and deficiency of plasmalogen synthesis through knockout of the gene encoding the peroxisomal membrane protein Gnpat leads to hypomyelination and premature death in mice (Malheiro et al. 2019).

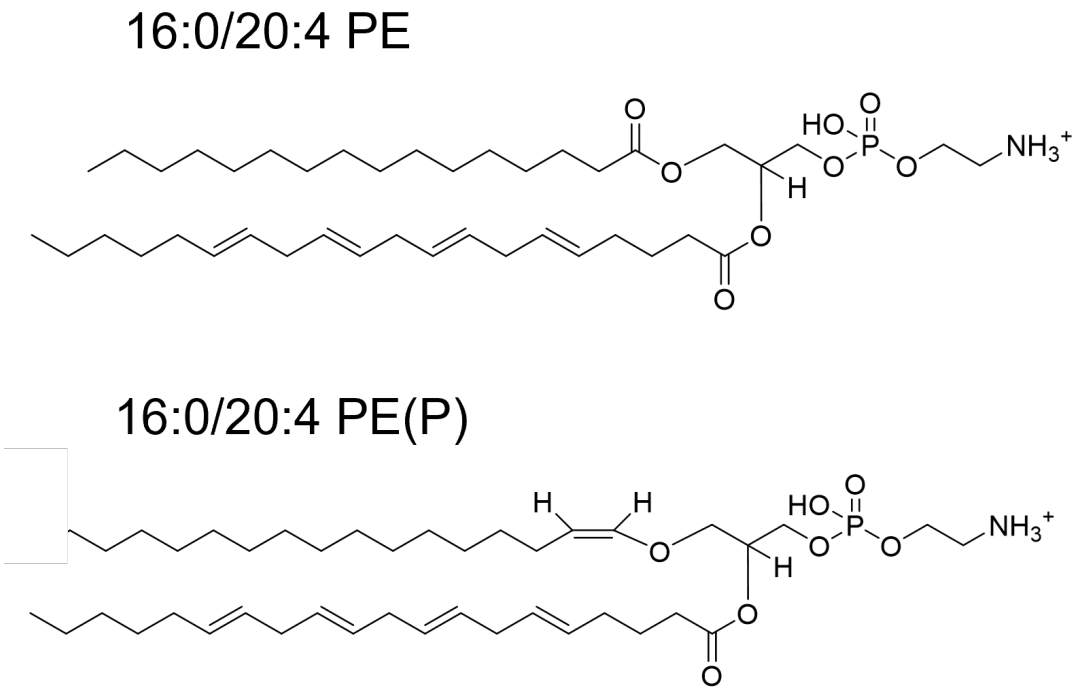

Figure 1.7: Structure of phosphatidylethanolamines

Phospholipids are usually attached via an ester linkage at the sn-1 position of the glycerol backbone (as in PE, top structure). In plasmalogens, the sn-1 glycerol linkage is through a vinyl ether bond (PE(P), below structure), and this leads to a distinct conformation of the molecule (Braverman et al. 2012). PE(P)s are highly enriched in myelin and confer tight membrane packing properties to the myelin sheath.

1.10 Aims

Despite the importance of brain lipid homeostasis to neurophysiological function, evidence of white matter abnormalities observed in inherited forms of FTD reported in MRI studies, and the proposed role for progranulin in lysosomal lipid catabolism, there is currently limited evidence from studies of post-mortem human brain supporting the potential role of lipid metabolic dysfunction and myelin defects in the precipitation of FTD. The aims of this thesis work are to understand how brain lipid metabolism and myelin content are affected in the heavily affected and relatively unaffected brain regions in carriers of the major familial mutations causing FTD with TDP-43 neuropathology. Comprehensive lipidomic and proteomic analysis was undertaken on post-mortem brain tissue of heavily affected frontal lobe grey and white matter and relatively unaffected parietal lobe grey and white matter from FTD-*GRN* (n = 6) and FTD-*C9orf72* (n = 11) cases, and age-matched neurologically normal controls (n = 11).

Aims:

(1) Determine how brain region-specific lipid metabolism and myelin content is affected in FTD cases with inherited *GRN* and *C9orf72* mutations.

(2) Determine how brain region-specific proteomic profiles differ in FTD cases with inherited *GRN* and *C9orf72* mutations.

(3) Identify whether levels of the myelin lipid galactosylceramide in plasma can be used as a biomarker of myelin defects in FTD.

Chapter 2: Disrupted myelin lipid metabolism differentiates frontotemporal dementia caused by *GRN* and *C9orf72* gene mutations

This chapter was published in *Acta Neuropathologica Communications* in 2023:

Marian, O.C., Teo, J.D., Lee, J.Y. Song, H., Kwok, J.B., Landin-Romero, R., Halliday, G & Don, A.S (2023) 'Disrupted myelin lipid metabolism differentiates frontotemporal dementia caused by GRN and C9orf72 gene mutations.' Acta Neuropathologica Communications 11, 52

I performed the majority of experiments (90%), analysed all data with assistance from JYL, and wrote the manuscript with ASD. JDT and HS contributed experimental work (10%), JBK obtained funding and performed genotyping, RLR and GH contributed to study design, case ascertainment, and editing of the manuscript, ASD conceived and planned the study, obtained funding and ethics approval, and wrote the manuscript.

In addition to the statements above, in cases where I am not the corresponding author of a published item, permission to include the published material has been granted by the corresponding author.

Oana Claudia Marian

30 June 2023

As supervisor for the candidature upon which this thesis is based, I can confirm that the authorship attribution statements above are correct.

Anthony S Don

30 June 2023

Acta Neuropathologica Communications

RESEARCH

Open Access

Disrupted myelin lipid metabolism differentiates frontotemporal dementia caused by *GRN* and *C9orf72* gene mutations

Oana C. Marian[1,2], Jonathan D. Teo[1,2], Jun Yup Lee[1,2], Huitong Song[1,2], John B. Kwok[2,3], Ramon Landin-Romero[3,4], Glenda Halliday[2,3] and Anthony S. Don[1,2*]

Abstract

Heterozygous mutations in the *GRN* gene and hexanucleotide repeat expansions in *C9orf72* are the two most common genetic causes of Frontotemporal Dementia (FTD) with TDP-43 protein inclusions. The triggers for neurodegeneration in FTD with *GRN* (FTD-*GRN*) or *C9orf72* (FTD-*C9orf72*) gene abnormalities are unknown, although evidence from mouse and cell culture models suggests that *GRN* mutations disrupt lysosomal lipid catabolism. To determine how brain lipid metabolism is affected in familial FTD with TDP-43 inclusions, and how this is related to myelin and lysosomal markers, we undertook comprehensive lipidomic analysis, enzyme activity assays, and western blotting on grey and white matter samples from the heavily-affected frontal lobe and less-affected parietal lobe of FTD-*GRN* cases, FTD-*C9orf72* cases, and age-matched neurologically-normal controls. Substantial loss of myelin-enriched sphingolipids (sulfatide, galactosylceramide, sphingomyelin) and myelin proteins was observed in frontal white matter of FTD-*GRN* cases. A less-pronounced, yet statistically significant, loss of sphingolipids was also observed in FTD-*C9orf72*. FTD-*GRN* was distinguished from FTD-*C9orf72* and control cases by increased acylcarnitines in frontal grey matter and marked accumulation of cholesterol esters in both frontal and parietal white matter, indicative of myelin break-down. Both FTD-*GRN* and FTD-*C9orf72* cases showed significantly increased lysosomal and phagocytic protein markers, however galactocerebrosidase activity, required for lysosomal catabolism of galactosylceramide and sulfatide, was selectively increased in FTD-*GRN*. We conclude that both *C9orf72* and *GRN* mutations are associated with disrupted lysosomal homeostasis and white matter lipid loss, but *GRN* mutations cause a more pronounced disruption to myelin lipid metabolism. Our findings support the hypothesis that hyperactive myelin lipid catabolism is a driver of gliosis and neurodegeneration in FTD-*GRN*. Since FTD-*GRN* is associated with white matter hyperintensities by MRI, our data provides important biochemical evidence supporting the use of MRI measures of white matter integrity in the diagnosis and management of FTD.

Keywords FTD, Progranulin, Lipidomics, Lysosome, Cholesterol, TDP-43

*Correspondence:
Anthony S. Don
anthony.don@sydney.edu.au
[1]Charles Perkins Centre, The University of Sydney, Camperdown, NSW 2006, Australia
[2]School of Medical Sciences, The University of Sydney, Camperdown, NSW 2006, Australia
[3]Brain and Mind Centre, The University of Sydney, Camperdown, NSW 2006, Australia
[4]School of Health Sciences, The University of Sydney, Camperdown, NSW 2006, Australia

Introduction

FTD is the second most common cause of younger-onset dementia, frequently manifesting before 65 years of age [1, 2]. It is characterised by atrophy of the frontal or temporal lobes and classified into three clinical syndromes: behavioural variant FTD (bvFTD), progressive non-fluent aphasia, and semantic dementia. BvFTD, typified by personality changes, socially inappropriate behaviour and cognitive deficits, is the most common [3]. Pathologically, FTD is associated with intraneuronal aggregates of hyperphosphorylated tau protein or hyperphosphorylated and proteolytically-cleaved 43 kDa TAR DNA-binding protein (TDP-43) in both neurons and glia [4].

A strong family history is reported in nearly half of all bvFTD cases [3]. The two most common genetic causes of familial FTD with TDP-43 inclusions are heterozygous mutations in the gene encoding progranulin (*GRN*), which accounts for 5–20% of inherited FTD [5, 6]; and hexanucleotide repeat (GGGGCC) expansions in a non-coding region of the *C9orf72* gene, accounting for approximately 20% of inherited FTD [7]. *C9orf72* repeat expansions are also the most common genetic cause of amyotrophic lateral sclerosis (ALS) [8].

Progranulin is a secreted glycoprotein that is highly expressed by activated microglia [6, 9], interacts with the neuronal receptor sortilin, and localises primarily to neuronal and microglial lysosomes [9, 10]. Heterozygous *GRN* mutations that cause FTD lead to nonsense-mediated decay of *GRN* mRNA and reduced progranulin protein levels [5, 6]. Loss of function mutations in both *GRN* alleles cause the severe lysosomal storage disorder neuronal ceroid lipofuscinosis (NCL), characterised by enlarged lysosomes and accumulation of the auto-fluorescent material lipofuscin [11, 12]. These features are also observed in brains of FTD-*GRN* cases and *Grn*-/- mice [13–16]. Mechanistic studies have demonstrated important functions for progranulin in regulating lysosomal acidification [17], the lysosomal import of proteins required for lipid catabolism [10], and activity of the lysosomal lipase glucocerebrosidase (GCase) [18, 19].

C9orf72 repeat expansions are associated with reduced *C9orf72* transcript levels, nuclear RNA foci that interfere with the function of RNA binding proteins, and inclusions comprising dipeptide repeat polymers derived from translation of the repeat expansions [8, 20, 21]. Whether one of these mechanisms predominates in causing neurodegeneration remains a subject of research, since both loss of normal *C9orf72* and gain of toxic function promote neurodegenerative phenotypes [22, 23]. Physiologically, C9orf72 is required for endosomal trafficking, autophagy and lysosomal biogenesis [23, 24]. Disrupted lysosomal function may therefore be common to both FTD-*GRN* and FTD-*C9orf72*.

Magnetic resonance imaging (MRI) studies show white matter hyperintensities, indicative of focal demyelination, in FTD-*GRN* but not FTD-*C9orf72* cases [25–27]. On the other hand, diffusion tensor imaging has shown reduced white matter integrity in both FTD-*GRN* and FTD-*C9orf72*, and in bvFTD more generally [28, 29]. Myelin is composed 70% (dry weight) of lipids [30]. The physiological turnover and maintenance of myelin is therefore predicted to require constitutive lipid catabolism in microglial and oligodendrocyte lysosomes. In this study we demonstrate that both FTD-*GRN* and FTD-*C9orf72* are characterised by significant lipid loss in frontal white matter. However, myelin lipid and protein loss was substantially greater in FTD-*GRN* cases and associated with a pronounced increase in cholesterol esters, suggesting that excess cholesterol and fatty acids resulting from myelin break-down are stored as cholesterol esters in white matter. Markers of phagocytic microglia, TREM2 and CD68, were increased in FTD-*C9orf72* and FTD-*GRN*, indicating that both gene defects promote a phagocytic microglial phenotype, however our evidence indicates that hyperactive myelin lipid catabolism differentiates FTD-*GRN* from FTD-*C9orf72* cases.

Materials and methods

Human brain tissue

Fresh frozen grey and white matter tissue samples from the superior frontal and superior parietal lobe of 11 FTD-*C9orf72* cases, 6 FTD-*GRN* cases, and 11 age-matched neurologically-normal controls were obtained from the Sydney Brain Bank and NSW Brain Tissue Resource Centre. Demographic and clinical information (sex, age at death, cause of death and post-mortem interval (PMI)) is provided in Table 1.

Approximately 100 mg of frozen brain tissue was homogenised for 1 min at 4 °C in 700 µL ice-cold HEPES buffer (50 mM, pH 7.4) containing 5 mM NaF, 2 mM Na_3VO_4, 10 mM KCl and cOmplete Mini EDTA-free Protease Inhibitor Cocktail (Roche #11836153001), using a bead beater with 425–600 mm acid washed glass beads (Sigma Aldrich #G8772). Samples were centrifuged at 4 °C for 1 min at 1000x*g* and the homogenate was transferred to a new tube, after which the beads were washed with a further 100 µL of ice-cold HEPES buffer, centrifuged, and the supernatant combined with the previous fraction. The homogenate was stored in 100 µL aliquots at -80 °C. Protein concentration of the homogenates was determined by bicinchoninic acid assay (Thermo Scientific #23225).

Lipid extraction

Lipids were extracted from 100 µL brain homogenate samples (~100 µg protein) using a two-phase methyl-tert-butyl ether (MTBE)/methanol/water

Table 1 Demographic information for cases used in this study. PMI: post-mortem interval. *Cases used for histological analysis. [#]Cases with co-occurring ALS.

Case ID	Gene Defect	Age	Sex	PMI (h)	Tissue pH	Cause of Death	TDP-43 Type
1	C9orf72	65	F	5	6.6	Bronchopneumonia	A
2	C9orf72	49	F	26	6.3	Aspiration pneumonia	B
3	C9orf72	66	M	9	6.2	Cardiorespiratory failure	B
4	C9orf72	81	F	14	6.6	Cardiorespiratory arrest	B
5[#]	C9orf72	68	F	9	6.3	Cardiorespiratory failure	A
6	C9orf72	75	F	46	6.3	Cardiorespiratory failure	A
7[#]	C9orf72	70	M	15	6.4	Cardiorespiratory failure	A
8*	C9orf72	61	M	39	6.3	Aspiration pneumonia	A
9*	C9orf72	69	F	24	5.6	Cardiorespiratory failure	B
10*	C9orf72	67	F	22	6.2	Cardiorespiratory failure	A
11*	C9orf72	83	M	13	5.9	Uraemia, bronchopneumonia	A
12	GRN (c.90_91insCTGS)	77	M	48	6.2	Aspiration pneumonia	A
13*	GRN (c.90_91insCTGS)	54	F	26	5.9	Aspiration pneumonia	A
14*	GRN (c.898 C>T)	54	F	21	5.8	Cardiorespiratory failure	A
15	GRN (c.898 C>T)	61	M	17	6.0	Cardiorespiratory failure	A
16	GRN (c.87dup)	64	M	13	5.6	Cardiorespiratory failure	A
17*	GRN (c.918 C>A)	68	F	29	6.1	Cardiorespiratory failure	A
18*	Control	69	M	16	6.6	Cardiac	-
19*	Control	60	M	25	6.7	Infection	-
20*	Control	71	F	16	6.2	Cancer	-
21	Control	66	M	23	6.7	Cardiac	-
22	Control	66	M	63	6.9	Cardiac	-
23	Control	69	F	39	6.7	Cardiac/ Respiratory	-
24	Control	73	M	9	6.5	Cancer	-
25	Control	51	F	41	7.0	Alcohol toxicity	-
26	Control	84	M	36	6.4	Severe pulmonary hypertension	-
27*	Control	80	F	29	6.3	Cardiorespiratory failure	-
28*	Control	84	F	16	5.7	Endocarditis	-

protocol [31]. Homogenate was combined with 850 µL MTBE and 250 µL methanol containing internal standards: 5 nmoles PC(19:0/19:0); 2 nmoles each of SM(d18:1/12:0), GluCer(d18:1/12:0), PS(17:0/17:0), PE(17:0/17:0), PG(17:0/17:0), CL(14:0/14:0/14:0/14:0), TG(17:0/17:0/17:0), and CholE(17:0); 1 nmole PA(17:0/17:0), PI(d7-18:1/15:0), and d7-Chol; 0.5 nmoles LacCer(d18:1/12:0), ST(d18:1/17:0), Cer(d18:1/17:0), DG(d7-18:1/15:0), MG(d7-18:1), LPC(17:0), LPE(17:1), LPS(17:1); and 0.2 nmoles Sph(d17:1), S1P(d17:1), LPA(17:0), and AcCa(d3-16:0). Samples were sonicated in a 4 °C water bath for 30 min. Phase separation was induced with the addition of 212 µL of mass spectrometry grade water, samples were vortexed and centrifuged at 2000x*g* for 5 min and the upper organic phase was collected in 5 mL glass tubes. The aqueous phase was extracted twice more with 500 µL MTBE and 150 µL methanol followed by sonication for 15 min and phase separation with 125 µL water. Organic phases from the three extractions were combined and dried under vacuum in a Savant SC210 SpeedVac (ThermoFisher Scientific). Lipids were reconstituted in 400 µL of HPLC grade methanol, then diluted 1:5 in 80% (v/v) methanol:20% water containing 1 mM ammonium formate and 0.2% formic acid.

Lipid quantification using liquid chromatography-tandem mass spectrometry (LC-MS/MS)

Lipidomic data was acquired with a ThermoFisher Q-Exactive HF-X mass spectrometer coupled to a Vanquish HPLC [31]. Lipids were resolved on a 2.1×100 mm Waters C18 HPLC column (1.7 µm pore size), using a 27 min binary gradient at a 0.28 mL/minute flow rate: 0 min, 80:20 A/B; 3 min, 80:20 A/B; 5.5 min, 55:45 A/B; 8 min, 36:65 A/B; 13 min, 15:85 A/B; 14 min, 0:100 A/B; 20 min, 0:100 A/B; 20.2 min, 70:30 A/B; 27 min, 70:30 A/B. Solvent A was 10 mM ammonium formate, 0.1% formic acid in acetonitrile:water (60:40); Solvent B was 10 mM ammonium formate, 0.1% formic acid in isopropanol:acetonitrile (90:10). Data was acquired in full scan/data-dependent MS^2 mode (resolution 60,000 FWHM, scan range 220–1600 *m/z*). Sample order was randomised, and data was collected in both positive and negative mode for each sample. The ten most abundant ions in each cycle were subjected to MS^2, with an isolation window of 1.4 *m/z*, collision energy 30 eV, resolution

17,500 FWHM, maximum integration time 110 ms and dynamic exclusion window 10 s. An exclusion list of background ions was based on a solvent blank. An inclusion list of the $[M+H]^+$ and $[M-H]^-$ ions for all internal standards was used. Mass accuracy was <5 ppm and %CV for peak elution time was <2% across the entire sample run.

LipidSearch software (version 4.2, Thermo Fisher) was used for lipid annotation, chromatogram alignment, and peak integration. Lipid annotation required both accurate precursor ion mass (5 ppm mass tolerance) and diagnostic product ions (8 ppm mass tolerance). Molar amounts for each lipid were calculated by taking the ratio to the class-specific internal standard, after which lipid levels were normalised to protein content.

Bis(monoacylglycero)phosphate (BMP) quantification

Resolution of BMP from its mass isomer PG was performed as described [19]. Lipid annotation, chromatogram alignment and peak integration were carried out with TraceFinder software (version 5.1, Thermo Fisher). Correct peak identification was confirmed with the use of commercial standards for BMP(18:1/18:1) and PG(18:1/18:1) (Avanti Polar Lipids #857135 and #840475, respectively). Molar amounts for BMP and PG were calculated relative to the PG(17:0/17:0) internal standard.

Western blots

Whole brain homogenates (10 µg protein for grey matter and 5 µg for white matter) were resolved on Bolt™ 4–12% Bis-Tris Plus gels (ThermoFisher Scientific #NW04125BOX) and transferred to polyvinylidene fluoride membranes. Membranes were blocked for 1 h at RT with 5% skim milk in Tris-buffered saline containing 0.1% Tween-20 (TBST), then incubated overnight at 4 °C with primary antibody in TBST with 3% bovine serum albumin (Sigma Aldrich #A7906). Membranes were then washed 3 times in TBST and incubated in horseradish peroxidase-conjugated secondary antibody diluted 1:5000 in TBST containing 5% skim milk for 2 h at RT. Membranes were imaged with ECL Ultra Western HRP Substrate (Millipore #WBULS0500) using a Bio-Rad ChemiDoc Touch. Bands were quantified by densitometry with Bio-Rad Image Lab software (v6.0.1). Membranes were then stripped with mild stripping buffer (1.5% w/v glycine, 0.1% w/v SDS, 0.1% v/v Tween20, pH 2.2), blocked with 5% skim milk in TBST for 1 h and re-probed with anti-β-actin (Abcam #ab8227, RRID #AB_2305186) or anti-GAPDH (Cell Signalling #2118, RRID #AB_561053) at 1:5000 dilution in TBST with 3% BSA overnight at 4 °C. A common sample was included on each gel as a loading control to normalise between membranes containing different samples.

The following primary antibodies were used at 1:1000 dilution unless specified: rabbit anti-MBP (Abcam, #ab40390, RRID #AB_1141521), rabbit anti-PLP (Abcam #ab28486, RRID #AB_776593) (diluted 1:2000), mouse anti-CNP (11-5B) (Abcam #ab6319, RRID #AB_2082593), mouse anti-NEFL (DA2) (Invitrogen #13–0400, RRID #AB_2532995), mouse anti-tubulin βIII (TUBB3) (BioLegend #801,202, RRID #AB_10063408) (diluted 1:5000), #rabbit anti-LAMP1 (D2D11) XP® (Cell Signalling #9091, RRID #AB_2687579), mouse anti-LAMP2 (Developmental Studies Hybridoma Bank #H4B4, RRID #AB_528129) (diluted 1:200), rabbit anti-Trem2 (Cell Signalling #91,068, RRID # AB_1961900), rabbit anti-CD68 (Abcam # ab213363, RRID #AB_2801637).

Enzyme activity assays

β-glucocerebrosidase (GCase) and β-galactocerebrosidase (GALC) activities were assayed with the fluorometric substrates 4-Methylumbelliferyl β-D-glucopyranoside (Sigma-Aldrich #M3633) and 4-Methylumbelliferyl β-D-galactopyranoside (Sigma-Aldrich #M1633), respectively. All reactions were carried out in triplicate in 96-well white Opti-Plates (PerkinElmer #6005290). For GCase activity, 1 µg homogenate protein was resuspended in 15 µL 0.1 M citric acid/0.2 M disodium phosphate (pH 5) and incubated with 30 µL of 10 mM substrate dissolved in 0.1 M citric acid/0.2 M disodium phosphate (pH 5), 0.5% sodium taurocholate, 0.25% Triton X-100 [32]. Plates were covered with sealing film, shaken, and incubated at 37 °C in the dark for 1 h. Reactions were stopped with 180 µL of ice-cold stop solution (0.2 M glycine/NaOH, pH 10.4). For GALC activity, 20 µg homogenate protein was resuspended in 25 µL citrate/phosphate buffer, pH 4.5, and incubated for 30 min with 25 µL of 1 mM substrate dissolved in 50 mM sodium citrate, pH 4.5, 125 mM NaCl, 0.5% Triton X-100. Reactions were stopped with 50 µL of ice-cold stop solution (0.5 M glycine/0.3 M NaOH, pH 10). Fluorescence was measured on a Tecan M200 Pro plate reader with excitation 360 nm and emission 446 nm. Relative activity was determined after subtraction of the substrate blank.

Immunohistochemistry

TDP-43 inclusions were detected with anti-phospho TDP-43 (pS409/410) (Cosmo Bio, CAC-TIP-PTD-M01, RRID # AB_1961900). The type and density of TDP-43 inclusions and dystrophic neurites was assessed by an experienced research neuropathologist.

Formalin-fixed and paraffin embedded Sect. (10 µm) from the superior frontal lobe of 4 FTD-*C9orf72* cases, 3 FTD-*GRN* cases and 5 age-matched controls, indicated by an asterisk in Table 1, were used for luxol fast blue (LFB) staining, and immunofluorescence staining for aspartoacylase (ASPA) and myelin basic protein (MBP).

These cases were those for which the tissue had not been subjected to extended fixation (>2 weeks). Sections were heated in an oven at 60 °C for 1 h, deparaffinised in 2×15 min changes of xylene, and rehydrated to deionised water following graded changes of ethanol from 100 to 50%. For LFB staining, sections were rehydrated to 95% ethanol, incubated in 0.1% LFB solution (#S3382, Sigma-Aldrich) at 60 °C for 17 h, then rinsed in 70% ethanol for 2.5 min, followed by distilled water until the water ran clear. Sections were then differentiated in 0.05% lithium carbonate solution for 30 s, then in 70% ethanol for 30 s, and rinsed in distilled water. Sections were then counterstained with 0.1% cresyl violet solution for 30 s and rinsed in distilled water, followed by 95% ethanol for 5 min. Sections were dehydrated in two changes of 100% ethanol, cleared in two changes of xylene, and coverslipped using DPX mounting medium. Myelination scores from 0 to 3 were assigned by two blinded observers, where 0 is complete absence of myelin and 3 is dense myelin [33].

For immunofluorescence, sections were incubated in sodium citrate antigen retrieval buffer (10 mM, pH 6.0, 0.05% Tween 20) at 85 °C for 10 min, blocked in PBS with 0.1% Triton X-100 (PBST), 5% normal goat serum and 0.1% bovine serum albumin (BSA) at RT for 2 h, and incubated overnight at 4 °C with primary antibodies rabbit anti-ASPA (Abcam #ab223269 EPR22072) and mouse anti-MBP (R&D #MAB42282), diluted 1:250 in blocking solution. Sections were incubated in secondary antibodies (AlexaFluor 488 Goat anti-mouse, Cell Signalling #4408, RRID: AB_10694704; and AlexaFluor 647 Goat anti-rabbit, Cell Signalling #4414, RRID: AB_10693544) diluted 1:250 in blocking solution for 2 h, and counterstained with 1 µg/mL diamidino-2-phenylindole dihydrochloride (DAPI). Autofluorescence was quenched with TrueBlack Plus autofluorescence eliminator (Biotium #23,014) per manufacturer's protocol. Sections were cover-slipped with ProLong Glass antifade mountant (Life Technologies #P36980) before imaging. Slides were imaged with a Zeiss Axioscan slide scanner. The density of ASPA-positive cells (co-localised ASPA and DAPI staining) in white matter was quantified using QuPath (version 0.3.2) [34].

Statistical analysis

Partial least squares-discriminant analysis (PLS-DA) of lipidomic data was carried out in MetaboAnalyst (version 5.0). Lipid levels were $\log_{10}$-transformed and filtered based on interquartile range prior to analysis. Missing values (not detected in that sample) were assigned a value of 1/5 of the minimum observed value for that lipid. Lipid class totals, and individual cholesterol ester or acylcarnitine species, were compared between the three sample groups using one-way ANOVA adjusted for age and PMI, followed by Tukey's post-hoc test. Values were natural log-transformed to improve normality and ANOVA p values were adjusted for false discovery rate using the Benjamini-Hochberg correction, with adjusted $p<0.05$ considered significant. These statistical tests were performed using the *car*, *olsrr*, *ggplot2*, *multcomp* and *dplyr* packages in R (version 4.0.3). The heatmap was generated in Tableau Desktop (version 2022.1.1).

Western blot, immunofluorescence, BMP levels, and enzyme activity data were analysed by one-way ANOVA with Tukey's post-hoc test, using GraphPad PRISM (version 9.3.1). Non-normally distributed data were natural log-transformed to achieve a normal distribution. LFB histological scores were subject to non-parametric Kruskall-Wallis test with Dunn's post-test. Spearman correlations were performed in GraphPad PRISM.

Results

Case demographics and TDP-43 pathology

This study used post-mortem brain tissue from FTD cases with *GRN* (n=6) and *C9orf72* (n=11) mutations, and neurologically normal controls (n=11) (Table 1). Mean age at death was 70.3±10.0 years for controls, 68.6±9.3 years for *C9orf72* cases and 63.0±8.8 years for *GRN* cases (ANOVA, F=1.17, $p=0.33$). Mean post-mortem interval (PMI) was 28.5±15.5 h for controls, 20.2±12.9 h for *C9orf72* cases and 25.7±12.4 h for *GRN* cases (F=0.99, $p=0.38$). All FTD-*GRN* and 7 out of 11 FTD-*C9orf72* cases exhibited type A TDP-43 inclusions [35], with the rest exhibiting type B. The severity of TDP-43 neuronal cytoplasmic inclusions in frontal grey matter (Fig. 1A-D) or glial cytoplasmic inclusions in frontal white matter (Fig. 1E) did not differ significantly between FTD-*GRN* and FTD-*C9orf72* cases (Fig. 1F-G), nor did the severity of TDP-43-positive dystrophic neurites (Fig. 1H-I), indicating that the FTD-*GRN* and FTD-*C9orf72* cases are well-matched neuropathologically.

Lipidomic profiles distinguishes FTD-*GRN* from control and FTD-*C9orf72* cases

Lipidomic analysis was performed on the superior frontal grey and white matter, which are heavily affected in bvFTD, and the less affected superior parietal grey and white matter [36, 37]. A total of 821 glycerophospholipid, phospholipid, lysophospholipid, sphingolipid, sterol and acylcarnitine species were quantified (Supplementary Data File 1). Applying partial least squares discriminant analysis (PLS-DA), FTD-*GRN* cases clustered distinctly from both control and FTD-*C9orf72* cases based on lipidomic data from frontal grey matter (Fig. 2A). This was driven by myelin-enriched sphingolipids, specifically sulfatides (ST), monohexosylceramides (Hex1Cer), and dihexosylceramides (Hex2Cer) (Fig. 2B). Hex1Cer comprises both glucosylceramide and galactosylceramide, structural isomers that are indistinguishable using

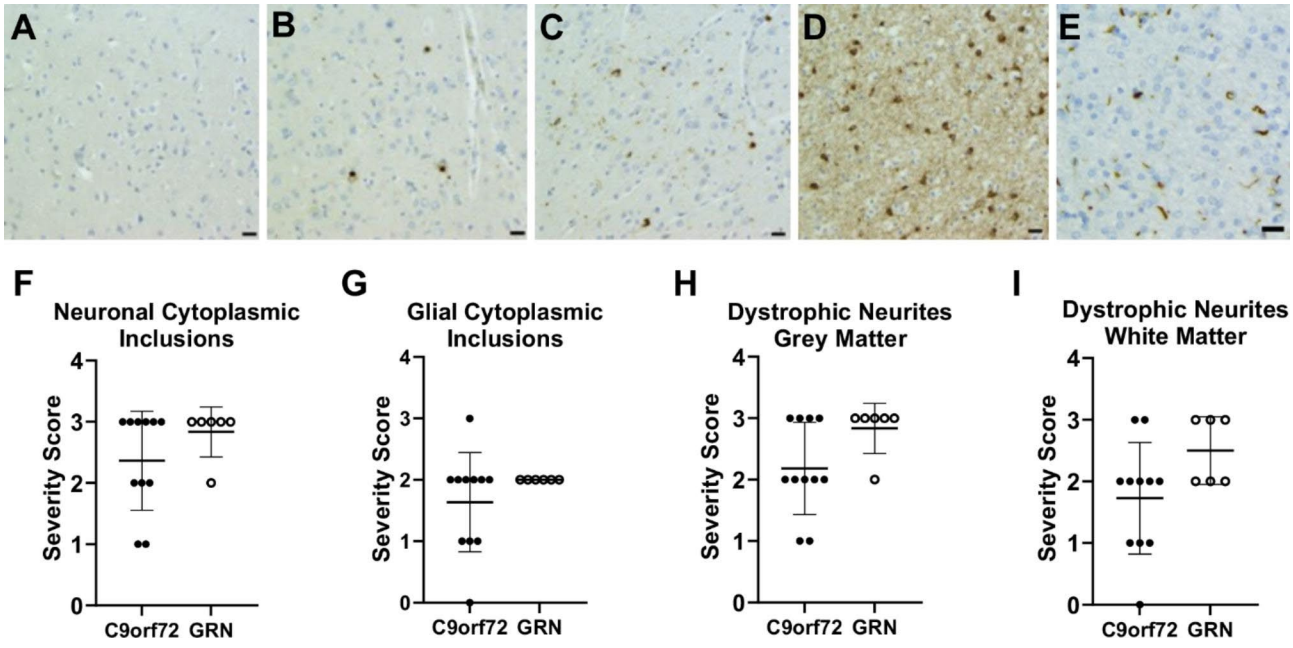

Fig. 1 TDP-43 cytoplasmic inclusions and dystrophic neurites are similar between FTD-*GRN* and FTD-*C9orf72* cases. (A-D) Representative images of phosphorylated TDP-43 staining in grey matter, showing (A) a control case with no TDP-43 inclusions, (B) mild (score = 1), (C) moderate (score = 2), and (D) severe (score = 3) TDP-43 pathology. (E) Abundant TDP-43-positive dystrophic neurites (score = 3) in frontal white matter of an FTD case. Scale bar, 20 μM. (F-I) Severity of (F) neuronal cytoplasmic TDP-43 inclusions in frontal grey matter, (G) glial cytoplasmic inclusions in frontal white matter, (H) TDP-43-positive dystrophic neurites in frontal grey matter, and (I) dystrophic neurites in frontal white matter of FTD-*C9orf72* (n = 11) and FTD-*GRN* (n = 6) cases

LC-MS/MS with reverse-phase chromatography. However, over 99% of Hex1Cer in the brain is galactosylceramide [38], which makes up 20–25% of myelin lipid [30]. ST (galactosylceramide sulfate) makes up a further 4–5% of myelin lipid [30]. PLS-DA did not effectively differentiate the three sample groups based on parietal grey matter lipids.

FTD-*GRN* cases also clustered distinctly from controls in frontal and parietal white matter (Fig. 2A), and this was driven by cholesterol esters (Fig. 2B). Many cholesterol ester species were increased by 1–2 orders of magnitude in FTD-*GRN* compared to FTD-*C9orf72* and control cases, particularly in parietal white matter (Fig. 2C-D).

Loss of myelin lipids in FTD-*GRN* and FTD-*C9orf72* cases

To complement the unsupervised statistical analysis of individual lipids and identify metabolic nodes affected by *GRN* or C*9orf72* mutations, lipid class totals were compared across the three sample groups using ANOVA adjusted for age and PMI (Fig. 3A and Supplementary Tables 1–4). The most significant changes were observed in frontal white matter, where 9 of the 27 lipid classes were significantly reduced in the FTD-*GRN* group. Statistically significant reductions in total ST, Hex2Cer, sphingomyelin (SM), Hex1Cer, lysophosphatidylcholine (LPC), and 1-O-alkyl-lysophosphatidylcholine [LPC(O)] were observed in both FTD-*GRN* and FTD-*C9orf72* relative to control cases, although the magnitude of lipid loss was greater in FTD-*GRN* cases (Fig. 3A-G). Phosphatidylinositol (PI), lysophosphatidylinositol (LPI), and ceramide were significantly reduced in frontal white matter of FTD-*GRN* but only trended lower in FTD-*C9orf72* cases (Fig. 3A). Similar trends with an overall loss of sphingolipids and phospholipids were observed in the parietal white matter, however these were not statistically significant. Instead, total cholesterol esters, lysophosphatidylethanolamine (LPE), and sphingosine, an intermediate metabolite in sphingolipid catabolism, were significantly increased in the FTD-*GRN* group (Fig. 3A).

In addition to the sphingolipids ST, Hex1Cer, and SM, myelin is highly enriched in unesterified cholesterol [30]. Although unesterified cholesterol levels trended downwards in white matter of FTD relative to the control cases, this was not statistically significant. However, the ratio of esterified to unesterified cholesterol was an order of magnitude higher in both frontal ($F = 24.6$, $p < 0.0001$) and parietal ($F = 49.2$, $p < 0.0001$) white matter of FTD-*GRN* cases (Fig. 2E-F).

A marked increase in acylcarnitines was observed in frontal grey matter of FTD-*GRN* cases (Fig. 3A and H). Examination of individual acylcarnitine species showed a preferential effect on acylcarnitines with 16–20 carbon acyl chains (Fig. 3I). Acylcarnitines also trended higher in FTD-*GRN* cases in the parietal grey matter, however no lipid classes reached statistical significance in this region.

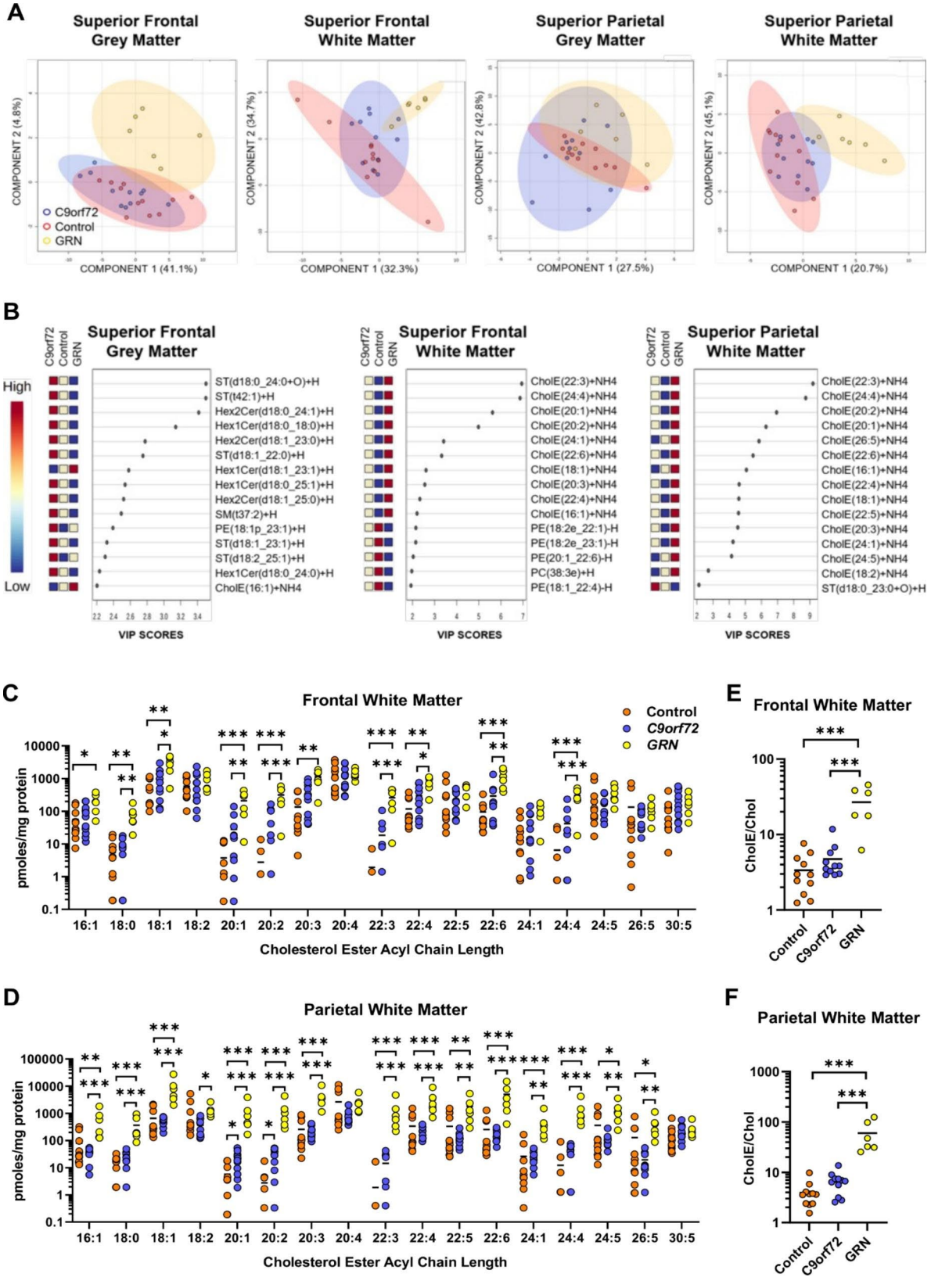

Fig. 2 Lipid profiles distinguish FTD-*GRN* from FTD-*C9orf72* and control cases. (A) PLS-DA scores plots for control (n = 11, orange), FTD-*C9orf72* (n = 11, blue), and FTD-*GRN* (n = 6, yellow) cases for each brain region, based on the untargeted lipidomic data. Component % refers to the percentage of variance explained by each principal component. (B) Variable Importance in the Projection (VIP) scores for the 15 features that contribute most to separation of the groups in PLS-DA. ST: sulfatide, Hex1Cer: monohexosylceramide, Hex2Cer: dihexosylceramide, SM: sphingomyelin, CholE: cholesterol ester, PC: phosphatidylcholine, PE: phosphatidylethanolamine. (C,D) Levels of CholE species in (C) frontal and (D) parietal white matter. Horizontal bars show mean. Missing values indicate that the specific CholE was below the limit of detection in that sample. Sample groups were compared by one-way ANOVA adjusted for PMI and age, and *p* values were corrected for false discovery rate. Results of Tukey's post-test are shown: *$p < 0.05$; **$p < 0.01$; ***$p < 0.001$. (E,F) Total cholesterol esters (CholE)/cholesterol (Chol) in (E) frontal and (F) parietal white matter

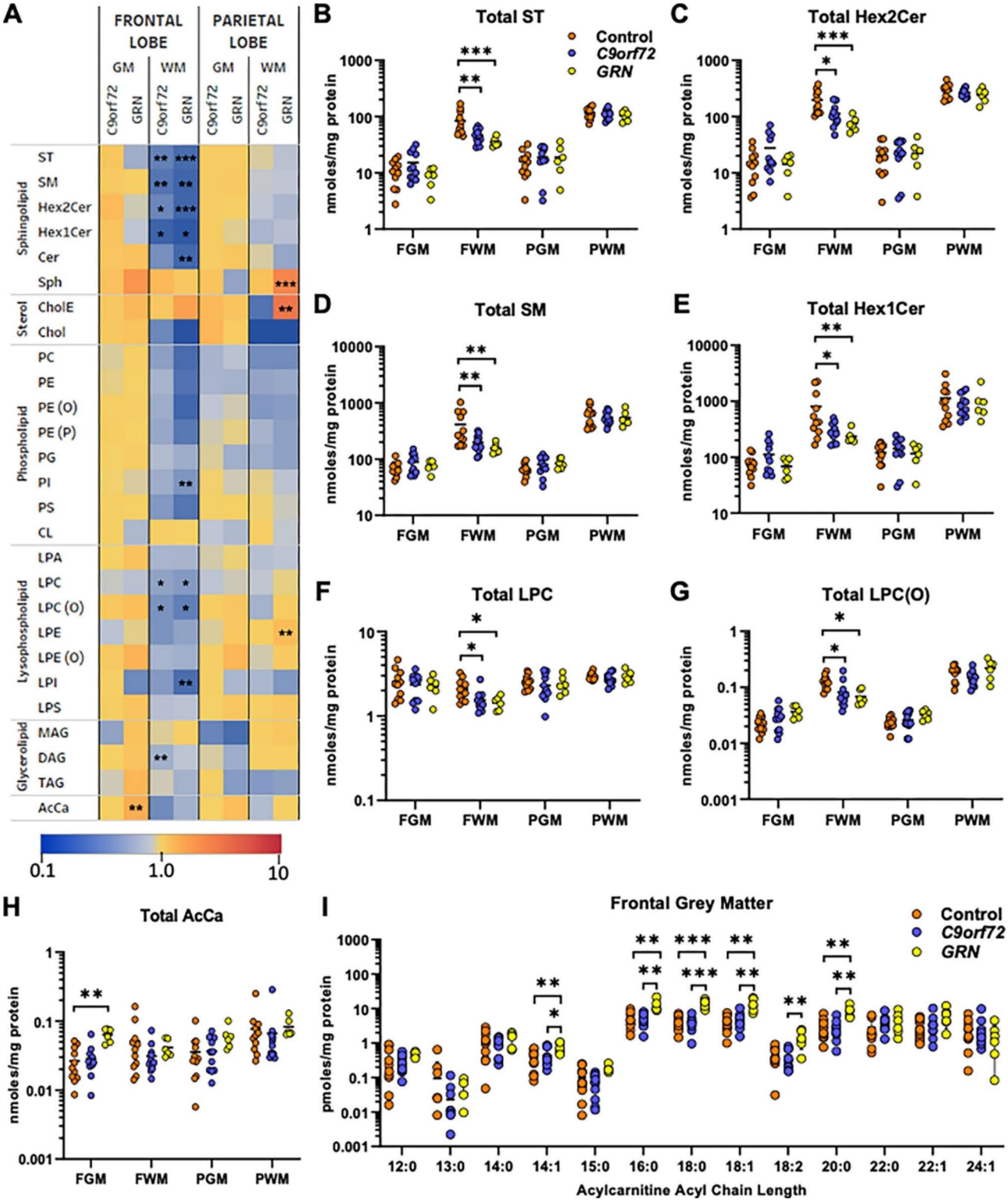

Fig. 3 Loss of myelin lipids is common to FTD-*GRN* and FTD-*C9orf72*. (A) Mean lipid class totals in FTD-*C9orf72* (n = 11) and FTD-*GRN* (n = 6) cases, expressed as a fold-change relative to the mean of the control group (n = 11) within each brain region. GM: grey matter, WM: white matter. Sample groups were compared by one-way ANOVA adjusted for PMI and age, with *p* values adjusted for false discovery rate. Asterisks indicate a significant difference compared to the control group in Tukey's post-test: $^{*}p < 0.05$; $^{**}p < 0.01$; $^{***}p < 0.001$. (B-H) Total lipid levels in each brain region. (I) Individual acylcarnitine (AcCa) species in frontal grey matter. Horizontal bar shows mean. FGM: Frontal Grey Matter; FWM: Frontal White Matter; PGM: Parietal Grey Matter; PWM: Parietal White Matter; ST: sulfatide; SM: sphingomyelin; Hex2Cer: dihexosylceramide; Hex1Cer: monohexosylceramide; Cer: ceramide; Sph: sphingosine; CholE: cholesterol ester; Chol: cholesterol; PC: phosphatidylcholine; PE: phosphatidylethanolamine; PE(O): alkyl-PE; PE(P): alkenyl-PE (PE plasmalogen); PG: phosphatidylglycerol; PI: phosphatidylinositol; PS: phosphatidylserine; CL: cardiolipin; LPA: lysophosphatidic acid; LPC: lysophosphatidylcholine; LPC(O): alkyl-LPC; LPE: lysophosphatidylethanolamine; LPE(O): alkyl-lysophosphatidylethanolamine; LPI: lysophosphatidylinositol; LPS: lysophosphatidylserine; MAG: monoacylglycerol; DAG: diacylglyerol; TAG: triacylglycerol; AcCa: acylcarnitine

FTD-*GRN* is characterised by severe myelin attrition

In agreement with our lipidomic data, western blotting showed significant loss of the myelin markers proteolipid protein (PLP) (ANOVA, F = 12.03, $p = 0.0003$), 2',3'-Cyclic nucleotide 3'-phosphodiesterase (CNP) (F = 11.64, $p = 0.0003$) and myelin basic protein (MBP) (F = 4.84, $p = 0.018$), in frontal white matter of FTD-*GRN* cases (Fig. 4A-B). Although PLP levels were reduced relative to controls in FTD-*C9orf72* cases, both PLP and CNP were significantly lower in FTD-*GRN* compared to FTD-*C9orf72* cases, indicating more severe myelin loss in FTD-*GRN* cases. In parietal white matter, PLP (F = 14.64,

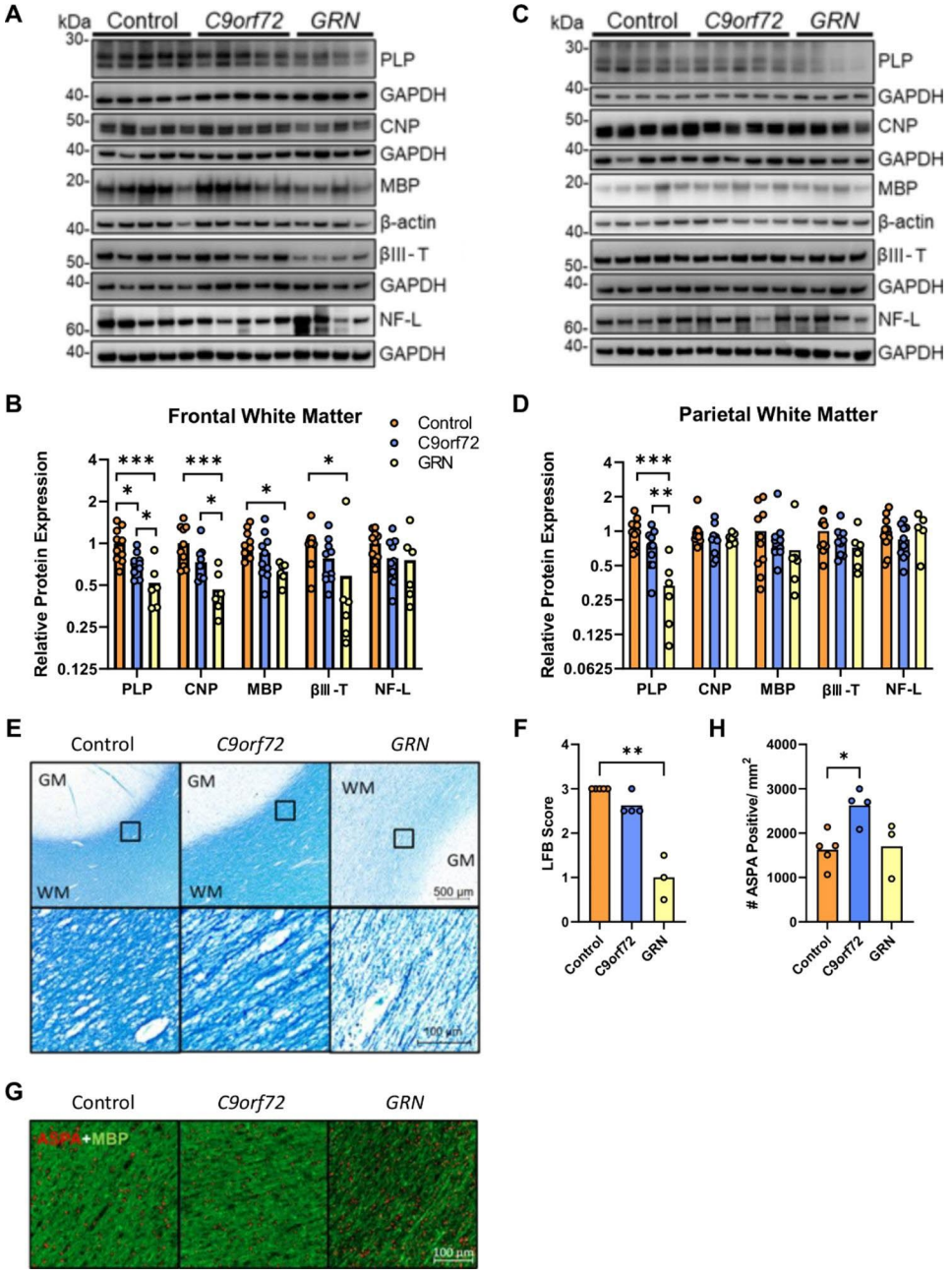

Fig. 4 Pronounced myelin loss in FTD-*GRN*. (A, C) Representative western blots and (B, D) densitometric quantification of PLP, CNP, MBP, βIII-tubulin (βIII-T) and neurofilament light chain (NF-L) in (A, B) superior frontal white matter, and (C, D) superior parietal white matter from control (n = 11), FTD-*C9orf72* (n = 11), and FTD-*GRN* (n = 6) cases. Protein levels were normalised to β-actin or GAPDH as a loading control, and are expressed relative to the mean of the control group. (E) Representative images and (F) myelination scores from LFB staining of superior frontal gyrus white matter from control (n = 5), FTD-*C9orf72* (n = 4), and FTD-*GRN* (n = 3) cases from which tissue fixed for < 2 weeks was available. (G) Representative ASPA (red) and MBP (green) staining in superior frontal gyrus white matter, and (H) ASPA-positive cell density. Groups were compared by one-way ANOVA with Tukey's post-test (B,D,H) or Kruskall-Wallis test with Dunn's post-test (F): *$p < 0.05$; **$p < 0.01$; ***$p < 0.001$

$p<0.0001$) was significantly reduced in FTD-*GRN* compared to both control and FTD-*C9orf72* cases, whereas CNP (F=0.88, $p=0.43$) and MBP (F=1.02, $p=0.38$) were unchanged across the three sample groups (Fig. 4C-D). The neuronal marker βIII-tubulin was significantly decreased in frontal (Fig. 4A-B) but not parietal (Fig. 4C-D) white matter of FTD-*GRN* cases, and was not significantly affected in FTD-*C9orf72* cases (Kruskal-Wallis test, frontal white matter: H=7.90, $p=0.019$; parietal white matter: ANOVA F=1.76, $p=0.19$). Axonal marker neurofilament-L trended down in frontal white matter of FTD-*GRN* and FTD-*C9orf72* cases, however this was not statistically significant (ANOVA F=2.32, $p=0.12$). No difference was observed for neurofilament-L levels in parietal white matter (ANOVA F=0.73, $p=0.49$).

Luxol fast blue staining confirmed the pronounced myelin loss in frontal white matter of FTD-*GRN* cases (Kruskal-Wallis H=9.47, $p=0.0002$) (Fig. 4E-F). Loss of myelin staining in FTD-*GRN* cases was uniform and without evidence of focal lesions or plaques. Despite the pronounced myelin loss, mature oligodendrocyte (ASPA-positive) cell density [33, 39] was not reduced in frontal white matter of FTD-*GRN* cases, and was 60% higher in FTD-*C9orf72* compared to control cases (F=6.15, $p=0.021$) (Fig. 4G-H).

Cholesterol esters are inversely correlated with myelin proteins and lipids

Myelin loss could explain the pronounced cholesterol ester accumulation in FTD-*GRN* cases, as cholesterol released from myelin is metabolised by phagocytic cells [40, 41]. Total cholesterol esters were inversely correlated with PLP, but not MBP or CNP, in frontal and parietal white matter (Table 2). Of all the lipids measured, ST and Hex1Cer are most unique to myelin in the CNS [42]. Cholesterol esters were inversely correlated with total Hex1Cer but not ST in frontal white matter, and both Hex1Cer and ST in parietal white matter. Since not all cholesterol esters were increased in FTD-*GRN* cases, we performed the same correlation analysis with CholE(22:6), an abundant cholesterol ester that was greatly increased in FTD-*GRN* (Fig. 1C-D). CholE(22:6) was inversely correlated with all five myelin markers (PLP, MBP, CNP, ST, Hex1Cer) in frontal white matter, and PLP, ST, and Hex1Cer in parietal white matter (Table 2). These inverse correlations support the hypothesis that cholesterol esters are indicative of myelin degradation.

Lysosomal and phagocytic markers are increased in both FTD-*GRN* and FTD-*C9orf72*

GRN mutations are proposed to disrupt lysosomal homeostasis, and hypomyelination is common to many lysosomal storage diseases, including neuronal ceroid lipofuscinosis (NCL) caused by homozygous *GRN* mutations [11, 12]. Reduced GCase activity has been reported in G*rn-/-* mice [19, 43], IPSC-derived neurons [18] and brain tissue from FTD-*GRN* cases [44, 45]. We observed no significant difference in GCase activity between FTD cases and controls, in frontal grey or white matter, or parietal white matter (Fig. 5A-C). However, galactocerebrosidase (GALC) activity, which is required for lysosomal degradation of Hex1Cer and ST, was 64% higher in frontal white matter of FTD-*GRN* ($p=0.004$), and 33% higher in FTD-*C9orf72* cases ($p=0.21$, not significant), relative to the controls (ANOVA F=6.94, $p=0.004$) (Fig. 5B).

Recent studies have also demonstrated loss of the endolysosomal lipid Bis(monoacylglycero)phosphate (BMP), particularly BMP(18:1/18:1) and BMP(22:6/22:6), in mouse models of *Grn* deficiency [19, 45]. We were able to confidently resolve the abundant BMP(18:1/18:1) species from its mass isomer PG(18:1/18:1), and show here that levels of this BMP were not significantly different in FTD cases compared to controls (Fig. 5D-G, all $p>0.05$ by one-way ANOVA), in agreement with another recent publication [45].

Further evidence for disrupted lysosomal homeostasis in FTD-*GRN* cases has come from reports showing increased levels of lysosomal proteins such as LAMP-1 and LAMP-2 [13, 44]. Western blotting showed increased LAMP-2 levels in frontal grey (F=12.2, $p=0.0003$) (Fig. 6A-B) and white matter (F=9.7, $p=0.0009$) (Fig. 6C-D) of both FTD-*GRN* and FTD-*C9orf72* cases, whereas levels were unchanged in parietal white matter

Table 2 Correlations between cholesterol esters and myelin markers in white matter. Spearman's correlation coefficient (r) and *p* value are shown for associations between myelin markers and total cholesterol ester (CholE) or CholE(22:6) in frontal and parietal white matter. Significant correlations are in bold font

	Frontal white matter				**Parietal white matter**			
	Total CholE		CholE(22:6)		Total CholE		CholE(22:6)	
	r	*p*	r	*p*	r	*p*	r	*p*
PLP	**-0.70**	**8.13×10^{-5}**	**-0.79**	**1.53×10^{-4}**	**-0.59**	**1.57×10^{-3}**	**-0.66**	**2.74×10^{-4}**
MBP	-0.20	0.32	**-0.48**	**0.014**	0.12	0.55	0.12	0.55
CNP	-0.38	0.052	**-0.43**	**0.030**	-0.10	0.64	-0.25	0.23
Total ST	-0.39	0.0501	**-0.52**	**6.07×10^{-3}**	**-0.50**	**6.85×10^{-3}**	**-0.52**	**4.27×10^{-3}**
Total Hex1Cer	**-0.52**	**7.07×10^{-3}**	**-0.46**	**0.020**	**-0.56**	**1.76×10^{-3}**	**-0.51**	**5.73×10^{-3}**

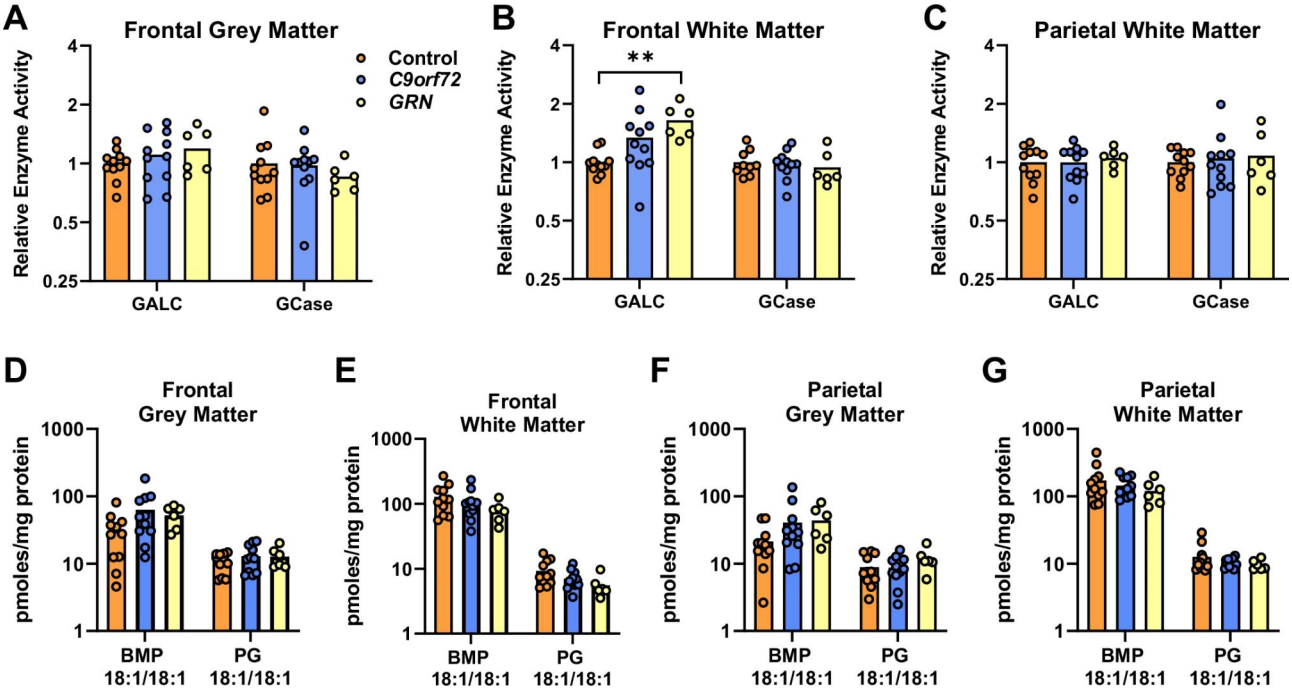

Fig. 5 Increased GALC activity in frontal white matter of FTD-*GRN* cases. (A-C) GALC and GCase enzyme activity in frontal white matter (A), parietal white matter (B) and frontal grey matter (C) of control (n = 11), FTD-*C9orf72* (n = 11), and FTD-*GRN* (n = 6) cases. Data is normalised to the mean of the control group. (D-G) Targeted lipidomic analysis of 18:1/18:1 BMP and 18:1/18:1 PG in frontal grey matter (D), frontal white matter (E), parietal grey matter (F), parietal white matter (G). Groups were compared by one-way ANOVA with Tukey's post-test: $^{**}p < 0.01$

(Fig. 6E-F). LAMP-1 was increased in frontal grey matter of FTD-*GRN* cases (F = 7.0, $p = 0.0042$), and parietal white matter of both FTD-*GRN* and FTD-*C9orf72* cases (F = 11.3, $p = 0.0004$), but was reduced in the frontal white matter of FTD-*C9orf72* cases compared to controls (F = 3.9, $p = 0.035$). Levels of the phagocytic microglial marker CD68 were significantly increased in frontal (F = 6.45, $p = 0.0049$) and parietal white matter of FTD-*C9orf72* (F = 3.9, $p = 0.034$), but not FTD-*GRN* cases. However, the microglial lipid receptor TREM2 [40, 46] was increased in frontal grey matter (F = 12.5, $p = 0.0002$) and parietal white matter (F = 33.6, $p < 0.0001$) of both FTD-*GRN* and FTD-*C9orf72* cases, and frontal white matter of FTD-*GRN* cases (F = 4.7, $p = 0.019$). These results indicate that lysosomal and microglial homeostasis is disrupted in both FTD-*C9orf72* and FTD-*GRN* cases, whereas lipid and myelin protein changes are more pronounced in FTD-*GRN* cases.

Discussion

This study presents the first comprehensive biochemical evidence that FTD-*GRN* is characterised by pronounced myelin loss. Significant loss of myelin-enriched sphingolipids was observed in white matter of both FTD-*GRN* and FTD-*C9orf72* cases, however FTD-*GRN* cases displayed a distinct lipidomic profile characterised by greater white matter lipid loss, increased levels of cholesterol esters in white matter, and increased acylcarnitines in grey matter. Levels of lysosomal markers and the microglial lipid receptor TREM2 were increased in both FTD-*C9orf72* and FTD-*GRN* cases, whereas galactocerebrosidase activity, required for catabolism of the myelin lipids galactosylceramide and ST, was only significantly increased in FTD-*GRN* cases. These changes point to a specific effect of *GRN* mutations in promoting myelin lipid catabolism and myelin degeneration, supported by the marked loss of myelin proteins and luxol fast blue staining in FTD-*GRN* relative to FTD-*C9orf72* and control cases. TDP-43 pathology did not differ significantly between the FTD-*GRN* and FTD-*C9orf72* cases, suggesting that heterozygous *GRN* mutations and *C9orf72* repeat expansions may promote TDP-43 deposition and bvFTD through distinct biochemical mechanisms.

Our study establishes that substantial white matter lipid loss is common to both FTD-*C9orf72* and FTD-*GRN*. Relative to age-matched controls, mean levels of the myelin-enriched sphingolipids ST, Hex1Cer, Hex2Cer, and SM were 43–64% lower in frontal white matter of FTD-*C9orf72* and 58–71% lower in FTD-*GRN* cases. Loss of phospholipids (PI) and lysophospholipids (LPC, LPI) in white matter of FTD-*GRN* cases probably also reflects myelin loss [42]. A previous study showed marked demyelination and gliosis in regions corresponding to white matter hyperintensities in a single FTD-*GRN* case [47]. Our study expands substantially on this, presenting several lines of biochemical evidence (myelin

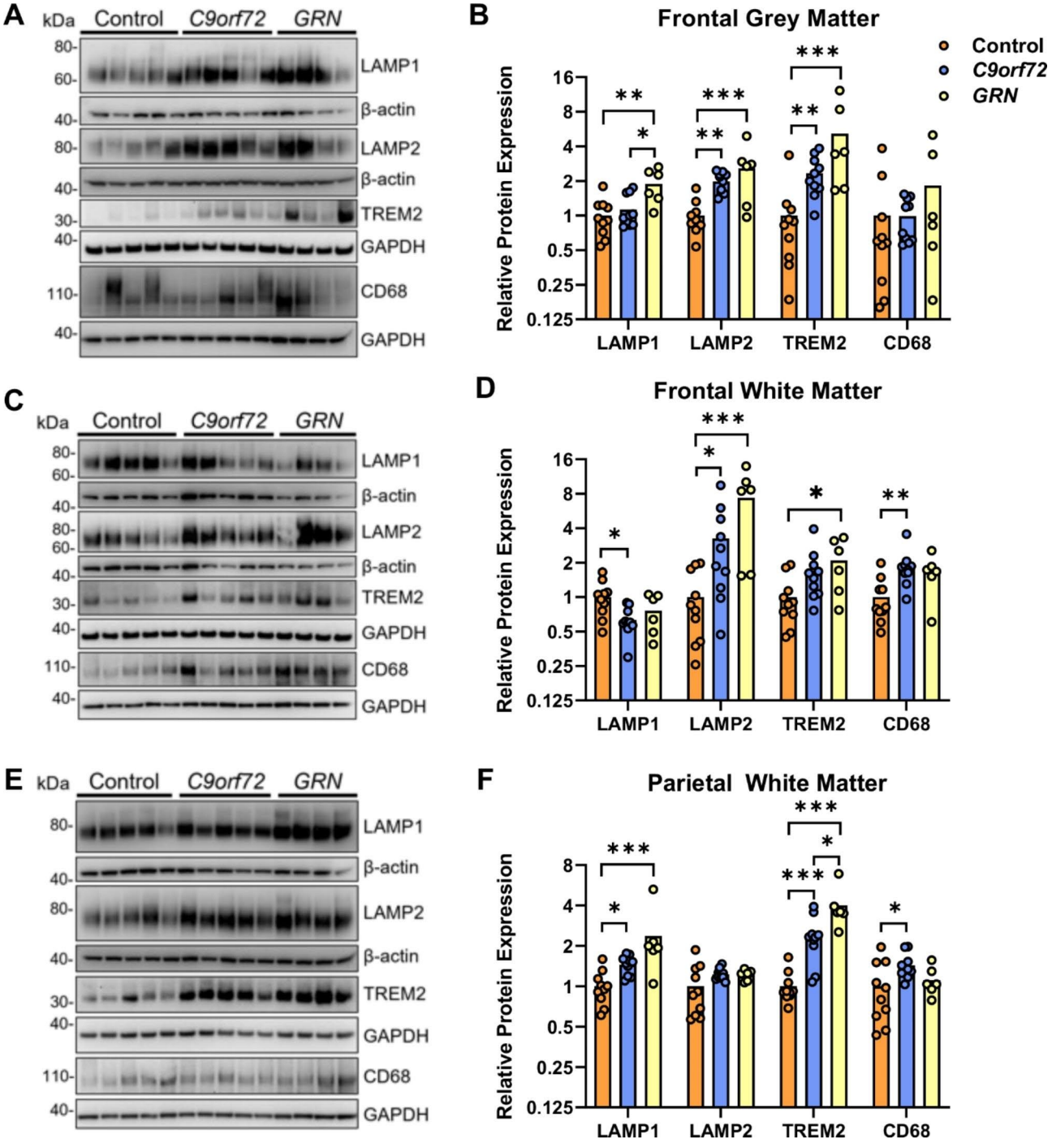

Fig. 6 Lysosomal and phagocytic markers are increased in both FTD-*GRN* and FTD-*C9orf72*. (A, C, E) Representative western blots and (B, D, F) densitometric quantification for LAMP1, LAMP2, TREM2 and CD68 in (A, B) frontal grey matter, (C, D) frontal white matter and (E, F) parietal white matter of control (n = 11), FTD-*C9orf72* (n = 11), and FTD-*GRN* (n = 6) cases. Protein levels were normalised to β-actin or GAPDH as a loading control, and expressed relative to the mean of the control group. Asterisks indicate significant difference in Tukey's post-test after one-way ANOVA: *$p < 0.05$; **$p < 0.01$; ***$p < 0.001$

lipid loss, myelin protein loss, and histological staining) from multiple FTD-*GRN* cases to demonstrate that pronounced myelin loss is characteristic of FTD-*GRN*. The observation of severe myelin loss in FTD-*GRN* but not FTD-*C9orf72* cases is in agreement with reported observations of white matter hyperintensities in FTD-*GRN* but not FTD-*C9orf72* cases [25–27]. However, our demonstration of significant lipid loss and a reduction in the major myelin protein PLP in frontal white matter of FTD-*C9orf72* cases demonstrates some myelin loss, in

agreement with a recent study reporting decreased MBP immunoreactivity in frontal cortex of FTD-*C9orf72* cases [48]. Mature oligodendrocyte density did not decrease in FTD-*GRN* cases, implying that demyelination does not stem from oligodendrocyte loss. However, given the significant frontal lobe atrophy in bvFTD [1], equivalent oligodendrocyte density likely indicates an overall loss of oligodendrocytes relative to the age-matched controls. This could explain the increased mature oligodendrocyte density in *FTD-C9orf72* cases.

FTD-*GRN* were differentiated from FTD-*C9orf72* cases by pronounced accumulation of cholesterol esters in white matter, relative to both protein content and unesterified cholesterol. Boland et al. very recently reported a modest increase in sterol esters in middle frontal gyrus of FTD cases with *GRN* mutations but not sporadic cases with TPD-43 inclusions [45], however it was unclear if grey or white matter was used and control cases were limiting. We observed significantly-increased cholesterol esters only in white matter. Cholesterol esters are formed during myelin break-down and accumulate in demyelinating conditions, as microglia and infiltrating macrophages phagocytose cholesterol released from compact myelin [40, 41, 49, 50]. Since cholesterol cannot be broken down by CNS cells, this free cholesterol is stored in esterified form and eventually cleared by excretion [51]. In the CNS, myelin phagocytosis and degradation is carried out by microglia and macrophages [40, 41, 52], which are the cell types that express *GRN* most abundantly. Although cholesterol ester accumulation in white matter of FTD-*GRN* cases is probably associated with excessive myelin break-down, it is also possible that this phenotype results from a defect in cholesterol break-down and clearance caused by *GRN* haploinsufficiency. In this regard, a recent study reported that *GRN* deficiency impairs clearance of myelin debris by cultured microglia [53]. Cholesterol overload in microglia triggers lysosome rupture and NLRP3 inflammasome activation [41], which could fuel neuroinflammation in FTD-*GRN* cases. Cholesterol ester formation also appears to be an important driver of amyloid β and neurofibrillary tangle pathology in Alzheimer's disease models [54, 55].

Diffusion tensor imaging studies have shown loss of white matter integrity in *C9orf72*, *GRN* and *MAPT* mutation carriers up to 30 years prior to estimated symptom onset [28, 29], suggesting that myelin deterioration begins early in FTD pathogenesis. Using post-mortem tissue samples, it is difficult to determine if white matter changes precede axon degeneration, or vice-versa. Loss of myelin markers in frontal white matter of FTD-*GRN* cases was accompanied by a significant reduction in βIII-tubulin but not neurofilament-L by western blotting. In contrast, we observed significant myelin lipid loss in FTD-*C9orf72* cases without evidence for loss of axonal markers by western blotting, although noting that this could be attributed to the more quantitative nature of our lipidomic analysis in comparison to western blotting and densitometry. In the less affected parietal white matter, the pronounced increase in cholesterol esters without significant loss of myelin lipids or axonal markers suggests that cholesterol ester storage is an early phenotype resulting from *GRN* haploinsufficiency.

Another differentiating feature of FTD-*GRN* was increased levels of long chain (C16-C20) acylcarnitines in frontal grey matter. Acylcarnitines are formed to import fatty acids into mitochondria for β-oxidation, and their accumulation is commonly associated with impaired β-oxidation of fatty acids [56]. Defective fatty acid β-oxidation can produce a brain energy deficit, which could partly explain the hypometabolic phenotype of FTD [57]. Acylcarnitine accumulation attributed to impaired β-oxidation of very long chain fatty acids in peroxisomes is a defining feature of X-linked adrenoleukodystrophy [58], also characterised by cholesterol ester accumulation [50]. Further research is required to determine if impaired fatty acid oxidation is a feature of FTD-*GRN*. Alternatively, the increased acylcarnitines could be indicative of a metabolic shift favouring lipid oxidation for energy production at the expense of lipid synthesis, thus causing myelin degeneration [59].

Levels of the microglial lipid receptor TREM2 were significantly higher in grey and white matter of both FTD-*GRN* and FTD-*C9orf72* cases, indicating the presence of phagocytic microglia. Lipid sensing by TREM2 promotes microglial activation and myelin phagocytosis [40, 52]. Our data therefore provides important evidence from human FTD cases confirming the observation that microglia from *C9orf72* and *Grn* knockout mice exhibit a phagocytic microglial phenotype [60, 61]. In addition to phagocytosing myelin, activated microglia promote neurodegeneration through increased secretion of inflammatory cytokines and complement proteins, and synaptic pruning [61, 62]. In fact, complement proteins secreted by *GRN*-/- microglia are sufficient to induce TDP-43 granules and cell death in excitatory neurons [62]. Our data also establishes that lysosomal protein markers LAMP-1, LAMP-2, and CD68 are deregulated in FTD-*C9orf72* cases, and demonstrates that this phenotype is shared with FTD-*GRN*. C9orf72 colocalises with Rab family proteins and regulates endocytosis, lysosome biogenesis and phagosome maturation [23, 63]. Prior work had shown increased LAMP-1 and CD68 immunoreactivity in ALS cases with *C9orf72* repeat expansions [63, 64], however *C9orf72-/-* motor neurons and those from ALS-*C9orf72* cases have fewer lysosomes, despite higher LAMP-2 content in lysosomal membranes [23].

Current evidence suggests that progranulin is required for full activity of lysosomal lipid hydrolases, particularly GCase [19, 43, 44]. Higher levels of the GCase substrate glucosylsphingosine have been reported in plasma of FTD-*GRN* cases [19], whereas another study showed unchanged levels in the inferior frontal gyrus [44]. Decreased GCase activity has been attributed to a role for progranulin in regulating the delivery of prosaposin to lysosomes and its proteolytic cleavage into saposins [10, 18], which serve as cofactors for lysosomal sphingolipid hydrolases such as GCase. Others have proposed a direct interaction between progranulin and GCase [43], or that progranulin regulates lysosomal enzyme functions through a direct interaction with BMP [19, 45]. Further evidence for lysosomal dysfunction comes from the recent demonstration of gangliosidosis in frontal cortex of FTD-*GRN* cases [45]. We did not find reduced BMP content in FTD-*GRN* cases compared to controls, indicating that not all molecular phenotypes of *Grn-/-* mice accurately reflect changes in FTD cases with heterozygous *GRN* mutations. GCase activity trended lower (14% reduction) in frontal grey matter of FTD-*GRN* cases, in line with modest reductions reported in two prior studies [44, 45], however this was not statistically significant. We note that GCase activity reductions are modest even in *Grn-/-* mice, with one study reporting a decrease of ~10% [44], and were not seen in mice bearing the R493X *Grn* mutation found in FTD [45].

In contrast to the absence of any change in GCase activity, the clear and significant increase in GALC activity in frontal white matter of FTD-*GRN* cases aligns with our observation of significantly reduced sulfatide and Hex1Cer levels in the same samples. GALC activity in frontal white matter of FTD-*C9orf72* cases was lower than FTD-*GRN* but higher than the control cases (not significant), in agreement with the lipidomic results. Increased GALC (b-galactosidase) activity was also seen in frontal cortex of *Grn-/-* mice [44], and *GALC* RNA levels are higher in motor cortex of ALS cases compared to age-matched controls [65]. Overall, decreased sphingolipids in FTD-*GRN* cases, together with increased levels of the sphingolipid catabolic intermediate sphingosine in parietal white matter, support the concept that *GRN* mutations disrupt brain sphingolipid metabolism. Future studies with cell culture models will be necessary to resolve whether *GRN* haploinsufficiency causes a block in lysosomal catabolism that leads to accumulation of cholesterol esters, sphingosine, and acylcarnitines; or whether these features are biomarkers of accelerated myelin break-down, as indicated by the increased GALC activity in frontal white matter.

Our lipidomic results with FTD cases are in broad agreement with a recent paper reporting decreased SM, ceramide, and some phospholipids, and increased cholesterol esters and triglycerides, in motor cortex white matter of ALS cases [65]. Decreased myelin-enriched sphingolipids (GalCer, ST, SM) are also observed in motor cortex of people with multiple system atrophy [66], which is characterised by a-synuclein aggregates in oligodendrocytes. In contrast, the more common synucleinopathy Parkinson's disease is characterised by increased BMP in the heavily-affected substantia nigra [67], and increased diacylglycerol in frontal cortex [68]. In Alzheimer's disease (AD), marked depletion of myelin sphingolipids and myelin proteins was seen in superior frontal grey matter, but not frontal white matter [69, 70]. Given that both AD and bvFTD affect the superior frontal lobe, it is interesting that the pattern of myelin loss differs between AD and bvFTD, with a much more pronounced effect on the frontal white matter seen in the familial bvFTD cases examined herein. Accordingly, the burden of white matter hyperintensities is higher in bvFTD than AD and is thought to contribute substantially to cognitive deficits [71, 72].

A limitation of our study was the absence of sporadic FTD cases. It will be important in future studies to determine whether the lipidomic signature and pronounced myelin loss in FTD-*GRN* cases is shared with a subset of sporadic FTD cases with TDP-43 inclusions. This seems likely, since (i) MRI studies have demonstrated loss of white matter integrity in sporadic bvFTD [72, 73] and (ii) rare variants in genes whose loss of function is associated with the severe inherited leukodystrophies hypomyelinating leukodystrophy (*TMEM106B* gene), Nasu-Hakola disease (*TREM2*), metachromatic leukodystrophy (*ARSA*), and cerebrotendinous xanthomatosis (*CYP27A1*), are also known to cause FTD with TDP-43 deposition [74].

In conclusion, this study presents the first evidence of severe myelin lipid loss in FTD-*GRN* and FTD-*C9orf72*. More severe white matter lipid and myelin protein loss in FTD-*GRN*, together with marked accumulation of cholesterol esters in white matter and increased GALC activity, imply a pronounced susceptibility for myelin lipid loss, leading to white matter attrition, in *GRN* mutation carriers. These results are consistent with a requirement for progranulin in restricting myelin lipid catabolism. In fact, our data shows that FTD-*GRN* displays features of metabolic leukodystrophies, including myelin loss, gliosis, and cholesterol ester storage [50]. MRI studies underscore the importance of myelin attrition in the behavioural deficits that define bvFTD [71, 72], and our data provides biochemical evidence underpinning the use of myelin MRI as a diagnostic and prognostic tool in

FTD management. Since myelin is essential for neuronal health and neurological functions, accelerated myelin loss may be a key driver of neurodegeneration caused by progranulin haploinsufficiency.

List of Abbreviations

AcCa	Acylcarnitine
AD	Alzheimer's disease
ALS	Amyotrophic Lateral Sclerosis
ASPA	Aspartoacylase
BMP	Bis(Monoacylglycero)Phosphate
BSA	Bovine Serum Albumin
bvFTD	Behavioural Variant FTD
C9orf72	Chromosome 9 open reading frame 72
Cer	Ceramide
Chol	Cholesterol
CholE	Cholesterol Ester
CL	Cardiolipin
CNP	2',3'-Cyclic Nucleotide 3'-Phosphodiesterase
DAG	Diacylglyerol
DAPI	Diamidino-2-Phenylindole Dihydrochloride
FTD	Frontotemporal Dementia
GALC	β-Galactocerebrosidase
GCase	β-Glucocerebrosidase
GRN	Progranulin
Hex1Cer	Monohexosylceramide
Hex2Cer	Dihexosylceramide
LFB	Luxol Fast Blue
LPA	Lysophosphatidic acid
LPC	Lysophosphatidylcholine
LPC(O)	Alkyl-LPC
LPE	Lysophosphatidylethanolamine
LPE(O)	Alkyl-Lysophosphatidylethanolamine
LPI	Lysophosphatidylinositol
LPS	Lysophosphatidylserine
MAG	Monoacylglycerol
MBP	Myelin Basic Protein
MRI	Magnetic Resonance Imaging
MTBE	Methyl-Tert-Butyl Ether
NCL	Neuronal Ceroid Lipofuscinosis
PC	Phosphatidylcholine
PE	Phosphatidylethanolamine
PE(O)	Alkyl-PE
PE(P)	Alkenyl-PE(PE plasmalogen)
PG	Phosphatidylglycerol
PI	Phosphatidylinositol
PLP	Myelin Proteolipid Protein
PLS-DA	Partial Least Squares-Discriminant Analysis
PMI	Post-Mortem Interval
PS	Phosphatidylserine
SM	Sphingomyelin
Sph	Sphingosine
ST	Sulfatide
TAG	Triacylglycerol
TBST	Tris Buffered Saline, 0.1% Tween 20
TDP-43	TAR DNA-binding protein 43

Supplementary Information

The online version contains supplementary material available at https://doi.org/10.1186/s40478-023-01544-7.

Supplementary Data File 1

Supplementary Table 1. Lipid Class Totals (nmoles/mg protein) in frontal white matter and one-way ANOVA results. BH FDR: Benjamini-Hochberg false discovery rate-corrected p value (q value). P values for Tukey's post-test are also given. **Supplementary Table 2**. Lipid Class Totals (nmoles/mg protein) in frontal grey matter and one-way ANOVA results. BH FDR: Benjamini-Hochberg false discovery rate-corrected p value (q value). P values for Tukey's post-test are also given. **Supplementary Table 3**. Lipid Class Totals (nmoles/mg protein) in parietal white matter and one-way ANOVA results. BH FDR: Benjamini-Hochberg false discovery rate-corrected p value (q value). P values for Tukey's post-test are also given. **Supplementary Table 4**. Lipid Class Totals (nmoles/mg protein) in parietal grey matter and one-way ANOVA results. BH FDR: Benjamini-Hochberg false discovery rate-corrected p value (q value). P values for Tukey's post-test are also given.

Acknowledgements
Brain tissue was provided by Sydney Brain Bank, which is supported by Neuroscience Research Australia, and the NSW Brain Tissue Resource Centre, University of Sydney, which is supported by award R28AA012725 from the National Institute of Alcohol Abuse and Alcoholism, National Institutes of Health, USA. We would like to thank Heather McCann from the Sydney Brain Bank for TDP-43 scoring, and gratefully acknowledge subsidised access to the Sydney Mass Spectrometry and Sydney Microscopy and Microanalysis core facilities.

Authors' contributions
OCM performed experiments, analysed data, and wrote the manuscript.
JDT and HS performed experiments.
JYL analysed data.
JBK obtained funding and performed genotyping.
RLR and GH contributed to study design, case ascertainment, and editing of the manuscript.
ASD conceived and planned the study, obtained funding and ethics approval, and wrote the manuscript.

Funding
This research was supported by Project grant APP1163249 (J.B.K. and A.S.D.) and Ideas grant APP1100626 (A.S.D.) from the National Health and Medical Research Council of Australia. O.C.M., H.S. and J.Y.L. are supported by Australian government Research Training Program scholarships. G.M.H. is supported by an NHMRC Senior Leadership Fellowship (1176607).

Data Availability
The complete lipidomic dataset is included as Supplementary Data File 1 and available at Metabolomics Workbench [75], study ST002452, DOI: https://doi.org/10.21228/M8BD85. All other raw data is available from the corresponding author upon reasonable request.

Declarations

Competing interests
The authors declare that they have no competing interests.

Ethics approval and consent to participate
This research project was carried out under University of Sydney Human Research Ethics Committee approval (#2019/750). Since the research used post-mortem brain bank tissue samples obtained from the Sydney Brain Bank and NSW Brain Tissue Resource Centre, consent to participate is not required.

Consent for publication
Not applicable.

Received: 6 March 2023 / Accepted: 12 March 2023
Published online: 27 March 2023

References

1. Olney NT, Spina S, Miller BL (2017) Frontotemporal Dementia. Neurologic clinics 35:339 – 74. https://doi.org/10.1016/j.ncl.2017.01.008
2. Hodges JR, Davies R, Xuereb J, Kril J, Halliday G (2003) Survival in frontotemporal dementia. Neurology 61:349–354. https://doi.org/10.1212/01.Wnl.0000078928.20107.52
3. Greaves CV, Rohrer JD (2019) An update on genetic frontotemporal dementia. J Neurol 266:2075–2086. https://doi.org/10.1007/s00415-019-09363-4
4. Neumann M, Sampathu DM, Kwong LK, Truax AC, Micsenyi MC, Chou TT, Bruce J, Schuck T, Grossman M, Clark CM, McCluskey LF, Miller BL, Masliah

E, Mackenzie IR, Feldman H, Feiden W, Kretzschmar HA, Trojanowski JQ, Lee VM (2006) Ubiquitinated TDP-43 in frontotemporal lobar degeneration and amyotrophic lateral sclerosis. Science 314:130–133. https://doi.org/10.1126/science.1134108

5. Cruts M, Gijselinck I, van der Zee J, Engelborghs S, Wils H, Pirici D, Rademakers R, Vandenberghe R, Dermaut B, Martin JJ, van Duijn C, Peeters K, Sciot R, Santens P, De Pooter T, Mattheijssens M, Van den Broeck M, Cuijt I, Vennekens K, De Deyn PP, Kumar-Singh S, Van Broeckhoven C (2006) Null mutations in progranulin cause ubiquitin-positive frontotemporal dementia linked to chromosome 17q21. Nature 442:920–924. https://doi.org/10.1038/nature05017
6. Baker M, Mackenzie IR, Pickering-Brown SM, Gass J, Rademakers R, Lindholm C, Snowden J, Adamson J, Sadovnick AD, Rollinson S, Cannon A, Dwosh E, Neary D, Melquist S, Richardson A, Dickson D, Berger Z, Eriksen J, Robinson T, Zehr C, Dickey CA, Crook R, McGowan E, Mann D, Boeve B, Feldman H, Hutton M (2006) Mutations in progranulin cause tau-negative frontotemporal dementia linked to chromosome 17. Nature 442:916–919. https://doi.org/10.1038/nature05016
7. Majounie E, Renton AE, Mok K, Dopper EGP, Waite A, Rollinson S, Chiò A, Restagno G, Nicolaou N, Simon-Sanchez J, van Swieten JC, Abramzon Y, Johnson JO, Sendtner M, Pamphlett R, Orrell RW, Mead S, Sidle KC, Houlden H, Rohrer JD, Morrison KE, Pall H, Talbot K, Ansorge O, Hernandez DG, Arepalli S, Sabatelli M, Mora G, Corbo M, Giannini F, Calvo A, Englund E, Borghero G, Floris GL, Remes AM, Laaksovirta H, McCluskey L, Trojanowski JQ, Van Deerlin VM, Schellenberg GD, Nalls MA, Drory VE, Lu C-S, Yeh T-H, Ishiura H, Takahashi Y, Tsuji S, Le Ber I, Brice A, Drepper C, Williams N, Kirby J, Shaw P, Hardy J, Tienari PJ, Heutink P, Morris HR, Pickering-Brown S, Traynor BJ (2012) Frequency of the C9orf72 hexanucleotide repeat expansion in patients with amyotrophic lateral sclerosis and frontotemporal dementia: a cross-sectional study. Lancet Neurol 11:323–330
8. DeJesus-Hernandez M, Mackenzie IR, Boeve BF, Boxer AL, Baker M, Rutherford NJ, Nicholson AM, Finch NA, Flynn H, Adamson J, Kouri N, Wojtas A, Sengdy P, Hsiung G-YR, Karydas A, Seeley WW, Josephs KA, Coppola G, Geschwind DH, Wszolek ZK, Feldman H, Knopman DS, Petersen RC, Miller BL, Dickson DW, Boylan KB, Graff-Radford NR, Rademakers R (2011) Expanded GGGGCC hexanucleotide repeat in noncoding region of C9ORF72 causes chromosome 9p-linked FTD and ALS. Neuron 72:245–256. https://doi.org/10.1016/j.neuron.2011.09.011
9. Hu F, Padukkavidana T, Vaegter CB, Brady OA, Zheng Y, Mackenzie IR, Feldman HH, Nykjaer A, Strittmatter SM (2010) Sortilin-mediated endocytosis determines levels of the frontotemporal dementia protein, progranulin. Neuron 68:654–667. https://doi.org/10.1016/j.neuron.2010.09.034
10. Zhou X, Sun L, Bracko O, Choi JW, Jia Y, Nana AL, Brady OA, Hernandez JCC, Nishimura N, Seeley WW, Hu F (2017) Impaired prosaposin lysosomal trafficking in frontotemporal lobar degeneration due to progranulin mutations. Nat Commun 8:15277. https://doi.org/10.1038/ncomms15277
11. Smith KR, Damiano J, Franceschetti S, Carpenter S, Canafoglia L, Morbin M, Rossi G, Pareyson D, Mole SE, Staropoli JF, Sims KB, Lewis J, Lin WL, Dickson DW, Dahl HH, Bahlo M, Berkovic SF (2012) Strikingly different clinicopathological phenotypes determined by progranulin-mutation dosage. Am J Hum Genet 90:1102–1107. https://doi.org/10.1016/j.ajhg.2012.04.021
12. Almeida MR, Macário MC, Ramos L, Baldeiras I, Ribeiro MH, Santana I (2016) Portuguese family with the co-occurrence of frontotemporal lobar degeneration and neuronal ceroid lipofuscinosis phenotypes due to progranulin gene mutation. Neurobiology of Aging 41:200.e1-00.e5
13. Gotzl JK, Mori K, Damme M, Fellerer K, Tahirovic S, Kleinberger G, Janssens J, van der Zee J, Lang CM, Kremmer E, Martin JJ, Engelborghs S, Kretzschmar HA, Arzberger T, Van Broeckhoven C, Haass C, Capell A (2014) Common pathobiochemical hallmarks of progranulin-associated frontotemporal lobar degeneration and neuronal ceroid lipofuscinosis. Acta Neuropathol 127:845–860. https://doi.org/10.1007/s00401-014-1262-6
14. Ahmed Z, Sheng H, Xu YF, Lin WL, Innes AE, Gass J, Yu X, Wuertzer CA, Hou H, Chiba S, Yamanouchi K, Leissring M, Petrucelli L, Nishihara M, Hutton ML, McGowan E, Dickson DW, Lewis J (2010) Accelerated lipofuscinosis and ubiquitination in granulin knockout mice suggest a role for progranulin in successful aging. Am J Pathol 177:311–324. https://doi.org/10.2353/ajpath.2010.090915
15. Ward ME, Chen R, Huang HY, Ludwig C, Telpoukhovskaia M, Taubes A, Boudin H, Minami SS, Reichert M, Albrecht P, Gelfand JM, Cruz-Herranz A, Cordano C, Alavi MV, Leslie S, Seeley WW, Miller BL, Bigio E, Mesulam MM, Bogyo MS, Mackenzie IR, Staropoli JF, Cotman SL, Huang EJ, Gan L, Green AJ (2017) Individuals with progranulin haploinsufficiency exhibit features of neuronal ceroid lipofuscinosis. Sci Transl Med 9. https://doi.org/10.1126/scitranslmed.aah5642
16. Evers BM, Rodriguez-Navas C, Tesla RJ, Prange-Kiel J, Wasser CR, Yoo KS, McDonald J, Cenik B, Ravenscroft TA, Plattner F, Rademakers R, Yu G, White CL 3rd, Herz J (2017) Lipidomic and transcriptomic basis of lysosomal dysfunction in Progranulin Deficiency. Cell Rep 20:2565–2574. https://doi.org/10.1016/j.celrep.2017.08.056
17. Tanaka Y, Suzuki G, Matsuwaki T, Hosokawa M, Serrano G, Beach TG, Yamanouchi K, Hasegawa M, Nishihara M (2017) Progranulin regulates lysosomal function and biogenesis through acidification of lysosomes. Hum Mol Genet 26:969–988. https://doi.org/10.1093/hmg/ddx011
18. Valdez C, Ysselstein D, Young TJ, Zheng J, Krainc D (2020) Progranulin mutations result in impaired processing of prosaposin and reduced glucocerebrosidase activity. Hum Mol Genet 29:716–726. https://doi.org/10.1093/hmg/ddz229
19. Logan T, Simon MJ, Rana A, Cherf GM, Srivastava A, Davis SS, Low RLY, Chiu CL, Fang M, Huang F, Bhalla A, Llapashtica C, Prorok R, Pizzo ME, Calvert MEK, Sun EW, Hsiao-Nakamoto J, Rajendra Y, Lexa KW, Srivastava DB, van Lengerich B, Wang J, Robles-Colmenares Y, Kim DJ, Duque J, Lenser M, Earr TK, Nguyen H, Chau R, Tsogtbaatar B, Ravi R, Skuja LL, Solanoy H, Rosen HJ, Boeve BF, Boxer AL, Heuer HW, Dennis MS, Kariolis MS, Monroe KM, Przybyla L, Sanchez PE, Meisner R, Diaz D, Henne KR, Watts RJ, Henry AG, Gunasekaran K, Astarita G, Suh JH, Lewcock JW, DeVos SL, Di Paolo G (2021) Rescue of a lysosomal storage disorder caused by Grn loss of function with a brain penetrant progranulin biologic. Cell 184:4651-68 e25. https://doi.org/10.1016/j.cell.2021.08.002
20. Mori K, Weng SM, Arzberger T, May S, Rentzsch K, Kremmer E, Schmid B, Kretzschmar HA, Cruts M, Van Broeckhoven C, Haass C, Edbauer D (2013) The C9orf72 GGGGCC repeat is translated into aggregating dipeptide-repeat proteins in FTLD/ALS. Science 339:1335-8. https://doi.org/10.1126/science.1232927
21. Gendron TF, Bieniek KF, Zhang YJ, Jansen-West K, Ash PE, Caulfield T, Daughrity L, Dunmore JH, Castanedes-Casey M, Chew J, Cosio DM, van Blitterswijk M, Lee WC, Rademakers R, Boylan KB, Dickson DW, Petrucelli L (2013) Antisense transcripts of the expanded C9ORF72 hexanucleotide repeat form nuclear RNA foci and undergo repeat-associated non-ATG translation in c9FTD/ALS. Acta Neuropathol 126:829–844. https://doi.org/10.1007/s00401-013-1192-8
22. Kwon I, Xiang S, Kato M, Wu L, Theodoropoulos P, Wang T, Kim J, Yun J, Xie Y, McKnight SL (2014) Poly-dipeptides encoded by the C9orf72 repeats bind nucleoli, impede RNA biogenesis, and kill cells. Science 345:1139–1145. https://doi.org/10.1126/science.1254917
23. Shi Y, Lin S, Staats KA, Li Y, Chang WH, Hung ST, Hendricks E, Linares GR, Wang Y, Son EY, Wen X, Kisler K, Wilkinson B, Menendez L, Sugawara T, Woolwine P, Huang M, Cowan MJ, Ge B, Koutsodendris N, Sandor KP, Komberg J, Vangoor VR, Senthilkumar K, Hennes V, Seah C, Nelson AR, Cheng TY, Lee SJ, August PR, Chen JA, Wisniewski N, Hanson-Smith V, Belgard TG, Zhang A, Coba M, Grunseich C, Ward ME, van den Berg LH, Pasterkamp RJ, Trotti D, Zlokovic BV, Ichida JK (2018) Haploinsufficiency leads to neurodegeneration in C9ORF72 ALS/FTD human induced motor neurons. Nat Med 24:313–325. https://doi.org/10.1038/nm.4490
24. Farg MA, Sundaramoorthy V, Sultana JM, Yang S, Atkinson RAK, Levina V, Halloran MA, Gleeson PA, Blair IP, Soo KY, King AE, Atkin JD (2014) C9ORF72, implicated in amytrophic lateral sclerosis and frontotemporal dementia, regulates endosomal trafficking. Hum Mol Genet 23:3579–3595. https://doi.org/10.1093/hmg/ddu068
25. Sudre CH, Bocchetta M, Cash D, Thomas DL, Woollacott I, Dick KM, van Swieten J, Borroni B, Galimberti D, Masellis M, Tartaglia MC, Rowe JB, Graff C, Tagliavini F, Frisoni G, Laforce R Jr, Finger E, de Mendonca A, Sorbi S, Ourselin S, Cardoso MJ, Rohrer JD (2017) Genetic Ftd Initiative G White matter hyperintensities are seen only in GRN mutation carriers in the GENFI cohort. Neuroimage Clin 15:171 – 80. https://doi.org/10.1016/j.nicl.2017.04.015
26. Paternico D, Premi E, Gazzina S, Cosseddu M, Alberici A, Archetti S, Cotelli MS, Micheli A, Turla M, Gasparotti R, Padovani A, Borroni B (2016) White matter hyperintensities characterize monogenic frontotemporal dementia with granulin mutations. Neurobiol Aging 38:176–180. https://doi.org/10.1016/j.neurobiolaging.2015.11.011
27. Ameur F, Colliot O, Caroppo P, Stroer S, Dormont D, Brice A, Azuar C, Dubois B, Le Ber I, Bertrand A (2016) White matter lesions in FTLD: distinct phenotypes characterize GRN and C9ORF72 mutations. Neurol Genet 2:e47. https://doi.org/10.1212/NXG.0000000000000047
28. Jiskoot LC, Bocchetta M, Nicholas JM, Cash DM, Thomas D, Modat M, Ourselin S, Rombouts S, Dopper EGP, Meeter LH, Panman JL, van Minkelen R, van der

Ende EL, Donker Kaat L, Pijnenburg YAL, Borroni B, Galimberti D, Masellis M, Tartaglia MC, Rowe J, Graff C, Tagliavini F, Frisoni GB, Laforce R Jr, Finger E, de Mendonca A, Sorbi S, Genetic Frontotemporal dementia I, Papma JM, van Swieten JC, Rohrer JD (2018) Presymptomatic white matter integrity loss in familial frontotemporal dementia in the GENFI cohort: A cross-sectional diffusion tensor imaging study. Ann Clin Transl Neurol 5:1025-36. https://doi.org/10.1002/acn3.601

29. Mahoney CJ, Simpson IJ, Nicholas JM, Fletcher PD, Downey LE, Golden HL, Clark CN, Schmitz N, Rohrer JD, Schott JM, Zhang H, Ourselin S, Warren JD, Fox NC (2015) Longitudinal diffusion tensor imaging in frontotemporal dementia. Ann Neurol 77:33–46. https://doi.org/10.1002/ana.24296
30. Quarles RH, Macklin WB, Morell P (2006) Myelin formation, structure and Biochemistry. In: Brady ST et al (eds) Basic Neurochemistry: Molecular, Cellular and Medical Aspects. Elsevier, pp 51–71
31. Couttas TA, Rustam YH, Song H, Qi Y, Teo JD, Chen J, Reid GE, Don AS (2020) A Novel Function of Sphingosine Kinase 2 in the Metabolism of Sphinga-4,14-Diene Lipids. Metabolites 10. https://doi.org/10.3390/metabo10060236
32. Oftedal L, Maple-Grødem J, Førland MGG, Alves G, Lange J (2020) Validation and assessment of preanalytical factors of a fluorometric in vitro assay for glucocerebrosidase activity in human cerebrospinal fluid. Sci Rep 10:22098. https://doi.org/10.1038/s41598-020-79104-5
33. Song H, McEwen HP, Duncan T, Lee JY, Teo JD, Don AS (2021) Sphingosine kinase 2 is essential for remyelination following cuprizone intoxication. Glia 69:2863–2881. https://doi.org/10.1002/glia.24074
34. Bankhead P, Loughrey MB, Fernández JA, Dombrowski Y, McArt DG, Dunne PD, McQuaid S, Gray RT, Murray LJ, Coleman HG, James JA, Salto-Tellez M, Hamilton PW (2017) QuPath: open source software for digital pathology image analysis. Sci Rep 7:16878. https://doi.org/10.1038/s41598-017-17204-5
35. Mackenzie IR, Neumann M, Baborie A, Sampathu DM, Du Plessis D, Jaros E, Perry RH, Trojanowski JQ, Mann DM, Lee VM (2011) A harmonized classification system for FTLD-TDP pathology. Acta Neuropathol 122:111–113. https://doi.org/10.1007/s00401-011-0845-8
36. Kril JJ, Halliday GM (2004) Clinicopathological staging of frontotemporal dementia severity: correlation with regional atrophy. Dement Geriatr Cogn Disord 17:311–315. https://doi.org/10.1159/000077161
37. Manera AL, Dadar M, Collins DL, Ducharme S, Frontotemporal Lobar Degeneration Neuroimaging I (2019) Deformation based morphometry study of longitudinal MRI changes in behavioral variant frontotemporal dementia. NeuroImage Clin 24:102079–102079. https://doi.org/10.1016/j.nicl.2019.102079
38. Vanier MT, Svennerholm L (1975) Chemical pathology of Krabbe's disease. III. Ceramide-hexosides and gangliosides of brain. Acta Paediatr Scand 64:641–648
39. Madhavarao CN, Moffett JR, Moore RA, Viola RE, Namboodiri MA, Jacobowitz DM (2004) Immunohistochemical localization of aspartoacylase in the rat central nervous system. J Comp Neurol 472:318–329. https://doi.org/10.1002/cne.20080
40. Nugent AA, Lin K, van Lengerich B, Lianoglou S, Przybyla L, Davis SS, Llapashtica C, Wang J, Kim DJ, Xia D, Lucas A, Baskaran S, Haddick PCG, Lenser M, Earr TK, Shi J, Dugas JC, Andreone BJ, Logan T, Solanoy HO, Chen H, Srivastava A, Poda SB, Sanchez PE, Watts RJ, Sandmann T, Astarita G, Lewcock JW, Monroe KM, Di Paolo G (2020) TREM2 regulates microglial cholesterol metabolism upon chronic phagocytic challenge. Neuron 105:837 – 54 e9. https://doi.org/10.1016/j.neuron.2019.12.007
41. Cantuti-Castelvetri L, Fitzner D, Bosch-Queralt M, Weil MT, Su M, Sen P, Ruhwedel T, Mitkovski M, Trendelenburg G, Lutjohann D, Mobius W, Simons M (2018) Defective cholesterol clearance limits remyelination in the aged central nervous system. Science 359:684–688. https://doi.org/10.1126/science.aan4183
42. Schmitt S, Castelvetri LC, Simons M (2015) Metabolism and functions of lipids in myelin. Biochim Biophys Acta 1851:999–1005. https://doi.org/10.1016/j.bbalip.2014.12.016
43. Zhou X, Paushter DH, Pagan MD, Kim D, Nunez Santos M, Lieberman RL, Overkleeft HS, Sun Y, Smolka MB, Hu F (2019) Progranulin deficiency leads to reduced glucocerebrosidase activity. PLoS ONE 14:e0212382. https://doi.org/10.1371/journal.pone.0212382
44. Arrant AE, Roth JR, Boyle NR, Kashyap SN, Hoffmann MQ, Murchison CF, Ramos EM, Nana AL, Spina S, Grinberg LT, Miller BL, Seeley WW, Roberson ED (2019) Impaired ß-glucocerebrosidase activity and processing in frontotemporal dementia due to progranulin mutations. Acta Neuropathol Commun 7:218. https://doi.org/10.1186/s40478-019-0872-6
45. Boland S, Swarup S, Ambaw YA, Malia PC, Richards RC, Fischer AW, Singh S, Aggarwal G, Spina S, Nana AL, Grinberg LT, Seeley WW, Surma MA, Klose C, Paulo JA, Nguyen AD, Harper JW, Walther TC, Farese RV Jr (2022) Deficiency of the frontotemporal dementia gene GRN results in gangliosidosis. Nat Commun 13:5924. https://doi.org/10.1038/s41467-022-33500-9
46. Wang Y, Cella M, Mallinson K, Ulrich JD, Young KL, Robinette ML, Gilfillan S, Krishnan GM, Sudhakar S, Zinselmeyer BH, Holtzman DM, Cirrito JR, Colonna M (2015) TREM2 lipid sensing sustains the microglial response in an Alzheimer's disease model. Cell 160:1061–1071. https://doi.org/10.1016/j.cell.2015.01.049
47. Woollacott IOC, Bocchetta M, Sudre CH, Ridha BH, Strand C, Courtney R, Ourselin S, Cardoso MJ, Warren JD, Rossor MN, Revesz T, Fox NC, Holton JL, Lashley T, Rohrer JD (2018) Pathological correlates of white matter hyperintensities in a case of progranulin mutation associated frontotemporal dementia. Neurocase 24:166–174. https://doi.org/10.1080/13554794.2018.1506039
48. Sirisi S, Querol-Vilaseca M, Dols-Icardo O, Pegueroles J, Montal V, Munoz L, Torres S, Ferrer-Raventos P, Iulita MF, Sanchez-Aced E, Blesa R, Illan-Gala I, Molina-Porcel L, Borrego-Ecija S, Sanchez-Valle R, Clarimon J, Belbin O, Fortea J, Lleo A (2022) Myelin loss in C9orf72 hexanucleotide expansion carriers. J Neurosci Res 100:1862–1875. https://doi.org/10.1002/jnr.25100
49. Wender M, Filipek-Wender H, Stanislawska J (1974) Cholesteryl esters of the brain in demyelinating diseases. Clin Chim Acta 54:269–275. https://doi.org/10.1016/0009-8981(74)90245-9
50. Theda C, Moser AB, Powers JM, Moser HW (1992) Phospholipids in X-linked adrenoleukodystrophy white matter: fatty acid abnormalities before the onset of demyelination. J Neurol Sci 110:195–204. https://doi.org/10.1016/0022-510x(92)90028-j
51. Chiang JYL, Ferrell JM (2020) Up to date on cholesterol 7 alpha-hydroxylase (CYP7A1) in bile acid synthesis. Liver Res 4:47–63. https://doi.org/10.1016/j.livres.2020.05.001
52. Cantoni C, Bollman B, Licastro D, Xie M, Mikesell R, Schmidt R, Yuede CM, Galimberti D, Olivecrona G, Klein RS, Cross AH, Otero K, Piccio L (2015) TREM2 regulates microglial cell activation in response to demyelination in vivo. Acta Neuropathol 129:429–447. https://doi.org/10.1007/s00401-015-1388-1
53. Wu Y, Shao W, Todd TW, Tong J, Yue M, Koga S, Castanedes-Casey M, Librero AL, Lee CW, Mackenzie IR, Dickson DW, Zhang YJ, Petrucelli L, Prudencio M (2021) Microglial lysosome dysfunction contributes to white matter pathology and TDP-43 proteinopathy in GRN-associated FTD. Cell Rep 36:109581. https://doi.org/10.1016/j.celrep.2021.109581
54. van der Kant R, Langness VF, Herrera CM, Williams DA, Fong LK, Leestemaker Y, Steenvoorden E, Rynearson KD, Brouwers JF, Helms JB, Ovaa H, Giera M, Wagner SL, Bang AG, Goldstein LSB (2019) Cholesterol Metabolism Is a Druggable Axis that Independently Regulates Tau and Amyloid-beta in iPSC-Derived Alzheimer's Disease Neurons. Cell Stem Cell 24:363 – 75 e9. https://doi.org/10.1016/j.stem.2018.12.013
55. Puglielli L, Konopka G, Pack-Chung E, Ingano LA, Berezovska O, Hyman BT, Chang TY, Tanzi RE, Kovacs DM (2001) Acyl-coenzyme A: cholesterol acyltransferase modulates the generation of the amyloid beta-peptide. Nat Cell Biol 3:905–912. https://doi.org/10.1038/ncb1001-905
56. Rinaldo P, Matern D, Bennett MJ (2002) Fatty acid Oxidation Disorders. Annu Rev Physiol 64:477–502. https://doi.org/10.1146/annurev.physiol.64.082201.154705
57. Jacova C, Hsiung G-YR, Tawankanjanachot I, Dinelle K, McCormick S, Gonzalez M, Lee H, Sengdy P, Bouchard-Kerr P, Baker M, Rademakers R, Sossi V, Stoessl AJ, Feldman HH, Mackenzie IR (2013) Anterior brain glucose hypometabolism predates dementia in progranulin mutation carriers. Neurology 81:1322–1331. https://doi.org/10.1212/WNL.0b013e3182a8237e
58. Turk BR, Theda C, Fatemi A, Moser AB (2020) X-linked adrenoleukodystrophy: Pathology, pathophysiology, diagnostic testing, newborn screening and therapies. Int J Dev neuroscience: official J Int Soc Dev Neurosci 80:52–72. https://doi.org/10.1002/jdn.10003
59. Viader A, Sasaki Y, Kim S, Strickland A, Workman Cayce S, Yang K, Gross Richard W, Milbrandt J (2013) Aberrant Schwann cell lipid metabolism linked to mitochondrial deficits leads to Axon Degeneration and Neuropathy. Neuron 77:886–898
60. Gotzl JK, Brendel M, Werner G, Parhizkar S, Sebastian Monasor L, Kleinberger G, Colombo AV, Deussing M, Wagner M, Winkelmann J, Diehl-Schmid J, Levin J, Fellerer K, Reifschneider A, Bultmann S, Bartenstein P, Rominger A, Tahirovic S, Smith ST, Madore C, Butovsky O, Capell A, Haass C (2019) Opposite microglial activation stages upon loss of PGRN or TREM2 result in reduced

cerebral glucose metabolism. EMBO Mol Med 11. https://doi.org/10.15252/emmm.201809711
61. Lall D, Lorenzini I, Mota TA, Bell S, Mahan TE, Ulrich JD, Davtyan H, Rexach JE, Muhammad A, Shelest O, Landeros J, Vazquez M, Kim J, Ghaffari L, O'Rourke JG, Geschwind DH, Blurton-Jones M, Holtzman DM, Sattler R, Baloh RH (2021) C9orf72 deficiency promotes microglial-mediated synaptic loss in aging and amyloid accumulation. Neuron 109:2275-91 e8. https://doi.org/10.1016/j.neuron.2021.05.020
62. Zhang J, Velmeshev D, Hashimoto K, Huang YH, Hofmann JW, Shi X, Chen J, Leidal AM, Dishart JG, Cahill MK, Kelley KW, Liddelow SA, Seeley WW, Miller BL, Walther TC, Farese RV Jr, Taylor JP, Ullian EM, Huang B, Debnath J, Wittmann T, Kriegstein AR, Huang EJ (2020) Neurotoxic microglia promote TDP-43 proteinopathy in progranulin deficiency. Nature 588:459–465. https://doi.org/10.1038/s41586-020-2709-7
63. O'Rourke JG, Bogdanik L, Yanez A, Lall D, Wolf AJ, Muhammad AK, Ho R, Carmona S, Vit JP, Zarrow J, Kim KJ, Bell S, Harms MB, Miller TM, Dangler CA, Underhill DM, Goodridge HS, Lutz CM, Baloh RH (2016) C9orf72 is required for proper macrophage and microglial function in mice. Science 351:1324–1329. https://doi.org/10.1126/science.aaf1064
64. Brettschneider J, Toledo JB, Van Deerlin VM, Elman L, McCluskey L, Lee VM, Trojanowski JQ (2012) Microglial activation correlates with disease progression and upper motor neuron clinical symptoms in amyotrophic lateral sclerosis. PLoS ONE 7:e39216. https://doi.org/10.1371/journal.pone.0039216
65. Sadler GL, Lewis KN, Narayana VK, De Souza DP, Mason J, McLean C, Gonsalvez DG, Turner BJ, Barton SK (2022) Lipid Metabolism Is Dysregulated in the Motor Cortex White Matter in Amyotrophic Lateral Sclerosis. Metabolites 12. https://doi.org/10.3390/metabo12060554
66. Don AS, Hsiao JH, Bleasel JM, Couttas TA, Halliday GM, Kim W (2014) Altered lipid levels provide evidence for myelin dysfunction in multiple system atrophy. Acta Neuropathol Commun 2:150. https://doi.org/10.1186/s40478-014-0150-6
67. Xicoy H, Brouwers JF, Wieringa B, Martens GJM (2020) Explorative combined lipid and transcriptomic profiling of Substantia Nigra and Putamen in Parkinson's Disease. Cells 9. https://doi.org/10.3390/cells9091966
68. Wood PL, Tippireddy S, Feriante J, Woltjer RL (2018) Augmented frontal cortex diacylglycerol levels in Parkinson's disease and Lewy Body Disease. PLoS ONE 13:e0191815. https://doi.org/10.1371/journal.pone.0191815
69. Cheng D, Jenner AM, Shui G, Cheong WF, Mitchell TW, Nealon JR, Kim WS, McCann H, Wenk MR, Halliday GM, Garner B (2011) Lipid pathway alterations in Parkinson's disease primary visual cortex. PLoS ONE 6:e17299. https://doi.org/10.1371/journal.pone.0017299
70. Couttas TA, Kain N, Suchowerska AK, Quek LE, Turner N, Fath T, Garner B, Don AS (2016) Loss of ceramide synthase 2 activity, necessary for myelin biosynthesis, precedes tau pathology in the cortical pathogenesis of Alzheimer's disease. Neurobiol Aging 43:89–100. https://doi.org/10.1016/j.neurobiolaging.2016.03.027
71. Huynh K, Piguet O, Kwok J, Dobson-Stone C, Halliday GM, Hodges JR, Landin-Romero R (2021) Clinical and biological Correlates of White Matter Hyperintensities in patients with behavioral-variant Frontotemporal Dementia and Alzheimer Disease. Neurology 96:e1743–e54. https://doi.org/10.1212/WNL.0000000000011638
72. Mahoney CJ, Ridgway GR, Malone IB, Downey LE, Beck J, Kinnunen KM, Schmitz N, Golden HL, Rohrer JD, Schott JM, Rossor MN, Ourselin S, Mead S, Fox NC, Warren JD (2014) Profiles of white matter tract pathology in frontotemporal dementia. Hum Brain Mapp 35:4163–4179. https://doi.org/10.1002/hbm.22468
73. Lam BY, Halliday GM, Irish M, Hodges JR, Piguet O (2014) Longitudinal white matter changes in frontotemporal dementia subtypes. Hum Brain Mapp 35:3547–3557
74. Lok HC, Kwok JB (2021) The role of White Matter Dysfunction and Leukoencephalopathy/Leukodystrophy genes in the aetiology of Frontotemporal Dementias: implications for Novel Approaches to therapeutics. Int J Mol Sci 22. https://doi.org/10.3390/ijms22052541
75. Sud M, Fahy E, Cotter D, Azam K, Vadivelu I, Burant C, Edison A, Fiehn O, Higashi R, Nair KS, Sumner S, Subramaniam S (2016) Metabolomics Workbench: an international repository for metabolomics data and metadata, metabolite standards, protocols, tutorials and training, and analysis tools. Nucleic Acids Res 44:D463–D470. https://doi.org/10.1093/nar/gkv1042

Publisher's Note

Chapter 3: Investigating proteomic changes in genetic FTD

3.1 Background

In chapter 2, our untargeted lipidomic mass spectrometry analysis coupled with western blotting, enzyme activity assays and histology led us to discover that dysfunctional brain lipid metabolism, lysosomal dysfunction and gliosis are features of FTD caused by both heterozygous *GRN* loss and *C9orf72* repeat expansions, however the mechanism and extent to which these features are observed appears to vary between the two FTD groups (Marian et al. 2023), and the underlying pathological mechanisms by which these gene mutations lead to FTD are still under investigation. Untargeted proteomic analysis provides a valuable tool to address these questions and complement our prior lipidomic findings.

Few studies have explored proteomic changes in FTD, and proteomic analyses of the most common inherited causes of FTD with TDP-43 proteinopathy, heterozygous *GRN* loss or *C9orf72* repeat expansions, are limited to a handful of studies (Umoh et al. 2018, Andrés-Benito et al. 2019, Miedema et al. 2022). Frontal cortex from FTD-*GRN* cases showed the greatest proteomic changes relating to immune processes in epithelial cells and mitochondrial dysfunction in neurons while in frontal cortex of FTD-*C9orf72* cases dysregulation in pathways including apoptosis, neurotransmission, phagocytosis and glial markers associated with neuroinflammation were observed (Umoh et al. 2018, Andrés-Benito et al. 2019, Miedema et al. 2022). No prior studies have examined the proteomic differences between FTD caused by *C9orf72* or *GRN* mutations.

Furthermore, previous studies in FTD have focussed on profiling changes in the heavily affected frontal and temporal lobes, but have not widely examined changes to less-affected brain regions. While FTD is a highly heterogeneous form of dementia, both FTD-*GRN* and FTD-*C9orf72* cases present with bvFTD, and therefore the neurodegenerative pattern of these groups is comparable. Examining less-affected regions such as the superior parietal lobe allows us to identify molecular changes attributed to the gene mutations without the effect of gross neuron degeneration and

changes to cellular composition that might be expected to dominate proteomic analysis of the frontal lobe.

In order to further investigate the changes underlying our previous findings, we undertook mass spectrometry-based proteomics for the comprehensive identification and relative quantitation of proteins in brain tissue samples from FTD cases carrying mutations in the *C9orf72* or *GRN* genes, and age-matched controls from the cases described in Chapter 2. The samples matched those used for our prior lipidomic analysis on grey and white matter of the heavily affected superior frontal lobe and relatively-unaffected superior parietal lobe.

3.2 Methods

3.2.1 Proteomic sample preparation

Post-mortem brain tissue from the superior frontal grey and white matter, and superior parietal grey and white matter from 11 FTD-*C9orf72*, 6 FTD-*GRN* and 11 age-matched, neurologically-normal control cases was homogenised as previously described in Chapter 2. All chemicals were purchased from Sigma-Aldrich unless specified. 100 µL of brain tissue homogenate containing protease and phosphatase inhibitors was denatured and reduced with 125 µL of 6 M urea, 9 M thiourea, 10 mM dithiothreitol and 0.1% sodium dodecyl sulfate for 1 h, followed by alkylation with 20 mM iodoacetamide for a further 1 h in the dark.

Samples were then subjected to chloroform/methanol precipitation to desalt and remove lipids and detergents as previously described (Wessel et al. 1984). All solvents were used ice-cold. Briefly, 800 µL methanol, and 200 µL of chloroform was added to the sample mixture and vortexed well between additions. Phase separation was induced with the addition of 600 µL water, the mixture was then vortexed and centrifuged at 9,000 x *g* for 1 min. The upper phase was carefully discarded, 1200 µL methanol was added to the remaining solution and vortexed, then the solution was centrifuged at 9,000 x *g* for 2 min to pellet the protein. The supernatant was discarded, the protein pellet was washed twice with 1000 µL methanol, then centrifuged 14,000 x *g* for 15 min and remaining pellet was dried under a stream of air. The dried protein pellet was resuspended in 50 mM HEPES buffer, pH 7.5 and protein quantification was carried out by Qubit fluorometric assay (ThermoFisher). 100 µg of protein was subject to trypsin digestion (1:33 trypsin: total protein) overnight at 25°C with Trypsin/Lys-C Mix, Mass Spec Grade (#V5072, Promega). Digests were acidified to 2% formic acid and 0.1% trifluoroacetic acid (TFA), peptides were desalted and concentrated by solid-phase extraction on hydrophilic-lipophilic balance (HLB) cartridges (#WAT094226, Waters) and eluate was dried under vacuum (Concentrator plus, Eppendorf). Peptides were resuspended in 50 mM HEPES and adjusted to a final pH >8.5, protein concentration was determined by Qubit fluorometric assay, and 15 µg of peptide per sample were labelled for relative quantitation with Tandem Mass Tags (TMT)

according to the manufacturer's protocol (#A37725, ThermoFisher). Samples within each biological group were randomly assigned to TMT 11-plex tags, including a pooled quality control (QC) sample in each set. Labelled peptides from each TMT 11-plex experiment were pooled and dried down under vacuum. Pooled experiments were reconstituted in 1000 µL 0.1% TFA and further concentrated and desalted by HLB and dried down under vacuum.

TMT labelling allows for relative protein quantitation through the chemical modification of the free amines of tryptic peptides within each sample with unique isobaric reporter tags. As a result, all peptides become labelled with a reporter tag corresponding to each sample. These isobaric reporter tags differ through the varying positional incorporation of stable isotopes. In MS^1, the isobaric nature of the tag allows for the same peptide, regardless of its unique label, to appear as a single precursor ion, but yields specific m/z fragments when cleaved by higher energy collisional dissociation (HCD) fragmentation (Thompson et al. 2003). The labelled samples are pooled at an equimolar ratio, and upon fragmentation, the TMT label is cleaved to yield relative quantitation for each peptide through the relative abundance of the reporter ions corresponding to each sample in conjunction with peptide fragmentation for identification.

3.2.2 Offline LC Fractionation

Pooled, TMT-labelled peptides were fractionated by offline reverse-phase liquid chromatography at mid-pH (pH 7.9) on an Agilent 1260 Infinity HPLC (Agilent Technologies). All solvents were LC-MS grade. Peptides were separated on a 15 cm column packed in-house with C_{18} resin (3.5µm XBridge BEH particles, Waters), across a 70-min binary gradient at a flow rate of 6 µL/min where solvent A comprised 10mM ammonium formate in water, pH 7.9, and solvent B comprised 90:10 acetonitrile:water. The following chromatography gradient was used: 0-13.5 min: 95:5 A/B; 13.5-14 min 90:10 A/B; 14-45 min 58:42 A/B; 45-47 min 10:90 A/B; 47-50 min 10:90 A/B; 50-53 min 95:5 A/B; 53-70 min 95:5 A/B. Pooled samples were reconstituted in 8 µL of 100% acetonitrile and 92 µL of solvent A, and 8 µL of reconstituted sample was diluted in a further 32 µL of solvent A and injected into the HPLC. Eluted fractions were collected every 3 min from 14-20 min, every

1 min from 20-44 min and every 2 min from 44-60 min. Eluted fractions were combined such that every 8th fraction was pooled for liquid chromatography tandem mass spectrometry (LC-MS/MS).

3.2.3 Proteomics

Proteomics was carried out with LC/MS-MS using a Dionex UltiMate 3000 UHPLC coupled to a Q-Exactive HF-X or Exploris Orbitrap mass spectrometer (Thermo Scientific). Peptide separation was carried out on a 75 µm x 45 cm column packed in-house with C_{18} resin (3.5µm particle size) over a 100-min binary gradient, where solvent A: 1% formic acid in water and solvent B: 1% formic acid in 80:20 acetonitrile:water. Flow rate was 450 nL/min from 0-14 min, 300 nL/min from 14-98 min, and 450 nL/min from 98-100 min with the following chromatography: 0-0.1 min: 97:3 A/B; 0.1-14 min 95:5 A/B; 14-90 min 55:45 A/B, 90-95 min 40:60 A/B, 95-100 min 2:98 A/B. MS data were acquired in full scan/data dependent MS^2 mode, in positive polarity. MS1 scan range was 300-1650 *m/z* at a resolution of 60,000, 3e6 automatic gain control (AGC) target and 50 ms injection time. The 15 most abundant ions in each precursor scan were taken for MS^2 fragmentation using HCD at a resolution of 60,000 with 0.7 *m/z* isolation window, 1e5 AGC and normalised collision energy of 30. Two technical replicates were run for each fraction, and bovine serum albumin blanks were run between samples to ensure no sample carry-over.

3.2.4 Data analysis

Analysis of raw data files was carried out in Proteome Discoverer (version 2.5, Thermo Scientific) and searched against the Swiss-Prot database for *Homo Sapiens* (UP000005640; organism ID 9606; 20,610 proteins, released 28th May 2020) using an in-house Mascot (Matrix Science) server with the following parameters: precursor mass tolerance 10 ppm, product mass tolerance 0.1 Da, trypsin digestion, maximum 2 missed cleavages; variable modifications: oxidation and acetylation (N-termini), fixed modifications: TMT 6-Plex (+229.1629, peptide N-terminal and lysine) and carbamidomethyl (cysteine residues). Relative quantitation was performed in Proteome

Discoverer (version 2.5) with the TMT 11-plex setting. Peptide spectral matches (PSM) were searched against a target decoy database (Percolator) with the false discovery rate set to 1%.

At the PSM level, TMT channels containing a single missing value had a value of 1 imputed. PSMs containing >1 missing values were discarded. PSMs were concatenated to the peptide and protein level using R (version 3.6.0). Proteins with >50% missing features were removed. Proteomics data were median normalised to the average of the control group and $\log_2$ transformed in Perseus (version 1.6.8.0) to ensure normality.

3.2.5 Statistical analysis

Differences between sample groups were compared by one-way ANOVA adjusted for Age and PMI covariates. ANOVA *p* values were adjusted for the false-discovery rate (FDR) using the Benjamini-Hochberg correction, followed by Tukey's posthoc test for multiple comparisons. Significance was held at $p < 0.05$. Statistical analyses were carried out in R (version 4.0.3) using the *car*, *olsrr*, *ggplot2*, *multcomp* and *dplyr* packages.

3.2.6 GO enrichment

Proteins with a minimum 25% fold change and significantly different between sample groups after FDR adjustment ($q < 0.05$) were subjected to Gene Ontology (GO) pathway enrichment for biological process and molecular function. Functional annotation was performed using DAVID (Huang et al. 2008, Huang et al. 2009).

3.2.7 Ingenuity Pathway Analysis

Proteins showing significantly different abundance between sample groups by FDR-adjusted *p*-value ($q < 0.05$) were subjected to enrichment for canonical pathways against the Ingenuity Knowledge Base using the default settings within Ingenuity Pathway Analysis software (Qiagen).

“Upregulated” and “downregulated" canonical pathways were identified on the basis of changes to protein abundance within each canonical pathway.

3.3 Results

3.3.1 Superior Frontal Grey Matter

In the superior frontal grey matter we identified 649,852 PSMs resulting in 77,657 peptides leading to identification of a total of 6,656 unique proteins.

Comparison between sample groups by one-way ANOVA adjusted for age at death and PMI yielded significantly different abundance of a total of 2,445 proteins after FDR correction.

With further filtering based on a 25% or greater fold-change, 691 proteins were increased and 297 were decreased in abundance in FTD-*GRN* cases compared with control cases (Figure 3.1 A, D). In FTD-*C9orf72* compared to control cases 50 proteins were increased, and 6 were decreased (Figure 3.1 B, D). Comparison of FTD-*GRN* and FTD-*C9orf72* proteomes showed differential expression of the abundance of 531 proteins between the two FTD groups (Figure 3.1 C, D). Abundance of 443 proteins was increased, and 88 proteins was decreased in FTD-*GRN* cases compared with FTD-*C9orf72* cases. The differences between the two FTD groups were driven by changes to protein abundance in the FTD-*GRN* group, which showed substantially more differentially expressed proteins relative to the controls compared with FTD-*C9orf72* cases.

Gene ontology (GO) enrichment on differentially expressed proteins between FTD-*GRN* cases and controls identified the most significant enrichment in the biological process terms *telomere organisation, nucleosome assembly, cell-cell adhesion, DNA templated transcription, initiation* and *mitochondrial energy transport, NADH to ubiquinone*. GO molecular functions identified terms related to the enriched biological processes including structural constituent of chromatin, protein binding and actin binding (Figure 3.2 A, B).

None of the identified GO biological processes or molecular functions remained significantly enriched after FDR correction in the comparison between FTD-*C9orf72* cases and controls (Figure 3.2 C, D). Enriched GO pathways identified in the comparison between FTD-*GRN* and FTD-*C9orf72* cases included similarly enriched biological processes to those identified between FTD-*GRN* cases

and controls, with the addition of *leukocyte migration* and *synaptic signalling* biological processes (Figure 3.2 E, F).

For further investigation of affected proteins, Ingenuity Pathway Analysis (IPA) was applied in parallel to identify canonical pathways that were enriched in differentially abundant proteins that met statistical significance by FDR-corrected *p*-value, and to predict activation or inhibition of identified pathways. The most strongly enriched pathway identified by IPA in differentially expressed proteins identified between FTD-*GRN* cases and controls was upregulation of *mitochondrial dysfunction*, followed by downregulation in *synaptogenesis signalling, oestrogen receptor signalling* and *oxidative phosphorylation* pathways (Figure 3.3 A). IPA identified downregulation of *synaptogenesis signalling, opioid signalling* and *endocannabinoid neuronal synapse* pathways in FTD-*C9orf72* cases compared to controls (Figure 3.3 B).

Proteins in the *mitochondrial dysfunction* pathway were increased, and proteins in the *oxidative phosphorylation* and *synaptogenesis signalling* pathways were decreased in FTD-*GRN* compared to FTD-*C9orf72* cases (Figure 3.3 C). Proteins within the *oxidative phosphorylation* and *mitochondrial dysfunction* pathways overlapped significantly. The *oxidative phosphorylation* pathway showed that most of the proteins decreased in FTD-*GRN* cases compared with FTD-*C9orf72* cases occurred in complex I, complex IV and complex V (Figure 3.4). Differentially expressed proteins within the *mitochondrial dysfunction/oxidative phosphorylation* pathway such as the mitochondrial complex I protein NDUFV3, complex IV MT-CO3 and complex V F0 subunit protein ATP5MC1 showed significantly decreased abundance in FTD-*GRN* cases compared with both FTD-*C9orf72* cases and controls, with a trend decrease in abundance observed in FTD-*C9orf72* cases, while the complex V F1 subunit protein ATP5F1C was significantly decreased in both FTD groups (Figure 3.5 A-D).

Within the *synaptogenesis signalling* pathway, the abundance of constituent proteins such as the NMDA and AMPA receptor subunits (GRIN2A and GRIA4, respectively), synaptotagmin 2 (SYT2), and the calcium/calmodulin-dependent protein kinase 2 (CAMK2A), were significantly reduced in both FTD groups compared with control cases, and significantly lower in FTD-*GRN* cases

compared with FTD-*C9orf72* cases in all proteins described with the exception of GRIN2A (Figure 3.5 E-H).

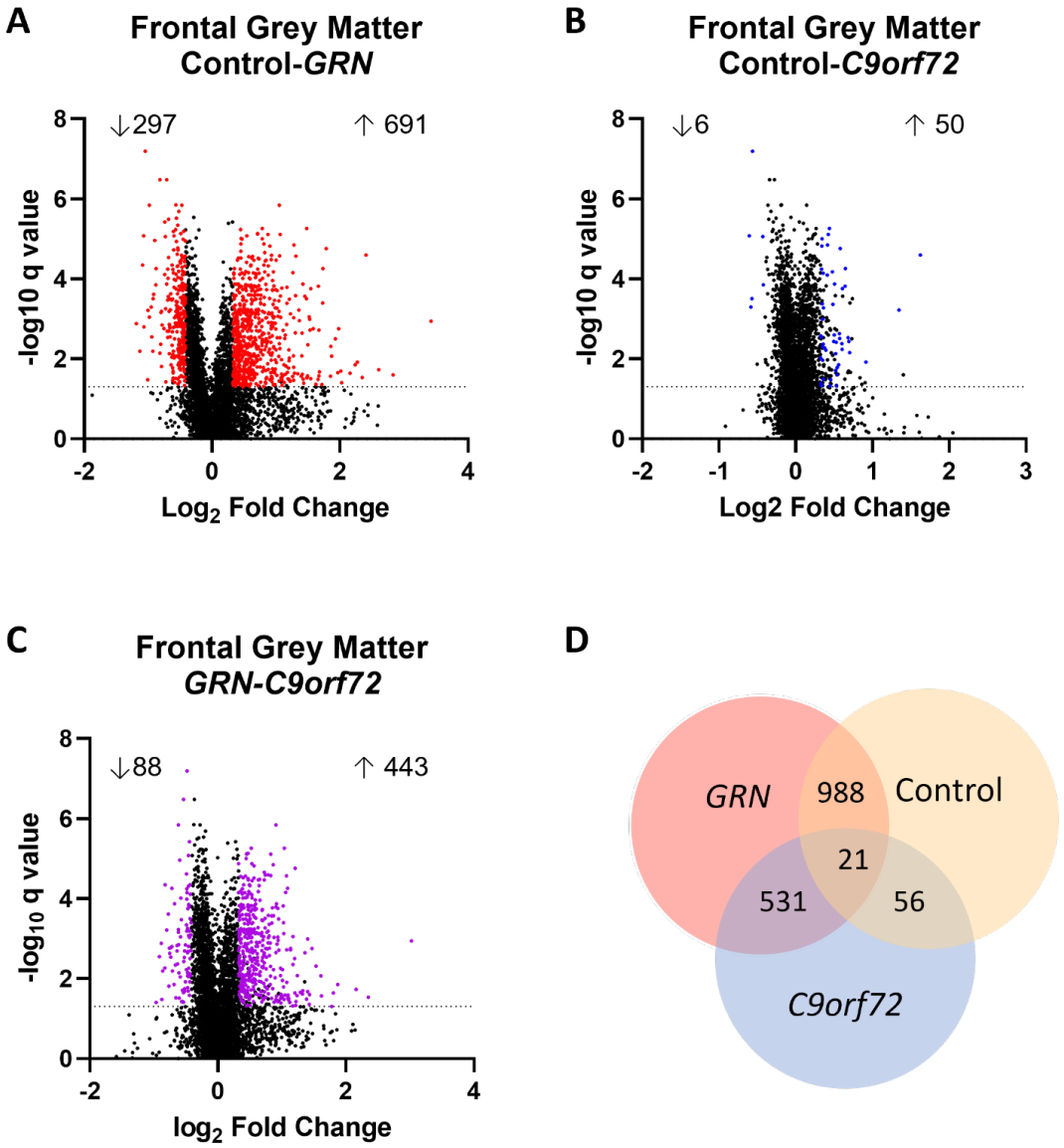

Figure 3.1: Differentially expressed proteins in frontal grey matter

Volcano plots showing differentially expressed proteins in (A) FTD-*GRN* cases compared to controls, (B) FTD-*C9orf72* cases compared with controls, (C) FTD-*GRN* cases compared with FTD-*C9orf72* cases. Differentially expressed proteins meeting FDR-adjusted *p*-value (*q*-value) < 0.05 by overall ANOVA, $p < 0.05$ in Tukey's post-hoc test and fold change greater than 25% indicated by coloured circles in each comparison. Dotted line indicates $q = 0.05$. Arrows indicate increase or decrease in number of differentially expressed proteins meeting all 3 criteria (D) Venn diagram summary of overlap of number of differentially expressed proteins between the 3 sample groups.

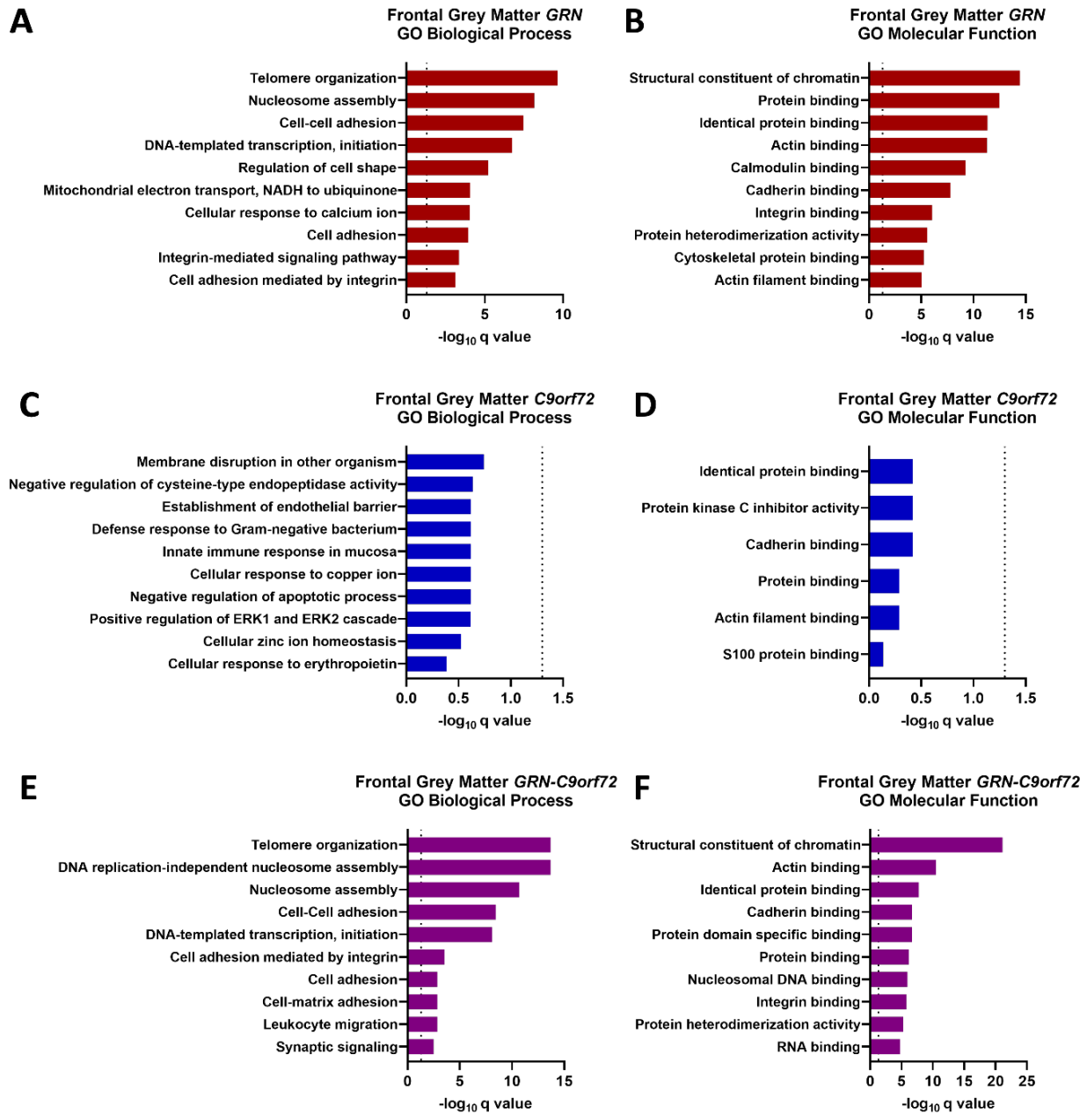

Figure 3.2: Gene ontology enrichment of differentially expressed proteins in frontal grey matter

Gene ontology (GO) enrichment of the 10 most highly enriched biological processes (A, C, E) and molecular functions (B, D, F) for differentially expressed proteins meeting criteria of FDR-corrected *p*-value < 0.05 and fold change greater than 25% between groups in (A, B) FTD-*GRN* cases compared to controls, (C, D) FTD-*C9orf72* cases compared with controls, (E, F) FTD-*GRN* cases compared with FTD-*C9orf72* cases. GO terms shown meet $p < 0.05$ significantly enriched proteins in a biological process or molecular function. Dotted line represents FDR corrected *p*-value (*q*-value) of 0.05 for GO term enrichment.

A *GRN*-Control

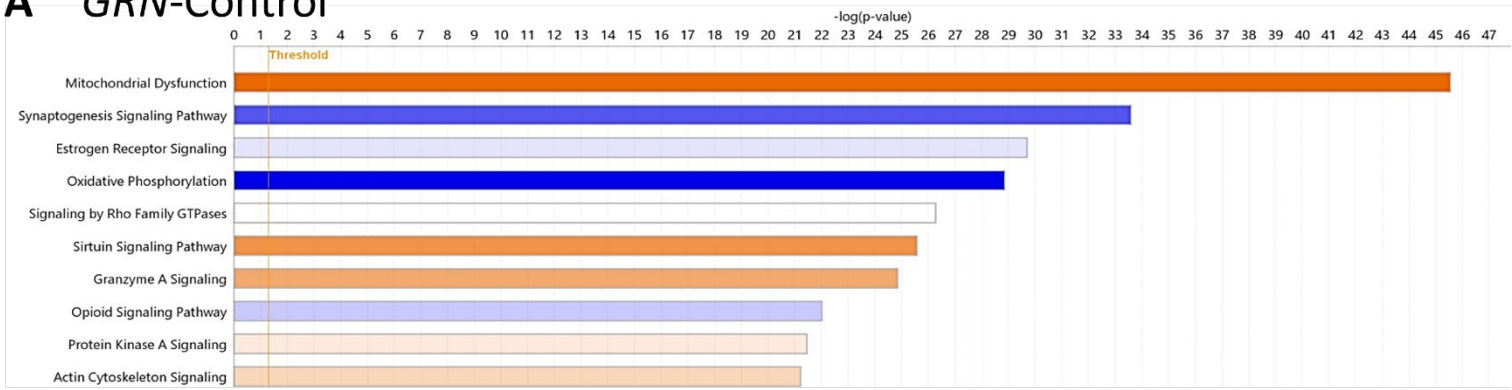

B *C9orf72*-Control

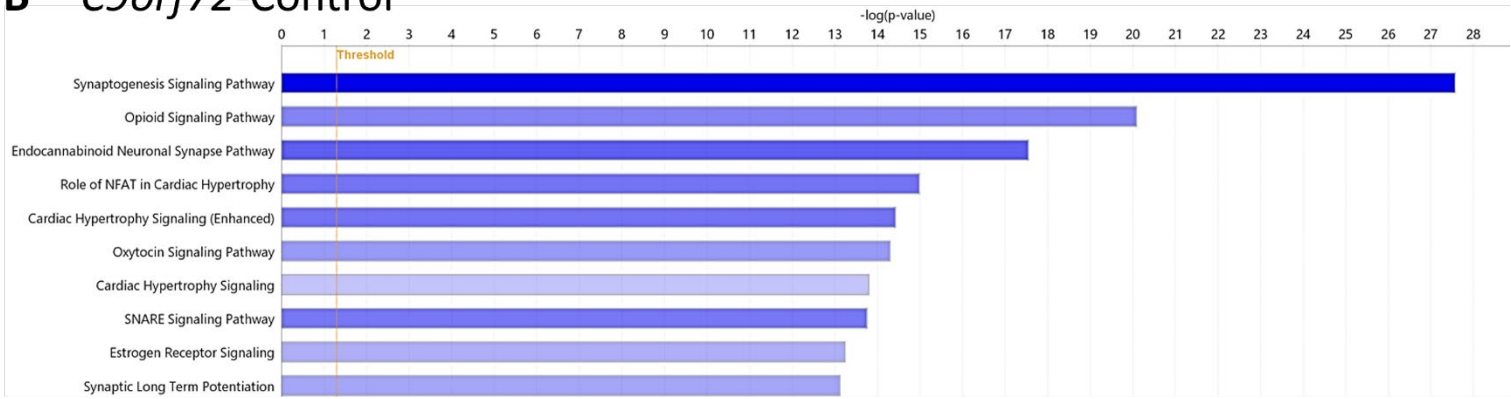

C *GRN-C9orf72*

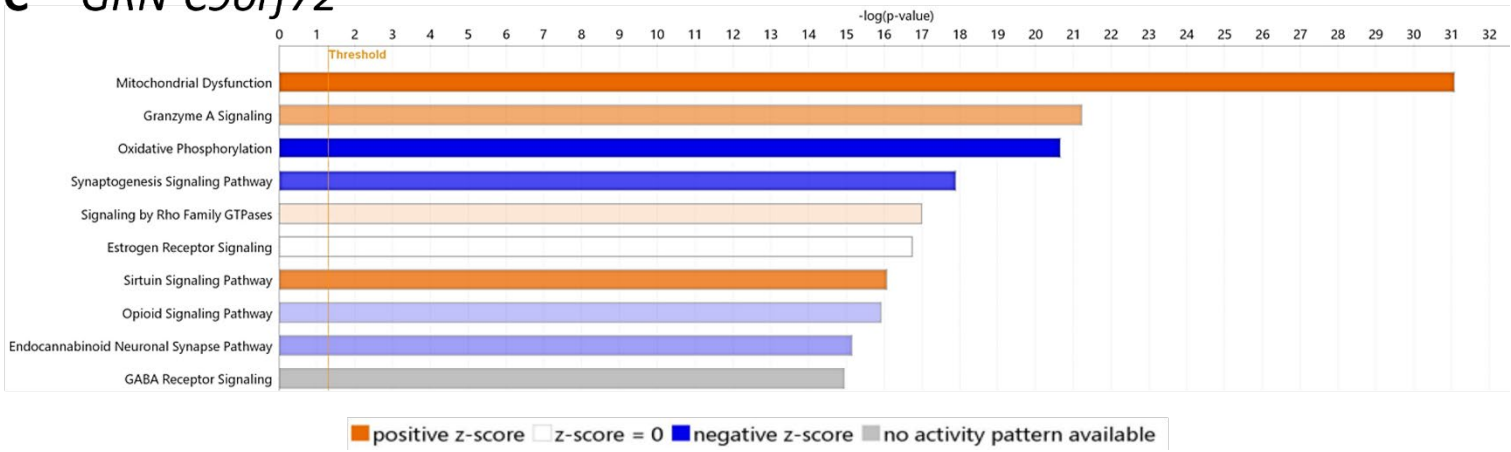

Figure 3.3: Ingenuity Pathway Analysis of differentially expressed proteins in superior frontal grey matter

Top 10 canonical pathways identified by Ingenuity Pathway Analysis as being enriched in the differentially expressed proteins meeting statistical significance following FDR-adjustment between (A) FTD-*GRN* cases and controls, (B) FTD-*C9orf72* cases and controls and (C) FTD-*GRN* and FTD-*C9orf72* cases. Vertical yellow line indicates *p*-value of 0.05 for significant enrichment of proteins within canonical pathways. Within each comparison, orange boxes indicate upregulated pathways, blue boxes indicate downregulated pathways, white boxes indicate pathways that have a z-score of 0 or are ineligible for analysis due to fewer than 4 proteins associated with the pathway, and grey boxes indicate that no activity prediction could be made.

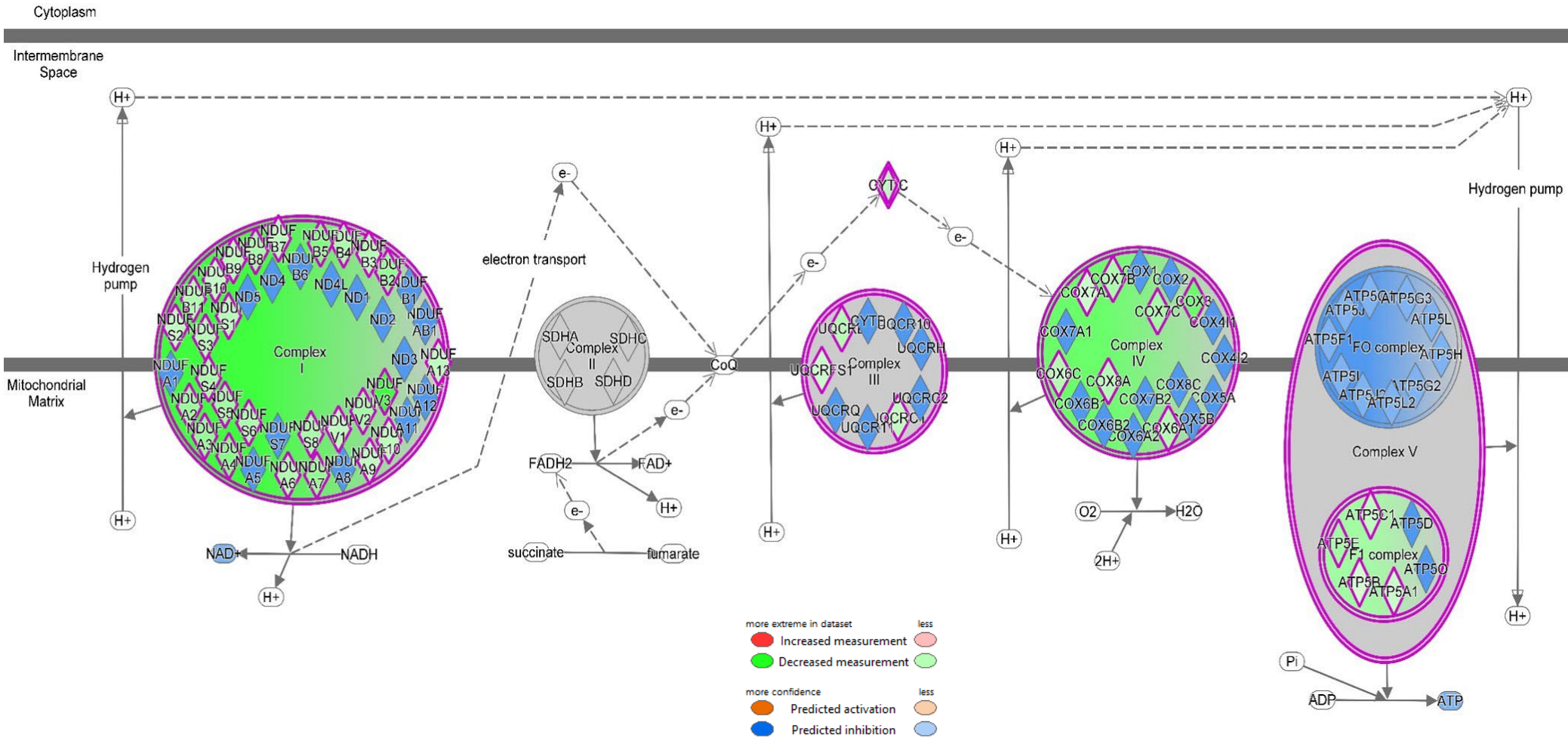

Figure 3.4: Differentially expressed proteins between FTD-GRN and FTD-C9orf72 cases identified in the oxidative phosphorylation pathway

Significantly affected proteins in FTD-*GRN* compared to FTD-*C9orf72* cases identified in the oxidative phosphorylation pathway. Shading indicates direction of protein abundance and predicted activation and inhibition of effector proteins. Schematic generated with Ingenuity Pathway Analysis.

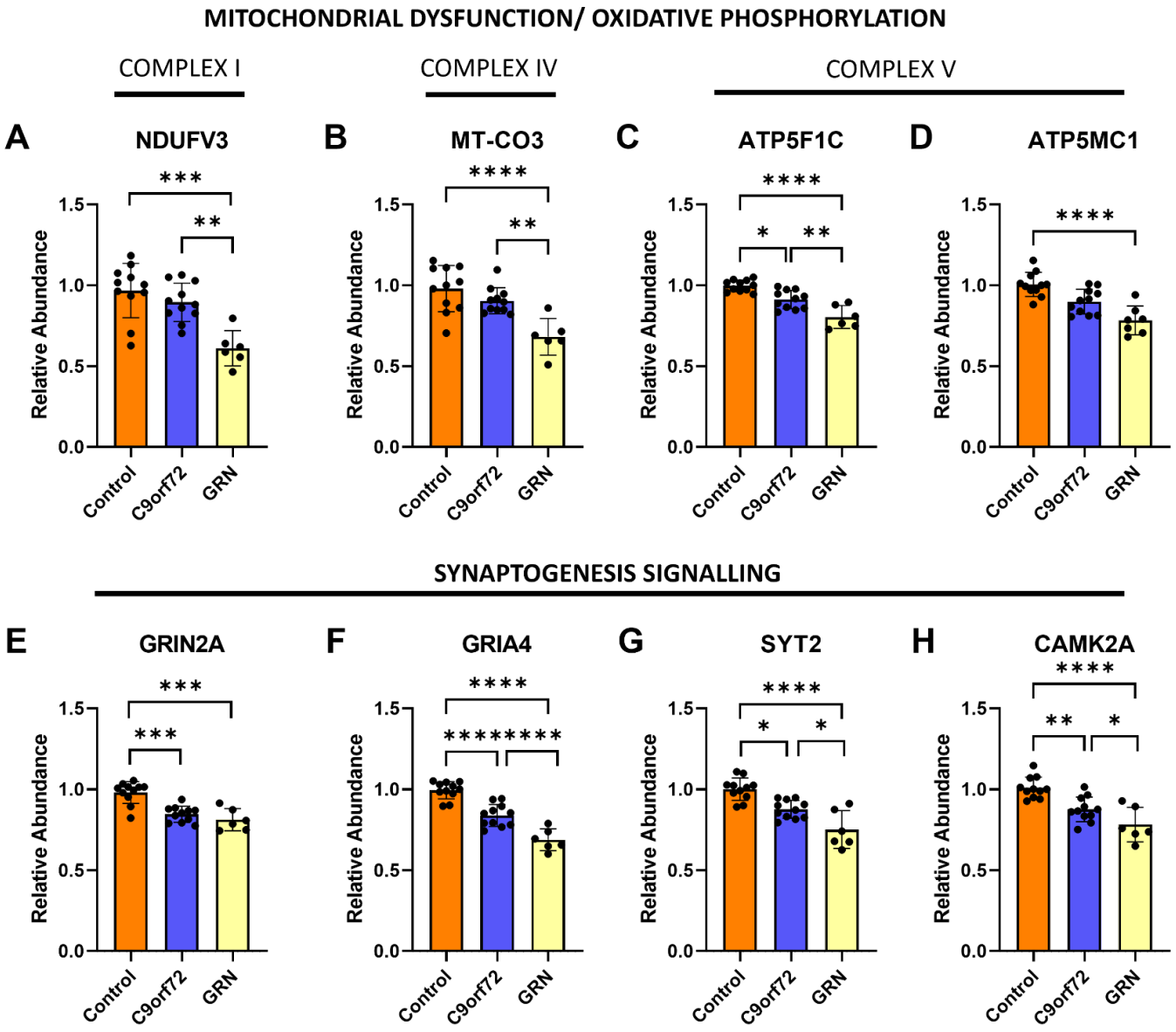

Figure 3.5: Differentially expressed proteins in frontal grey matter

Relative abundance of selected differentially expressed proteins identified in (A-D) mitochondrial dysfunction/oxidative phosphorylation pathways, (E-H) synaptogenesis signalling pathways. Protein abundances significantly altered following one-way ANOVA adjusted for PMI and age, with *p*-values adjusted for the false discovery rate. Asterisks indicate a significant difference compared to the control group in Tukey's post-test: *$p < 0.05$; **$p < 0.01$; ***$p < 0.001$, ****$p < 0.0001$.

3.3.2 Superior Frontal White Matter

In the heavily affected superior frontal white matter we identified 494,777 PSMs, resulting in 63,791 peptides and yielding a total of 5,984 unique proteins.

Comparison between sample groups by one-way ANOVA adjusted for age at death and PMI yielded significantly different abundance of a total of 1,175 proteins after FDR correction.

Further filtering on the basis of >25% fold change in the comparison of FTD-*GRN* cases with controls showed an increase in the abundance of 314 proteins and decreased abundance of 89 proteins (Figure 3.6 A, D). FTD-*C9orf72* cases showed increases in 58 and a decrease in 8 proteins compared with control cases (Figure 3.6 B, D). Comparison of the two FTD groups showed differential expression of the abundance of 98 proteins, with 93 increased and 5 decreased in FTD-*GRN* cases compared with FTD-*C9orf72* cases (Figure 3.6 C, D).

GO enrichment identified *cell-cell and cell-matrix adhesion*, and *complement activation*, *classical pathway* as the most enriched biological processes in FTD-*GRN* cases compared to controls, and enriched molecular functions including *actin*- and *actin-filament binding, calmodulin binding, cadherin binding and antigen binding* (Figure 3.7 A, B). Comparing FTD-*C9orf72* and controls, *cell-cell adhesion* was the single enriched biological process and *calcium-dependent protein binding* the only significantly enriched molecular function(Figure 3.7 C, D). *Epithelial cell-cell adhesion* was the only enriched biological process identified between the two FTD groups, and no significant molecular function enrichments were observed (Figure 3.7 E, F).

IPA identified *EIF2 signalling* as the most strongly enriched canonical pathway in both FTD-*GRN* and FTD-*C9orf72* cases compared with controls, with *mTOR signalling* also highly enriched. In FTD-*GRN* cases compared with controls, *remodelling of epithelial adherens junctions and integrin signalling* were upregulated, and *14-3-3 mediated signalling* was downregulated (Figure 3.8 A, B). Comparison between FTD-*GRN* and FTD-*C9orf72* cases showed upregulation of *remodelling of epithelial adherens junction* and *EIF2 signalling*, downregulation of *mTOR signalling* and enrichment of the *phagosome maturation* pathway (Figure 3.8 C).

Significant overlap was observed between proteins identified in the *EIF2* and *mTOR signalling* pathways, which is unsurprising as both pathways are involved in the regulation of protein synthesis (Saxton et al. 2017, Adomavicius et al. 2019). Abundance of the *EIF2* and *mTOR signalling* pathway constituent proteins AKT3 was decreased in FTD-*GRN* cases compared with controls, while levels of both RHEB and EIF3D were increased in both FTD groups compared with control cases (Figure 3.9 A-C). The abundance of GPNMB, a cell adhesion pathway protein was significantly increased in both FTD groups compared with control cases, and higher in FTD-*GRN* compared with FTD-*C9orf72* cases (Figure 3.9 D). Within the *remodelling of epithelial adherens junctions* pathway, abundance of the catenin alpha 2 protein CTNNA2, responsible for cellular adhesion was increased in both FTD groups, while abundance of the late endosome protein RAB7A was increased in FTD-*GRN* cases compared with both FTD-*C9orf72* and control cases (Figure 3.9 E-F) (Fanjul-Fernández et al. 2013). The abundance of the *phagosome maturation* pathway proteins, the lysosomal proteases cathepsins D and Z, CTSD and CTSZ, respectively, were both increased in FTD-*GRN* cases compared to both FTD-*C9orf72* and control cases, while CTSD was also increased in FTD-*C9orf72* cases compared to controls (Figure 3.9 G-H).

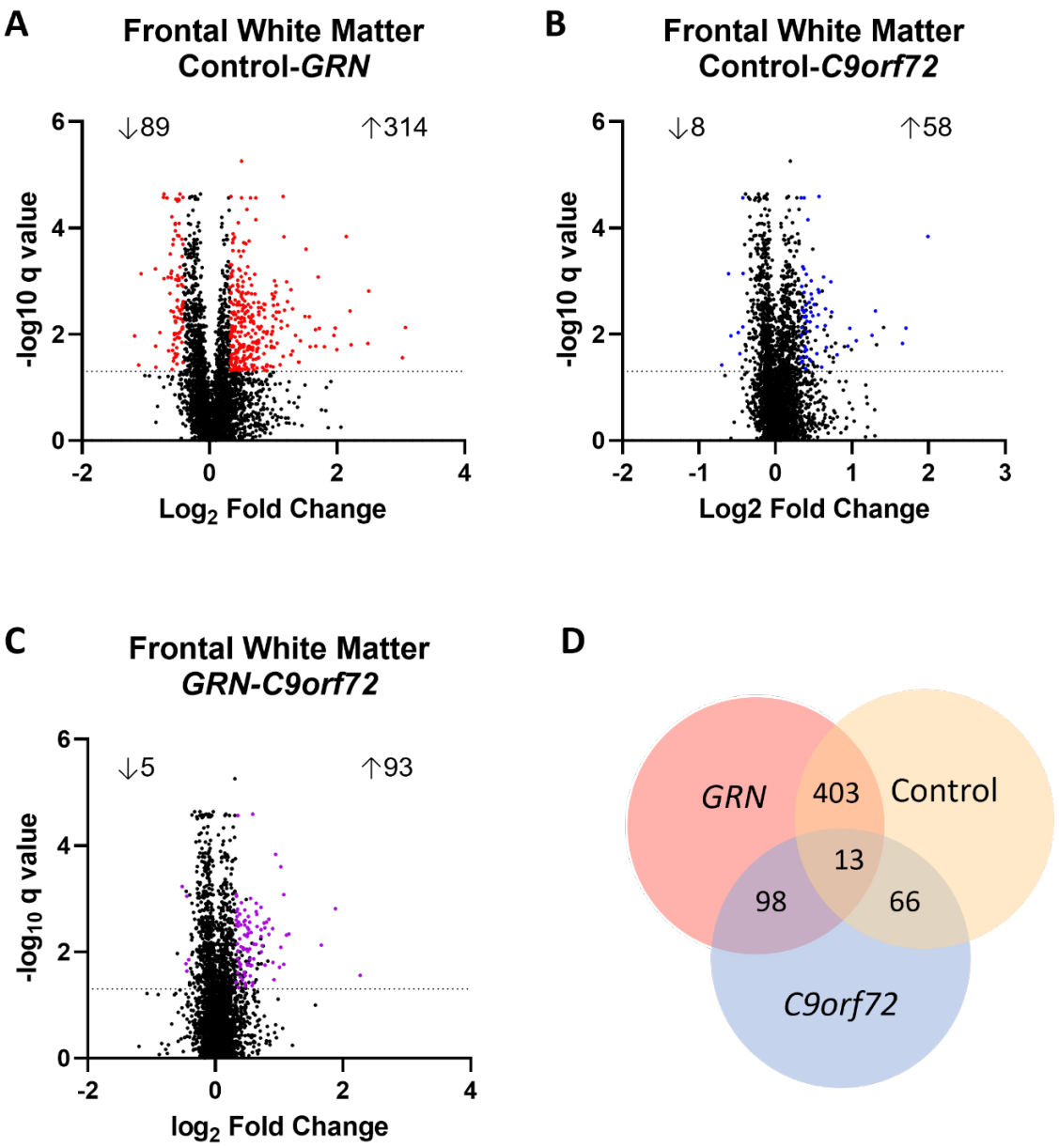

Figure 3.6: Differentially expressed proteins in superior frontal white matter

Volcano plots showing differentially expressed proteins in (A) FTD-*GRN* cases compared to controls, (B) FTD-*C9orf72* cases compared with controls, (C) FTD-*GRN* cases compared with FTD-*C9orf72* cases. Differentially expressed proteins meeting by FDR-adjusted *p*-value (*q*-value) < 0.05 by overall ANOVA, *p* < 0.05 in Tukey's post-hoc test and fold change greater than 25% indicated by coloured circles in each comparison. Dotted line indicates *q* = 0.05. Arrows indicate increase or decrease in number of differentially expressed proteins meeting all 3 criteria (D) Venn diagram summary of overlap of number of differentially expressed proteins between the 3 sample groups.

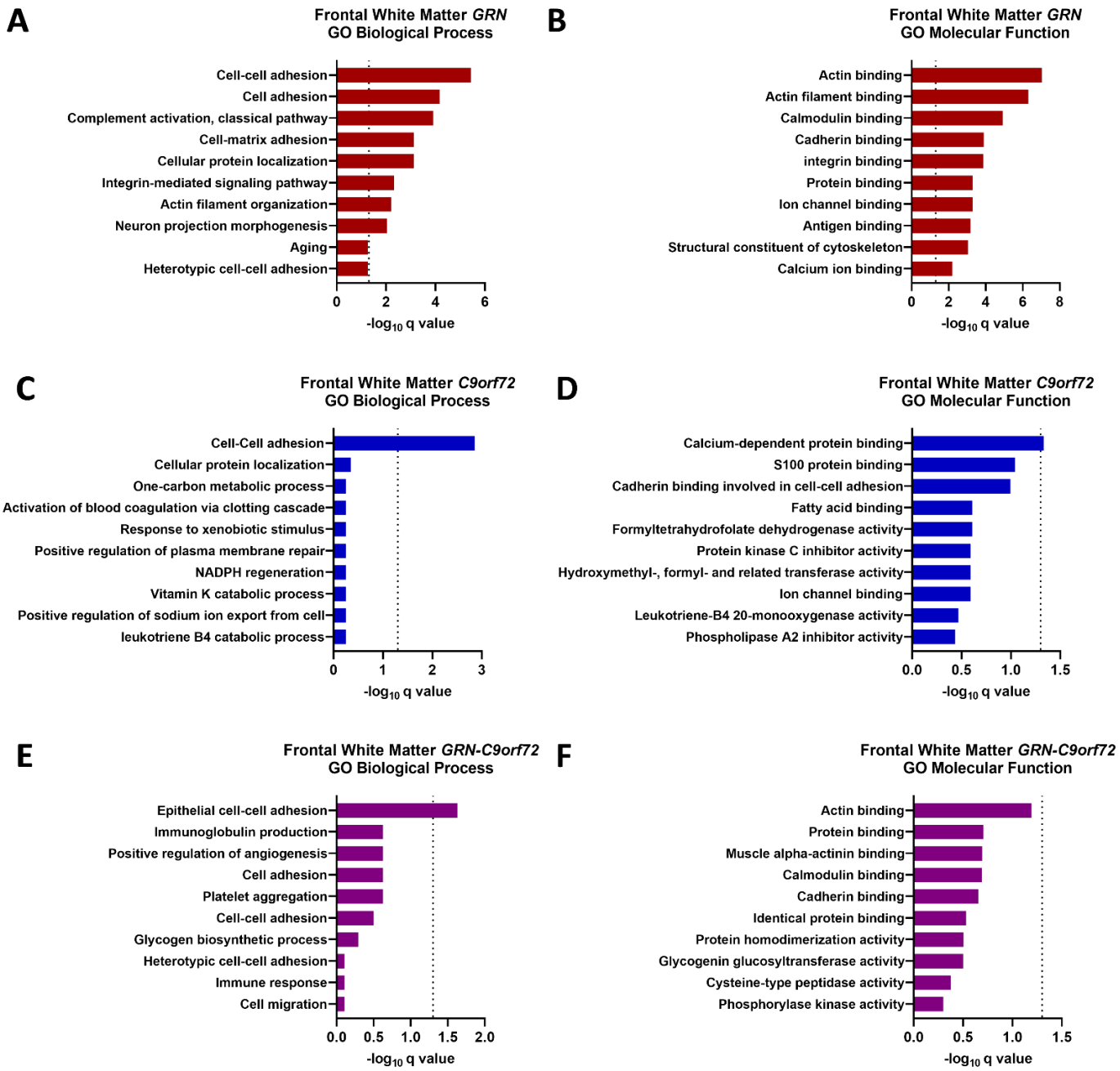

Figure 3.7: Gene ontology enrichment of differentially expressed proteins in frontal white matter

Gene ontology (GO) enrichment of the 10 most highly enriched biological processes (A, C, E) and molecular functions (B, D, F) for differentially expressed proteins meeting criteria of FDR-corrected p-value < 0.05 and fold change greater than 25% between groups in (A, B) FTD-GRN cases compared to controls, (C, D) FTD-C9orf72 cases compared with controls, (E, F) FTD-GRN cases compared with FTD-C9orf72 cases. GO terms shown meet p < 0.05 significantly enriched proteins in a biological process or molecular function. Dotted line represents FDR corrected p-value (q-value) of 0.05 for GO term enrichment.

A *GRN*-Control

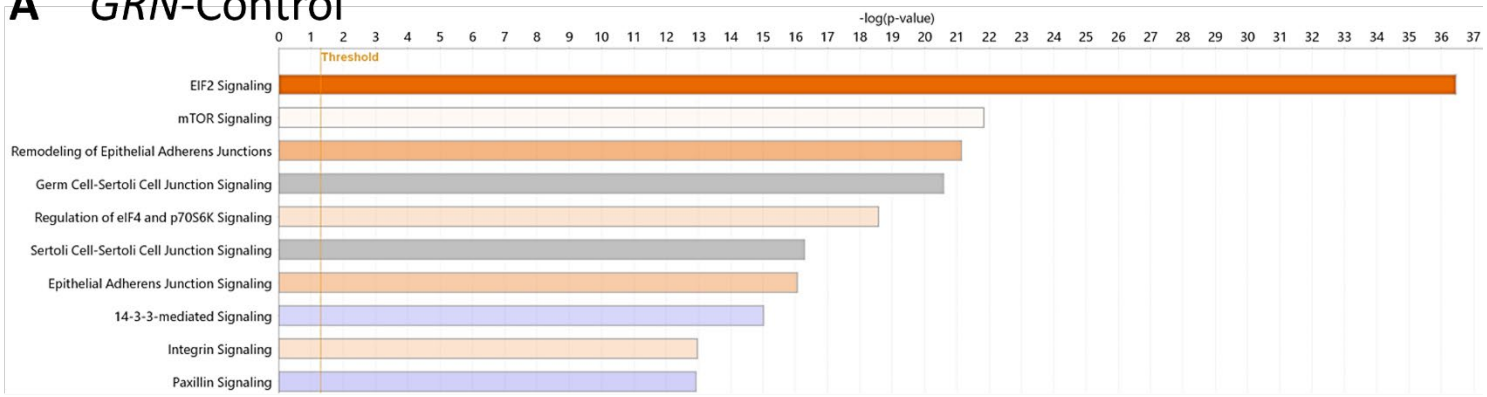

B *C9orf72*-Control

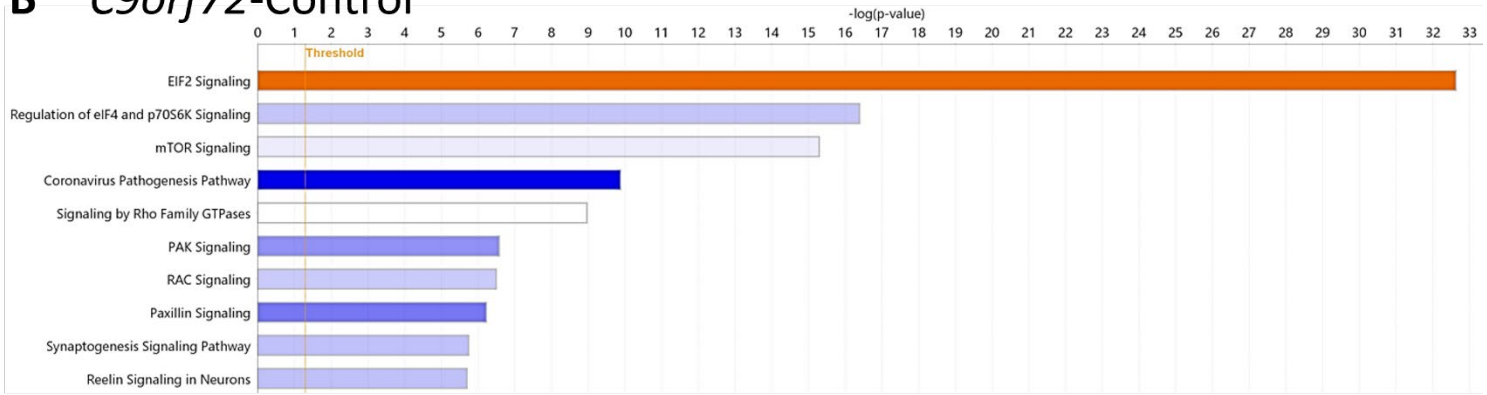

C *GRN-C9orf72*

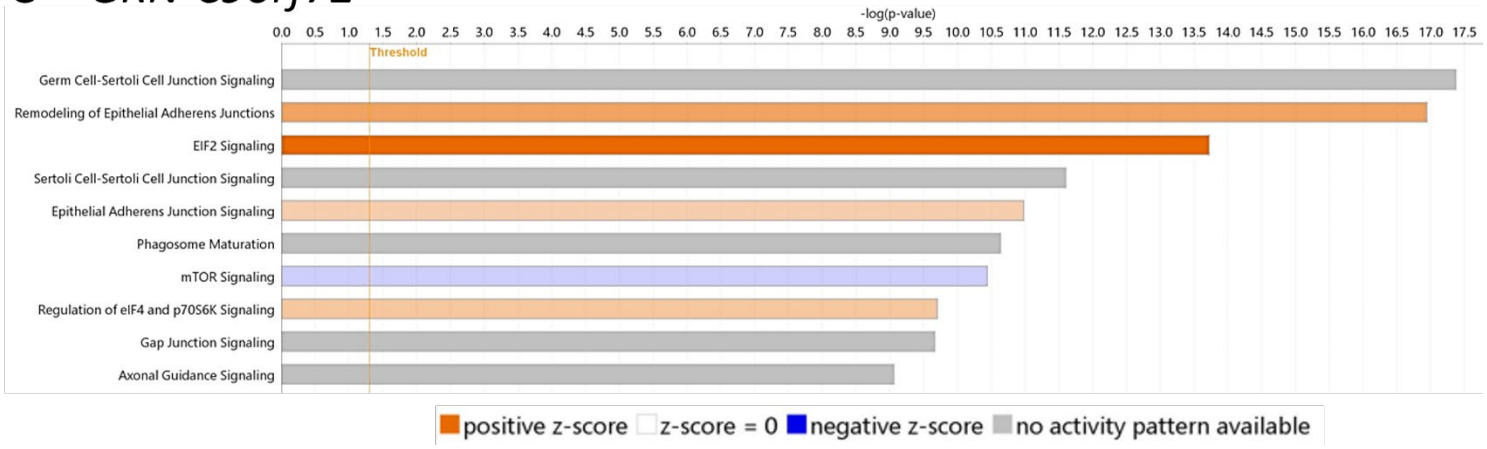

Figure 3.8: Ingenuity Pathway Analysis of differentially expressed proteins in frontal white matter

Top 10 canonical pathways identified by Ingenuity Pathway Analysis as being enriched in the differentially expressed proteins meeting statistical significance following FDR-adjustment between (A) FTD-*GRN* cases and controls, (B) FTD-*C9orf72* cases and controls and (C) FTD-*GRN* and FTD-*C9orf72* cases. Vertical yellow line indicates *p*-value of 0.05 for significant enrichment of proteins within canonical pathways. Within each comparison, orange boxes indicate upregulated pathways, blue boxes indicate downregulated pathways, white boxes indicate pathways that have a z-score of 0 or are ineligible for analysis due to fewer than 4 proteins associated with the pathway, and grey boxes indicate that no activity prediction could be made.

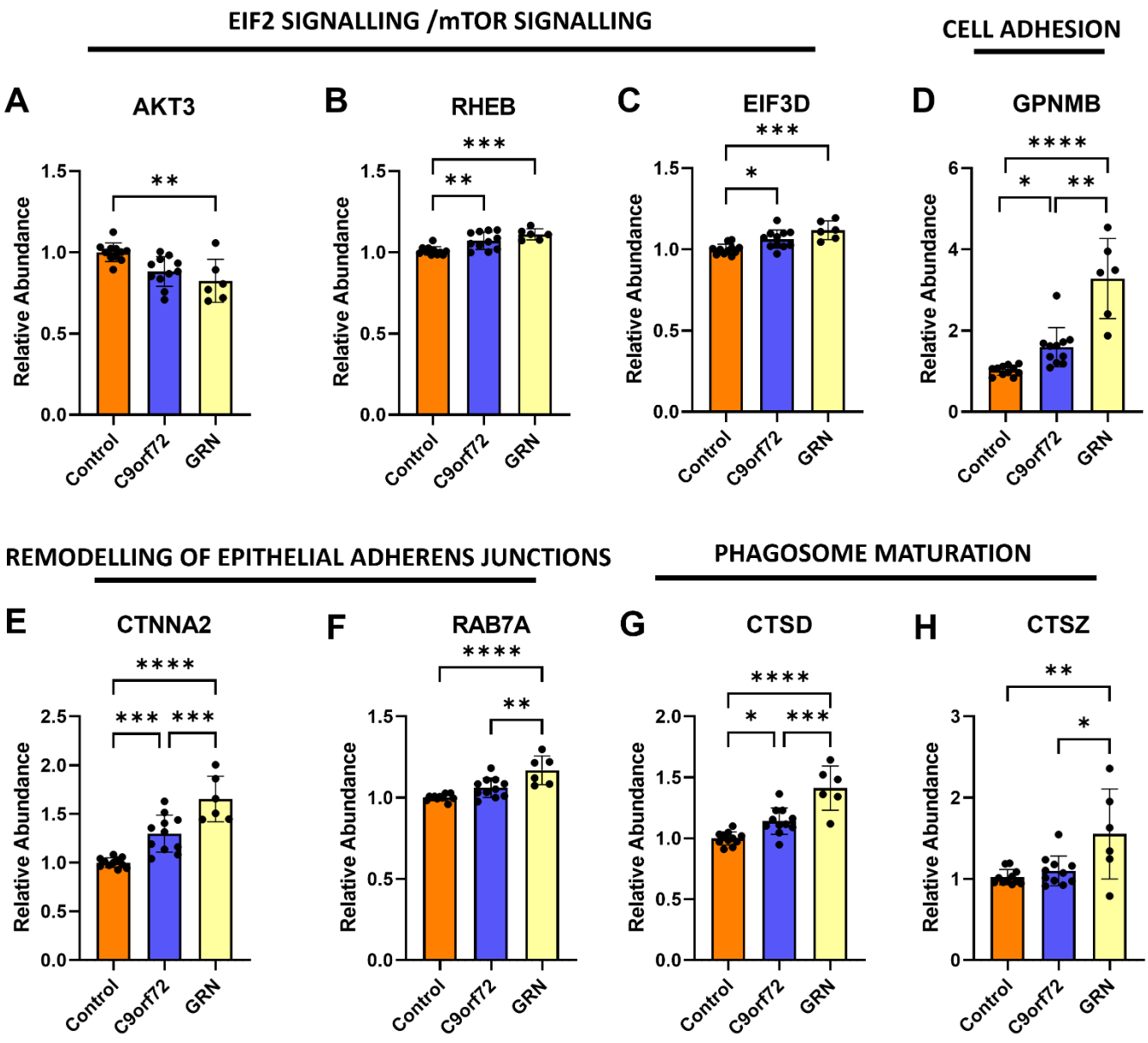

Figure 3.9: Differentially expressed proteins in frontal white matter

Relative abundance of selected differentially expressed proteins identified in (A-C) EIF2 signalling/mTOR signalling, (D) cell adhesion, (E-F) remodelling of epithelial adherens junctions, (G-H) phagosome maturation. Protein abundances significantly altered following one-way ANOVA adjusted for PMI and age, with p-values adjusted for the false discovery rate. Asterisks indicate a significant difference compared to the control group in Tukey's post-test: *$p < 0.05$; **$p < 0.01$; ***$p < 0.001$, ****$p < 0.0001$.

3.3.3 Superior Parietal Grey Matter

In the superior parietal grey matter tandem mass spectrometry proteomics identified 456,952 PSMs, resulting in 62,459 peptides and yielded a total of 5,547 unique proteins after data filtering.

Following comparison between sample groups by one-way ANOVA adjusted for age at death and PMI, the abundance of a total of 27 proteins were significantly different after FDR correction (Figure 3.10).

Applying a minimum 25% change in protein abundance produced 3 proteins that were increased in FTD-*GRN* compared to control cases (APOD, MOB3A, GM2A), and 4 that were decreased (TARS2, MT-ATP8, FAM162A, SLC4A7). No proteins were significantly altered in FTD-*C9orf72* compared to control cases (Figure 3.10 B, D). Comparison of the two FTD groups showed differential abundance of 2 proteins, with 1 increased (APOD) and 1 decreased (MT-ATP8) in FTD-*GRN* compared with FTD-*C9orf72* cases (Figure 3.11 C-F). Differences in these proteins between the two FTD groups were driven by altered protein abundance in the FTD-*GRN* group (Figure 3.11), which may indicate that these changes are a direct result of *GRN* mutations as opposed to the general effect of neurodegeneration in FTD.

GO enrichment for the comparison between FTD-*GRN* cases and controls yielded a single enriched biological process and molecular function, both related to lipid transport, however, the enriched pathways did not meet significance following FDR correction (Figure 3.12). Comparisons between FTD-*C9orf72* cases and controls, and between the two FTD groups did not identify any significant enrichments.

Similarly, due to the small number of differentially expressed proteins in this brain region, IPA did not identify significant changes in canonical pathways.

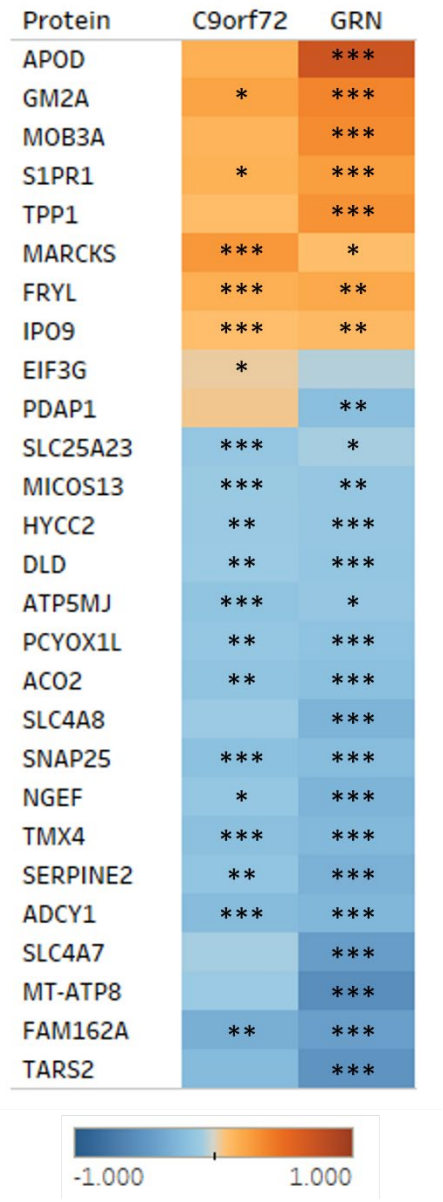

Figure 3.10: Differentially expressed proteins in the superior parietal grey matter

Abundance of proteins significantly altered following one-way ANOVA adjusted for PMI and age, with *p*-values adjusted for the false discovery rate. Heatmap showing log2 transformed fold change compared with control group. Asterisks indicate a significant difference compared to the control group in Tukey's post-test: *$p < 0.05$; **$p < 0.01$; ***$p < 0.001$.

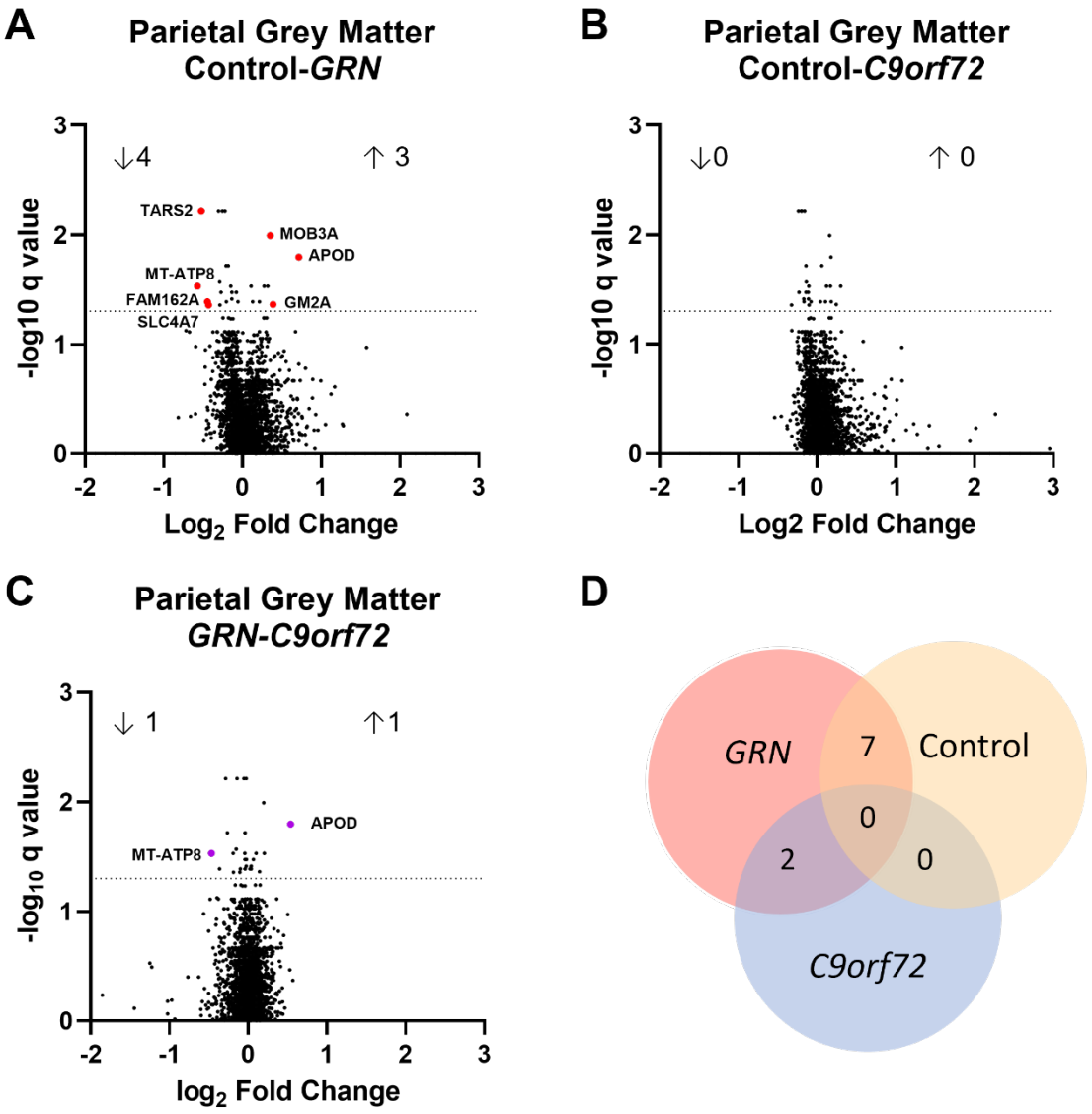
A
Parietal Grey Matter
Control-GRN
↓4
↑ 3
TARS2
MOB3A
APOD
MT-ATP8
FAM162A
GM2A
SLC4A7
-log10 q value
Log2 Fold Change
B
Parietal Grey Matter
Control-C9orf72
↓0
↑ 0
-log10 q value
Log2 Fold Change
C
Parietal Grey Matter
GRN-C9orf72
↓ 1
↑1
APOD
MT-ATP8
-log10 q value
log2 Fold Change
D
GRN
7
Control
0
2
0
C9orf72

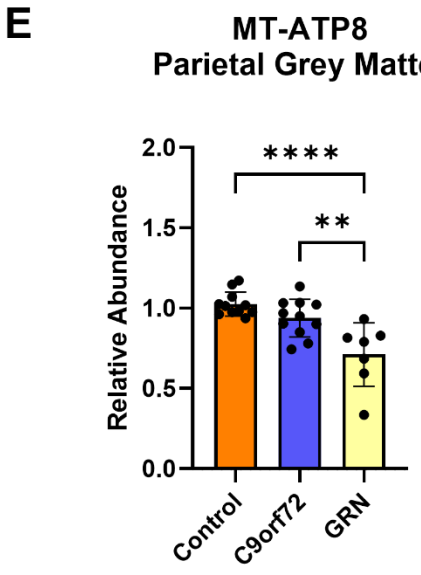
E
MT-ATP8
Parietal Grey Matter
****
**
Relative Abundance
Control
C9orf72
GRN

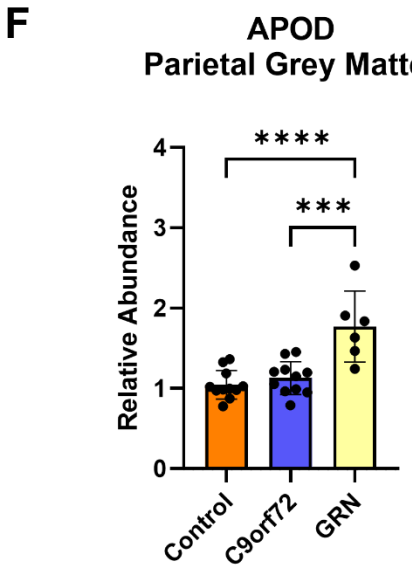
F
APOD
Parietal Grey Matter
****
***
Relative Abundance
Control
C9orf72
GRN

Figure 3.11: Differentially expressed proteins in superior parietal grey matter

Volcano plots showing differentially expressed proteins in (A) FTD-*GRN* cases compared to controls, (B) FTD-*C9orf72* cases compared with controls, (C) FTD-*GRN* cases compared with FTD-*C9orf72* cases. Differentially expressed proteins meeting FDR-adjusted *p*-value (*q*-value) < 0.05 and fold change greater than 25% are indicated by coloured circles in each comparison. Dotted line indicates *q* = 0.05. Arrows indicate increase or decrease in number of differentially expressed proteins meeting *q*-value and fold change criteria (D) Venn diagram summary of overlap of number of differentially expressed proteins between the 3 sample groups, abundance of (E) MT-ATP8 and (F) APOD in each sample. Asterisks indicate a significant difference compared to the control group in Tukey's post-test: *$p < 0.05$; **$p < 0.01$; ***$p < 0.001$, ****$p < 0.0001$.

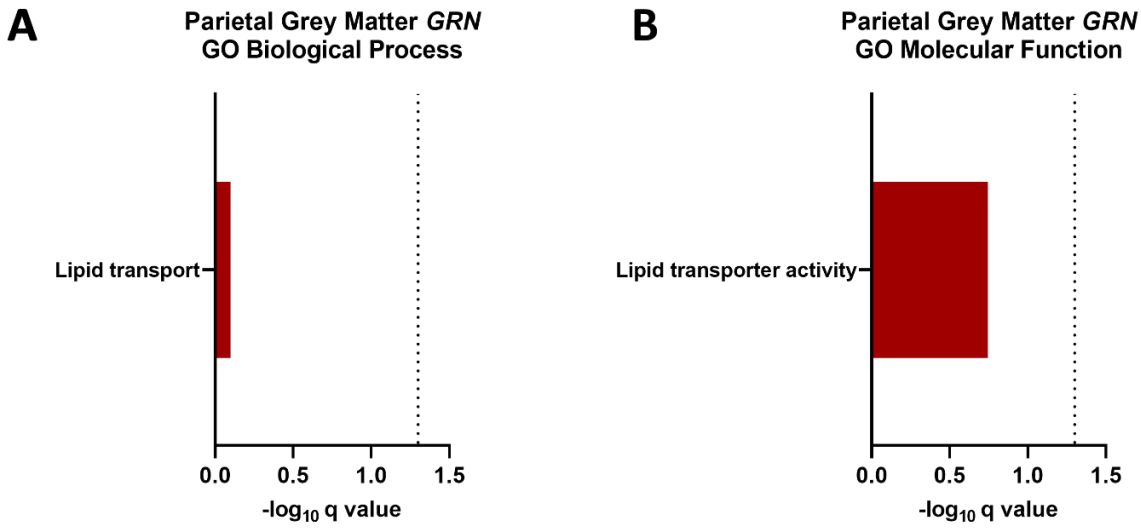

Figure 3.12: Gene ontology enrichment of differentially expressed proteins in superior parietal white matter

Gene ontology (GO) enrichment of enriched biological processes (A) and molecular functions (B) for differentially expressed proteins (FDR-adjusted p < 0.05 and > 25% fold-change) in FTD-*GRN* cases compared to controls. Dotted line represents FDR corrected *p*-value (*q*-value) of 0.05 for GO term enrichment

3.3.4 Superior Parietal White Matter

In the superior parietal white matter we identified 453,020 PSMs, resulting in 56,106 peptides and yielding a total of 5,220 identified proteins. Comparison between sample groups by one-way ANOVA adjusted for age at death and PMI yielded significantly different abundance of a total of 503 proteins after FDR correction.

Further filtering of significant proteins by fold change in the comparison of FTD-*GRN* cases with controls showed an increase in 144 proteins and decrease in 14 proteins (Figure 3.13 A, D). FTD-*C9orf72* cases showed significant differences in the abundance of 16 proteins, all increased compared with control cases (Figure 3.13 B, D). Comparison of the two FTD groups showed 60 increased and 4 decreased proteins in FTD-*GRN* cases compared with FTD-*C9orf72* cases (Figure 3.13 C, D).

The comparison between FTD-*GRN* cases and controls yielded several enriched GO terms. The most highly enriched biological processes were *cell-cell adhesion*, *nucleosome positioning, integrin-mediated signalling, and hydrogen peroxide biosynthetic process*, while for molecular functions, *protein binding* and *structural constituent of chromatin* were most enriched (Figure 3.14 A, B). No significant enrichments identified for protein pathways between FTD-*C9orf72* cases and controls met the FDR-correction threshold (Figure 3.14 C, D). Likewise, comparison between the two FTD groups showed no significant enrichment for biological process, while enriched molecular functions were observed, most significantly in *calcium-dependent protein binding* and *protein homodimerization activity* (Figure 3.14 E, F).

IPA identified numerous enriched pathways in all 3 comparisons, several of which were common between all comparisons, such as the *germ cell-Sertoli cell junction signalling* and *integrin signalling* pathways (Figure 3.15). In FTD-*GRN* cases compared to controls, downregulated *14-3-3 mediated signalling* and upregulated *epithelial adherens junction signalling* pathways were identified (Figure 3.15 A). Comparing FTD-*C9orf72* cases and controls identified downregulated *IL-22 signalling* and *mevalonate pathway I* (Figure 3.15 B). Pathways affected in the comparison

between FTD-*GRN* and FTD-*C9orf72* cases included *epithelial adherens junction signalling* and *integrin signalling* (Figure 3.15 C).

Further inspection of the *epithelial adherens junction signalling* pathway showed increased abundance of ANAX2 in both FTD groups and increased abundance of CTNN2 in FTD-*GRN* cases compared to both FTD-*C9orf72* cases and controls, while FTD-*C9orf72* cases showed a trend increase, exhibiting similar changes to abundance observed in the frontal white matter (Figure 3.16 A-B). *Mevalonate pathway* proteins HMGCS1 and MVK were significantly decreased in both FTD cases compared to controls and significantly lower in FTD-*GRN* cases compared to FTD-*C9orf72* cases (Figure 3.16 C-D). *14-3-3 signalling* and *IL-22 signalling* pathways showed overlap of protein constituents. Levels of both AKT3 and MAPK were significantly lower in both FTD groups compared with controls (Figure 3.16 E-F). *Integrin signalling* pathway protein ILK showed increased abundance in both FTD groups compared with controls, and also significantly increased in FTD-*GRN* cases compared with FTD-C9orf72 cases (Figure 3.16 G). GPNMB abundance was markedly increased in FTD-*GRN* cases compared with both FTD-*C9orf72* cases and controls, with *C9orf72* cases showing a trend increase in this brain region (Figure 3.16 H).

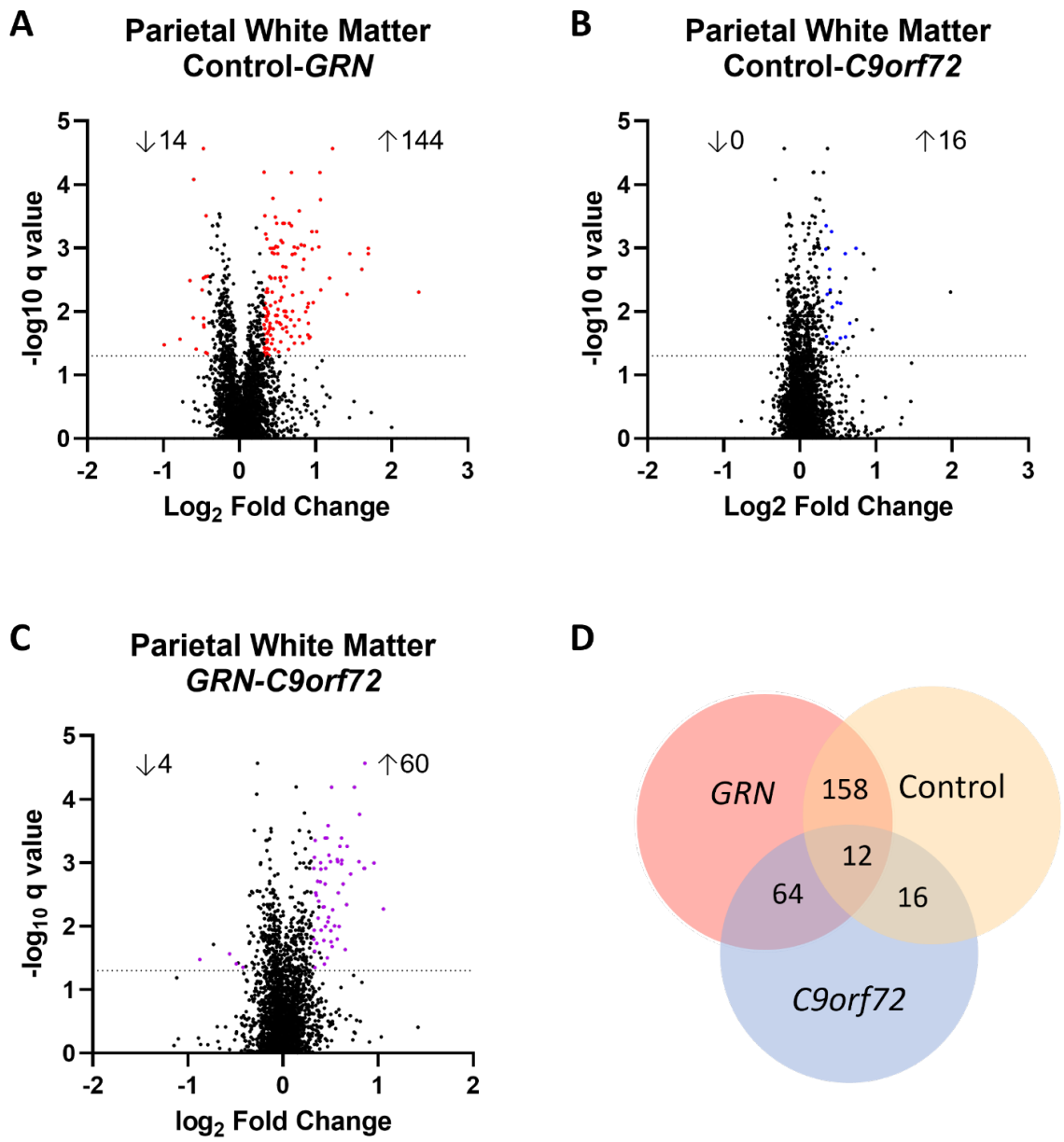

Figure 3.13: Differentially expressed proteins in superior parietal white matter

Volcano plots showing differentially expressed proteins in (A) FTD-*GRN* cases compared to controls, (B) FTD-*C9orf72* cases compared with controls, (C) FTD-*GRN* cases compared with FTD-*C9orf72* cases. Differentially expressed proteins meeting by FDR-adjusted *p*-value (*q*-value) < 0.05 by overall ANOVA, $p < 0.05$ in Tukey's post-hoc test and fold change greater than 25% indicated by coloured circles in each comparison. Dotted line indicates $q = 0.05$. Arrows indicate increase or decrease in number of differentially expressed proteins meeting all 3 criteria (D) Venn diagram summary of overlap of number of differentially expressed proteins between the 3 sample groups.

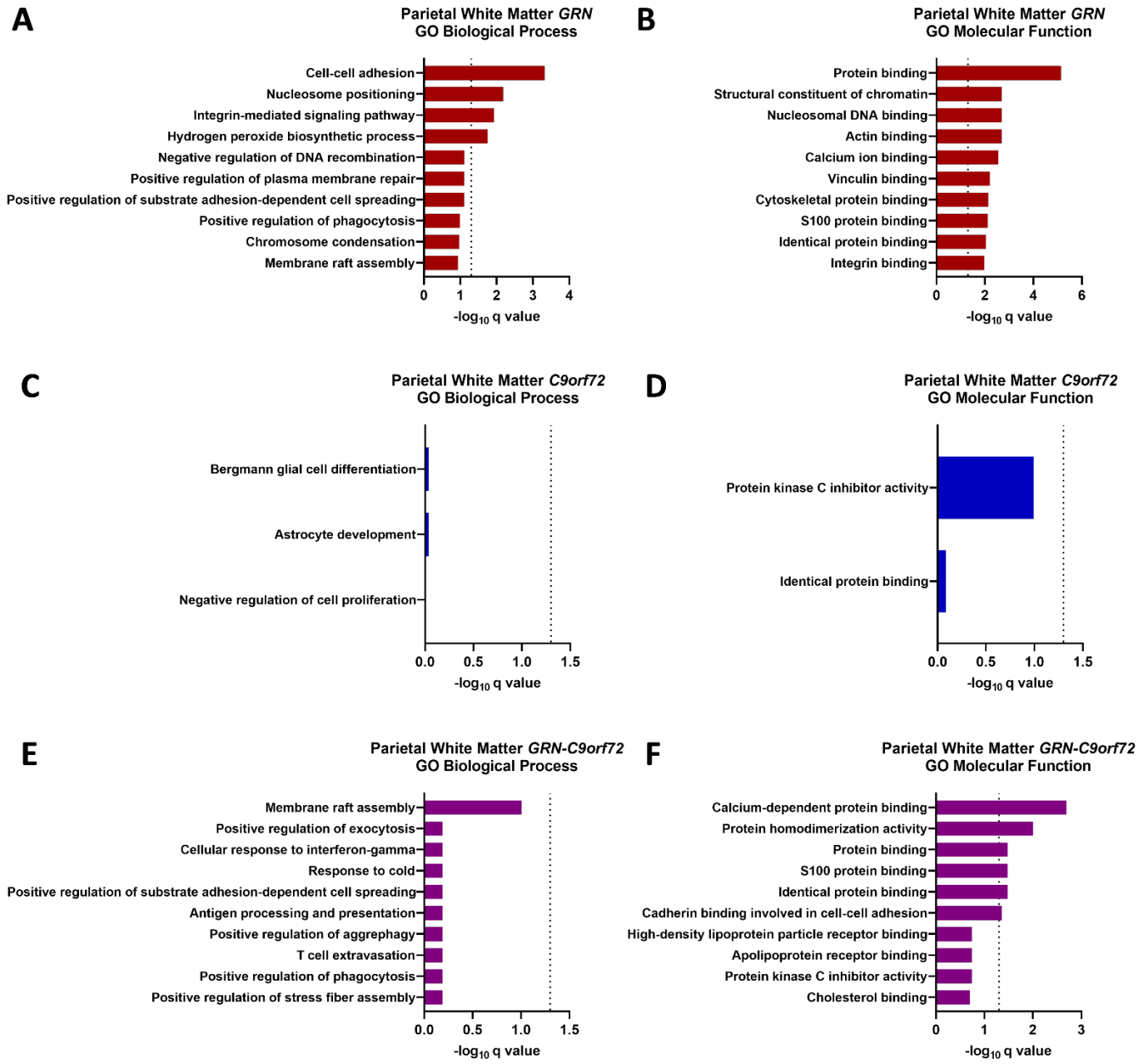

Figure 3.14: Gene ontology enrichment of differentially expressed proteins in parietal white matter

Gene ontology (GO) enrichment of the 10 most highly enriched biological processes (A, C, E) and molecular functions (B, D, F) for differentially expressed proteins meeting criteria of FDR-corrected p-value < 0.05 and fold change greater than 25% between groups in (A, B) FTD-GRN cases compared to controls, (C, D) FTD-C9orf72 cases compared with controls, (E, F) FTD-GRN cases compared with FTD-C9orf72 cases. GO terms shown meet p < 0.05 significantly enriched proteins in a biological process or molecular function. Dotted line represents FDR corrected p-value (q-value) of 0.05 for GO term enrichment.

A *GRN*-Control

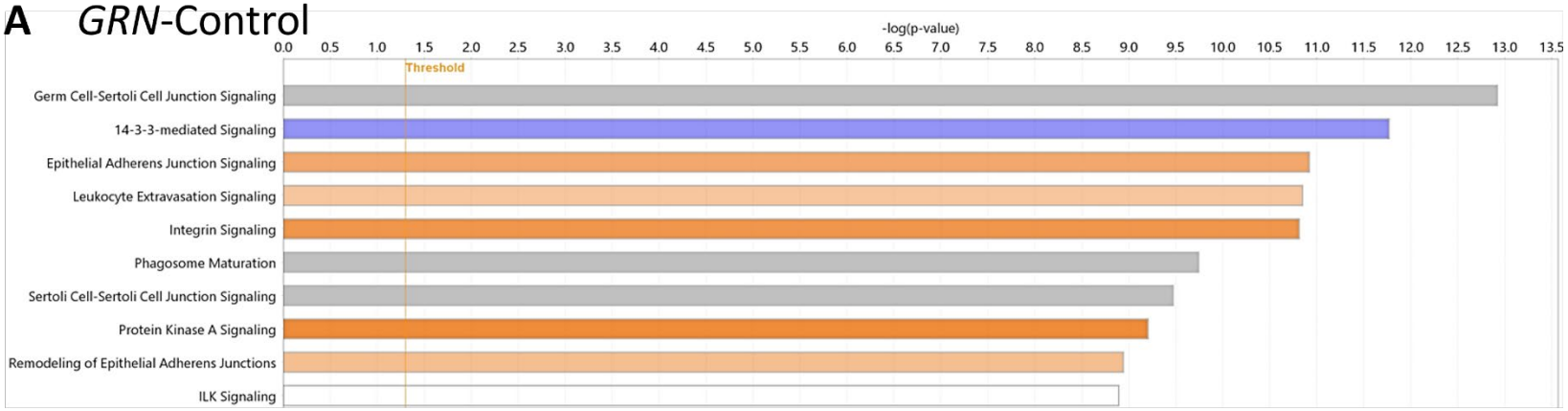

B *C9orf72*-Control

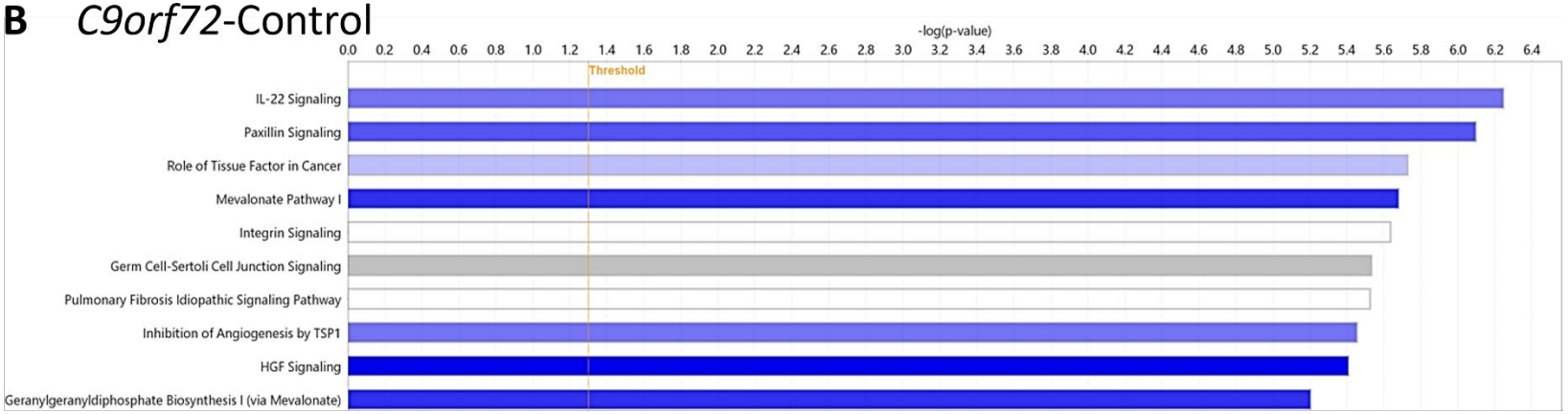

C *GRN-C9orf72*

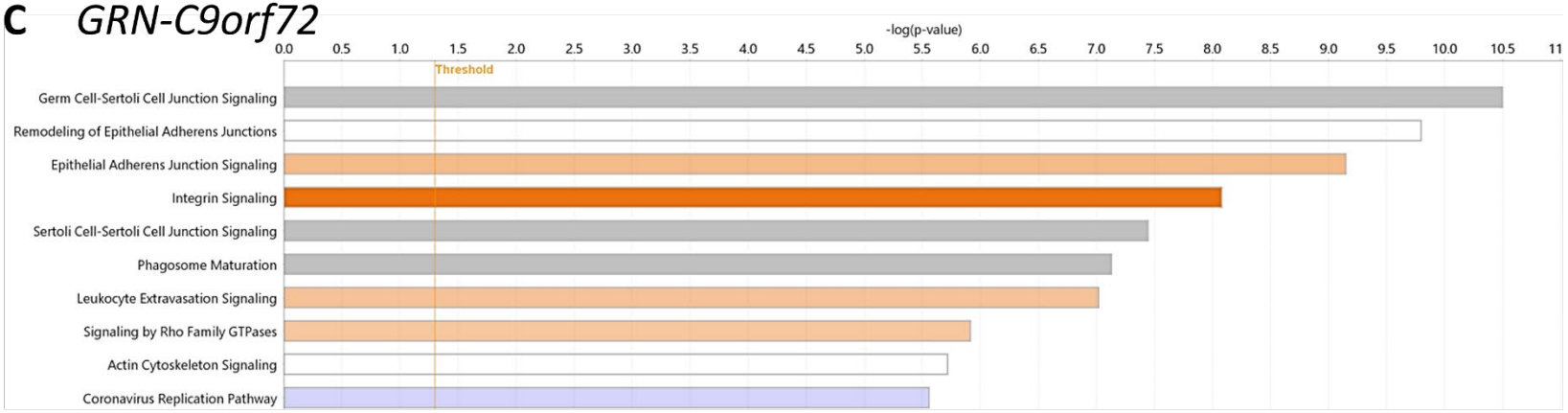

Figure 3.15: Ingenuity Pathway Analysis of differentially expressed proteins in parietal white matter

Top 10 canonical pathways identified by Ingenuity Pathway Analysis as being enriched in the differentially expressed proteins meeting statistical significance following FDR-adjustment between (A) FTD-*GRN* cases and controls, (B) FTD-*C9orf72* cases and controls and (C) FTD-*GRN* and FTD-*C9orf72* cases. Vertical yellow line indicates *p*-value of 0.05 for significant enrichment of proteins within canonical pathways. Within each comparison, orange boxes indicate upregulated pathways, blue boxes indicate downregulated pathways, white boxes indicate pathways that have a z-score of 0 or are ineligible for analysis due to fewer than 4 proteins associated with the pathway, and grey boxes indicate that no activity prediction could be made.

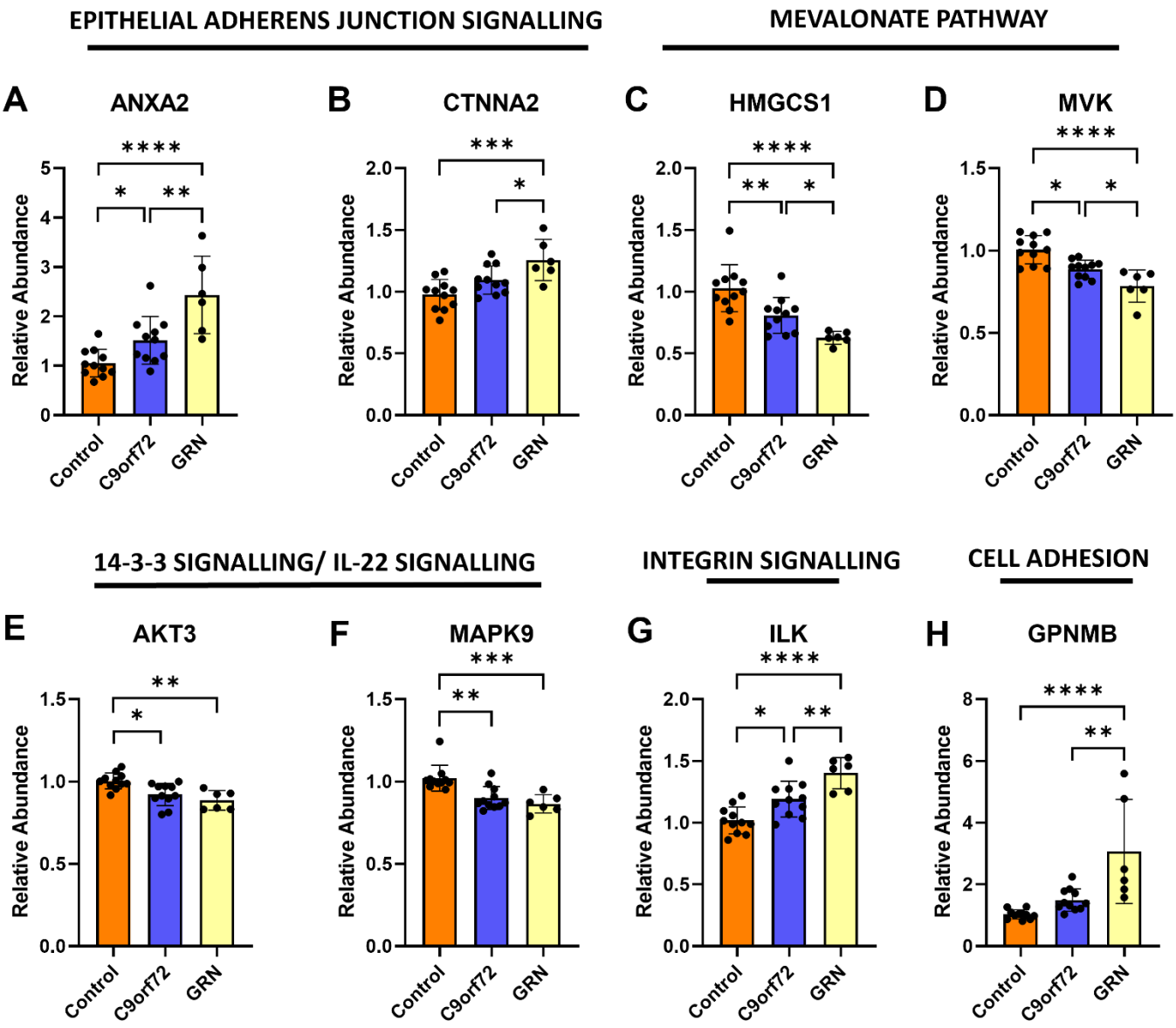

Figure 3.16: Differentially expressed proteins in parietal white matter

Relative abundance of selected differentially expressed proteins identified in (A, B) epithelial adherends junction signalling, (C-D) mevalonate pathway, (E, F) 14-3-3 signalling/ IL-22 signalling (G), integrin signalling, (H) cell adhesion. Protein abundances significantly altered following one-way ANOVA adjusted for PMI and age, with p-values adjusted for the false discovery rate. Asterisks indicate a significant difference compared to the control group in Tukey's post-test: *$p < 0.05$; **$p < 0.01$; ***$p < 0.001$, ****$p < 0.0001$.

3.4 Discussion

This chapter describes the first proteomic analysis of post-mortem FTD brain from cases carrying *GRN* and *C9orf72* mutations compared with normal controls. We discovered that the proteomic signatures of FTD with TDP-43 neuropathology differ between cases with *GRN* and *C9orf72* mutations more than within the genotype groups and describe proteomic changes in the relatively unaffected parietal lobe (Mahoney et al. 2012, Cash et al. 2018) for the first time. The most significant changes were observed in the heavily-affected frontal grey matter, while the least significant changes occurred in the relatively-unaffected parietal grey matter. Proteomic changes in all brain regions were more substantial in FTD-*GRN* cases than FTD-C*9orf72* cases, reflecting more aggressive neurodegeneration in FTD-*GRN* cases (Rohrer et al. 2010, Ameur et al. 2016). Interestingly, proteomic changes were significantly greater in parietal white compared to parietal grey matter of FTD-*GRN* and FTD-*C9orf72* cases, in agreement with our lipidomic findings (Marian et al. 2023). This suggests that FTD impacts on white matter prior to grey matter, and implies that degeneration of myelin and neuronal axons precede neuronal loss.

In the heavily affected superior frontal grey matter, one of the most significant changes to the proteome between the two FTD groups was decreased abundance of mitochondrial respiratory complex proteins in FTD-*GRN* cases compared with FTD-*C9orf72* cases. In line with these results, in chapter 2, we demonstrated acylcarnitine accumulation in this brain region in FTD-*GRN* cases alone, suggestive of impaired mitochondrial function, as acylcarnitines are formed to transport fatty acids into the mitochondria for β-oxidation (Rinaldo et al. 2002, Marian et al. 2023). Mitochondrial dysfunction has been described as a feature of Alzheimer's disease (AD) and Parkinson's disease (PD), and recently in FTD-*GRN* cases as well as ALS cases carrying *C9orf72* repeat expansions (Lin et al. 2006, Mehta et al. 2021, Miedema et al. 2022). Subunits from all respiratory chain complexes were decreased in FTD-*GRN* cases compared with controls, however when compared with FTD-*C9orf72* cases, the components that were differentially affected in FTD-*GRN* cases were primarily complex I, IV and V (ATP synthase). Similar findings are observed in the parietal grey matter, where abundance of the mitochondrial ATP synthase subunits MT-ATP8 and ATP5MJ are both significantly decreased in FTD-*GRN* cases, while ATP5MJ alone is decreased in FTD-*C9orf72* cases. Mitochondrially-

encoded MT-ATP8 is a component of the F0 subunit of ATP synthase, and its loss has been associated with mitochondrial dysfunction, impaired energy production and increased production of reactive oxygen species (ROS) (Houštěk et al. 2006, Morava et al. 2006, Weiss et al. 2012). Abundance of the mitochondrial threonyl tRNA synthetase TARS2 is also significantly decreased specifically in FTD-*GRN* cases in the parietal grey matter, which may indicate that synthesis of mitochondrially-encoded proteins is decreased in these cases (Zheng et al. 2021).

Homozygous *GRN* loss leads to the lysosomal storage disease neuronal ceroid lipofuscinosis (NCL), and interestingly, a well-described pathological feature of NCL is accumulation of the lipophilic subunit C of mitochondrial ATP synthase (SCMAS) within lipofuscin deposits in neuronal lysosomes (Ezaki et al. 1995). SCMAS accumulation is thought to result from abnormal lysosomal catabolic function, and has also been described in lysosomal lipofuscin inclusions in FTD-*GRN* cases (Gotzl et al. 2014, Palmer 2015, Ward et al. 2017). While it is unclear whether previously described accumulation of undegraded SCMAS and the loss of mitochondrial proteins we observe in FTD-*GRN* cases are closely connected pathologically, myelin degeneration has been proposed to alter neuronal energetics and promote mitochondrial stress (Dutta et al. 2006, Lee et al. 2012, Ravera et al. 2015). Neurons are not thought to readily utilise β-oxidation for energy production, however disrupted β-oxidation in glial cells has the potential to disrupt neuronal energetics indirectly, as upon neurons rely heavily on these cell types for the provision of energy substrates (Bélanger et al. 2011). Oligodendrocytes provide energy substrates to neurons for ATP production, and myelin decreases the energetic demand on neurons by providing insulation to neuronal axons and concentrating voltage gated sodium ion channels at the nodes of Ranvier (Pedraza et al. 2001, Dutta et al. 2006, Fünfschilling et al. 2012, Lee et al. 2012). Neurons are energetically demanding cells and generate the majority of their ATP through oxidative phosphorylation, a process that produces high levels of ROS (Massaad et al. 2011, Zheng et al. 2016). In the absence of myelin, the increased energy demand on neurons from increased ATP production is likely to produce high levels of ROS, which in turn has the potential to lead to oxidative stress, damaging mitochondria and promoting neurodegeneration (Nolfi-Donegan et al. 2020, Sinenko et al. 2021, Ullah et al. 2021). Our previous findings indicate that demyelination is a pronounced feature in the corresponding frontal white matter in FTD-*GRN* cases, and more

severe than in FTD-*C9orf72* cases, which has the potential to destabilise neuronal energetics, promote mitochondrial dysfunction and promote clearance of damaged mitochondria (Martins et al. 2015, Marian et al. 2023).

The *synaptogenesis signalling* pathway was downregulated in the frontal grey matter in both FTD groups but was more pronounced in FTD-*GRN* cases. This is exemplified by decreased abundance of glutamatergic NMDA and AMPA receptor subunits (GRIN2A, GRIA4), the NMDA receptor-binding calcium/calmodulin-dependent protein kinase 2A (CAMK2A) and synaptotagmin 2 (SYT2), important for Ca^{2+} dependent neurotransmitter release (Lisman et al. 2002, Pang et al. 2006). Synaptic dysfunction has been described as a feature of FTD cases previously, and increased microglial-mediated synaptic pruning has been described in both FTD-*GRN* and FTD-*C9orf72* cases (Ferrer 1999, Lui et al. 2016, Murley et al. 2018, Lall et al. 2021). Additionally, NMDA receptor hypofunction has previously been reported in a mouse model of FTD (Warmus et al. 2014). Consistent with these findings, the NMDA receptor antagonist memantine, while widely used to treat the glutamate-mediated excitotoxicity symptoms of AD, is not a beneficial treatment in FTD cases (Parsons et al. 2007, Boxer et al. 2013). Importantly, synaptic transmission is an energetically demanding process, and the mitochondrial dysfunction signature we observe in both FTD groups in this brain region may impact the capacity for synaptic transmission (Harris et al. 2012). Additionally, our chapter 2 results showed significantly lower levels of the abundant neuronal marker βIII-tubulin and a trend decrease of the axonal marker neurofilament light in FTD-*GRN* cases in the frontal white matter, which may indicate that the downregulated synaptic signalling pathway observed in the frontal grey matter may partially result from a gross loss of neurons, reflecting the general neurodegenerative process (Marian et al. 2023).

In the heavily affected superior frontal white matter, *cell adhesion* and related pathways such as *remodelling of epithelial adherens junctions* and *integrin binding* were upregulated in both FTD groups, and similarly, this feature was observed in the parietal white matter. This may be a result of active remodelling of the extracellular matrix following neurodegeneration, and accordingly, related molecular function GO terms, such as *actin and cadherin binding* are also enriched in the frontal grey matter, but more notably in FTD-*GRN* cases (Pinheiro et al. 2018, Tewari et al. 2022).

A pronounced increase in the abundance of glycoprotein nonmetastatic melanoma protein B (GPNMB) was observed in the heavily affected frontal white matter in both FTD groups, while in the less-affected parietal white matter GPNMB increase was observed in FTD-*GRN* cases only. Proteomic analysis of brain samples from aged *Grn*-/- mice similarly identified a pronounced increase of GPNMB levels, and its increased abundance was confirmed in FTD-*GRN* cases by immunostaining, with the most pronounced increase observed in the frontal white matter and colocalising with the microglial marker Iba1 (Huang et al. 2020). GPNMB is highly expressed in microglia, and is thought to play a role in phagocytosis, particularly in response to lipid accumulation (Li et al. 2010, Satoh et al. 2019). GPNMB upregulation has been shown in response to demyelination, and upon lipid accumulation following pharmacological inhibition of the lysosomal lipase glucocerebrosidase (Vardi et al. 2016, Moloney et al. 2018, Taghizadeh et al. 2022). Its accumulation has also previously been reported in brain tissue of AD, PD, ALS motor neurons and CSF of adrenoleukodystrophy cases, potentially signifying a common disease mechanism involving lysosomal dysfunction and demyelination in these neurodegenerative diseases, which is in line with our findings of more pronounced demyelination in FTD-*GRN* cases compared with FTD-*C9orf72* cases in this brain region (Nagahara et al. 2017, Moloney et al. 2018, Satoh et al. 2019, Taghizadeh et al. 2022, Marian et al. 2023).

Phagosome maturation was also identified as an enriched pathway in the frontal white matter. Increased abundance of the lysosomal protease cathepsin D (CTSD) was observed in both FTD groups while cathepsin Z (CTSZ) was increased only in FTD-*GRN* cases. Progranulin has been shown to regulate the function of CTSD, essential for the cleavage of prosaposin into individual saposins A-D (Beel et al. 2017, Valdez et al. 2017). Increased levels of both CTSD and CTSZ was similarly observed in frontal cortex from *Grn* -/- mice and CTSD accumulation has also been observed in frontal cortex of FTD-*GRN* cases (Gotzl et al. 2014, Huang et al. 2020). Under physiological conditions, both *GRN* and *C9orf72* have roles related to lysosomal function, and therefore these findings may be indicative of an increased degradative compensation for the accumulation in the number or size of lysosomes in both FTD-*GRN* and FTD-*C9orf72* cases as noted by other groups (O'Rourke et al. 2016, Evers et al. 2017, Ward et al. 2017).

In the less-affected parietal grey matter region, a single enriched pathway was identified in lipid transport in FTD-*GRN* cases compared to controls, but did not meet significance following FDR correction. Isobaric labelling, allowing for relative quantitation of protein levels robustly across individual samples ensured that all identified proteins could be directly compared across the 3 sample groups. However, a phenomenon of isobaric labelling is the potential of ion interference to dampen the observed fold change (Savitski et al. 2013, Li et al. 2014). The lack of significant GO enrichments can likely be attributed to the reasonably stringent criteria potentially masking some of the more subtle protein changes in the less-affected brain regions.

It is interesting to note that proteomic changes in the parietal lobe are more severe in the WM than the GM, and a substantial proportion of the significantly affected proteins identified in the GM occur in proteins involved in lipid metabolism (APOD, GM2A, S1PR1, HYCC2). Apolipoprotein D (APOD) was significantly increased between FTD-*GRN* and FTD-*C9orf72* cases. APOD is a lipid transporter induced by oxidative stress and inflammation and proposed to have neuroprotective roles through its antioxidant activity, playing a role in preventing lipid peroxidation (Ganfornina et al. 2008, Bhatia et al. 2012, Bhatia et al. 2013). Abundance of the ganglioside GM2 activator protein (GM2A) was also strongly increased in both FTD groups and especially in FTD-*GRN* cases. GM2 activator protein acts to facilitate breakdown of gangliosides, sialic acid-containing lipids enriched in neuronal cell membranes, in a similar mechanism to which saposins facilitate function of sphingolipid catabolic enzymes (Schnaar et al. 2014, Sandhoff 2016). Interestingly, progranulin is thought to play a role in ganglioside catabolism through its interaction with the ganglioside catabolic enzyme hexosaminidase A, with a recent study showed evidence of ganglioside accumulation FTD-*GRN* cases (Chen et al. 2018, Boland et al. 2022). Increased abundance of GM2A may be indicative of increased catabolism of GM2 gangliosides in both FTD groups in this brain region, or a consequence of increased lysosomal content, indicating common dysregulation in FTD caused by these gene mutations.

In the less affected parietal white matter region, reduced abundance of proteins involved in the *mevalonate pathway* were observed in both FTD groups. The mevalonate pathway is responsible for production of isoprenoid and sterol precursors for cholesterol synthesis (Buhaescu et al. 2007). Decreased abundance of the HMG CoA synthase enzyme HMGCS1,

responsible for the synthesis of HMG-CoA, and mevalonate kinase enzyme MVK, which catalyses the first committed step for the mevalonate pathway were observed in both FTD groups, but were most pronounced in FTD-*GRN* cases. This is an interesting finding in light of our chapter 2 results, where we uncovered significant accumulation of cholesterol esters in FTD-*GRN* cases, with a trend decrease in unesterified cholesterol in both FTD groups in this brain region. In light of the concomitant phagocytic and lysosomal alterations observed in this brain region we hypothesised that impaired turnover of cholesterol released from myelin may be being stored as cholesterol esters (Cantuti-Castelvetri et al. 2018, Marian et al. 2023). To this end, impaired lysosomal function and impaired lipid degradation pathways have been shown to be an early pathological finding in *Grn*-/- mice (Huang et al. 2020). Impaired cholesterol clearance has been shown to decrease the rate of cholesterol synthesis and impair remyelination, and the accumulation of esterified cholesterol in the parietal white matter of FTD-*GRN* cases may explain the more prominent loss in the enzymes required to produce cholesterol synthesis precursors (Lund et al. 2003, Cantuti-Castelvetri et al. 2018, Berghoff et al. 2022). Importantly, the mevalonate pathway is also responsible for the formation of ubiquinone, a mitochondrial electron transporter with antioxidant properties, essential for protecting mitochondrial DNA against oxidative damage and preventing membrane lipid peroxidation (Pobezhimova et al. 2000, Crane 2001).

A challenge of profiling post-mortem human brain samples is the difficulty in teasing apart changes that result specifically from the genetic causes underlying inherited FTD from those changes resulting from the neurodegenerative process common to FTD in general. Therefore, it would be beneficial to determine whether the proteomic changes we observe in these cases are shared with sporadic FTD cases, in order to better understand the gene versus general FTD changes. Additionally, applying cell-type enrichment methods would improve our understanding of the contribution of distinct cell types to the proteomic changes observed and potentially identify cell-type specific dysregulated pathways.

3.5 Conclusion

In this chapter we describe proteomic changes in post-mortem brain tissue from FTD cases carrying the most common genetic mutations leading to behavioural variant FTD with TDP-43 pathology, heterozygous loss of *GRN* and *C9orf72* repeat expansions. For the first time, we describe proteomic changes to both heavily affected and less affected brain regions, including in understudied white matter, and relate these changes to our matched lipidomic findings. We have determined that FTD-*GRN* and FTD-*C9orf72* cases show strong dysregulation in both grey and white matter regions, however, FTD-*GRN* cases show a stronger protein dysregulation signature than FTD-*C9orf72* cases in all brain regions profiled. We have uncovered dysregulated pathways in common between the two FTD groups, including significant loss of mitochondrial and synaptic proteins in grey matter, which was more pronounced in FTD-*GRN* cases compared with FTD-*C9orf72* cases. In white matter, *phagosome maturation* pathway proteins were increased and *mevalonate pathway* proteins were decreased, and we observe agreement between our proteomic and lipidomic findings. Further investigation into proteomic changes in sporadic FTD cases would further our understanding of the mechanisms by which inherited gene mutations predispose to FTD.

Chapter 4: Investigating the myelin lipid galactosylceramide as a plasma biomarker of FTD

4.1 Background

Myelin is highly enriched in cholesterol and two glycosphingolipids that are relatively unique to myelin: galactosylceramide and sulfatide (Schmitt et al. 2015). Galactosylceramide (GalCer, also known as cerebroside) and sulfatide (ST) constitute approximately 19% and 4%, respectively, of the dry weight composition of myelin in the CNS (O'Brien et al. 1965). Myelin GalCer is preferentially formed from very long chain ceramides, constituting a sphingosine backbone and commonly a C22-C24 N-acyl chain. In the CNS, these lipids are synthesised exclusively by ceramide synthase 2 in oligodendrocytes (Laviad et al. 2008, Teo et al. 2023).

Whereas GalCer makes up over 99% of hexosylceramide (HexCer) in the CNS, its structural isomer Glucosylceramide (GluCer) is the more abundant isomer in organs other than the brain (Vanier et al. 1975, Reza et al. 2021). GalCer and GluCer differ only in the orientation of a single hydroxyl group on the hexose headgroup (Figure 4.1). Since these isomers cannot be distinguished on the basis of mass or through conventional lipidomic analyses employing reverse-phase LC-MS/MS, they are generally referred to as HexCer. Separation of GalCer and GluCer requires specialised normal phase chromatography (Boutin et al. 2016) or differential ion mobility separation (Xu et al. 2019) coupled to mass spectrometry. Alternatively, the isomers can be distinguished using traditional biochemical methods following thin layer chromatography (Vanier et al. 1975).

Recent, unpublished research by our collaborators at the Brain and Mind Centre, University of Sydney, has identified several novel deleterious mutations in genes that are crucially involved in myelin lipid biosynthesis or catabolism, in people diagnosed with FTD. These include *ARSA, FA2H, ASPA CYP27A1*, and peroxisomal biogenesis (*PEX*) genes. As with *GRN*, homozygous mutation of these genes results in severe demyelinating disorders (Edvardson et al. 2008, Waterham et al. 2012, Beytía Mde et al. 2014, Nie et al. 2014, Cesani et al. 2016) . Due to their rarity, it has not been established whether these novel mutations cause FTD

through disrupted brain lipid metabolism, however the strong association of *GRN* mutations with white matter (WM) loss and tendency for WM loss to feature prominently in all FTD cases suggests that these mutations may be causal (Lok et al. 2021, Marian et al. 2023).

Our collaborators (A/Prof Woojin Kim and A/Prof John Kwok) also observed that plasma HexCer levels are generally lower in people with FTD, although no statistically significant reduction in total HexCer was reported (Kim et al. 2018). Separation of GalCer and GluCer has previously been achieved, with the primary goal being to investigate how levels of GluCer are altered (Gegg et al. 2015, Boutin et al. 2016, Hamler et al. 2017, Logan et al. 2021). Previous publications detailing HexCer isomer separation methods have not reported quantification of GalCer in plasma, and the utility of GalCer as a peripheral diagnostic and prognostic biomarker of CNS myelin integrity in FTD has not been explored.

In order to determine whether levels of GalCer in plasma can be used as a biomarker of myelin defects in FTD, we developed a method to separate GalCer from GluCer in plasma samples, using HILIC chromatography coupled to tandem mass spectrometry. This method was applied to both sporadic bvFTD cases and the FTD cases carrying mutations that are postulated to affect WM integrity. We determined that plasma levels of galactosylceramide from FTD patients are significantly reduced in both sporadic FTD cases and FTD cases carrying novel mutation compared with control cases. Due to the sensitivity of the chromatography to minor perturbations in sample preparation, solvent composition, or instrument sensitivity, further investigation is required to determine a reference range for control cases.

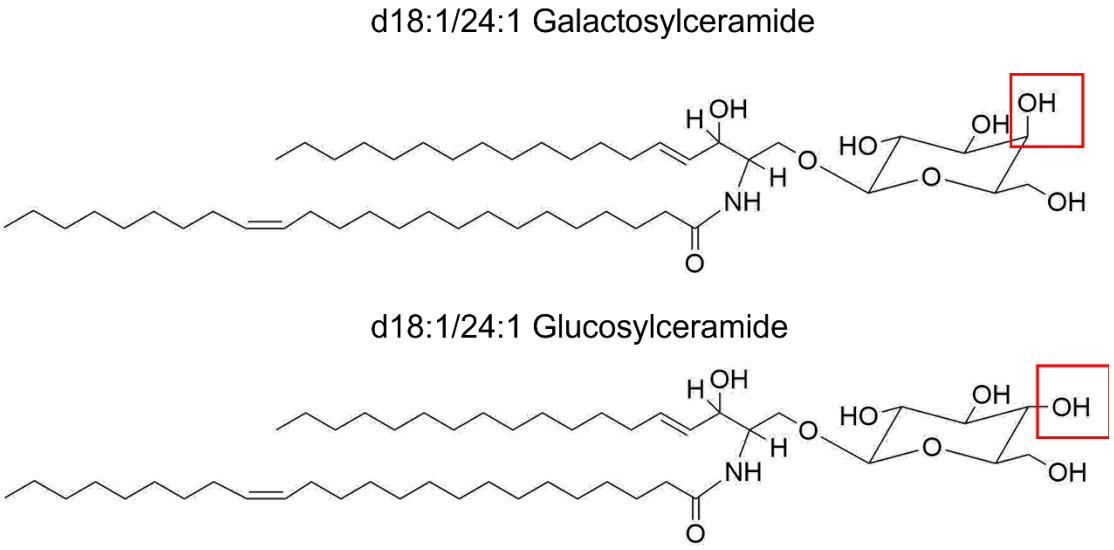

Figure 4.1: Structure of the isomers Galactosylceramide and Glucosylceramide

GalCer and GluCer differ in structure by the orientation of the of C-4 hydroxyl group of the hexose headgroup (shown within the red boxes).

4.2 Methods

4.2.1 Mouse brain samples

Mice deficient for ceramide synthase 2 in oligodendrocytes ($CerS2^{\Delta O/\Delta O}$) and floxed gene controls ($CerS2^{fl/fl}$) were generated as described in (Teo et al. 2023). Whole brain homogenates and isolated myelin were prepared as described (Teo et al. 2023).

4.2.2 Human plasma samples

Plasma samples were obtained from the FRONTIER Clinic at the Brain and Mind Centre, from a preliminary cohort of 17 of each sporadic FTD patients, FTD patients carrying novel mutations, and age-matched controls (Table 4.1), and a validation cohort of 14 sporadic FTD patients and age-matched controls (Table 4.2). Plasma samples were collected between 2008 and 2018 and stored at -80°C until further use. Samples were obtained under Human Research Ethics Committee approval from South Eastern Sydney Local Health Service (10/192) and The University of New South Wales (10/092).

4.2.3 Whole exome sequencing

Whole exome sequencing and bioinformatics were carried out as previously described (Dobson-Stone et al. 2020). Candidate variants were then prioritized in terms of the following criteria:

(1) Variants in genes that have been associated with white matter pathology; (2) Ultra-rare in human population (allele frequency < 0.00001) using public access databases such as EXAC; (3) Loss-of-function mutations such as stop-gain or frameshift mutations; (4) Mutation classified as ‘pathogenic’ or ‘likely pathogenic’ in public access database such as ClinVAR.

Table 4.1: Demographic information for preliminary cohort

** Denotes samples with matched serum. bvFTD = behavioural variant FTD, CBD = corticobasal degeneration, PNFA = progressive non-fluent aphasia, SD = semantic dementia, AD = Alzheimer's disease, dbSNP = Database for Single Nucleotide Polymorphisms.*

Control			Sporadic bvFTD				FTD Novel Mutation Carriers							
Case ID	**Sex**	**Age**	**Case ID**	**Sex**	**Age**	**Clinical Syndrome**	**Case ID**	**Sex**	**Age**	**Clinical Syndrome**	**Affected Gene**	**Base position (build hg19)**	**Protein**	**dbSNP**
*C1	M	68	F2	F	65	bvFTD	M1	M	75	bvFTD	*ASPA* (Kaul et al. 1994, Tahmaz et al. 2001)	3384956	p.L99X	rs759524474
C2	M	71	F3	F	65	bvFTD	M2	F	51	bvFTD	*PEX1* (Barth et al. 2001, Waterham et al. 2012)	92132417	p.L665V	rs1252221734
*C4	F	73	F4	F	68	bvFTD	*M3	M	66	bvFTD	*LAMA2* (Beytía Mde et al. 2014, Arreguin et al. 2020)	129663524	p.R1450X	rs200923373
C5	M	74	F5	M	67	bvFTD	*M4	M	58	bvFTD	*GJA1* (Kajiwara et al. 2018)	121768924	p.A311fs	rs778110855
*C6	F	75	F6	M	68	bvFTD	*M6	M	66	bvFTD	*ARSA* (Stoeck et al. 2016, Penati et al. 2017)	51065818	p.G81S	rs759524474
*C7	F	75	F7	M	61	bvFTD	M7	M	82	CBD	*CLIP1* (Larti et al. 2015)	122825676	p.M382fs	Novel
*C8	F	65	F8	M	60	bvFTD	*M8	F	57	PNFA	*CYP27A1* (Nie et al. 2014)	219678909	p.R395C	rs121908096
C9	M	72	F9	M	72	bvFTD	M9	M	73	CBD	*LAMA2* (Beytía Mde et al. 2014, Arreguin et al. 2020)	129513995	p.K594Nfs *4	Novel
*C10	M	64	F10	F	55	bvFTD	M10	F	60	PFNA		129498995	p.G484V	rs781424807
*C11	M	68	F11	M	69	bvFTD	*M11	F	68	Logopenic		129470131	p.R306H	rs1023922833
*C12	F	80	F12	M	55	bvFTD	*M12	F	63	PFNA		129807739	p.H2620Y	rs746069321
C13	M	74	F13	M	63	bvFTD	*M13	M	82	PFNA	*PEX1* (Barth et al. 2001, Waterham et al. 2012)	92134096	p.P674L	rs141509344
*C14	M	72	F14	M	74	bvFTD	M14	F	63	SD Left	*PEX5* (Barth et al. 2001, Waterham et al. 2012)	7351635	p.W159X	Novel
C15	F	70	F15	M	68	bvFTD	*M15	M	70	AD	*PPT1* (Metelitsina et al. 2016, Sheth et al. 2018)	40555167	p.R48X	rs137852700
*C16	F	76	F16	M	65	bvFTD	*M16	M	73	SD right	*FA2H* (Eckhardt et al. 2005, Edvardson et al. 2008)	74752890	p.H48R	rs761645282
C17	F	70	F17	M	75	bvFTD	*M17	F	63	CBD	*TBK1* (Gijselinck et al. 2015, Wang et al. 2017)	64860723	p.R134H	s1264687081
*C18	M	75	F18	M	62	bvFTD	M18	F	61	bvFTD	GJA1 (Kajiwara et al. 2018)	121768924	p.A311fs	rs778110855

Table 4.2: Demographic information for validation cohort

Control			Sporadic bvFTD			
Case ID	**Sex**	**Age**	**Case ID**	**Sex**	**Age**	**Clinical Syndrome**
V_C1	F	68	V_F1	M	68	bvFTD
V_C2	F	70	V_F2	M	66	bvFTD
V_C3	F	75	V_F3	M	69	bvFTD
V_C4	F	80	V_F4	M	73	bvFTD
V_C5	F	66	V_F5	F	58	bvFTD
V_C6	F	71	V_F6	F	60	bvFTD
V_C7	M	60	V_F7	M	66	bvFTD
V_C8	M	58	V_F8	F	64	bvFTD
V_C9	F	66	V_F9	M	56	bvFTD
V_C10	F	57	V_F10	M	64	bvFTD
V_C11	M	56	V_F11	F	68	bvFTD
V_C12	F	76	V_F12	F	77	bvFTD
V_C13	F	67	V_F13	F	56	bvFTD
V_C14	M	72	V_F14	F	60	bvFTD

4.2.4 Lipid extraction

Lipids were extracted from 50 µL plasma samples using the two-phase methyl-tert-butyl ether (MTBE)/methanol/water protocol (Matyash et al. 2008, Couttas et al. 2020). Plasma was combined with 850 µL MTBE and 250 µL HPLC grade methanol containing 400 pmoles GluCer(d18:1_12:0) internal standard (#860543, Avanti Polar Lipids). Samples were sonicated in a 4℃ water bath for 30 min. Phase separation was induced with the addition of 212 µL of mass-spectrometry grade water, samples were vortexed and centrifuged at 2000 x *g* for 5 min, and the upper organic phase was collected in 5 mL glass tubes. The lower phase was extracted twice more with the addition of 500 µL MTBE and 150 µL methanol followed by sonication for 15 min and phase separation with 125 µL water. The upper phase was collected into the same vial from all 3 extractions and dried down under vacuum on low heat in a Savant SC210 SpeedVac (ThermoFisher Scientific). Lipids were reconstituted by 15 minutes of sonication at 4°C in 100 µL of 100% HPLC grade methanol, and stored at -30°C for up to a week before analysis. For the isomer separation assay, samples were briefly vortexed and diluted 1:50 into 99% acetonitrile, 2% methanol, 0.75% water, 0.25% formic acid, and 2.5 mM

ammonium formate (mass spectrometry grade solvents, Fisher Scientific) immediately prior to running, to equate their solvent composition to the mobile phase used for the HPLC.

4.2.5 Lipidomics

Lipidomics was performed by targeted liquid chromatography-tandem mass spectrometry (LC-MS/MS). For GluCer/GalCer isomer separation lipids were detected using a Sciex 6500+ QTRAP mass spectrometer coupled to a Shimadzu Nexera HPLC. Lipids were resolved on a 2.1 x 150 mm Agilent InfinityLab Poroshell 120 HILIC-Z HPLC column (2.7 µm pore size), with column oven at 30°C and an isocratic solvent comprising 97% acetonitrile, 2% methanol, 0.75% water, 0.25% formic acid, and 2.5 mM ammonium formate. Run time was 20 min, and flow rate 0.1 mL/min.

ST and HexCer were quantified with a TSQ Altis triple quadrupole mass spectrometer coupled to a Vanquish HPLC (Thermo Scientific). Lipids were resolved on a 3 x 150 mm Agilent ZORBAX Eclipse XDB-C8 column (5 µm pore size), with column oven at 30°C using an isocratic solvent comprising 2 mM ammonium formate and 0.2% formic acid in 100% methanol. Run time was 10 min at a flow rate of 0.4 mL/min.

Data was acquired in full scan/data-dependent MS^2 mode, using the parameters in Table 4.3 for GluCer/GalCer separation, or Table 4.4 for ST and HexCer quantification. For both assays, sample order was randomised, and data was collected in positive ion mode. SciexOS software (version 1.7) or TraceFinder (version 5.1) were used for isomer separation and ST/HexCer assays, respectively, for lipid annotation, chromatogram alignment, and peak integration. The diagnostic 264.3 *m/z* sphingosine product ion was used for all transitions (Figure 4.2). Individual lipids were expressed as ratios to the d18:1/12:0 GluCer internal standard (#860543, Avanti Polar Lipids), then multiplied by the amount of internal standard added to calculate molar amounts for each lipid. Commercial GalCer(d18:1/24:1) (#860432) and GluCer(d18:1/24:1) (#860549) standards for optimisation were from Avanti Polar Lipids.

Table 4.3: Selected reaction monitoring parameters used for isomer separation targeted mass spectrometry data acquisition

Compound	Precursor m/z	Product m/z	Collision Energy (V)	Min Dwell Time (ms)	RF Lens (V)	Expected Elution Time (min) GluCer/GalCer
d18:1/12:0 HexCer	644.6	264.3	37	179.735	80	14.7/-
d18:1/16:0 HexCer	700.6	264.3	37	179.735	80	13.7/12.8
d18:1/18:1 HexCer	726.7	264.3	37	179.735	80	13.8/13.2
d18:1/18:0 HexCer	728.6	264.3	37	179.735	80	13.2/12.4
d18:1/20:0 HexCer	756.6	264.3	37	179.735	80	12.9/12.1
d18:1/22:1 HexCer	782.7	264.3	37	179.735	80	12.6/11.8
d18:1/22:0 HexCer	784.7	264.3	37	179.735	80	12.7/11.9
d18:1/23:1 HexCer	796.7	264.3	37	179.735	80	12.4/11.7
d18:1/23:0 HexCer	798.7	264.3	37	179.735	80	12.7/11.9
d18:1/24:1 HexCer	810.7	264.3	37	179.735	80	12.3/11.5
d18:1/24:0 HexCer	812.7	264.3	37	179.735	80	13.0/12.3

Table 4.4: Selected reaction monitoring parameters used for ST and HexCer targeted mass spectrometry data acquisition

Compound	Precursor m/z	Product m/z	Collision Energy (V)	Min Dwell Time (ms)	RF Lens (V)
d18:1/12:0 HexCer	644.5	264.3	34	72.933	87
d18:1/16:0 HexCer	700.6	264.3	34	72.933	87
d18:1/18:0 HexCer	728.6	264.3	34	72.933	87
d18:1/20:0 HexCer	756.6	264.3	34	72.933	87
d18:1/22:1 HexCer	782.7	264.3	34	72.933	87
d18:1/22:0 HexCer	784.7	264.3	34	72.933	87
d18:1/24:1 HexCer	810.7	264.3	34	72.933	87
d18:1/24:0 HexCer	812.7	264.3	34	72.933	87
d18:1/17:0 ST	794.5	264.3	43	72.933	100
d18:1/18:0 ST	808.6	264.3	43	72.933	100
d18:1/20:0 ST	836.6	264.3	43	72.933	100
d18:1/22:1 ST	862.7	264.3	43	72.933	100
d18:1/22:0 ST	864.7	264.3	43	72.933	100
d18:1/24:1 ST	890.6	264.3	43	72.933	100
d18:1/24:0 ST	892.7	264.3	43	72.933	100

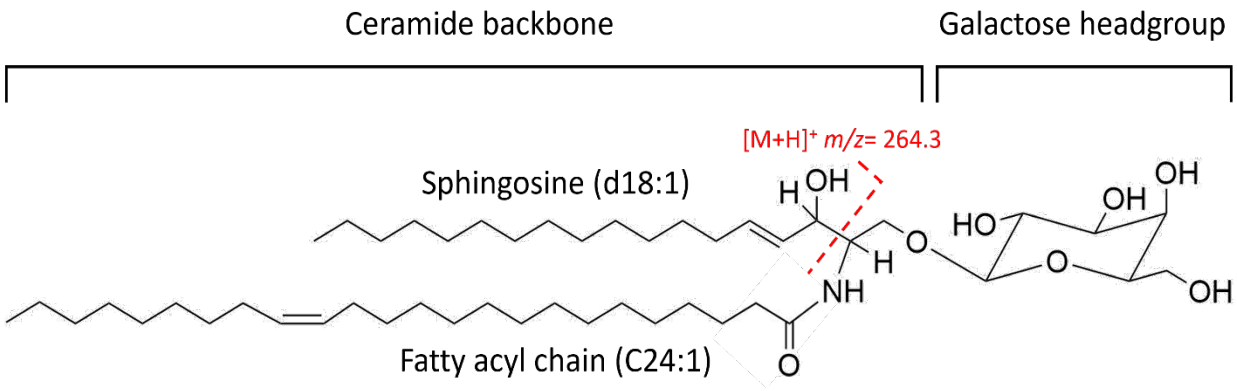

Figure 4.2: Structure of the most abundant form of GalCer in the brain, GalCer (d18:1/24:1)

Fragmentation of the protonated precursor ion yields a diagnostic sphingosine product fragment ion.

4.2.6 Statistical analysis

Data were first assessed for normality and if not normally distributed, data were natural log-transformed to achieve a normal distribution. Data were compared between sample groups by unpaired t-test, one-way ANOVA, followed by Tukey's post-hoc test, or non-parametric Kruskal-Wallis test followed by Dunn's post-test in GraphPad Prism (Version 9.4.1). $p < 0.05$ was considered statistically significant.

4.3 Results

4.3.1 Case Demographics

Mean age ± standard deviation for preliminary case cohort plasma donors was 71.9 ± 4.1 years for controls, 65.4 ± 5.7 for sporadic bvFTD cases and 66.5 ± 8.5 for FTD cases carrying novel mutations (ANOVA F = 4.98, p = 0.0109). An additional 14 sporadic bvFTD and 14 control samples were obtained to validate our preliminary results (Table 4.2). These validation cohort cases had mean age 67.3 ± 7.4 years for controls and 64.6 ± 7.4 years for sporadic FTD cases (t = 1.02, p = 0.317).

4.3.2 Optimisation of isomer separation assay

We aimed to develop a method to separate and quantify the isomers GluCer and GalCer in plasma samples using LC-MS/MS, initially adapted from the method described by Shaner and colleagues (Shaner et al. 2009). This method utilised a normal phase 250 mm silica column and 8 min isocratic chromatography with 97:2:1 acetonitrile/methanol/acetic acid containing 5 mM ammonium acetate. We tested this method with a HILIC (hydrophilic interaction chromatography) column that we had in our lab.

The HPLC solvent composition was varied to achieve optimal separation of the isomers, while maintaining signal intensity. Increasing the proportion of methanol and reducing the acetonitrile increased the signal intensity of commercial d18:1/24:1 GluCer and GalCer standards slightly, possibly due to improved solubility of the analytes in the mobile phase, however the isomers could no longer be resolved. Following several alterations, a mobile phase composition of 97% acetonitrile, 2% methanol, 0.75% water, 0.25% formic acid, and 2.5 mM ammonium formate was found to allow detection of the analytes of interest while resolving the HexCer isomers (Figure 4.3). Commercial d18:1/24:1 GluCer and GalCer lipid standards were used to ensure the correct identification of the isomers by retention time. Using our separation method and solvent system, GalCer consistently elutes earlier than GluCer.

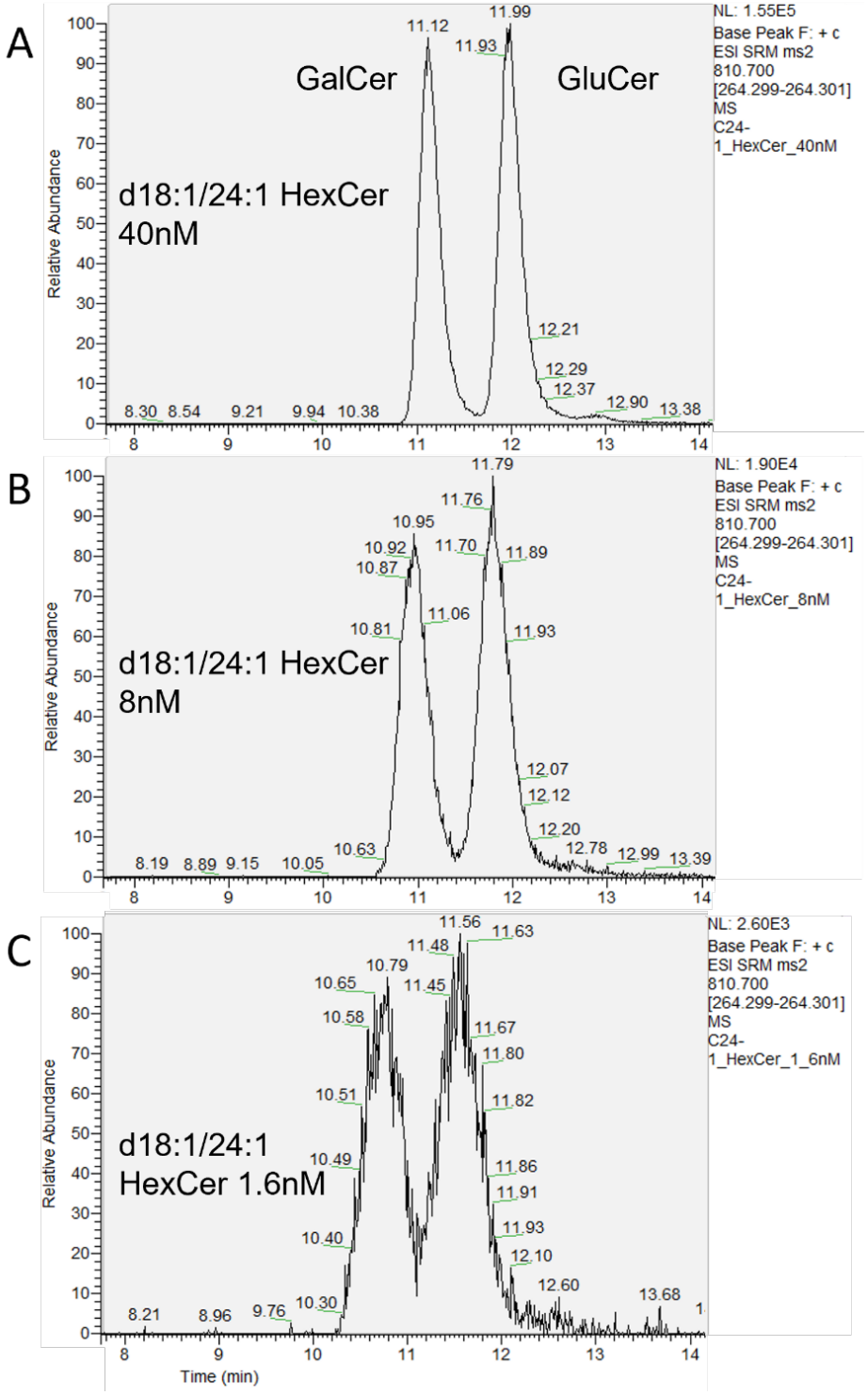

Figure 4.3: Chromatographic separation of GalCer and GluCer

Detection of commercial C24:1 GalCer and GluCer standards diluted into the mobile phase (97% acetonitrile, 2% methanol, 0.75% water, 0.25% formic acid, and 2.5 mM ammonium formate) and run using our isomer separation assay. Equimolar concentrations of GalCer and GluCer standards were run at (A) 40 nM, (B) 8 nM, (C) 1.6 nM.

Trial experiments with d18:1/24:1 GalCer and GluCer standards indicated that the lipids had to be reconstituted in the HPLC solvent for effective separation, and even minor deviations from the starting conditions affected elution time and separation. We were particularly interested in the recovery of the dominant GalCer species occurring in the CNS which are highly hydrophobic due to their long and very-long chain ceramide backbones. However, we were concerned that reconstitution of dried lipid extracts (following lipid extraction) directly into the above HPLC starting solvent would result in poor lipid recovery. This was tested by subjecting 50 µL human plasma test samples to the two-phase extraction protocol, followed by reconstitution of the dried lipid extracts in the HPLC mobile phase (97% acetonitrile, 2% methanol 0.75% water, 0.25% formic acid, and 2.5 mM ammonium formate) or in 100% methanol. The latter was subsequently diluted 1:50 into the mobile phase without methanol, to match the composition of the mobile phase.

Using our optimised HILIC chromatography coupled to tandem mass spectrometry, we were able to successfully separate and identify the structural isomers GluCer and GalCer in human plasma. Reconstitution into 100% methanol improved recovery of very long-chain HexCer species compared to reconstitution directly into the mobile phase (Figure 4.4). We observed improved peak detection in the plasma sample reconstituted in 100% methanol despite the 50-fold dilution compared to the sample reconstituted directly into mobile phase solvent. As 1:50 dilution of the reconstituted sample limits the amount of plasma lipid that can be assayed, injection of the sample reconstituted in 100% methanol without further dilution into the mobile phase was also trialled, however this incompatibility with the mobile phase solvent caused the analytes to elute with the solvent front.

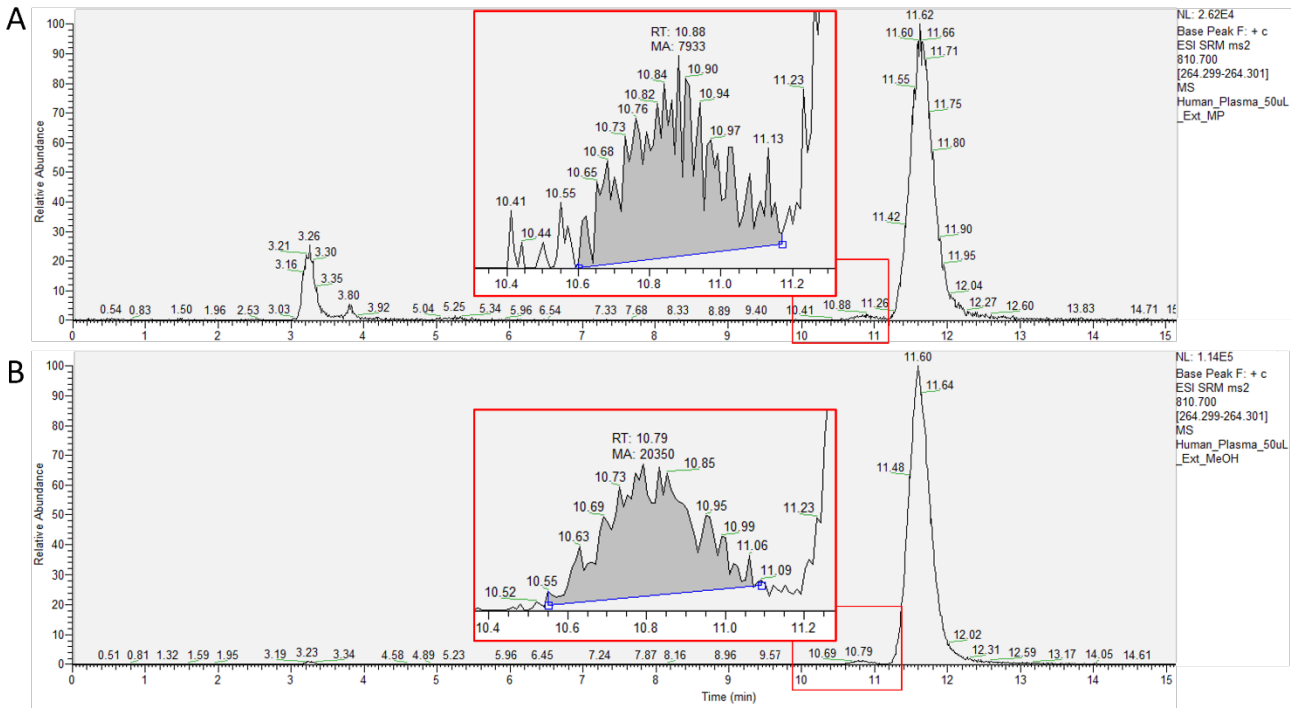

Figure 4.4: Reconstitution of human plasma samples into 100% methanol improves recovery of very long chain GalCer

Chromatograms showing C24:1 HexCer extracted ion chromatograms from 50 µL of the same trial human plasma sample reconstituted into 100 µL of (A) mobile phase, or (B) 100% methanol and subsequently diluted 1:50 into the mobile phase minus methanol. GalCer peak shown in red boxes.

GluCer is abundant in human plasma, approximately 50 times more abundant compared with GalCer (Figure 4.5). A trial human plasma sample was then used to determine which major GluCer/GalCer species could be separated and detected in human plasma using this method. The column flow rate was reduced to 0.1 mL/min to improve isomer separation, and the number of scans across each peak was reduced, which allowed for an increase in cycle time to 60 ms. This resulted in detectible peaks for d18:1/16:0, d18:1/18:0, d18:1/20:0, d18:1/22:0, d18:1/22:1, d18:1/23:0 and d18:1/24:1 GalCer in human plasma (representative chromatograms shown in Figure 4.5).

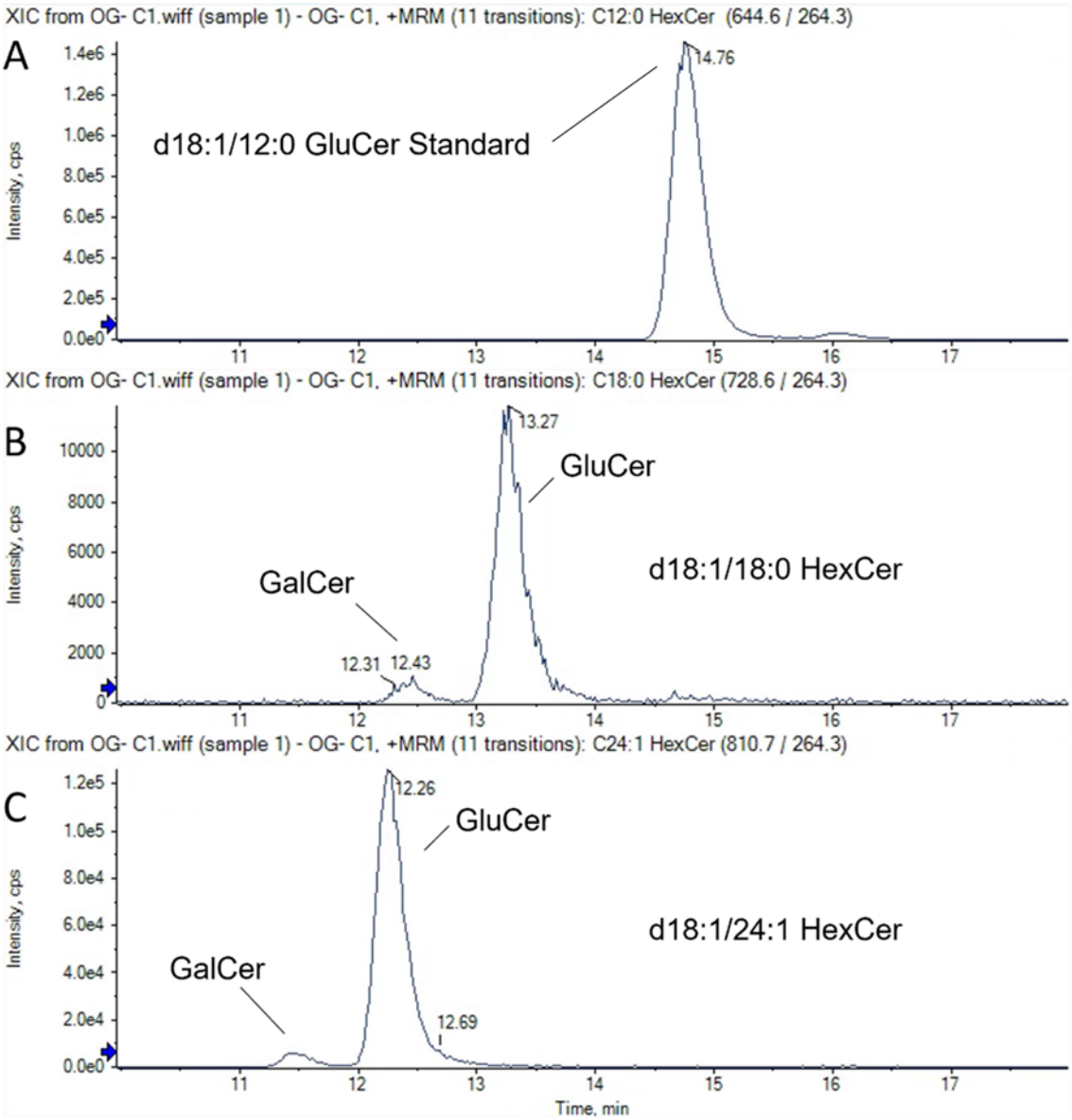

Figure 4.5 GluCer is the dominant HexCer isomer in human plasma

Chromatogram showing separation of (A) d18:1/12:0 GluCer internal standard, (B) d18:1/18:0 and (C) d18:1/24:1 forms of GalCer and GluCer in a human plasma sample.

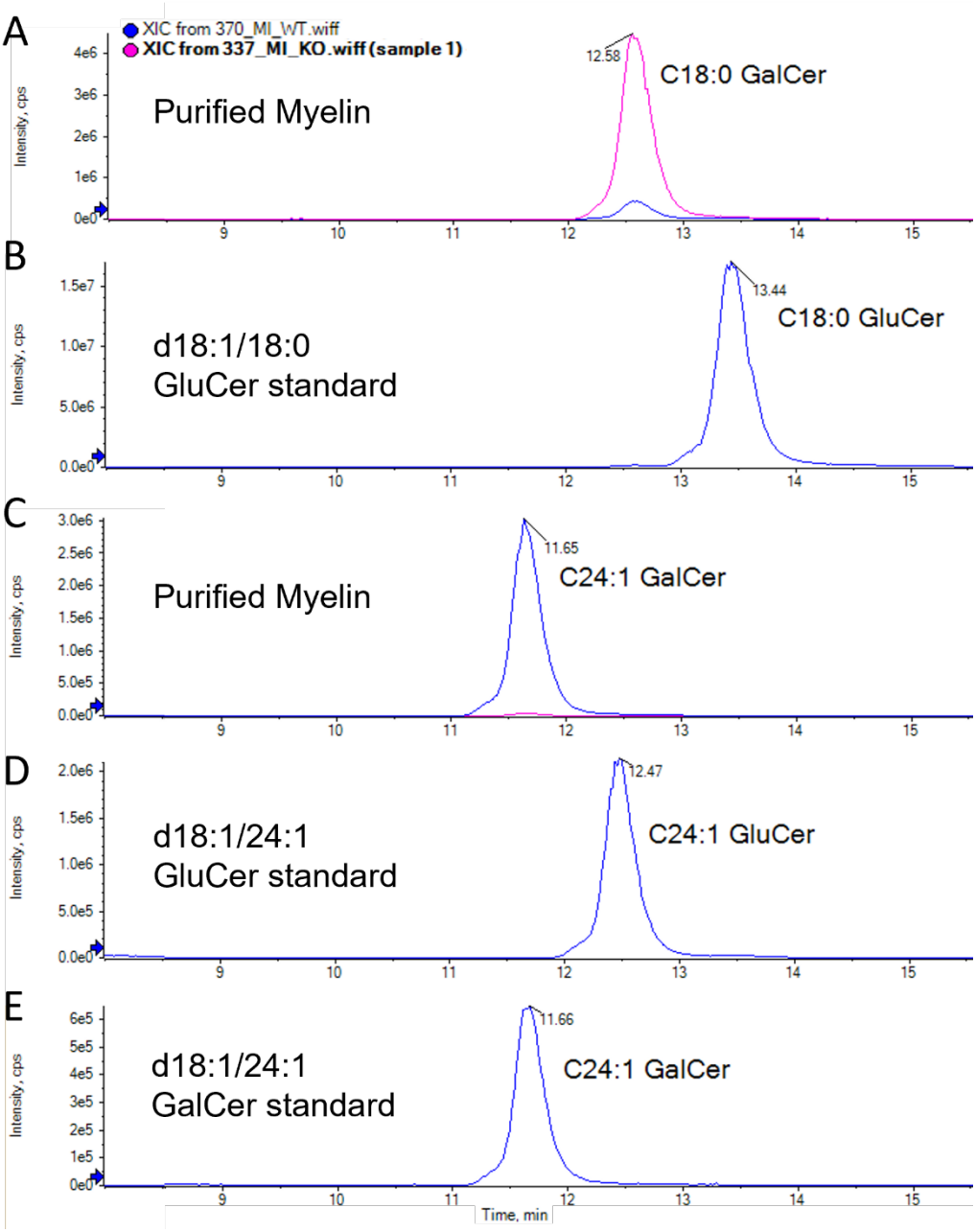

Figure 4.6 Myelin HexCer content is comprised almost exclusively of GalCer

Chromatograms show (A, B) HexCer (d18:1/18:0) and (C–E) HexCer (d18:1/24:1) peaks in purified myelin from a CerS2ΔO/ΔO (pink) and a CerS2fl/fl (blue) mouse (A, C), a synthetic GluCer (d18:1/18:0) standard (B), a synthetic GluCer (d18:1/24:1) standard (D), and a synthetic GalCer (d18:1/24:1) standard (E). Peaks corresponding to GalCer but not GluCer were observed in all myelin samples. The GalCer (d18:1/18:0) peak was higher and GalCer (d18:1/24:1) much lower in myelin from CerS2ΔO/ΔO mice, compared to CerS2fl/fl. Image from (Teo et al. 2023).

4.3.3 Novel mutation carriers show reduced levels of circulating GalCer in plasma

We next sought to use our isomer separation assay to determine if plasma GalCer levels are altered in people with FTD, including those carrying mutations that have been associated with white matter defects (Table 4.1). Circulating plasma GalCer levels were significantly different in both sporadic FTD cases and FTD cases with mutations affecting white matter compared to control cases in five of the seven GalCer species quantified. (Figure 4.7A) The most significantly affected species were GalCer (d18:1/18:0), GalCer (d18:1/20:0) and GalCer (d18:1/24:1) (Table 4.5 Figure 4.7A). Plasma GalCer levels did not differ significantly between sporadic FTD cases and FTD cases carrying novel mutations (Figure 4.7A).

We tested whether expressing GalCer levels as a relative percentage of corresponding total hexosylceramide (e.g. d18:1/24:1 GalCer relative to total d18:1/24:1 hexosylceramide (GluCer+GalCer)) would allow for better differentiation between groups by reducing inter-sample variability (Figure 4.7B). We did not observe good differentiation between sample groups using this approach, and while the trend differences could still be observed between groups, the only change observed was a significant decrease in % C24:1 GalCer in FTD cases with novel mutations compared with controls (ANOVA F = 3.32, $p = 0.045$), while sporadic FTD cases displayed a trend reduction in % C24:1 GalCer compared with control cases (Figure 4.7B).

Table 4.5: Summary ANOVA results of absolute GalCer species quantified in human plasma from controls, sporadic FTD cases, and FTD cases with novel mutations

Lipid	F	*p*-value	ANOVA *p*-value summary
d18:1/16:0 GalCer	1.59	0.21	ns
d18:1/18:0 GalCer	9.25	0.0004	***
d18:1/20:0 GalCer	8.94	0.0006	***
d18:1/22:0 GalCer	8.56	0.0007	***
d18:1/22:1 GalCer	1.34	0.27	ns
d18:1/23:0 GalCer	4.30	0.0191	*
d18:1/24:1 GalCer	9.17	0.0004	***

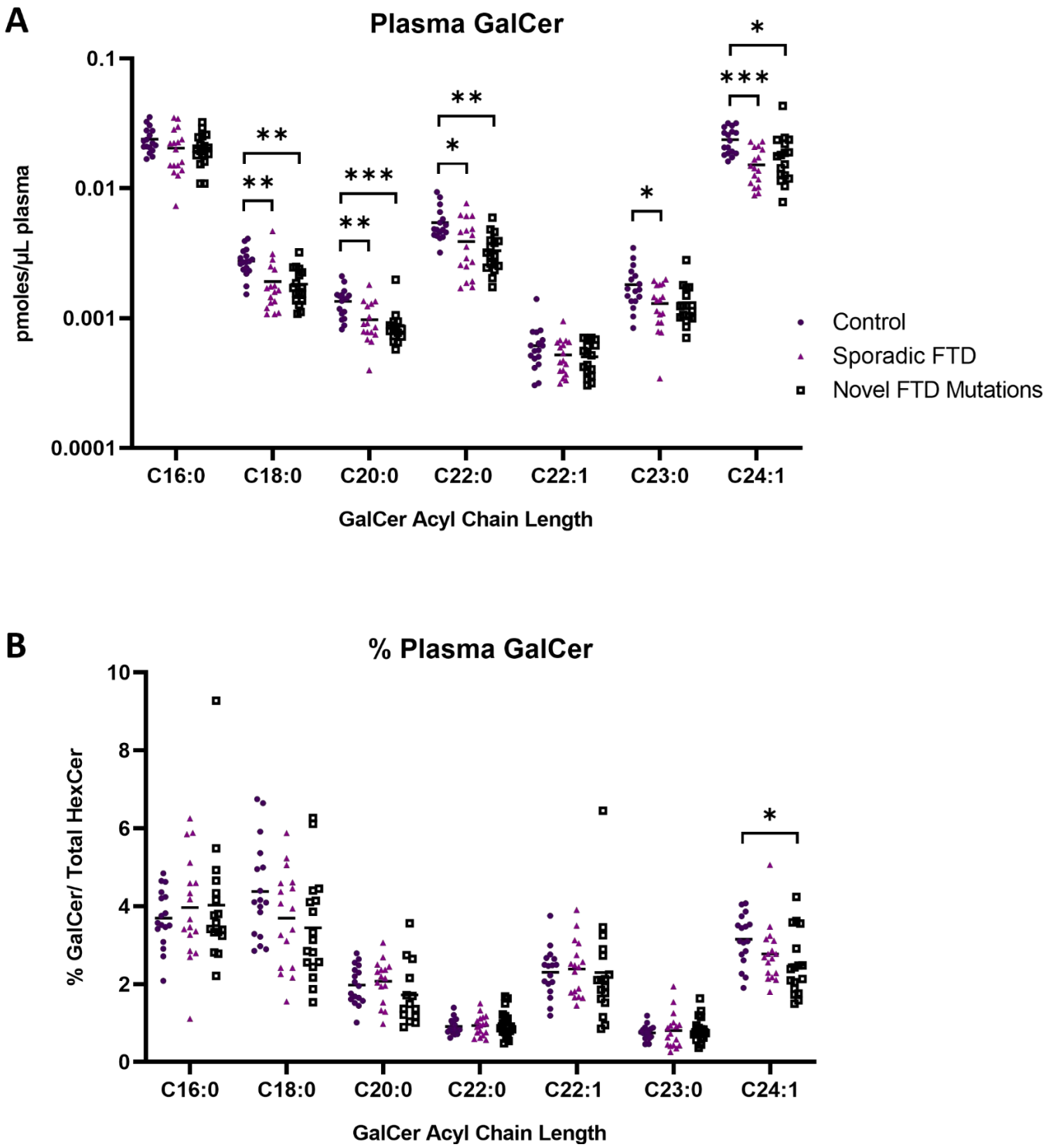

Figure 4.7: FTD cases show reduced plasma GalCer levels when compared to controls

(A) All quantified absolute GalCer levels shown in pmoles/µL (normalised to internal standard), (B) GalCer levels expressed at a percentage of their respective total hexosylceramide.

Individual values and mean (horizontal bar) are marked on the scatter plot. Asterisks indicate significant difference in post-hoc tests: *p < 0.05; **p < 0.01; ***p < 0.001; ****p < 0.0001.

4.3.4 Serum samples do not recapitulate plasma results

As serum is more generally more consistent and easier to collect than plasma, we tested whether we could apply our method to separate the hexosylceramide isomers in human serum. For this, we obtained serum samples matched to a subset of the plasma obtained from novel mutation carriers (n=10) and normal controls (n=11) (cases with serum samples indicated by * in Table 1).

We were able to successfully separate the isomers in the matched serum samples, however the significant reduction of d18:1/18:0 and d18:1/24:1 GalCer in plasma of FTD cases was not seen with the matched serum samples. Unpaired t-tests show a significant decrease to levels of both %C18:0 GalCer (t= 4.05, p = 0.0007) (Figure 4.8A) and %C24:1 GalCer (t = 6.64, p = 0.000002) in plasma samples from FTD cases compared to control cases (Figure 4.8B). In contrast, matched serum samples show no significant difference in %GalCer between the two groups in any of the lipids profiled. Serum therefore appears to be unsuitable for differentiation of FTD from control cases based on GalCer levels.

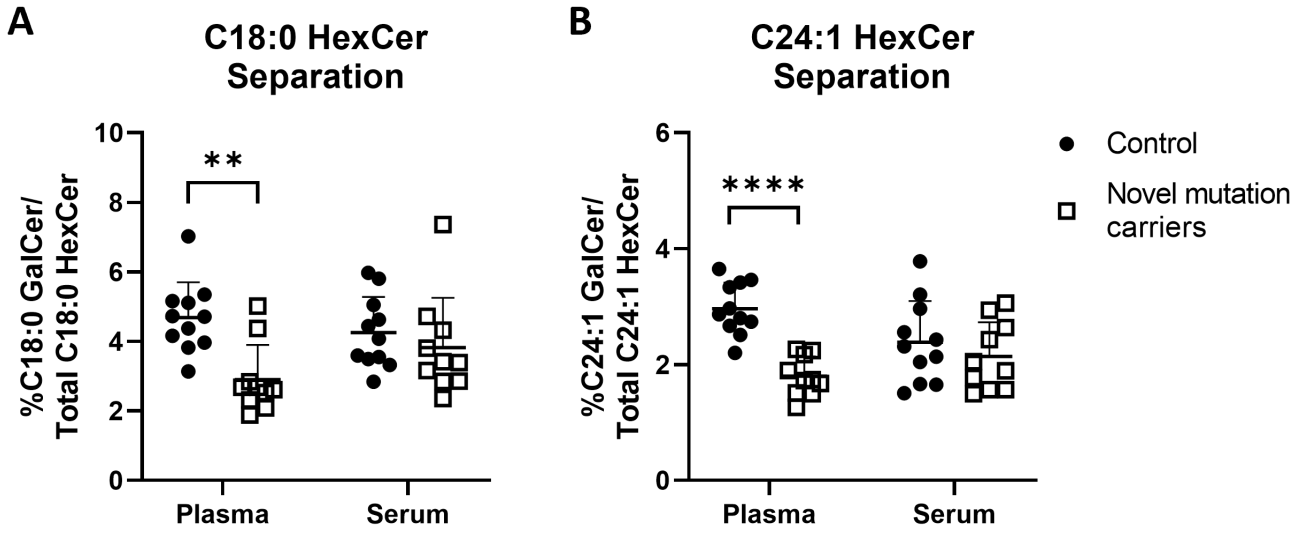

Figure 4.8 Matched plasma and serum samples show different levels of %GalCer

(A) %C18:0 and (B) %C24:1 GalCer levels expressed at a percentage of their corresponding total hexosylceramide. Individual values including mean (horizontal bar) and SD (vertical bars) are marked on the scatter plot. Asterisks indicate significant difference in unpaired t-tests: *p < 0.05; **p < 0.01; ***p < 0.001; ****p < 0.0001.

4.3.5 No changes to plasma galactosylceramide levels were observed in a small validation cohort of sporadic FTD cases.

In order to expand on our preliminary findings, plasma GalCer levels were quantified in a small validation cohort of plasma samples from 14 sporadic FTD cases and 14 controls (Figure 4.9). Validation cohort samples were run alongside the initial cohort of samples to facilitate direct comparison of GalCer levels between the two sample sets.

The findings from the original case cohort was replicated in the repeat analysis, however there was no difference in GalCer levels between sporadic FTD cases and controls in the validation cohort (Figure 4.9A). This was driven by significantly lower GalCer levels in the control cases from the validation compared to the preliminary cohort, as exemplified by GalCer d18:1/24:1 (ANOVA F = 11.64, $p < 0.0001$). Interestingly, there was no significant difference in GalCer d18:1/24:1 levels between preliminary and validation sporadic FTD cases (Figure 4.9A).

As this observation may have been driven by extraction batch effects, we analysed GalCer d18:1/24:1 as a percentage of total HexCer d18:1/24:1 (%C24:1 GalCer) to control for potential decreased extraction efficiency in the validation cohort. Once again, the validation control cases showed significantly lower levels of %C24:1 GalCer in the validation control group compared with the preliminary control cohort (ANOVA F = 5.52, $p = 0.02$), despite the sporadic FTD cases from the validation cohort showing no difference to those in the preliminary cohort (Figure 4.9B).

Despite the differences observed in plasma GalCer levels between the control cases, when the preliminary and validation cohorts were combined, both the sporadic FTD and novel mutation carrier FTD group showed significantly decreased plasma d18:1/18:0 GalCer (ANOVA F = 8.78, $p = 0.0004$) and d18:1/24:1 GalCer (ANOVA F = 11.66, $p < 0.0001$) levels compared to controls, recapitulating our preliminary findings (Figure 4.9C and 4.9D, respectively).

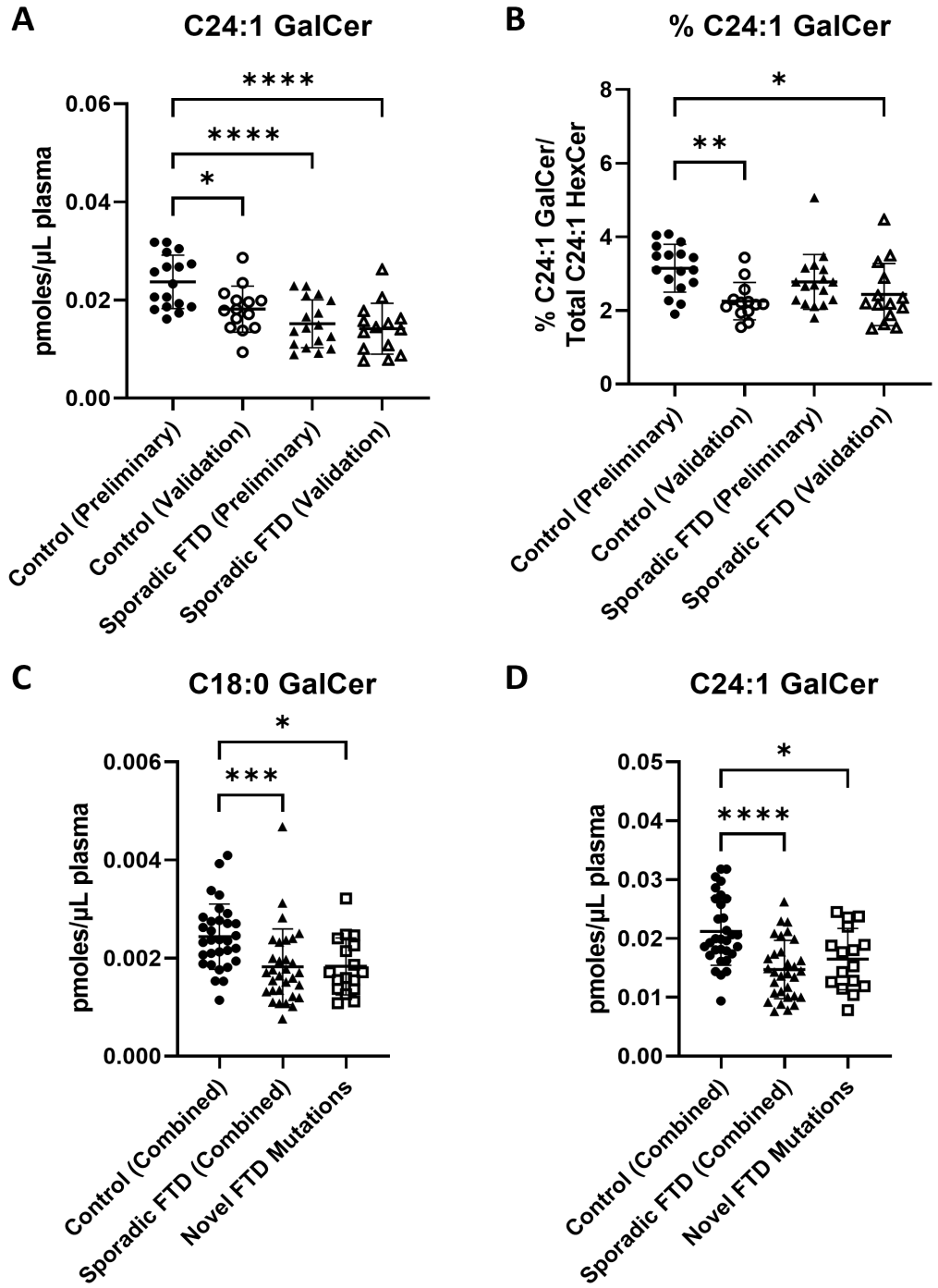

Figure 4.9: Control plasma samples show significant differences in GalCer levels between cohorts

Preliminary and validation control cases show significantly different levels in both (A) absolute C24:1 GalCer levels and (B) %C24:1 GalCer expressed at a percentage of total C24:1 hexosylceramide. (C) Significant reduction in absolute d18:1/18:0 GalCer and (D) absolute d18:1/24:1 GalCer levels in the combined sporadic FTD cases and FTD cases carrying novel mutations compared with combined controls. Individual values including mean (horizontal bar) and SD (vertical bars) are marked on the scatter plot. Asterisks indicate significant difference in post-hoc and t-tests: *p≤0.05; **p< 0.01; ***p<0.001; ****p<0.0001.

4.3.6 Plasma sulfatides are reduced in FTD cases carrying novel mutations

As we established that levels of circulating GalCer are lower in FTD cases compared to control cases, we were also interested in profiling the plasma levels of sulfatide (ST), which is a direct derivative of GalCer. Since sulfated GluCer is not found in humans (Reza et al. 2021), we employed standard reverse phase LC-MS/MS for sulfatide quantification (Song et al. 2021, Teo et al. 2023), as STs were not detected with our GalCer/GluCer separation method. Our plasma samples were not extracted with ST internal standard, therefore we normalised detected STs to the HexCer internal standard.

All profiled STs (Table 4.4) were successfully detected and quantified in the plasma samples. The preliminary and validation control case cohorts exhibited significant differences in the levels of ST(d18:1/18:0) (ANOVA F= 4.69, p = 0.0053), but not ST(d18:1/24:1) (Figure 4.10). Similar to our GalCer results, ST levels in the two sporadic FTD case cohorts were not significantly different.

As we had no way to determine which of the control cohorts was representative of the 'true' control plasma ST level, or whether the differences observed were simply a product of natural biological variation, we analysed the ST levels in the combined preliminary and validation case cohorts together.

In line with our GalCer results, significantly lower ST levels are observed in both sporadic and mutation-carrying FTD cases compared with control cases for d18:1/20:0 ST, d18:1/22:1 ST (Kruskal-Wallis H= 15.49, p = 0.0004), d18:1/24:0 ST and d18:1/24:1 ST (ANOVA F = 6.03, p = 0.0037). C18:0 ST levels were not significantly different between groups (Figure 4.11). Unlike our plasma GalCer results, where both sporadic FTD cases and novel mutation carriers display significantly lower levels of plasma GalCer compared with controls but not between FTD groups, plasma STs are significantly lower in FTD cases carrying novel mutations compared to both control cases and sporadic FTD cases for d18:1/20:0 ST (ANOVA F = 12.63, p <0.0001), d18:1/22:0 ST (ANOVA F = 18.36, p <0.0001) and d18:1/24:0 ST (ANOVA F = 18.64, p <0.0001) (Figure 4.11).

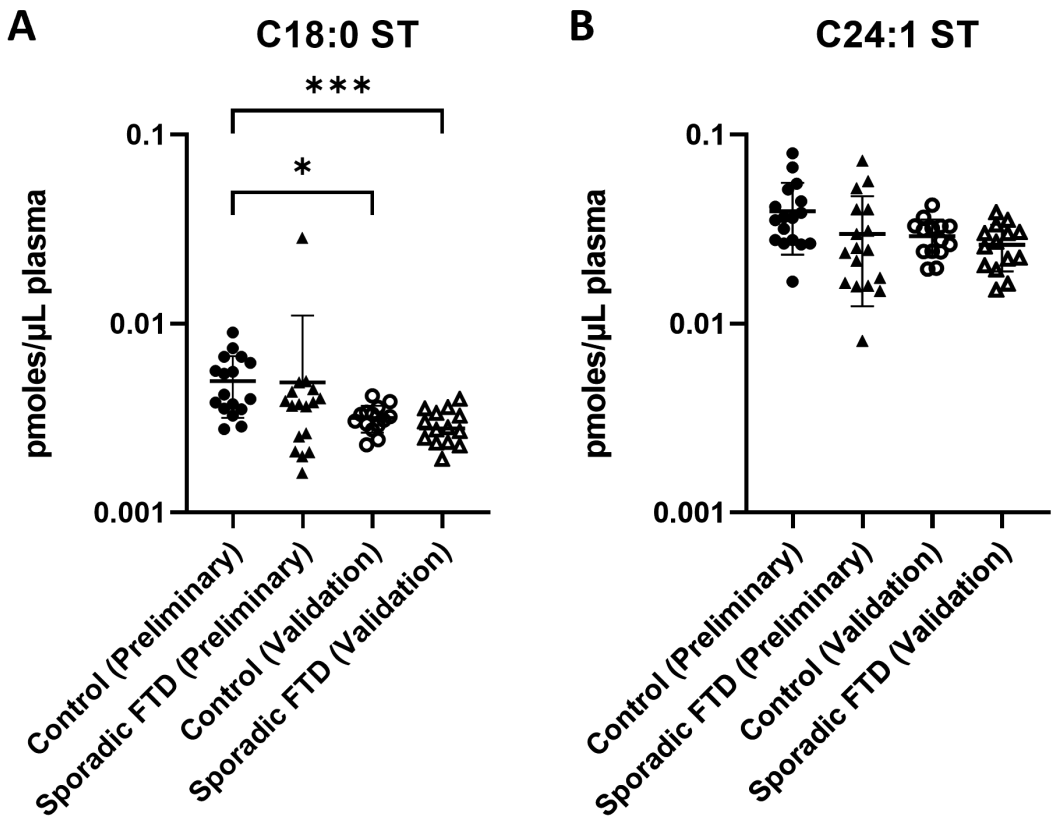

Figure 4.10: Control plasma samples show significant differences in some ST levels between cohorts

Preliminary and validation control cases show significantly different levels in (A) d18:1/18:0 ST, but not (B) d18:1/24:1 ST levels. Individual values including mean (horizontal bar) and SD (vertical bars) are marked on the scatter plot. Asterisks indicate significant difference in post-hoc and t-tests: *p≤0.05; **p< 0.01; ***p<0.001; ****p<0.0001.

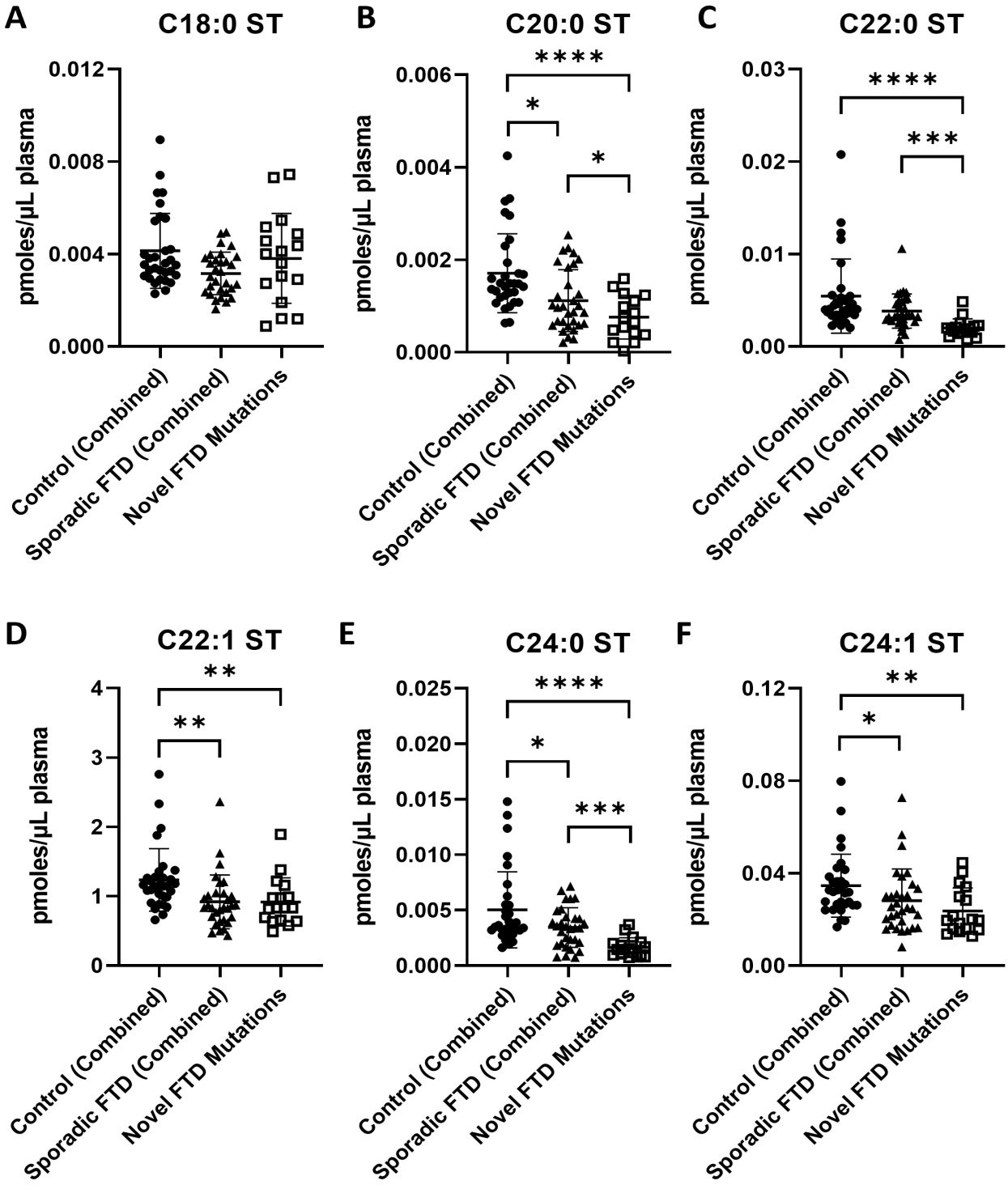

Figure 4.11: Plasma sulfatide levels are significantly reduced in FTD cases carrying novel mutations

Absolute levels of plasma sulfatides (pmoles/µL plasma) shown for (A) C18:0 ST, (B) C20:0 ST, (C), C22:0 ST (D) C22:1 ST, (E) C24:0 ST and (F) C24:1 ST. Individual values including mean (horizontal bar) and SD (vertical bars) are marked on the scatter plot. Asterisks indicate significant difference in post-hoc tests: *p≤0.05; **p< 0.01; ***p<0.001; ****p<0.0001.

4.4 Discussion

In this study we optimised a method for separation of GalCer and GluCer in human plasma and serum, and used this method to demonstrate that levels of multiple GalCer species are significantly lower in the plasma of a preliminary cohort of 34 FTD cases compared to 17 controls, which supports our hypothesis that myelin lipid metabolism is disrupted in FTD. GalCer levels were lower in FTD cases with or without identified mutations in genes affecting WM integrity, suggesting that this is a general property of FTD. However, GalCer levels were not significantly reduced in FTD cases from the sporadic FTD validation cohort, and this was attributed to reduced GalCer levels in the control cases within this cohort. When preliminary and validation cohorts were combined, our initial findings were recapitulated. We determined that serum GalCer measurements were not able to differentiate between study groups, and plasma appears to be a more appropriate matrix for identifying GalCer changes. Plasma ST levels were also lower in FTD cases compared to controls. Plasma ST levels showed a discrimination between FTD groups for several ST species, with FTD cases carrying novel mutations displaying lower circulating ST compared with both sporadic FTD cases and controls. Plasma GalCer and ST therefore have diagnostic potential as indicators of FTD and may be valuable measures for tracking CNS disease progression in people with FTD.

Dysfunctional brain lipid metabolism has been a topic of recent investigation as a potential causative factor in the development of FTD, and MRI studies have noted the presence of White Matter Hyperintensities (WMH) in the brains of FTD cases, which may be indicative of myelin degeneration (Andrés-Benito et al. 2021, Huynh et al. 2021, Logan et al. 2021, Boland et al. 2022, Marian et al. 2023). Circulating lipids are of interest as diagnostic and prognostic biomarkers, however no suitable biomarkers have emerged as yet (Ahmed et al. 2014, Kim et al. 2018, Jääskeläinen et al. 2019, Phan et al. 2020).

The majority of previously published methods for the separation of GluCer/GalCer have focussed on profiling brain GluCer levels as homozygous or heterozygous deficiency in the gene encoding the glucosylceramide catabolic enzyme, *GBA1* are known to cause the most common lysosomal storage disease Gaucher's disease or Parkinson's disease, respectively (Gegg et al. 2015, Boutin et al. 2016, Hamler et al. 2017). A robust lipidomic method for the quantification of GalCer, the less abundant isomer in plasma, has however not previously

been described. Interestingly, a recent study reported successful separation of GalCer and GluCer in human plasma using HILIC chromatography, but with the use of a gradient and different solvents. The authors profiled plasma from people with FTD with and without *GRN* mutations, however they did not report any changes to either GluCer or GalCer in these cases (Logan et al. 2021). It would be of interest to compare our methods and determine which produces more robust and sensitive results.

The difference observed in the GalCer levels between the two cohorts of healthy controls could reflect standard biological variation, or could result from extraction batch effects, or variations associated with the collection, preparation and storage of plasma samples (Surma et al. 2015, Halvey et al. 2021). The isomer separation assay appears to be particularly sensitive to the solvent composition that the samples are dissolved in prior to chromatography, and preparation of samples as separate batches may fuel this problem, leading to inconsistent results. However, GalCer levels were quite well matched in the sporadic FTD cases from both sample cohorts, suggesting that this is not the source of the variance between the two sets of control samples. Our findings are driven by the assumption that the combined control groups are representative of the healthy plasma lipidome within the population. We cannot exclude the possibility that the control cases in the validation cohort may display a more accurate reflection of circulating GalCer and ST levels in the healthy population. Due to our small sample groups, it is not possible to make a conclusion, however the non-significant trend reduction in GalCer levels observed in sporadic FTD cases in either cohort compared with the validation control cases suggests that our preliminary observations of lower plasma GalCer in FTD cases are likely to hold true. A larger cohort of control samples would be needed to determine a control reference range for GalCer, and how this varies with age. We verified the long-term stability of our lipid extracts and determined that extracts reconstituted in 100% methanol are stable at -30°C, with samples showing consistent results after several months of storage.

In agreement with our findings in chapter 2, lipid metabolic dysfunction appears to be a general feature of FTD, with plasma from both sporadic FTD cases and FTD cases carrying mutations in genes that have variously been associated with WM deficiencies showing significant decreases in long and very-long chain GalCer species. We have established that people with FTD carrying novel mutations appear to display a functional lipid metabolic

impairment, however as there were no significant differences between plasma GalCer levels in sporadic FTD cases and those carrying novel mutations, it is not possible to separate the effect of the novel mutations from the effect of FTD. Plasma ST levels were, however, able to discriminate between the two FTD groups, with novel mutation carriers displaying lower ST than sporadic FTD cases for several species. In future studies, it would be important to determine if similarly reduced GalCer and ST levels are seen in cases with the common genetic mutations in *C9orf72*, *GRN* and *MAPT*.

Although profiling of GalCer is theoretically a more selective reporter of myelin since it is almost exclusive to myelin, our results suggest that reduced plasma ST appears to be a more robust indicator for diagnosing FTD. Quantification of plasma STs using reversed phase chromatography produced more robust results compared to the isomer separation assay, as the assay is more sensitive and unlike the isomer separation assay, does not require dilution into the mobile phase. This increase in sensitivity may have led to the enhanced discrimination between the two FTD groups. For the purposes of potential diagnostic utility this an important consideration.

STs are found in extra-neural tissue such as kidney, liver and pancreas, however these STs occur in minor quantities compared to that occurring in brain (Mirzaian et al. 2015). The structure of STs also differs between different tissues: In brain, the very-long chain C24:1, C24:0 ST and their 2-hydroxylated counterparts predominate, whereas in pancreatic islets of Langerhans, shorter acyl chain C16:0 STs are abundant, and there are a lack of hydroxylated species. In the kidney papillae, approximately half of STs are based on a C20 sphingosine backbone, rather than the major C18 sphingoid base seen in the CNS (Hsu et al. 1998, Fredman et al. 2000, Marsching et al. 2014). This is thought to lend different membrane physicochemical properties to those required for myelin (Fredman et al. 2000). Our targeted assay focussed on detection of long and very-long chain STs derived from an 18:1 sphingosine backbone. Therefore, it is reasonable to postulate that a substantial proportion of the ST we profiled in plasma could have originated from the CNS.

As myelin-enriched ST species, while not myelin-specific, are broadly decreased in plasma of WM mutation carriers as well as some species in sporadic FTD cases, this may indicate that lipid metabolic dysfunction may be a phenomenon of FTD cases that is not restricted to CNS lipids exclusively. To this end, previous studies undertaking serum and plasma lipidomics have

uncovered changes to the lipidome in bvFTD cases compared with controls, especially noting increases in the levels of triglycerides and cholesterol, potentially highlighting changes to eating habits in bvFTD cases (Kim et al. 2018, Phan et al. 2020, Wang et al. 2020).

It is interesting to note that despite the heterogeneity of the novel gene mutations and their varying clinical presentations, the plasma GalCer and ST levels in these cases tend to be closely clustered. This may indicate that novel mutations in unique genes required for white matter function may impact myelin lipid metabolism with similar consequences. For example, peroxisomes (*PEX* genes) are required for plasmalogen synthesis and turnover of very long-chain fatty acids, while *FA2H* is required for the formation of hydroxylated very long-chain myelin lipids and *ARSA* is required for the catabolism of STs and their turnover (Alderson et al. 2004, Eckhardt et al. 2005, Hein et al. 2008, Cesani et al. 2016, Honsho et al. 2017). These gene mutations all have the potential to result in impairments in the structural integrity of myelin. Our findings may be indicative of the inter-dependency of functional lipid metabolic pathways in ensuring myelin integrity, which is exemplified by our mouse CerS2 results, showing that the acyl chain composition of galactosylceramides is essential for myelin integrity (Teo et al. 2023).

It is unknown exactly by what mechanism myelin lipids enter the plasma, and whether from the CNS or PNS. It has been postulated that CNS GalCer may enter the periphery via transport from the CSF on apolipoprotein E-associated lipoproteins, or within lipid-laden nanostructures (Han et al. 2003, Harrington et al. 2009). Increased levels of CSF GalCer and STs have been reported in demyelinating disorders, however the relationship between brain demyelination, CSF and plasma or serum changes appears to be variable (Lubetzki et al. 1989, Haghighi et al. 2013, Saville et al. 2017). If CNS GalCer and ST are transported or excreted into the plasma, it may be expected that increased myelin degeneration may lead to increased levels of these lipids in the periphery. For example, In the lysosomal storage disease metachromatic leukodystrophy (MLD), deficiency of *ARSA*, encoding the lysosomal lipase responsible for degradation of ST and lysosulfatide leads to their accumulation in myelinating cells, causing subsequent demyelination and neurodegeneration. Plasma CSF and ST levels, especially C18:0 ST, are elevated in MLD cases (Saville et al. 2017, Cao et al. 2020). However, myelin lipids are constantly being turned over (Yeung et al. 2014). Decreased plasma levels of GalCer and STs in FTD cases, and especially those carrying novel mutations may indicate that

turnover of myelin lipids is reduced in the brains of people with FTD. As the brain is highly lipid rich, it may be particularly susceptible to lipid metabolic dysfunction caused by novel mutations in genes necessary for white matter integrity, which may lead to impaired myelin lipid turnover and subsequent demyelination, resulting in decreased levels of detectable GalCer and ST in the periphery. Additionally, the presence of WMH observed in bvFTD cases by MRI may be indicative of demyelination and may lead to similar outcomes in the sporadic FTD cases (Huynh et al. 2021). It is likely that FTD-*GRN* cases also exhibit an impairment in myelin lipid catabolism and turnover, as accumulation of cholesterol esters are seen alongside demyelination in brain white matter (Marian et al. 2023).

Given our chapter 2 findings of reduced myelin lipids but accumulation of sphingosine in brain tissue of FTD-*GRN* cases, where progranulin similarly appears to play a significant role in lipid metabolic regulation, it is reasonable to posit that the reduction in very long chain GalCer and ST in the plasma of bvFTD and FTD cases carrying WM mutations may be accompanied by an accumulation of galactosylsphingosine or sphingosine, metabolites of GalCer and ST. Logan and colleagues described accumulation of glucosylsphingosine, a substrate of glucocerebrosidase, in plasma from FTD-*GRN* cases (Logan et al. 2021). GalCer and ST analysis of matched CSF from the cases described in this study would allow us to clarify the relationship between brain-derived lipids and corresponding lipids in the circulation.

Several studies have reported an increase in CSF ST, but not GalCer, in people with the inflammatory demyelinating disease multiple sclerosis (MS), while another found no difference in CSF ST, however both serum anti-ST and anti-GalCer antibodies were elevated in MS cases (Haghighi et al. 2012, Haghighi et al. 2013, Novakova et al. 2018, Novakova et al. 2023). When stratified by disease course, MS cases with the relapsing-remitting course, characterised by periods of active demyelination interspersed with periods of remission and remyelination showed increases to serum GalCer occurring prior to clinical relapse, however, there were no increases to serum GalCer in their primary progressive disease course counterparts, where remission periods are not observed (Lubetzki et al. 1989). In the progressive forms of MS, mature oligodendrocytes are significantly lost, and the remyelination capacity of the CNS is reduced (Berghoff et al. 2022). Taken together, these results may indicate that the detection of myelin lipids in the periphery may be dependent on the remyelination capacity and bulk availability of myelin lipids in the CNS.

In vascular dementia (VAD), higher CSF ST levels are seen in comparison to both Alzheimer's Disease cases and controls, which is thought to arise as a result of intermittent demyelinating insults leading to a marked efflux of myelin lipids in VAD compared to the slower demyelinating course observed in AD (Fredman et al. 1992, Blomqvist et al. 2017). It is likely that blood-brain barrier (BBB) dysfunction plays a role in the increased presence of STs in the CSF, and indeed it has been proposed that CSF STs on a background of BBB dysfunction may be originating from the serum (Fredman et al. 1992, Blomqvist et al. 2017). In contrast, in elderly individuals with white matter lesions (WML), lower baseline CSF ST was shown to be predictive of more pronounced progression of WML, which the authors attributed to a potential decline in the remyelination capacity of these individuals (Jonsson et al. 2012). While WMH have been reported in the brains of both FTD and Alzheimer's disease cases, it has been reported that WMH are more severe in bvFTD cases compared to those observed in Alzheimer's disease (Huynh et al. 2021). Profiling plasma levels of GalCer and ST in Alzheimer's disease cases would be valuable to determine whether a reduction in circulating myelin lipids is a general feature of neurodegeneration, or an FTD-specific finding considering the more pronounced white matter dysfunction seen in FTD cases by MRI.

The relationship between CNS myelin lipids and those detected in the periphery is not straightforward. Further investigation is required to determine how plasma GalCer and ST relate to the CNS pathological findings in FTD, however the observation of decreased myelin lipids in the plasma of FTD cases indicates that myelin lipid metabolism is impacted in FTD. It is distinctly possible that over time, impaired myelin lipid turnover in the CNS can be observed in the periphery as a decrease in myelin lipids in FTD cases compared with healthy controls.

4.5 Conclusion

In this study we have demonstrated that we are able to separate the structural isomers GalCer and GluCer in several biological matrices. However, the assay sensitivity is susceptible to changes in solvent composition and MS instrument sensitivity. We have determined that reduced plasma galactosphingolipids appear to be a feature of FTD, with FTD cases display significantly lower levels of GalCer and ST in the plasma, especially in the very-long chain species that are enriched in myelin. FTD cases with white matter mutations may have a more pronounced role in myelin lipid metabolism as these cases displayed significantly reduced levels of ST compared with sporadic FTD cases. Further investigation is required to determine whether this phenomenon is seen in FTD cases alone, and whether it is shared with the common inherited forms of FTD caused by *C9orf72*, *GRN* or *MAPT* mutations, or is common to other neurodegenerative diseases such as Alzheimer's disease.

Chapter 5: Summary and Future Directions

Heterozygous loss of function mutations in the *GRN* gene or hexanucleotide repeat expansions in the *C9orf72* gene are the most common causes of inherited FTD, leading to bvFTD with TDP-43 neuropathology (Rademakers et al. 2012). The mechanisms by which these gene mutations cause FTD is still unknown, however, white matter abnormalities observed in bvFTD cases in MRI studies suggests that brain lipid metabolism may play a role in the pathogenesis of FTD. Despite a growing body of evidence from MRI studies that white matter changes occur as an early feature of FTD, the biochemical and neuropathological correlates of these MRI features have not been established. This thesis contributes novel insights into the biochemical basis of FTD caused by either *GRN* or *C9orf72* gene mutations in post-mortem human brain tissue utilising a multi-omic approach encompassing untargeted mass spectrometry-based lipidomics and proteomics and describes a novel isomer separation method to enable quantification of the myelin lipid galactosylceramide as a putative biomarker of myelin degeneration in plasma. This work establishes lipid metabolic dysfunction and myelin defects as key drivers in the precipitation of FTD due to *GRN* and *C9orf72* mutations and identifies lipid metabolic dysfunction as a feature of bvFTD pathogenesis in general.

Our results demonstrate that pronounced myelin degeneration identified by lipidomic, histological and immunoblotting techniques is a common feature of the major inherited forms of FTD caused by either *GRN* or *C9orf72* mutations, but is a more pronounced feature of FTD-*GRN* cases. We have established that these features are present even in the relatively unaffected parietal white matter in the absence of overt neuronal degeneration, exemplified by significant accumulation of cholesterol esters in FTD-*GRN* cases, indicating that FTD-*GRN* cases appear to have a pronounced susceptibility to myelin lipid loss, distinguishing them from FTD-*C9orf72* cases. Proteomic analysis supported these findings by demonstrating increased abundance of phagocytic markers and decreased mevalonate pathway synthesis proteins in both FTD groups, but more severely in FTD-*GRN* cases.

Proteomic findings identified mitochondrial dysfunction as a common dysregulated pathway in grey matter of both FTD-*GRN* and FTD-*C9orf72* cases, however FTD-*GRN* cases showed significant decrease in abundance of respiratory complex proteins compared to FTD-*C9orf72*

cases, in agreement with our lipidomic findings of selective accumulation of acylcarnitines in the frontal grey matter of FTD-*GRN* cases alone. These features were similarly observed in the less affected parietal lobe in addition to lipid metabolic protein changes, identifying these changes as early markers of FTD pathogenesis caused by either *GRN* or *C9orf72* mutations.

This thesis describes a novel lipidomic method to quantify the myelin lipid GalCer in plasma. Successful separation of the structural isomers GluCer and GalCer enabled quantification of the less abundant myelin-enriched isomer GalCer in human plasma. Myelin galactosphingolipids are significantly lower in plasma of both sporadic FTD cases and FTD cases carrying mutations in genes necessary for white matter integrity, identifying decreased circulating myelin lipids as a feature of bvFTD. This work establishes the signature of altered sphingolipid metabolism as a feature of the periphery in addition to the CNS, and establishes the potential for these lipids to serve as diagnostic and prognostic plasma biomarkers in FTD.

It has been established that bvFTD carriers show evidence of white matter hyperintensities by MRI (Huynh et al. 2021). In future, lipidomic and proteomic investigation of sporadic FTD cases would improve our understanding of whether the pathological changes observed in FTD-*GRN* and FTD-*C9orf72* cases are a consequence of their genetic risk factors, or are shared with sporadic FTD cases. The neuropathological correlates of white matter hyperintensities by MRI have not been widely investigated. Our findings establish a biochemical basis for the white matter hyperintensities observed in MRI studies of FTD cases, identifying myelin degeneration and gliosis as significant drivers of neurodegeneration. These findings support the use of MRI techniques in the diagnosis of FTD, and future longitudinal studies investigating the correlations between neuroimaging and biochemical findings have the potential to improve our understanding of disease progression and associated neuropathology.

This work highlights the importance of investigating white matter changes in neurodegenerative diseases. Future studies should aim to examine changes to white matter in addition to grey matter brain regions to provide greater understanding of the contribution of myelin loss to neurodegeneration, and to clarify whether myelin degeneration may precede neurodegeneration in sporadic FTD cases through investigation of the biochemical mechanisms underlying myelin dysfunction. This has the potential to expand our understanding not only of the pathogenesis of FTD, but other neurodegenerative diseases.

At present, our understanding of the specific lipidomic and proteomic changes observed in these cases is largely limited by the brain regions from which they were sampled. Any given sampling region contains a variety of cell types, and in the absence of additional techniques to separate cell types or visualise the tissue using histology from matched cases, contribution of the cell types involved in pathways of interest are inferred based on their sampling region. Immunohistochemical techniques were used to cross-validate our major findings, however this is not often possible. Cell-type enrichment of our proteomic data as recently performed by Miedema and colleagues (Miedema et al. 2022) would inform the contribution of specific cell-types to the proteomic changes observed, increasing our understanding of the interaction between dysregulated pathways and the cell types involved. Advances in lipidomic and proteomic mass spectrometry imaging techniques also hold the potential to provide spatial and cell-type specific resolution to overcome these challenges, and would be a valuable tool for future investigation (Krijnen et al. 2023, Vandenbosch et al. 2023).

Investigating pathological changes in post-mortem brain tissue is valuable as it overcomes the problem of attempting translation of *in-vitro* or animal models into meaningful discoveries for human pathology. However, the relationship between the drivers and consequences of observed pathological changes is difficult to dissect. In an attempt to circumvent this problem, we profiled both heavily-affected frontal cortex and less affected parietal cortex samples to determine the contribution of the gene mutations in the absence of overt neurodegeneration. Post-mortem, age-dependent pathological changes are often studied in experimental mouse models, which have the potential to provide valuable insight into the effects of genetic risk factors in the absence of the heterogeneity observed in humans, however, they do not necessarily recapitulate human disease. An example of this can be seen in the fact that *Grn* deficiency in mice does not follow gene-dosage-dependent impairment as it does in humans, and homozygous *Grn* loss must be employed in mice in order to recapitulate the major pathological features of FTD-*GRN* cases (Gotzl et al. 2014). Future studies may benefit from the adoption of large animal models that share a more similar CNS neuroanatomy to humans as an alternative to better recapitulate the neuropathology caused by these genetic defects (Mitchell et al. 2023).

FTD is a neurodegenerative disease prone to frequent misdiagnosis due to the potential for symptoms to mirror psychiatric disorders (Woolley et al. 2011, Shinagawa et al. 2016). This

thesis establishes the potential for providing more diagnostic certainty in FTD by tracking disease onset and progression through profiling peripheral plasma levels of GalCer and ST. Assessment of plasma levels of GalCer and ST from cases with genetic FTD such as FTD-*GRN* cases would help clarify the relationship between brain and circulating myelin lipid levels in light of the pronounced demyelination we observe in these cases. Additionally, analysis of CSF samples would provide insight into whether the changes to myelin-enriched lipids observed in FTD cases in the periphery originate from the CNS, or are indicative of a general lipid metabolic dysfunction. This assay may have potential as a biomarker in other demyelinating neurodegenerative diseases such as multiple sclerosis.

Current therapies for FTD are lacking and limited to symptomatic treatment (Balachandran et al. 2021). This thesis identifies a rationale for the development of novel therapeutic approaches to target the demyelination contributing to neurodegeneration in genetic FTD caused by *GRN* and *C9orf72* mutations. Approaches to slow or prevent the progression of demyelination through strategies to promote remyelination or modulate autophagy to reduce demyelination or boost myelin lipid turnover are worthy avenues for investigation (Nutma et al. 2021, Zhou et al. 2023).

Despite the importance of brain lipid homeostasis to neurophysiological function, research has largely focussed on the contribution of grey matter to neurodegenerative disease pathogenesis. Myelin and oligodendrocytes are essential for neuronal health and this thesis identifies white matter brain regions as having substantial pathological implications in FTD caused by *GRN* and *C9orf72* gene mutations. In summary, this thesis contributes the first comprehensive biochemical study into the aetiology of genetic frontotemporal dementia caused by mutations in the *GRN* and *C9orf72* genes. This work establishes dysfunctional brain lipid metabolism as an early and significant driver of neurodegeneration in FTD cases and highlights the potential for new diagnostic and therapeutic approaches to target the lipid metabolic dysfunction identified in bvFTD.

Reference List

Abdul-Hammed, M., B. Breiden, G. Schwarzmann and K. Sandhoff (2017). "Lipids regulate the hydrolysis of membrane bound glucosylceramide by lysosomal β-glucocerebrosidase." J Lipid Res **58**(3): 563-577.

Adomavicius, T., M. Guaita, Y. Zhou, M. D. Jennings, Z. Latif, A. M. Roseman and G. D. Pavitt (2019). "The structural basis of translational control by eIF2 phosphorylation." Nature Communications **10**(1): 2136.

Agosta, F., S. Galantucci, G. Magnani, A. Marcone, D. Martinelli, M. Antonietta Volontè, . . . M. Filippi (2015). "MRI signatures of the frontotemporal lobar degeneration continuum." Hum Brain Mapp **36**(7): 2602-2614.

Ahmed, R. M., M. MacMillan, L. Bartley, G. M. Halliday, M. C. Kiernan, J. R. Hodges and O. Piguet (2014). "Systemic metabolism in frontotemporal dementia." Neurology **83**(20): 1812-1818.

Ahmed, Z., I. R. A. Mackenzie, M. L. Hutton and D. W. Dickson (2007). "Progranulin in frontotemporal lobar degeneration and neuroinflammation." Journal of Neuroinflammation **4**(1): 7.

Ahmed, Z., H. Sheng, Y. F. Xu, W. L. Lin, A. E. Innes, J. Gass, . . . J. Lewis (2010). "Accelerated lipofuscinosis and ubiquitination in granulin knockout mice suggest a role for progranulin in successful aging." Am J Pathol **177**(1): 311-324.

Akgoc, Z., M. Sena-Esteves, D. R. Martin, X. Han, A. d'Azzo and T. N. Seyfried (2015). "Bis(monoacylglycero)phosphate: a secondary storage lipid in the gangliosidoses." Journal of Lipid Research **56**(5): 1005-1006.

Alderson, N. L., B. M. Rembiesa, M. D. Walla, A. Bielawska, J. Bielawski and H. Hama (2004). "The Human FA2H Gene Encodes a Fatty Acid 2-Hydroxylase*." Journal of Biological Chemistry **279**(47): 48562-48568.

Almeida, M. R., M. C. Macário, L. Ramos, I. Baldeiras, M. H. Ribeiro and I. Santana (2016). "Portuguese family with the co-occurrence of frontotemporal lobar degeneration and neuronal ceroid lipofuscinosis phenotypes due to progranulin gene mutation." Neurobiology of Aging **41**: 200.e201-200.e205.

Ameur, F., O. Colliot, P. Caroppo, S. Ströer, D. Dormont, A. Brice, . . . A. Bertrand (2016). "White matter lesions in FTLD: distinct phenotypes characterize GRN and C9ORF72 mutations." Neurology Genetics **2**(1): e47.

Amick, J., A. Roczniak-Ferguson and S. M. Ferguson (2016). "C9orf72 binds SMCR8, localizes to lysosomes, and regulates mTORC1 signaling." Mol Biol Cell **27**(20): 3040-3051.

Ando, S., Y. Tanaka, Y. Toyoda and K. Kon (2003). "Turnover of Myelin Lipids in Aging Brain." Neurochemical Research **28**(1): 5-13.

Andrés-Benito, P., E. Gelpi, M. Jové, N. Mota-Martorell, È. Obis, M. Portero-Otin, . . . I. Ferrer (2021). "Lipid alterations in human frontal cortex in ALS-FTLD-TDP43 proteinopathy spectrum are partly related to peroxisome impairment." Neuropathology and Applied Neurobiology **47**(4): 544-563.

Andrés-Benito, P., E. Gelpi, M. Povedano, K. Ausín, J. Fernández-Irigoyen, E. Santamaría and I. Ferrer (2019). "Combined Transcriptomics and Proteomics in Frontal Cortex Area 8 in Frontotemporal Lobar Degeneration Linked to C9ORF72 Expansion." J Alzheimers Dis **68**(3): 1287-1307.

Ardesch, D. J., L. H. Scholtens, S. C. de Lange, L. Roumazeilles, A. A. Khrapitchev, T. M. Preuss, . . . M. P. van den Heuvel (2021). "Scaling Principles of White Matter Connectivity in the Human and Nonhuman Primate Brain." Cerebral Cortex **32**(13): 2831-2842.

Arrant, A. E., J. R. Roth, N. R. Boyle, S. N. Kashyap, M. Q. Hoffmann, C. F. Murchison, . . . E. D. Roberson (2019). "Impaired β-glucocerebrosidase activity and processing in frontotemporal dementia due to progranulin mutations." Acta Neuropathologica Communications **7**(1): 218.

Arreguin, A. J. and H. Colognato (2020). "Brain Dysfunction in LAMA2-Related Congenital Muscular Dystrophy: Lessons From Human Case Reports and Mouse Models." Front Mol Neurosci **13**: 118.

Bain, H. D. C., Y. S. Davidson, A. C. Robinson, S. Ryan, S. Rollinson, A. Richardson, . . . D. M. A. Mann (2019). "The role of lysosomes and autophagosomes in frontotemporal lobar degeneration." Neuropathol Appl Neurobiol **45**(3): 244-261.

Baker, M., I. R. Mackenzie, S. M. Pickering-Brown, J. Gass, R. Rademakers, C. Lindholm, . . . M. Hutton (2006). "Mutations in progranulin cause tau-negative frontotemporal dementia linked to chromosome 17." Nature **442**(7105): 916-919.

Balachandran, S., E. L. Matlock, M. L. Conroy and C. E. Lane (2021). "Behavioral Variant Frontotemporal Dementia: Diagnosis and Treatment Interventions." Current Geriatrics Reports **10**(3): 101-107.

Banworth, M. J. and G. Li (2018). "Consequences of Rab GTPase dysfunction in genetic or acquired human diseases." Small GTPases **9**(1-2): 158-181.

Barth, P. G., J. Gootjes, H. Bode, P. Vreken, C. B. Majoie and R. J. Wanders (2001). "Late onset white matter disease in peroxisome biogenesis disorder." Neurology **57**(11): 1949-1955.

Bateman, A., D. Belcourt, H. Bennett, C. Lazure and S. Solomon (1990). "Granulins, a novel class of peptide from leukocytes." Biochemical and Biophysical Research Communications **173**(3): 1161-1168.

Becker, I., L. Wang-Eckhardt, A. Yaghootfam, V. Gieselmann and M. Eckhardt (2008). "Differential expression of (dihydro)ceramide synthases in mouse brain: oligodendrocyte-specific expression of CerS2/Lass2." Histochemistry and Cell Biology **129**(2): 233-241.

Beel, S., M. Moisse, M. Damme, L. De Muynck, W. Robberecht, L. Van Den Bosch, . . . P. Van Damme (2017). "Progranulin functions as a cathepsin D chaperone to stimulate axonal outgrowth in vivo." Hum Mol Genet **26**(15): 2850-2863.

Bélanger, M., I. Allaman and Pierre J. Magistretti (2011). "Brain Energy Metabolism: Focus on Astrocyte-Neuron Metabolic Cooperation." Cell Metabolism **14**(6): 724-738.

Berghoff, S. A., L. Spieth and G. Saher (2022). "Local cholesterol metabolism orchestrates remyelination." Trends Neurosci **45**(4): 272-283.

Berghoff, S. A., L. Spieth and G. Saher (2022). "Local cholesterol metabolism orchestrates remyelination." Trends in Neurosciences **45**(4): 272-283.

Beytía Mde, L., G. Dekomien, S. Hoffjan, V. Haug, C. Anastasopoulos and J. Kirschner (2014). "High creatine kinase levels and white matter changes: clinical and genetic spectrum of congenital muscular dystrophies with laminin alpha-2 deficiency." Mol Cell Probes **28**(4): 118-122.

Bhatia, S., A. M. Jenner, H. Li, K. Ruberu, A. S. Spiro, C. E. Shepherd, . . . B. Garner (2013). "Increased Apolipoprotein D Dimer Formation in Alzheimer's Disease Hippocampus is Associated with Lipid Conjugated Diene Levels." Journal of Alzheimer's Disease **35**: 475-486.

Bhatia, S., B. Knoch, J. Wong, Woojin S. Kim, Paul L. Else, Aaron J. Oakley and B. Garner (2012). "Selective reduction of hydroperoxyeicosatetraenoic acids to their hydroxy derivatives by apolipoprotein D: implications for lipid antioxidant activity and Alzheimer's disease." Biochemical Journal **442**(3): 713-721.

Björkhem, I., D. Lütjohann, U. Diczfalusy, L. Ståhle, G. Ahlborg and J. Wahren (1998). "Cholesterol homeostasis in human brain: turnover of 24S-hydroxycholesterol and evidence for a cerebral origin of most of this oxysterol in the circulation." Journal of Lipid Research **39**(8): 1594-1600.

Blomqvist, M., J. Borén, H. Zetterberg, K. Blennow, J.-E. Månsson and M. Ståhlman (2017). "High-throughput analysis of sulfatides in cerebrospinal fluid using automated extraction and UPLC-MS/MS." Journal of Lipid Research **58**(7): 1482-1489.

Boland, S., S. Swarup, Y. A. Ambaw, P. C. Malia, R. C. Richards, A. W. Fischer, . . . R. V. Farese (2022). "Deficiency of the frontotemporal dementia gene GRN results in gangliosidosis." Nature Communications **13**(1): 5924.

Borroni, B., F. Ferrari, D. Galimberti, B. Nacmias, C. Barone, S. Bagnoli, . . . A. Padovani (2014). "Heterozygous TREM2 mutations in frontotemporal dementia." Neurobiol Aging **35**(4): 934.e937-910.

Bosio, A., E. Binczek and W. Stoffel (1996). "Functional breakdown of the lipid bilayer of the myelin membrane in central and peripheral nervous system by disrupted galactocerebroside synthesis." Proceedings of the National Academy of Sciences **93**(23): 13280-13285.

Boutin, M., Y. Sun, J. J. Shacka and C. Auray-Blais (2016). "Tandem Mass Spectrometry Multiplex Analysis of Glucosylceramide and Galactosylceramide Isoforms in Brain Tissues at Different Stages of Parkinson Disease." Anal Chem **88**(3): 1856-1863.

Boxer, A. L., D. S. Knopman, D. I. Kaufer, M. Grossman, C. Onyike, N. Graf-Radford, . . . B. L. Miller (2013). "Memantine in patients with frontotemporal lobar degeneration: a multicentre, randomised, double-blind, placebo-controlled trial." Lancet Neurol **12**(2): 149-156.

Braverman, N. E. and A. B. Moser (2012). "Functions of plasmalogen lipids in health and disease." Biochimica et Biophysica Acta (BBA) - Molecular Basis of Disease **1822**(9): 1442-1452.

Brettschneider, J., J. B. Toledo, V. M. Van Deerlin, L. Elman, L. McCluskey, V. M. Y. Lee and J. Q. Trojanowski (2012). "Microglial Activation Correlates with Disease Progression and Upper Motor Neuron Clinical Symptoms in Amyotrophic Lateral Sclerosis." PLOS ONE **7**(6): e39216.

Brody, B. A., H. C. Kinney, A. S. Kloman and F. H. Gilles (1987). "Sequence of central nervous system myelination in human infancy. I. An autopsy study of myelination." J Neuropathol Exp Neurol **46**(3): 283-301.

Bryleva, E. Y., M. A. Rogers, C. C. Y. Chang, F. Buen, B. T. Harris, E. Rousselet, . . . T.-Y. Chang (2010). "ACAT1 gene ablation increases 24(S)-hydroxycholesterol content in the brain and ameliorates amyloid pathology in mice with AD." Proceedings of the National Academy of Sciences **107**(7): 3081-3086.

Buhaescu, I. and H. Izzedine (2007). "Mevalonate pathway: A review of clinical and therapeutical implications." Clinical Biochemistry **40**(9): 575-584.

Buratti, E., T. Dörk, E. Zuccato, F. Pagani, M. Romano and F. E. Baralle (2001). "Nuclear factor TDP-43 and SR proteins promote in vitro and in vivo CFTR exon 9 skipping." The EMBO Journal **20**(7): 1774-1784.

Burrell, J. R., M. C. Kiernan, S. Vucic and J. R. Hodges (2011). "Motor Neuron dysfunction in frontotemporal dementia." Brain **134**(9): 2582-2594.

Cantuti-Castelvetri, L., D. Fitzner, M. Bosch-Queralt, M. T. Weil, M. Su, P. Sen, . . . M. Simons (2018). "Defective cholesterol clearance limits remyelination in the aged central nervous system." Science **359**(6376): 684-688.

Cao, K. H., G. Zhang, L. Jacobsen and J. Wu (2020). "LC-MS/MS assays to quantify sulfatides and lysosulfatide in cerebrospinal fluid of metachromatic leukodystrophy patients." Bioanalysis **12**(22): 1621-1633.

Caroppo, P., I. Le Ber, A. Camuzat, F. Clot, L. Naccache, F. Lamari, . . . A. Brice (2014). "Extensive White Matter Involvement in Patients With Frontotemporal Lobar Degeneration: Think PrognanulinWhite Matter Involvement in Patients With FTLDWhite Matter Involvement in Patients With FTLD." JAMA Neurology **71**(12): 1562-1566.

Cash, D. M., M. Bocchetta, D. L. Thomas, K. M. Dick, J. C. van Swieten, B. Borroni, . . . J. Warren (2018). "Patterns of gray matter atrophy in genetic frontotemporal dementia: results from the GENFI study." Neurobiology of Aging **62**: 191-196.

Cenik, B., C. F. Sephton, B. Kutluk Cenik, J. Herz and G. Yu (2012). "Progranulin: a proteolytically processed protein at the crossroads of inflammation and neurodegeneration." J Biol Chem **287**(39): 32298-32306.

Cesani, M., L. Lorioli, S. Grossi, G. Amico, F. Fumagalli, I. Spiga, . . . A. Biffi (2016). "Mutation Update of ARSA and PSAP Genes Causing Metachromatic Leukodystrophy." Hum Mutat **37**(1): 16-27.

Chan, R. B., T. G. Oliveira, E. P. Cortes, L. S. Honig, K. E. Duff, S. A. Small, . . . G. Di Paolo (2012). "Comparative lipidomic analysis of mouse and human brain with Alzheimer disease." The Journal of Biological Chemistry **287**(4): 2678-2688.

Chen-Plotkin, A. S., M. Martinez-Lage, P. M. A. Sleiman, W. Hu, R. Greene, E. M. Wood, . . . V. M. Van Deerlin (2011). "Genetic and Clinical Features of Progranulin-Associated Frontotemporal Lobar Degeneration." Archives of Neurology **68**(4): 488-497.

Chen-Plotkin, A. S., T. L. Unger, M. D. Gallagher, E. Bill, L. K. Kwong, L. Volpicelli-Daley, . . . V. M. Y. Lee (2012). "TMEM106B, the risk gene for frontotemporal dementia, is regulated by the microRNA-132/212 cluster and affects progranulin pathways." The Journal of neuroscience : the official journal of the Society for Neuroscience **32**(33): 11213-11227.

Chen-Plotkin, A. S., J. Xiao, F. Geser, M. Martinez-Lage, M. Grossman, T. Unger, . . . V. M. Y. Lee (2009). "Brain progranulin expression in GRN-associated frontotemporal lobar degeneration." Acta Neuropathologica **119**(1): 111.

Chen, Y., J. Jian, A. Hettinghouse, X. Zhao, K. D. R. Setchell, Y. Sun and C. J. Liu (2018). "Progranulin associates with hexosaminidase A and ameliorates GM2 ganglioside accumulation and lysosomal storage in Tay-Sachs disease." J Mol Med (Berl) **96**(12): 1359-1373.

Chiang, J. Y. L. and J. M. Ferrell (2020). "Up to date on cholesterol 7 alpha-hydroxylase (CYP7A1) in bile acid synthesis." Liver Research **4**(2): 47-63.

Christomanou, H., A. Chabás, T. Pámpols and A. Guardiola (1989). "Activator protein deficient Gaucher's disease. A second patient with the newly identified lipid storage disorder." Klin Wochenschr **67**(19): 999-1003.

Cignarella, F., F. Filipello, B. Bollman, C. Cantoni, A. Locca, R. Mikesell, . . . L. Piccio (2020). "TREM2 activation on microglia promotes myelin debris clearance and remyelination in a model of multiple sclerosis." Acta Neuropathol **140**(4): 513-534.

Coetzee, T., N. Fujita, J. Dupree, R. Shi, A. Blight, K. Suzuki, . . . B. Popko (1996). "Myelination in the absence of galactocerebroside and sulfatide: normal structure with abnormal function and regional instability." Cell **86**(2): 209-219.

Couttas, T. A., Y. H. Rustam, H. Song, Y. Qi, J. D. Teo, J. Chen, . . . A. S. Don (2020). "A Novel Function of Sphingosine Kinase 2 in the Metabolism of Sphinga-4,14-Diene Lipids." Metabolites **10**(6).

Coyle-Gilchrist, I. T. S., K. M. Dick, K. Patterson, P. Vázquez Rodríquez, E. Wehmann, A. Wilcox, . . . J. B. Rowe (2016). "Prevalence, characteristics, and survival of frontotemporal lobar degeneration syndromes." Neurology **86**(18): 1736-1743.

Crane, F. L. (2001). "Biochemical Functions of Coenzyme Q10." Journal of the American College of Nutrition **20**(6): 591-598.

Cruchaga, C., C. Graff, H.-H. Chiang, J. Wang, A. L. Hinrichs, N. Spiegel, . . . A. Goate (2011). "Association of TMEM106B Gene Polymorphism With Age at Onset in Granulin Mutation Carriers and Plasma Granulin Protein Levels." Archives of Neurology **68**(5): 581-586.

Cruts, M., I. Gijselinck, J. van der Zee, S. Engelborghs, H. Wils, D. Pirici, . . . C. Van Broeckhoven (2006). "Null mutations in progranulin cause ubiquitin-positive frontotemporal dementia linked to chromosome 17q21." Nature **442**(7105): 920-924.

Davidson, J. M., R. S. Chung and A. Lee (2022). "The converging roles of sequestosome-1/p62 in the molecular pathways of amyotrophic lateral sclerosis (ALS) and frontotemporal dementia (FTD)." Neurobiology of Disease **166**: 105653.

de Araujo, M. E. G., G. Liebscher, M. W. Hess and L. A. Huber (2020). "Lysosomal size matters." Traffic **21**(1): 60-75.

DeJesus-Hernandez, M., I. R. Mackenzie, B. F. Boeve, A. L. Boxer, M. Baker, N. J. Rutherford, . . . R. Rademakers (2011). "Expanded GGGGCC hexanucleotide repeat in noncoding region of C9ORF72 causes chromosome 9p-linked FTD and ALS." Neuron **72**(2): 245-256.

Dobson-Stone, C., M. Hallupp, H. Shahheydari, A. M. G. Ragagnin, Z. Chatterton, F. Carew-Jones, . . . J. B. Kwok (2020). "CYLD is a causative gene for frontotemporal dementia - amyotrophic lateral sclerosis." Brain **143**(3): 783-799.

Double, K. L., V. N. Dedov, H. Fedorow, E. Kettle, G. M. Halliday, B. Garner and U. T. Brunk (2008). "The comparative biology of neuromelanin and lipofuscin in the human brain." Cell Mol Life Sci **65**(11): 1669-1682.

Dutta, R., J. McDonough, X. Yin, J. Peterson, A. Chang, T. Torres, . . . B. D. Trapp (2006). "Mitochondrial dysfunction as a cause of axonal degeneration in multiple sclerosis patients." Annals of Neurology **59**(3): 478-489.

Düvel, K., J. L. Yecies, S. Menon, P. Raman, A. I. Lipovsky, A. L. Souza, . . . B. D. Manning (2010). "Activation of a metabolic gene regulatory network downstream of mTOR complex 1." Mol Cell **39**(2): 171-183.

Eckhardt, M., A. Yaghootfam, S. N. Fewou, I. Zöller and V. Gieselmann (2005). "A mammalian fatty acid hydroxylase responsible for the formation of alpha-hydroxylated galactosylceramide in myelin." Biochem J **388**(Pt 1): 245-254.

Edvardson, S., H. Hama, A. Shaag, J. M. Gomori, I. Berger, D. Soffer, . . . O. Elpeleg (2008). "Mutations in the fatty acid 2-hydroxylase gene are associated with leukodystrophy with spastic paraparesis and dystonia." Am J Hum Genet **83**(5): 643-648.

Evers, B. M., C. Rodriguez-Navas, R. J. Tesla, J. Prange-Kiel, C. R. Wasser, K. S. Yoo, . . . J. Herz (2017). "Lipidomic and Transcriptomic Basis of Lysosomal Dysfunction in Progranulin Deficiency." Cell reports **20**(11): 2565-2574.

Ezaki, J., L. S. Wolfe and E. Kominami (1995). "Defect of proteolysis of mitochondrial ATP synthase subunit C in neuronal ceroid lipofuscinosis." Gerontology **41 Suppl 2**: 259-269.

Fanjul-Fernández, M., V. Quesada, R. Cabanillas, J. Cadiñanos, T. Fontanil, Á. Obaya, . . . C. López-Otín (2013). "Cell–cell adhesion genes CTNNA2 and CTNNA3 are tumour suppressors frequently mutated in laryngeal carcinomas." Nature Communications **4**(1): 2531.

Farg, M. A., V. Sundaramoorthy, J. M. Sultana, S. Yang, R. A. K. Atkinson, V. Levina, . . . J. D. Atkin (2014). "C9ORF72, implicated in amytrophic lateral sclerosis and frontotemporal dementia, regulates endosomal trafficking." Human Molecular Genetics **23**(13): 3579-3595.

Feng, T., S. Mai, J. M. Roscoe, R. R. Sheng, M. Ullah, J. Zhang, . . . F. Hu (2020). "Loss of TMEM106B and PGRN leads to severe lysosomal abnormalities and neurodegeneration in mice." EMBO reports **21**(10): e50219.

Feng, T., R. R. Sheng, S. Solé-Domènech, M. Ullah, X. Zhou, C. S. Mendoza, . . . F. Hu (2020). "A role of the frontotemporal lobar degeneration risk factor TMEM106B in myelination." Brain **143**(7): 2255-2271.

Ferrer, I. (1999). "Neurons and their dendrites in frontotemporal dementia." Dement Geriatr Cogn Disord **10 Suppl 1**: 55-60.

Finch, N., M. Baker, R. Crook, K. Swanson, K. Kuntz, R. Surtees, . . . R. Rademakers (2009). "Plasma progranulin levels predict progranulin mutation status in frontotemporal dementia patients and asymptomatic family members." Brain **132**(3): 583-591.

Fredman, P., J.-E. Månsson, B.-M. Rynmark, K. Josefsen, A. Ekblond, L. Halldner, . . . K. Buschard (2000). "The glycosphingolipid sulfatide in the islets of Langerhans in rat pancreas is processed through recycling: possible involvement in insulin trafficking." Glycobiology **10**(1): 39-50.

Fredman, P., A. Wallin, K. Blennow, P. Davidsson, C. G. Gottfries and L. Svennerholm (1992). "Sulfatide as a biochemical marker in cerebrospinal fluid of patients with vascular dementia." Acta Neurol Scand **85**(2): 103-106.

Fünfschilling, U., L. M. Supplie, D. Mahad, S. Boretius, A. S. Saab, J. Edgar, . . . K.-A. Nave (2012). "Glycolytic oligodendrocytes maintain myelin and long-term axonal integrity." Nature **485**(7399): 517-521.

Gallagher, M. D., E. Suh, M. Grossman, L. Elman, L. McCluskey, J. C. Van Swieten, . . . A. S. Chen-Plotkin (2014). "TMEM106B is a genetic modifier of frontotemporal lobar degeneration with C9orf72 hexanucleotide repeat expansions." Acta Neuropathologica **127**(3): 407-418.

Ganfornina, M. D., S. Do Carmo, J. M. Lora, S. Torres-Schumann, M. Vogel, M. Allhorn, . . . D. Sanchez (2008). "Apolipoprotein D is involved in the mechanisms regulating protection from oxidative stress." Aging Cell **7**(4): 506-515.

Gass, J., A. Cannon, I. R. Mackenzie, B. Boeve, M. Baker, J. Adamson, . . . R. Rademakers (2006). "Mutations in progranulin are a major cause of ubiquitin-positive frontotemporal lobar degeneration." Hum Mol Genet **15**(20): 2988-3001.

Gegg, M. E., L. Sweet, B. H. Wang, L. S. Shihabuddin, S. P. Sardi and A. H. Schapira (2015). "No evidence for substrate accumulation in Parkinson brains with GBA mutations." Mov Disord **30**(8): 1085-1089.

Ghidoni, R., L. Benussi, M. Glionna, M. Franzoni and G. Binetti (2008). "Low plasma progranulin levels predict progranulin mutations in frontotemporal lobar degeneration." Neurology **71**(16): 1235-1239.

Gieselmann, V., S. Franken, D. Klein, J. E. Mansson, R. Sandhoff, R. Lüllmann Rauch, . . . N. Schaeren-Wiemers (2003). "Metachromatic leukodystrophy: consequences of sulphatide accumulation." Acta Paediatr Suppl **92**(443): 74-79; discussion 45.

Gijselinck, I., C. Van Broeckhoven and M. Cruts (2008). "Granulin mutations associated with frontotemporal lobar degeneration and related disorders: an update." Hum Mutat **29**(12): 1373-1386.

Gijselinck, I., S. Van Mossevelde, J. van der Zee, A. Sieben, S. Philtjens, B. Heeman, . . . C. Van Broeckhoven (2015). "Loss of TBK1 is a frequent cause of frontotemporal dementia in a Belgian cohort." Neurology **85**(24): 2116-2125.

Gomez-Sanchez, J. A., L. Carty, M. Iruarrizaga-Lejarreta, M. Palomo-Irigoyen, M. Varela-Rey, M. Griffith, . . . K. R. Jessen (2015). "Schwann cell autophagy, myelinophagy, initiates myelin clearance from injured nerves." J Cell Biol **210**(1): 153-168.

Goodier, J. L., A. O. Soares, G. C. Pereira, L. R. DeVine, L. Sanchez, R. N. Cole and J. L. García-Pérez (2020). "C9orf72-associated SMCR8 protein binds in the ubiquitin pathway and with proteins linked with neurological disease." Acta Neuropathologica Communications **8**(1): 110.

Gorno-Tempini, M. L., A. E. Hillis, S. Weintraub, A. Kertesz, M. Mendez, S. F. Cappa, . . . M. Grossman (2011). "Classification of primary progressive aphasia and its variants." Neurology **76**(11): 1006-1014.

Götzl, J. K., M. Brendel, G. Werner, S. Parhizkar, L. Sebastian Monasor, G. Kleinberger, . . . C. Haass (2019). "Opposite microglial activation stages upon loss of PGRN or TREM2 result in reduced cerebral glucose metabolism." EMBO Mol Med **11**(6).

Gotzl, J. K., K. Mori, M. Damme, K. Fellerer, S. Tahirovic, G. Kleinberger, . . . A. Capell (2014). "Common pathobiochemical hallmarks of progranulin-associated frontotemporal lobar degeneration and neuronal ceroid lipofuscinosis." Acta Neuropathol **127**(6): 845-860.

Greaves, C. V. and J. D. Rohrer (2019). "An update on genetic frontotemporal dementia." Journal of neurology **266**(8): 2075-2086.

Haghighi, S., A. Lekman, S. Nilsson, M. Blomqvist and O. Andersen (2012). "Myelin glycosphingolipid immunoreactivity and CSF levels in multiple sclerosis." Acta Neurologica Scandinavica **125**(1): 64-70.

Haghighi, S., A. Lekman, S. Nilsson, M. Blomqvist and O. Andersen (2013). "Increased CSF sulfatide levels and serum glycosphingolipid antibody levels in healthy siblings of multiple sclerosis patients." Journal of the Neurological Sciences **326**(1): 35-39.

Halvey, P., V. Farutin, L. Koppes, N. S. Gunay, D. A. Pappas, A. M. Manning and I. Capila (2021). "Variable blood processing procedures contribute to plasma proteomic variability." Clinical Proteomics **18**(1): 5.

Hamilton, J. A., C. J. Hillard, A. A. Spector and P. A. Watkins (2007). "Brain Uptake and Utilization of Fatty Acids, Lipids and Lipoproteins: Application to Neurological Disorders." Journal of Molecular Neuroscience **33**(1): 2-11.

Hamler, R., N. Brignol, S. W. Clark, S. Morrison, L. B. Dungan, H. H. Chang, . . . R. E. Boyd (2017). "Glucosylceramide and Glucosylsphingosine Quantitation by Liquid Chromatography-Tandem Mass Spectrometry to Enable In Vivo Preclinical Studies of Neuronopathic Gaucher Disease." Analytical Chemistry **89**(16): 8288-8295.

Han, X., H. Cheng, J. D. Fryer, A. M. Fagan and D. M. Holtzman (2003). "Novel Role for Apolipoprotein E in the Central Nervous System: MODULATION OF SULFATIDE CONTENT*." Journal of Biological Chemistry **278**(10): 8043-8051.

Harrington, M. G., A. N. Fonteh, E. Oborina, P. Liao, R. P. Cowan, G. McComb, . . . A. F. Hühmer (2009). "The morphology and biochemistry of nanostructures provide evidence for synthesis and signaling functions in human cerebrospinal fluid." Cerebrospinal Fluid Research **6**(1): 10.

Harris, Julia J., R. Jolivet and D. Attwell (2012). "Synaptic Energy Use and Supply." Neuron **75**(5): 762-777.

He, Y., K. Phan, S. Bhatia, R. Pickford, Y. Fu, Y. Yang, . . . W. S. Kim (2021). "Increased VLCFA-lipids and ELOVL4 underlie neurodegeneration in frontotemporal dementia." Scientific Reports **11**(1): 21348.

He, Z., C. H. P. Ong, J. Halper and A. Bateman (2003). "Progranulin is a mediator of the wound response." Nature Medicine **9**(2): 225-229.

Hein, S., P. Schönfeld, S. Kahlert and G. Reiser (2008). "Toxic effects of X-linked adrenoleukodystrophy-associated, very long chain fatty acids on glial cells and neurons from rat hippocampus in culture." Human Molecular Genetics **17**(12): 1750-1761.

Heo, D., J. P. Ling, G. C. Molina-Castro, A. J. Langseth, A. Waisman, K. A. Nave, . . . D. E. Bergles (2022). "Stage-specific control of oligodendrocyte survival and morphogenesis by TDP-43." Elife **11**.

Hildebrand, C., S. Remahl, H. Persson and C. Bjartmar (1993). "Myelinated nerve fibres in the CNS." Progress in Neurobiology **40**(3): 319-384.

Hiraiwa, M., B. M. Martin, Y. Kishimoto, G. E. Conner, S. Tsuji and J. S. O'Brien (1997). "Lysosomal proteolysis of prosaposin, the precursor of saposins (sphingolipid activator proteins): its mechanism and inhibition by ganglioside." Arch Biochem Biophys **341**(1): 17-24.

Ho, W. Y., J.-C. Chang, K. Lim, A. Cazenave-Gassiot, A. T. Nguyen, J. C. Foo, . . . S.-C. Ling (2021). "TDP-43 mediates SREBF2-regulated gene expression required for oligodendrocyte myelination." Journal of Cell Biology **220**(9).

Hodges, J. R., R. Davies, J. Xuereb, J. Kril and G. Halliday (2003). "Survival in frontotemporal dementia." Neurology **61**(3): 349-354.

Hodges, J. R., K. Patterson, S. Oxbury and E. Funnell (1992). "Semantic dementia. Progressive fluent aphasia with temporal lobe atrophy." Brain **115 (Pt 6)**: 1783-1806.

Hogan, D. B., N. Jetté, K. M. Fiest, J. I. Roberts, D. Pearson, E. E. Smith, . . . C. J. Maxwell (2016). "The Prevalence and Incidence of Frontotemporal Dementia: a Systematic Review." Can J Neurol Sci **43 Suppl 1**: S96-s109.

Honsho, M. and Y. Fujiki (2017). "Plasmalogen homeostasis – regulation of plasmalogen biosynthesis and its physiological consequence in mammals." FEBS Letters **591**(18): 2720-2729.

Horton, J. D., N. A. Shah, J. A. Warrington, N. N. Anderson, S. W. Park, M. S. Brown and J. L. Goldstein (2003). "Combined analysis of oligonucleotide microarray data from transgenic and knockout mice identifies direct SREBP target genes." Proceedings of the National Academy of Sciences **100**(21): 12027-12032.

Hosios, A. M., M. E. Wilkinson, M. C. McNamara, K. C. Kalafut, M. E. Torrence, J. M. Asara and B. D. Manning (2022). "mTORC1 regulates a lysosome-dependent adaptive shift in intracellular lipid species." Nature Metabolism **4**(12): 1792-1811.

Houštěk, J., A. Pícková, A. Vojtíšková, T. Mráček, P. Pecina and P. Ješina (2006). "Mitochondrial diseases and genetic defects of ATP synthase." Biochimica et Biophysica Acta (BBA) - Bioenergetics **1757**(9): 1400-1405.

Hsu, F.-F., A. Bohrer and J. Turk (1998). "Electrospray ionization tandem mass spectrometric analysis of sulfatide.: Determination of fragmentation patterns and characterization of molecular species expressed in brain and in pancreatic islets." Biochimica et Biophysica Acta (BBA) - Lipids and Lipid Metabolism **1392**(2): 202-216.

Hu, F., T. Padukkavidana, C. B. Vægter, O. A. Brady, Y. Zheng, I. R. Mackenzie, . . . S. M. Strittmatter (2010). "Sortilin-Mediated Endocytosis Determines Levels of the Frontotemporal Dementia Protein, Progranulin." Neuron **68**(4): 654-667.

Hu, F., T. Padukkavidana, C. B. Vaegter, O. A. Brady, Y. Zheng, I. R. Mackenzie, . . . S. M. Strittmatter (2010). "Sortilin-mediated endocytosis determines levels of the frontotemporal dementia protein, progranulin." Neuron **68**(4): 654-667.

Huang, D. W., B. T. Sherman and R. A. Lempicki (2008). "Bioinformatics enrichment tools: paths toward the comprehensive functional analysis of large gene lists." Nucleic Acids Research **37**(1): 1-13.

Huang, D. W., B. T. Sherman and R. A. Lempicki (2009). "Systematic and integrative analysis of large gene lists using DAVID bioinformatics resources." Nature Protocols **4**(1): 44-57.

Huang, M., E. Modeste, E. Dammer, P. Merino, G. Taylor, D. M. Duong, . . . T. Kukar (2020). "Network analysis of the progranulin-deficient mouse brain proteome reveals pathogenic mechanisms shared in human frontotemporal dementia caused by GRN mutations." Acta Neuropathologica Communications **8**(1): 163.

Hullin-Matsuda, F., C. Luquain-Costaz, J. Bouvier and I. Delton-Vandenbroucke (2009). "Bis(monoacylglycero)phosphate, a peculiar phospholipid to control the fate of cholesterol: Implications in pathology." Prostaglandins Leukot Essent Fatty Acids **81**(5-6): 313-324.

Huynh, K., O. Piguet, J. Kwok, C. Dobson-Stone, G. M. Halliday, J. R. Hodges and R. Landin-Romero (2021). "Clinical and Biological Correlates of White Matter Hyperintensities in Patients With Behavioral-Variant Frontotemporal Dementia and Alzheimer Disease." Neurology **96**(13): e1743-e1754.

Iguchi, Y., M. Katsuno, J.-i. Niwa, S. Takagi, S. Ishigaki, K. Ikenaka, . . . G. Sobue (2013). "Loss of TDP-43 causes age-dependent progressive motor neuron degeneration." Brain **136**(5): 1371-1382.

Jääskeläinen, O., E. Solje, A. Hall, K. Katisko, V. Korhonen, M. Tiainen, . . . S.-K. Herukka (2019). "Low Serum High-Density Lipoprotein Cholesterol Levels Associate with the C9orf72 Repeat Expansion in Frontotemporal Lobar Degeneration Patients." Journal of Alzheimer's Disease **72**: 127-137.

Jacova, C., G.-Y. R. Hsiung, I. Tawankanjanachot, K. Dinelle, S. McCormick, M. Gonzalez, . . . I. R. Mackenzie (2013). "Anterior brain glucose hypometabolism predates dementia in progranulin mutation carriers." Neurology **81**(15): 1322-1331.

Jahn, O., S. B. Siems, K. Kusch, D. Hesse, R. B. Jung, T. Liepold, . . . H. B. Werner (2020). "The CNS Myelin Proteome: Deep Profile and Persistence After Post-mortem Delay." Frontiers in Cellular Neuroscience **14**.

Jahn, O., S. Tenzer and H. B. Werner (2009). "Myelin Proteomics: Molecular Anatomy of an Insulating Sheath." Molecular Neurobiology **40**(1): 55-72.

Jakobsson, A., R. Westerberg and A. Jacobsson (2006). "Fatty acid elongases in mammals: Their regulation and roles in metabolism." Progress in Lipid Research **45**(3): 237-249.

Jian, J., Q.-Y. Tian, A. Hettinghouse, S. Zhao, H. Liu, J. Wei, . . . C.-j. Liu (2016). "Progranulin Recruits HSP70 to β-Glucocerebrosidase and Is Therapeutic Against Gaucher Disease." EBioMedicine **13**: 212-224.

Jiskoot, L. C., M. Bocchetta, J. M. Nicholas, D. M. Cash, D. Thomas, M. Modat, . . . J. D. Rohrer (2018). "Presymptomatic white matter integrity loss in familial frontotemporal dementia in the GENFI cohort: A cross-sectional diffusion tensor imaging study." Annals of clinical and translational neurology **5**(9): 1025-1036.

Johnson, J. K., J. Diehl, M. F. Mendez, J. Neuhaus, J. S. Shapira, M. Forman, . . . B. L. Miller (2005). "Frontotemporal lobar degeneration: demographic characteristics of 353 patients." Arch Neurol **62**(6): 925-930.

Jonsson, M., H. Zetterberg, S. Rolstad, A. Edman, A. A. Gouw, M. Bjerke, . . . A. Wallin (2012). "Low cerebrospinal fluid sulfatide predicts progression of white matter lesions: The LADIS study." Dement Geriatr Cogn Disord **34**(1): 61-67.

Jurevics, H. and P. Morell (1995). "Cholesterol for Synthesis of Myelin Is Made Locally, Not Imported into Brain." Journal of Neurochemistry **64**(2): 895-901.

Kajiwara, Y., E. Wang, M. Wang, W. C. Sin, K. J. Brennand, E. Schadt, . . . B. Zhang (2018). "GJA1 (connexin43) is a key regulator of Alzheimer's disease pathogenesis." Acta Neuropathologica Communications **6**(1): 144.

Käkelä, R., P. Somerharju and J. Tyynelä (2003). "Analysis of phospholipid molecular species in brains from patients with infantile and juvenile neuronal-ceroid lipofuscinosis using liquid chromatography-electrospray ionization mass spectrometry." Journal of Neurochemistry **84**(5): 1051-1065.

Kao, A. W., A. McKay, P. P. Singh, A. Brunet and E. J. Huang (2017). "Progranulin, lysosomal regulation and neurodegenerative disease." Nature Reviews Neuroscience **18**(6): 325-333.

Kaul, R., G. P. Gao, M. Aloya, K. Balamurugan, A. Petrosky, K. Michals and R. Matalon (1994). "Canavan disease: mutations among Jewish and non-Jewish patients." Am J Hum Genet **55**(1): 34-41.

Kertesz, A., P. McMonagle, M. Blair, W. Davidson and D. G. Munoz (2005). "The evolution and pathology of frontotemporal dementia." Brain **128**(Pt 9): 1996-2005.

Kim, J., M. Kundu, B. Viollet and K.-L. Guan (2011). "AMPK and mTOR regulate autophagy through direct phosphorylation of Ulk1." Nature Cell Biology **13**(2): 132-141.

Kim, W. S., E. Jary, R. Pickford, Y. He, R. M. Ahmed, O. Piguet, . . . G. M. Halliday (2018). "Lipidomics Analysis of Behavioral Variant Frontotemporal Dementia: A Scope for Biomarker Development." Frontiers in Neurology **9**(104).

Kishimoto, Y., M. Hiraiwa and J. S. O'Brien (1992). "Saposins: structure, function, distribution, and molecular genetics." J Lipid Res **33**(9): 1255-1267.

Krijnen, K., J. D. Keelor, S. Böhm, S. R. Ellis, C. Köster, J. Höhndorf, . . . I. G. M. Anthony (2023). "A Multimodal SIMS/MALDI Mass Spectrometry Imaging Source with Secondary Electron Imaging Capabilities for Use with timsTOF Instruments." Journal of the American Society for Mass Spectrometry **34**(4): 720-727.

Krueger, C. E., D. L. Dean, H. J. Rosen, C. Halabi, M. Weiner, B. L. Miller and J. H. Kramer (2010). "Longitudinal rates of lobar atrophy in frontotemporal dementia, semantic dementia, and Alzheimer's disease." Alzheimer Dis Assoc Disord **24**(1): 43-48.

Kulkarni, K., D. S. Snyder and T. J. McIntosh (1999). "Adhesion between Cerebroside Bilayers." Biochemistry **38**(46): 15264-15271.

Lall, D., I. Lorenzini, T. A. Mota, S. Bell, T. E. Mahan, J. D. Ulrich, . . . R. H. Baloh (2021). "C9orf72 deficiency promotes microglial-mediated synaptic loss in aging and amyloid accumulation." Neuron **109**(14): 2275-2291.e2278.

Lam, B. Y. K., G. M. Halliday, M. Irish, J. R. Hodges and O. Piguet (2014). "Longitudinal white matter changes in frontotemporal dementia subtypes." Human brain mapping **35**(7): 3547-3557.

Larti, F., K. Kahrizi, L. Musante, H. Hu, E. Papari, Z. Fattahi, . . . H. Najmabadi (2015). "A defect in the CLIP1 gene (CLIP-170) can cause autosomal recessive intellectual disability." European Journal of Human Genetics **23**(3): 331-336.

Laviad, E. L., L. Albee, I. Pankova-Kholmyansky, S. Epstein, H. Park, A. H. Merrill and A. H. Futerman (2008). "Characterization of Ceramide Synthase 2: TISSUE DISTRIBUTION, SUBSTRATE SPECIFICITY, AND INHIBITION BY SPHINGOSINE 1-PHOSPHATE*." Journal of Biological Chemistry **283**(9): 5677-5684.

Lebel, C. and C. Beaulieu (2011). "Longitudinal development of human brain wiring continues from childhood into adulthood." J Neurosci **31**(30): 10937-10947.

Lee, C. W., J. N. Stankowski, J. Chew, C. N. Cook, Y. W. Lam, S. Almeida, . . . L. Petrucelli (2017). "The lysosomal protein cathepsin L is a progranulin protease." Mol Neurodegener **12**(1): 55.

Lee, E. B., S. Porta, G. Michael Baer, Y. Xu, E. Suh, L. K. Kwong, . . . J. Q. Trojanowski (2017). "Expansion of the classification of FTLD-TDP: distinct pathology associated with rapidly progressive frontotemporal degeneration." Acta Neuropathol **134**(1): 65-78.

Lee, H., I. R. A. Mackenzie, M. F. Beg, K. Popuri, R. Rademakers, D. Wittenberg and G.-Y. R. Hsiung (2022). "White-matter abnormalities in presymptomatic GRN and C9orf72 mutation carriers." Brain Communications **5**(1).

Lee, J. Y., O. C. Marian and A. S. Don (2021). "Defective Lysosomal Lipid Catabolism as a Common Pathogenic Mechanism for Dementia." Neuromolecular Med.

Lee, Y., B. M. Morrison, Y. Li, S. Lengacher, M. H. Farah, P. N. Hoffman, . . . J. D. Rothstein (2012). "Oligodendroglia metabolically support axons and contribute to neurodegeneration." Nature **487**(7408): 443-448.

Leibiger, C., J. Deisel, A. Aufschnaiter, S. Ambros, M. Tereshchenko, B. M. Verheijen, . . . R. J. Braun (2018). "TDP-43 controls lysosomal pathways thereby determining its own clearance and cytotoxicity." Human Molecular Genetics **27**(9): 1593-1607.

Li, B., A. P. Castano, T. E. Hudson, B. T. Nowlin, S. L. Lin, J. V. Bonventre, . . . J. S. Duffield (2010). "The melanoma-associated transmembrane glycoprotein Gpnmb controls trafficking of cellular debris for degradation and is essential for tissue repair." Faseb j **24**(12): 4767-4781.

Li, H., K.-B. Hwang, D.-G. Mun, H. Kim, H. Lee, S.-W. Lee and E. Paek (2014). "Estimating Influence of Cofragmentation on Peptide Quantification and Identification in iTRAQ Experiments by Simulating Multiplexed Spectra." Journal of Proteome Research **13**(7): 3488-3497.

Lin, M. T. and M. F. Beal (2006). "Mitochondrial dysfunction and oxidative stress in neurodegenerative diseases." Nature **443**(7113): 787-795.

Lisman, J., H. Schulman and H. Cline (2002). "The molecular basis of CaMKII function in synaptic and behavioural memory." Nature Reviews Neuroscience **3**(3): 175-190.

Liu, W. J., L. Ye, W. F. Huang, L. J. Guo, Z. G. Xu, H. L. Wu, . . . H. F. Liu (2016). "p62 links the autophagy pathway and the ubiqutin–proteasome system upon ubiquitinated protein degradation." Cellular & Molecular Biology Letters **21**(1): 29.

Logan, T., M. J. Simon, A. Rana, G. M. Cherf, A. Srivastava, S. S. Davis, . . . G. Di Paolo (2021). "Rescue of a lysosomal storage disorder caused by Grn loss of function with a brain penetrant progranulin biologic." Cell **184**(18): 4651-4668.e4625.

Lok, H. C. and J. B. Kwok (2021). "The Role of White Matter Dysfunction and Leukoencephalopathy/Leukodystrophy Genes in the Aetiology of Frontotemporal Dementias: Implications for Novel Approaches to Therapeutics." Int J Mol Sci **22**(5).

Lubetzki, C., Y. Thuillier, A. Galli, O. Lyon-Caen, F. Lhermitte and B. Zalc (1989). "Galactosylceramide: a reliable serum index of demyelination in multiple sclerosis." Ann Neurol **26**(3): 407-409.

Lui, H., J. Zhang, Stefanie R. Makinson, Michelle K. Cahill, Kevin W. Kelley, H.-Y. Huang, . . . Eric J. Huang (2016). "Progranulin Deficiency Promotes Circuit-Specific Synaptic Pruning by Microglia via Complement Activation." Cell **165**(4): 921-935.

Lund, E. G., J. M. Guileyardo and D. W. Russell (1999). "cDNA cloning of cholesterol 24-hydroxylase, a mediator of cholesterol homeostasis in the brain." Proceedings of the National Academy of Sciences **96**(13): 7238-7243.

Lund, E. G., C. Xie, T. Kotti, S. D. Turley, J. M. Dietschy and D. W. Russell (2003). "Knockout of the Cholesterol 24-Hydroxylase Gene in Mice Reveals a Brain-specific Mechanism of Cholesterol Turnover*." Journal of Biological Chemistry **278**(25): 22980-22988.

Luoma, A. M., F. Kuo, O. Cakici, M. N. Crowther, A. R. Denninger, R. L. Avila, . . . D. A. Kirschner (2015). "Plasmalogen phospholipids protect internodal myelin from oxidative damage." Free Radical Biology and Medicine **84**: 296-310.

Ma, S., I. Y. Attarwala and X.-Q. Xie (2019). "SQSTM1/p62: A Potential Target for Neurodegenerative Disease." ACS Chemical Neuroscience **10**(5): 2094-2114.

Mackenzie, I. R., M. Neumann, A. Baborie, D. M. Sampathu, D. Du Plessis, E. Jaros, . . . V. M. Lee (2011). "A harmonized classification system for FTLD-TDP pathology." Acta Neuropathol **122**(1): 111-113.

Mackenzie, I. R. A., P. Frick, F. A. Grässer, T. F. Gendron, L. Petrucelli, N. R. Cashman, . . . M. Neumann (2015). "Quantitative analysis and clinico-pathological correlations of different dipeptide repeat protein pathologies in C9ORF72 mutation carriers." Acta Neuropathologica **130**(6): 845-861.

Mackenzie, I. R. A. and M. Neumann (2016). "Molecular neuropathology of frontotemporal dementia: insights into disease mechanisms from postmortem studies." Journal of Neurochemistry **138**(S1): 54-70.

Mahoney, C. J., J. Beck, J. D. Rohrer, T. Lashley, K. Mok, T. Shakespeare, . . . J. D. Warren (2012). "Frontotemporal dementia with the C9ORF72 hexanucleotide repeat expansion: clinical, neuroanatomical and neuropathological features." Brain **135**(3): 736-750.

Mahoney, C. J., G. R. Ridgway, I. B. Malone, L. E. Downey, J. Beck, K. M. Kinnunen, . . . J. D. Warren (2014). "Profiles of white matter tract pathology in frontotemporal dementia." Human Brain Mapping **35**(8): 4163-4179.

Mahoney, C. J., I. J. A. Simpson, J. M. Nicholas, P. D. Fletcher, L. E. Downey, H. L. Golden, . . . N. C. Fox (2015). "Longitudinal diffusion tensor imaging in frontotemporal dementia." Annals of neurology **77**(1): 33-46.

Malheiro, A. R., B. Correia, T. Ferreira da Silva, D. Bessa-Neto, P. P. Van Veldhoven and P. Brites (2019). "Leukodystrophy caused by plasmalogen deficiency rescued by glyceryl 1-myristyl ether treatment." Brain Pathology **29**(5): 622-639.

Marian, O. C., J. D. Teo, J. Y. Lee, H. Song, J. B. Kwok, R. Landin-Romero, . . . A. S. Don (2023). "Disrupted myelin lipid metabolism differentiates frontotemporal dementia caused by GRN and C9orf72 gene mutations." Acta Neuropathologica Communications **11**(1): 52.

Marian, O. C., C. Tran and A. S. Don (2020). Chapter 23 - Altered lipid metabolic homeostasis in the pathogenesis of Alzheimer's disease. Lipid Signaling and Metabolism. J. M. Ntambi, Academic Press**:** 469-504.

Marsching, C., M. Rabionet, D. Mathow, R. Jennemann, C. Kremser, S. Porubsky, . . . R. Sandhoff (2014). "Renal sulfatides: sphingoid base-dependent localization and region-specific compensation of CerS2-dysfunction." J Lipid Res **55**(11): 2354-2369.

Martens, L. H., J. Zhang, S. J. Barmada, P. Zhou, S. Kamiya, B. Sun, . . . R. V. Farese, Jr. (2012). "Progranulin deficiency promotes neuroinflammation and neuron loss following toxin-induced injury." J Clin Invest **122**(11): 3955-3959.

Martins, C., H. Hůlková, L. Dridi, V. Dormoy-Raclet, L. Grigoryeva, Y. Choi, . . . A. V. Pshezhetsky (2015). "Neuroinflammation, mitochondrial defects and neurodegeneration in mucopolysaccharidosis III type C mouse model." Brain **138**(Pt 2): 336-355.

Massaad, C. A. and E. Klann (2011). "Reactive oxygen species in the regulation of synaptic plasticity and memory." Antioxid Redox Signal **14**(10): 2013-2054.

Matsuda, J. (2008). Sphingolipid Activator Proteins. Experimental Glycoscience: Glycobiology. N. Taniguchi, A. Suzuki, Y. Ito et al. Tokyo, Springer Japan**:** 125-129.

Matyash, V., G. Liebisch, T. V. Kurzchalia, A. Shevchenko and D. Schwudke (2008). "Lipid extraction by methyl-tert-butyl ether for high-throughput lipidomics*s." Journal of Lipid Research **49**(5): 1137-1146.

Meeter, L. H., L. D. Kaat, J. D. Rohrer and J. C. van Swieten (2017). "Imaging and fluid biomarkers in frontotemporal dementia." Nature Reviews Neurology **13**(7): 406-419.

Mehta, A. R., J. M. Gregory, O. Dando, R. N. Carter, K. Burr, J. Nanda, . . . B. T. Selvaraj (2021). "Mitochondrial bioenergetic deficits in C9orf72 amyotrophic lateral sclerosis motor neurons cause dysfunctional axonal homeostasis." Acta Neuropathol **141**(2): 257-279.

Metelitsina, T. I., D. J. Waggoner and M. A. Grassi (2016). "BATTEN DISEASE CAUSED BY A NOVEL MUTATION IN THE PPT1 GENE." Retin Cases Brief Rep **10**(3): 211-213.

Miedema, S. S. M., M. O. Mol, F. T. W. Koopmans, D. C. Hondius, P. van Nierop, K. Menden, . . . A. B. Smit (2022). "Distinct cell type-specific protein signatures in GRN and MAPT genetic subtypes of frontotemporal dementia." Acta Neuropathologica Communications **10**(1): 100.

Mirzaian, M., G. Kramer and B. J. H. M. Poorthuis (2015). "Quantification of sulfatides and lysosulfatides in tissues and body fluids by liquid chromatography-tandem mass spectrometry[S]." Journal of Lipid Research **56**(4): 936-943.

Mitchell, N. L., K. N. Russell, G. K. Barrell, I. Tammen and D. N. Palmer (2023). "Characterization of neuropathology in ovine CLN5 and CLN6 neuronal ceroid lipofuscinoses (Batten disease)." Developmental Neurobiology **n/a**(n/a).

Moloney, E. B., A. Moskites, E. J. Ferrari, O. Isacson and P. J. Hallett (2018). "The glycoprotein GPNMB is selectively elevated in the substantia nigra of Parkinson's disease patients and increases after lysosomal stress." Neurobiology of Disease **120**: 1-11.

Morava, E., R. J. Rodenburg, F. Hol, M. de Vries, A. Janssen, L. van den Heuvel, . . . J. Smeitink (2006). "Clinical and biochemical characteristics in patients with a high mutant load of the mitochondrial T8993G/C mutations." American Journal of Medical Genetics Part A **140A**(8): 863-868.

Moreno-García, A., A. Kun, O. Calero, M. Medina and M. Calero (2018). "An Overview of the Role of Lipofuscin in Age-Related Neurodegeneration." Front Neurosci **12**: 464.

Moreno, F., G. D. Rabinovici, A. Karydas, Z. Miller, S. C. Hsu, A. Legati, . . . L. T. Grinberg (2015). "A novel mutation P112H in the TARDBP gene associated with frontotemporal lobar degeneration without motor neuron disease and abundant neuritic amyloid plaques." Acta Neuropathologica Communications **3**(1): 19.

Murley, A. G. and J. B. Rowe (2018). "Neurotransmitter deficits from frontotemporal lobar degeneration." Brain **141**(5): 1263-1285.

Nagahara, Y., M. Shimazawa, K. Ohuchi, J. Ito, H. Takahashi, K. Tsuruma, . . . H. Hara (2017). "GPNMB ameliorates mutant TDP-43-induced motor neuron cell death." Journal of Neuroscience Research **95**(8): 1647-1665.

Nana, A. L., M. Sidhu, S. E. Gaus, J.-H. L. Hwang, L. Li, Y. Park, . . . W. W. Seeley (2019). "Neurons selectively targeted in frontotemporal dementia reveal early stage TDP-43 pathobiology." Acta neuropathologica **137**(1): 27-46.

Nave, K.-A. (2010). "Myelination and support of axonal integrity by glia." Nature **468**(7321): 244-252.

Nave, K.-A. and H. B. Werner (2014). "Myelination of the Nervous System: Mechanisms and Functions." Annual Review of Cell and Developmental Biology **30**(1): 503-533.

Neary, D., J. S. Snowden, L. Gustafson, U. Passant, D. Stuss, S. Black, . . . D. F. Benson (1998). "Frontotemporal lobar degeneration: a consensus on clinical diagnostic criteria." Neurology **51**(6): 1546-1554.

Neumann, J., J. Bras, E. Deas, S. S. O'Sullivan, L. Parkkinen, R. H. Lachmann, . . . N. W. Wood (2009). "Glucocerebrosidase mutations in clinical and pathologically proven Parkinson's disease." Brain **132**(Pt 7): 1783-1794.

Neumann, M., L. K. Kwong, A. C. Truax, B. Vanmassenhove, H. A. Kretzschmar, V. M. Van Deerlin, . . . V. M.-Y. Lee (2007). "TDP-43-Positive White Matter Pathology in Frontotemporal Lobar Degeneration With Ubiquitin-Positive Inclusions." Journal of Neuropathology & Experimental Neurology **66**(3): 177-183.

Neumann, M., D. M. Sampathu, L. K. Kwong, A. C. Truax, M. C. Micsenyi, T. T. Chou, . . . V. M. Lee (2006). "Ubiquitinated TDP-43 in frontotemporal lobar degeneration and amyotrophic lateral sclerosis." Science **314**(5796): 130-133.

Nie, S., G. Chen, X. Cao and Y. Zhang (2014). "Cerebrotendinous xanthomatosis: a comprehensive review of pathogenesis, clinical manifestations, diagnosis, and management." Orphanet J Rare Dis **9**: 179.

Nilsson, O. and L. Svennerholm (1982). "Accumulation of glucosylceramide and glucosylsphingosine (psychosine) in cerebrum and cerebellum in infantile and juvenile Gaucher disease." J Neurochem **39**(3): 709-718.

Nolfi-Donegan, D., A. Braganza and S. Shiva (2020). "Mitochondrial electron transport chain: Oxidative phosphorylation, oxidant production, and methods of measurement." Redox Biology **37**: 101674.

Norton, W. T. and L. A. Autilio (1966). "The lipid composition of purified bovine brain myelin." J Neurochem **13**(4): 213-222.

Norton, W. T. and S. E. Poduslo (1973). "MYELINATION IN RAT BRAIN: CHANGES IN MYELIN COMPOSITION DURING BRAIN MATURATION1." Journal of Neurochemistry **21**(4): 759-773.

Novakova, L., M. Henricsson, E. Björnson, M. Axelsson, J. Borén, I. Rosenstein, . . . M. Blomqvist (2023). "Cerebrospinal fluid sulfatide isoforms lack diagnostic utility in separating progressive from relapsing-remitting multiple sclerosis." Multiple Sclerosis and Related Disorders **74**: 104705.

Novakova, L., A. K. Singh, M. Axelsson, M. Ståhlman, M. Adiels, C. Malmeström, . . . M. Blomqvist (2018). "Sulfatide isoform pattern in cerebrospinal fluid discriminates progressive MS from relapsing-remitting MS." Journal of Neurochemistry **146**(3): 322-332.

Nutma, E., M. C. Marzin, S. A. Cillessen and S. Amor (2021). "Autophagy in white matter disorders of the CNS: mechanisms and therapeutic opportunities." J Pathol **253**(2): 133-147.

O'Brien, J. S. and G. Rouser (1964). "The fatty acid composition of brain sphingolipids: sphingomyelin, ceramide, cerebroside, and cerebroside sulfate." J Lipid Res **5**(3): 339-342.

O'Brien, J. S. and E. L. Sampson (1965). "Lipid composition of the normal human brain: gray matter, white matter, and myelin." J Lipid Res **6**(4): 537-544.

O'Rourke, J. G., L. Bogdanik, A. Yáñez, D. Lall, A. J. Wolf, A. K. Muhammad, . . . R. H. Baloh (2016). "C9orf72 is required for proper macrophage and microglial function in mice." Science **351**(6279): 1324-1329.

Ohashi, K., J.-i. Osuga, R. Tozawa, T. Kitamine, H. Yagyu, M. Sekiya, . . . S. Ishibashi (2003). "Early Embryonic Lethality Caused by Targeted Disruption of the 3-Hydroxy-3-methylglutaryl-CoA Reductase Gene*." Journal of Biological Chemistry **278**(44): 42936-42941.

Olney, N. T., S. Spina and B. L. Miller (2017). "Frontotemporal Dementia." Neurologic clinics **35**(2): 339-374.

Onyike, C. U. and J. Diehl-Schmid (2013). "The epidemiology of frontotemporal dementia." International review of psychiatry (Abingdon, England) **25**(2): 130-137.

Palmer, D. N. (2015). "The relevance of the storage of subunit c of ATP synthase in different forms and models of Batten disease (NCLs)." Biochimica et Biophysica Acta (BBA) - Molecular Basis of Disease **1852**(10, Part B): 2287-2291.

Pang, W. and F. Hu (2021). "Cellular and physiological functions of C9ORF72 and implications for ALS/FTD." Journal of Neurochemistry **157**(3): 334-350.

Pang, Z. P., E. Melicoff, D. Padgett, Y. Liu, A. F. Teich, B. F. Dickey, . . . T. C. Südhof (2006). "Synaptotagmin-2 Is Essential for Survival and Contributes to Ca²⁺ Triggering of Neurotransmitter Release in Central and Neuromuscular Synapses." The Journal of Neuroscience **26**(52): 13493-13504.

Park, H. K. and S. J. Chung (2013). "New perspective on parkinsonism in frontotemporal lobar degeneration." J Mov Disord **6**(1): 1-8.

Parsons, C. G., A. Stöffler and W. Danysz (2007). "Memantine: a NMDA receptor antagonist that improves memory by restoration of homeostasis in the glutamatergic system--too little activation is bad, too much is even worse." Neuropharmacology **53**(6): 699-723.

Paternico, D., E. Premi, S. Gazzina, M. Cosseddu, A. Alberici, S. Archetti, . . . B. Borroni (2016). "White matter hyperintensities characterize monogenic frontotemporal dementia with granulin mutations." Neurobiol Aging **38**: 176-180.

Pedraza, L., J. K. Huang and D. R. Colman (2001). "Organizing Principles of the Axoglial Apparatus." Neuron **30**(2): 335-344.

Penati, R., F. Fumagalli, V. Calbi, M. E. Bernardo and A. Aiuti (2017). "Gene therapy for lysosomal storage disorders: recent advances for metachromatic leukodystrophy and mucopolysaccaridosis I." Journal of Inherited Metabolic Disease **40**(4): 543-554.

Petrov, A. M., M. R. Kasimov and A. L. Zefirov (2016). "Brain Cholesterol Metabolism and Its Defects: Linkage to Neurodegenerative Diseases and Synaptic Dysfunction." Acta Naturae **8**(1): 58-73.

Phan, K., Y. He, R. Pickford, S. Bhatia, J. S. Katzeff, J. R. Hodges, . . . W. S. Kim (2020). "Uncovering pathophysiological changes in frontotemporal dementia using serum lipids." Scientific Reports **10**(1): 3640.

Pinheiro, D. and Y. Bellaïche (2018). "Mechanical Force-Driven Adherens Junction Remodeling and Epithelial Dynamics." Developmental Cell **47**(1): 3-19.

Pobezhimova, T. P. and V. K. Voinikov (2000). "Biochemical and physiological aspects of ubiquinone function." Membr Cell Biol **13**(5): 595-602.

Popuri, K., M. F. Beg, H. Lee, R. Balachandar, L. Wang, V. Sossi, . . . G.-Y. R. Hsiung (2021). "FDG-PET in presymptomatic C9orf72 mutation carriers." NeuroImage: Clinical **31**: 102687.

Rademakers, R., M. Neumann and I. R. Mackenzie (2012). "Advances in understanding the molecular basis of frontotemporal dementia." Nature Reviews Neurology **8**(8): 423-434.

Rascovsky, K., J. R. Hodges, D. Knopman, M. F. Mendez, J. H. Kramer, J. Neuhaus, . . . B. L. Miller (2011). "Sensitivity of revised diagnostic criteria for the behavioural variant of frontotemporal dementia." Brain : a journal of neurology **134**(Pt 9): 2456-2477.

Ravera, S. and I. Panfoli (2015). "Role of myelin sheath energy metabolism in neurodegenerative diseases." Neural Regen Res **10**(10): 1570-1571.

Renaud, L., V. Picher-Martel, P. Codron and J.-P. Julien (2019). "Key role of UBQLN2 in pathogenesis of amyotrophic lateral sclerosis and frontotemporal dementia." Acta Neuropathologica Communications **7**(1): 103.

Renton, Alan E., E. Majounie, A. Waite, J. Simón-Sánchez, S. Rollinson, J. R. Gibbs, . . . Bryan J. Traynor (2011). "A Hexanucleotide Repeat Expansion in C9ORF72 Is the Cause of Chromosome 9p21-Linked ALS-FTD." Neuron **72**(2): 257-268.

Reza, S., M. Ugorski and J. Suchański (2021). "Glucosylceramide and galactosylceramide, small glycosphingolipids with significant impact on health and disease." Glycobiology **31**(11): 1416-1434.

Rinaldo, P., D. Matern and M. J. Bennett (2002). "Fatty Acid Oxidation Disorders." Annual Review of Physiology **64**(1): 477-502.

Rink, J., E. Ghigo, Y. Kalaidzidis and M. Zerial (2005). "Rab Conversion as a Mechanism of Progression from Early to Late Endosomes." Cell **122**(5): 735-749.

Roczniak-Ferguson, A., C. S. Petit, F. Froehlich, S. Qian, J. Ky, B. Angarola, . . . S. M. Ferguson (2012). "The Transcription Factor TFEB Links mTORC1 Signaling to Transcriptional Control of Lysosome Homeostasis." Science Signaling **5**(228): ra42-ra42.

Rohrer, J. D., G. R. Ridgway, M. Modat, S. Ourselin, S. Mead, N. C. Fox, . . . J. D. Warren (2010). "Distinct profiles of brain atrophy in frontotemporal lobar degeneration caused by progranulin and tau mutations." NeuroImage **53**(3): 1070-1076.

Rohrer, J. D., J. D. Warren, R. Omar, S. Mead, J. Beck, T. Revesz, . . . M. N. Rossor (2008). "Parietal lobe deficits in frontotemporal lobar degeneration caused by a mutation in the progranulin gene." Arch Neurol **65**(4): 506-513.

Rubino, E., I. Rainero, A. Chiò, E. Rogaeva, D. Galimberti, P. Fenoglio, . . . L. Pinessi (2012). "SQSTM1 mutations in frontotemporal lobar degeneration and amyotrophic lateral sclerosis." Neurology **79**(15): 1556-1562.

Ruskamo, S., A. Raasakka, J. S. Pedersen, A. Martel, K. Škubník, T. Darwish, . . . P. Kursula (2022). "Human myelin proteolipid protein structure and lipid bilayer stacking." Cellular and Molecular Life Sciences **79**(8): 419.

Ryan, C. L., D. C. Baranowski, B. P. Chitramuthu, S. Malik, Z. Li, M. Cao, . . . A. Bateman (2009). "Progranulin is expressed within motor neurons and promotes neuronal cell survival." BMC neuroscience **10**: 130-130.

Sadler, G. L., K. N. Lewis, V. K. Narayana, D. P. De Souza, J. Mason, C. McLean, . . . S. K. Barton (2022). "Lipid Metabolism Is Dysregulated in the Motor Cortex White Matter in Amyotrophic Lateral Sclerosis." Metabolites **12**(6).

Safaiyan, S., N. Kannaiyan, N. Snaidero, S. Brioschi, K. Biber, S. Yona, . . . M. Simons (2016). "Age-related myelin degradation burdens the clearance function of microglia during aging." Nature neuroscience **19**(8): 995-998.

Saftig, P. and J. Klumperman (2009). "Lysosome biogenesis and lysosomal membrane proteins: trafficking meets function." Nature Reviews Molecular Cell Biology **10**(9): 623-635.

Saher, G., B. Brügger, C. Lappe-Siefke, W. Möbius, R.-i. Tozawa, M. C. Wehr, . . . K.-A. Nave (2005). "High cholesterol level is essential for myelin membrane growth." Nature Neuroscience **8**(4): 468-475.

Samra, K., A. M. MacDougall, A. Bouzigues, M. Bocchetta, D. M. Cash, C. V. Greaves, . . . G. F. d. Initiative (2023). "Genetic forms of primary progressive aphasia within the GENetic Frontotemporal dementia Initiative (GENFI) cohort: comparison with sporadic primary progressive aphasia." Brain Communications **5**(2).

Sandhoff, K. (2013). "Metabolic and cellular bases of sphingolipidoses." Biochem Soc Trans **41**(6): 1562-1568.

Sandhoff, K. (2016). "Neuronal sphingolipidoses: Membrane lipids and sphingolipid activator proteins regulate lysosomal sphingolipid catabolism." Biochimie **130**: 146-151.

Satoh, J. I., Y. Kino, M. Yanaizu, T. Ishida and Y. Saito (2019). "Microglia express GPNMB in the brains of Alzheimer's disease and Nasu-Hakola disease." Intractable Rare Dis Res **8**(2): 120-128.

Saville, J. T., N. J. C. Smith, J. M. Fletcher and M. Fuller (2017). "Quantification of plasma sulfatides by mass spectrometry: Utility for metachromatic leukodystrophy." Analytica Chimica Acta **955**: 79-85.

Savitski, M. M., T. Mathieson, N. Zinn, G. Sweetman, C. Doce, I. Becher, . . . M. Bantscheff (2013). "Measuring and Managing Ratio Compression for Accurate iTRAQ/TMT Quantification." Journal of Proteome Research **12**(8): 3586-3598.

Saxton, R. A. and D. M. Sabatini (2017). "mTOR Signaling in Growth, Metabolism, and Disease." Cell **168**(6): 960-976.

Schaeren-Wiemers, N., P. Van Der Bijl and M. E. Schwab (1995). "The UDP-Galactose:Ceramide Galactosyltransferase: Expression Pattern in Oligodendrocytes and Schwann Cells During Myelination and Substrate Preference for Hydroxyceramide." Journal of Neurochemistry **65**(5): 2267-2278.

Schmitt, S., L. C. Castelvetri and M. Simons (2015). "Metabolism and functions of lipids in myelin." Biochim Biophys Acta **1851**(8): 999-1005.

Schnaar, R. L., R. Gerardy-Schahn and H. Hildebrandt (2014). "Sialic acids in the brain: gangliosides and polysialic acid in nervous system development, stability, disease, and regeneration." Physiol Rev **94**(2): 461-518.

Seelaar, H., J. D. Rohrer, Y. A. Pijnenburg, N. C. Fox and J. C. van Swieten (2011). "Clinical, genetic and pathological heterogeneity of frontotemporal dementia: a review." J Neurol Neurosurg Psychiatry **82**(5): 476-486.

Sellier, C., M. L. Campanari, C. Julie Corbier, A. Gaucherot, I. Kolb-Cheynel, M. Oulad-Abdelghani, . . . N. Charlet-Berguerand (2016). "Loss of C9ORF72 impairs autophagy and synergizes with polyQ Ataxin-2 to induce motor neuron dysfunction and cell death." Embo j **35**(12): 1276-1297.

Settembre, C., C. Di Malta, V. A. Polito, M. G. Arencibia, F. Vetrini, S. Erdin, . . . A. Ballabio (2011). "TFEB Links Autophagy to Lysosomal Biogenesis." Science **332**(6036): 1429-1433.

Shaner, R. L., J. C. Allegood, H. Park, E. Wang, S. Kelly, C. A. Haynes, . . . A. H. Merrill, Jr. (2009). "Quantitative analysis of sphingolipids for lipidomics using triple quadrupole and quadrupole linear ion trap mass spectrometers." J Lipid Res **50**(8): 1692-1707.

Shankaran, S. S., A. Capell, A. T. Hruscha, K. Fellerer, M. Neumann, B. Schmid and C. Haass (2008). "Missense Mutations in the Progranulin Gene Linked to Frontotemporal Lobar Degeneration with Ubiquitin-immunoreactive Inclusions Reduce Progranulin Production and Secretion*." Journal of Biological Chemistry **283**(3): 1744-1753.

Shao, Q., M. Yang, C. Liang, L. Ma, W. Zhang, Z. Jiang, . . . J.-F. Chen (2020). "C9orf72 and smcr8 mutant mice reveal MTORC1 activation due to impaired lysosomal degradation and exocytosis." Autophagy **16**(9): 1635-1650.

Sherman, D. L. and P. J. Brophy (2005). "Mechanisms of axon ensheathment and myelin growth." Nature Reviews Neuroscience **6**(9): 683-690.

Sheth, J., M. Mistri, R. Bhavsar, D. Pancholi, M. Kamate, N. Gupta, . . . F. Sheth (2018). "Batten disease: biochemical and molecular characterization revealing novel PPT1 and TPP1 gene mutations in Indian patients." BMC Neurology **18**(1): 203.

Shi, Y., S. Lin, K. A. Staats, Y. Li, W. H. Chang, S. T. Hung, . . . J. K. Ichida (2018). "Haploinsufficiency leads to neurodegeneration in C9ORF72 ALS/FTD human induced motor neurons." Nat Med **24**(3): 313-325.

Shinagawa, S., J. A. Catindig, N. R. Block, B. L. Miller and K. P. Rankin (2016). "When a Little Knowledge Can Be Dangerous: False-Positive Diagnosis of Behavioral Variant Frontotemporal Dementia among Community Clinicians." Dement Geriatr Cogn Disord **41**(1-2): 99-108.

Siintola, E., S. Partanen, P. Strömme, A. Haapanen, M. Haltia, J. Maehlen, . . . J. Tyynelä (2006). "Cathepsin D deficiency underlies congenital human neuronal ceroid-lipofuscinosis." Brain **129**(Pt 6): 1438-1445.

Simons, C., D. Dyment, S. J. Bent, J. Crawford, M. D'Hooghe, A. Kohlschütter, . . . N. I. Wolf (2017). "A recurrent de novo mutation in TMEM106B causes hypomyelinating leukodystrophy." Brain **140**(12): 3105-3111.

Simons, M., E. M. Krämer, C. Thiele, W. Stoffel and J. Trotter (2000). "Assembly of myelin by association of proteolipid protein with cholesterol- and galactosylceramide-rich membrane domains." J Cell Biol **151**(1): 143-154.

Simons, M. and K. A. Nave (2015). "Oligodendrocytes: Myelination and Axonal Support." Cold Spring Harb Perspect Biol **8**(1): a020479.

Sindelar, P. J., Z. Guan, G. Dallner and L. Ernster (1999). "The protective role of plasmalogens in iron-induced lipid peroxidation." Free Radic Biol Med **26**(3-4): 318-324.

Sinenko, S. A., T. Y. Starkova, A. A. Kuzmin and A. N. Tomilin (2021). "Physiological Signaling Functions of Reactive Oxygen Species in Stem Cells: From Flies to Man." Front Cell Dev Biol **9**: 714370.

Sirisi, S., M. Querol-Vilaseca, O. Dols-Icardo, J. Pegueroles, V. Montal, L. Muñoz, . . . A. Lleó (2022). "Myelin loss in C9orf72 hexanucleotide expansion carriers." J Neurosci Res **100**(10): 1862-1875.

Siuda, J., S. Fujioka and Z. K. Wszolek (2014). "Parkinsonian syndrome in familial frontotemporal dementia." Parkinsonism Relat Disord **20**(9): 957-964.

Smith, K. R., J. Damiano, S. Franceschetti, S. Carpenter, L. Canafoglia, M. Morbin, . . . S. F. Berkovic (2012). "Strikingly different clinicopathological phenotypes determined by progranulin-mutation dosage." Am J Hum Genet **90**(6): 1102-1107.

Snowden, J. S., D. Neary and D. M. Mann (2002). "Frontotemporal dementia." Br J Psychiatry **180**: 140-143.

Song, H., H. P. McEwen, T. Duncan, J. Y. Lee, J. D. Teo and A. S. Don (2021). "Sphingosine kinase 2 is essential for remyelination following cuprizone intoxication." Glia **69**(12): 2863-2881.

Songsrirote, K., Z. Li, D. Ashford, A. Bateman and J. Thomas-Oates (2010). "Development and application of mass spectrometric methods for the analysis of progranulin N-glycosylation." Journal of Proteomics **73**(8): 1479-1490.

Spillantini, M. G., T. D. Bird and B. Ghetti (1998). "Frontotemporal Dementia and Parkinsonism Linked to Chromosome 17: A New Group of Tauopathies." Brain Pathology **8**(2): 387-402.

Stoeck, K., M. N. Psychogios, A. Ohlenbusch, R. Steinfeld and J. Schmidt (2016). "Late-Onset Metachromatic Leukodystrophy with Early Onset Dementia Associated with a Novel Missense Mutation in the Arylsulfatase A Gene." Journal of Alzheimer's Disease **51**: 683-687.

Sudre, C. H., M. Bocchetta, D. Cash, D. L. Thomas, I. Woollacott, K. M. Dick, . . . J. D. Rohrer (2017). "White matter hyperintensities are seen only in GRN mutation carriers in the GENFI cohort." Neuroimage Clin **15**: 171-180.

Sudre, C. H., M. Bocchetta, C. Heller, R. Convery, M. Neason, K. M. Moore, . . . G. On behalf of (2019). "White matter hyperintensities in progranulin-associated frontotemporal dementia: A longitudinal GENFI study." NeuroImage. Clinical **24**: 102077-102077.

Sullivan, P. M., X. Zhou, A. M. Robins, D. H. Paushter, D. Kim, M. B. Smolka and F. Hu (2016). "The ALS/FTLD associated protein C9orf72 associates with SMCR8 and WDR41 to regulate the autophagy-lysosome pathway." Acta Neuropathologica Communications **4**(1): 51.

Surma, M. A., R. Herzog, A. Vasilj, C. Klose, N. Christinat, D. Morin-Rivron, . . . J. L. Sampaio (2015). "An automated shotgun lipidomics platform for high throughput, comprehensive, and quantitative analysis of blood plasma intact lipids." Eur J Lipid Sci Technol **117**(10): 1540-1549.

Taghizadeh, L. A., C. J. King, D. R. Nascene, A. O. Gupta, P. J. Orchard, L. Higgins, . . . T. C. Lund (2022). "Glycoprotein nonmetastatic melanoma protein B (GNMPB) as a novel biomarker for cerebral adrenoleukodystrophy." Sci Rep **12**(1): 7985.

Tahmaz, F. E., S. Sam, G. E. Hoganson and F. Quan (2001). "A partial deletion of the aspartoacylase gene is the cause of Canavan disease in a family from Mexico." J Med Genet **38**(3): E9.

Tanaka, Y., J. K. Chambers, T. Matsuwaki, K. Yamanouchi and M. Nishihara (2014). "Possible involvement of lysosomal dysfunction in pathological changes of the brain in aged progranulin-deficient mice." Acta Neuropathologica Communications **2**(1): 78.

Tanaka, Y., G. Suzuki, T. Matsuwaki, M. Hosokawa, G. Serrano, T. G. Beach, . . . M. Nishihara (2017). "Progranulin regulates lysosomal function and biogenesis through acidification of lysosomes." Human Molecular Genetics **26**(5): 969-988.

Tartaglia, M. C., Y. Zhang, C. Racine, V. Laluz, J. Neuhaus, L. Chao, . . . M. Weiner (2012). "Executive dysfunction in frontotemporal dementia is related to abnormalities in frontal white matter tracts." J Neurol **259**(6): 1071-1080.

Teo, J. D., O. C. Marian, A. G. Spiteri, M. Nicholson, H. Song, J. X. Y. Khor, . . . A. S. Don (2023). "Early microglial response, myelin deterioration and lethality in mice deficient for very long chain ceramide synthesis in oligodendrocytes." Glia **71**(4): 1120-1141.

Tewari, B. P., L. Chaunsali, C. E. Prim and H. Sontheimer (2022). "A glial perspective on the extracellular matrix and perineuronal net remodeling in the central nervous system." Frontiers in Cellular Neuroscience **16**.

Thompson, A., J. Schäfer, K. Kuhn, S. Kienle, J. Schwarz, G. Schmidt, . . . C. Hamon (2003). "Tandem mass tags: a novel quantification strategy for comparative analysis of complex protein mixtures by MS/MS." Anal Chem **75**(8): 1895-1904.

Tolbert, N. E. (1981). "Metabolic pathways in peroxisomes and glyoxysomes." Annu Rev Biochem **50**: 133-157.

Tozawa, R.-i., S. Ishibashi, J.-i. Osuga, H. Yagyu, T. Oka, Z. Chen, . . . N. Yamada (1999). "Embryonic Lethality and Defective Neural Tube Closure in Mice Lacking Squalene Synthase*." Journal of Biological Chemistry **274**(43): 30843-30848.

Trivedi, P. C., J. J. Bartlett and T. Pulinilkunnil (2020). "Lysosomal Biology and Function: Modern View of Cellular Debris Bin." Cells **9**(5).

Tsai, R. M. and A. L. Boxer (2014). "Treatment of frontotemporal dementia." Curr Treat Options Neurol **16**(11): 319.

Ullah, H., A. Di Minno, C. Santarcangelo, H. Khan and M. Daglia (2021). "Improvement of Oxidative Stress and Mitochondrial Dysfunction by β-Caryophyllene: A Focus on the Nervous System." Antioxidants (Basel) **10**(4).

Umoh, M. E., E. B. Dammer, J. Dai, D. M. Duong, J. J. Lah, A. I. Levey, . . . N. T. Seyfried (2018). "A proteomic network approach across the ALS-FTD disease spectrum resolves clinical phenotypes and genetic vulnerability in human brain." EMBO Molecular Medicine **10**(1): 48-62.

Vaccaro, A. M., M. Motta, M. Tatti, S. Scarpa, L. Masuelli, M. Bhat, . . . R. Salvioli (2010). "Saposin C mutations in Gaucher disease patients resulting in lysosomal lipid accumulation, saposin C deficiency, but normal prosaposin processing and sorting." Hum Mol Genet **19**(15): 2987-2997.

Valdez, C., Y. C. Wong, M. Schwake, G. Bu, Z. K. Wszolek and D. Krainc (2017). "Progranulin-mediated deficiency of cathepsin D results in FTD and NCL-like phenotypes in neurons derived from FTD patients." Human Molecular Genetics **26**(24): 4861-4872.

Valdez, C., D. Ysselstein, T. J. Young, J. Zheng and D. Krainc (2019). "Progranulin mutations result in impaired processing of prosaposin and reduced glucocerebrosidase activity." Human Molecular Genetics.

Valori, C. F. and M. Neumann (2021). "Contribution of RNA/DNA Binding Protein Dysfunction in Oligodendrocytes in the Pathogenesis of the Amyotrophic Lateral Sclerosis/Frontotemporal Lobar Degeneration Spectrum Diseases." Frontiers in Neuroscience **15**(1078).

Van Damme, P., A. Van Hoecke, D. Lambrechts, P. Vanacker, E. Bogaert, J. van Swieten, . . . W. Robberecht (2008). "Progranulin functions as a neurotrophic factor to regulate neurite outgrowth and enhance neuronal survival." J Cell Biol **181**(1): 37-41.

Van Deerlin, V. M., P. M. A. Sleiman, M. Martinez-Lage, A. Chen-Plotkin, L.-S. Wang, N. R. Graff-Radford, . . . V. M. Y. Lee (2010). "Common variants at 7p21 are associated with frontotemporal lobar degeneration with TDP-43 inclusions." Nature Genetics **42**: 234.

Vandenbosch, M., S. M. Mutuku, M. J. Q. Mantas, N. H. Patterson, T. Hallmark, M. Claesen, . . . S. R. Ellis (2023). "Toward Omics-Scale Quantitative Mass Spectrometry Imaging of Lipids in Brain Tissue Using a Multiclass Internal Standard Mixture." Analytical Chemistry **95**(51): 18719-18730.

Vanier, M. T. and L. Svennerholm (1975). "Chemical pathology of Krabbe's disease. III. Ceramide-hexosides and gangliosides of brain." Acta Paediatr Scand **64**(4): 641-648.

Vardi, A., H. Zigdon, A. Meshcheriakova, A. D. Klein, C. Yaacobi, R. Eilam, . . . A. H. Futerman (2016). "Delineating pathological pathways in a chemically induced mouse model of Gaucher disease." The Journal of Pathology **239**(4): 496-509.

Velakoulis, D., M. Walterfang, R. Mocellin, C. Pantelis and C. McLean (2009). "Frontotemporal dementia presenting as schizophrenia-like psychosis in young people: clinicopathological series and review of cases." British Journal of Psychiatry **194**(4): 298-305.

Vieira, R. T., L. Caixeta, S. Machado, A. C. Silva, A. E. Nardi, O. Arias-Carrión and M. G. Carta (2013). "Epidemiology of early-onset dementia: a review of the literature." Clinical practice and epidemiology in mental health : CP & EMH **9**: 88-95.

Waite, A. J., D. Bäumer, S. East, J. Neal, H. R. Morris, O. Ansorge and D. J. Blake (2014). "Reduced C9orf72 protein levels in frontal cortex of amyotrophic lateral sclerosis and frontotemporal degeneration brain with the C9ORF72 hexanucleotide repeat expansion." Neurobiol Aging **35**(7): 1779.e1775-1779.e1713.

Wang, J., W. Y. Ho, K. Lim, J. Feng, G. Tucker-Kellogg, K. A. Nave and S. C. Ling (2018). "Cell-autonomous requirement of TDP-43, an ALS/FTD signature protein, for oligodendrocyte survival and myelination." Proc Natl Acad Sci U S A **115**(46): E10941-E10950.

Wang, L.-C., T. E. Kennedy and G. Almazan (2017). "A novel function of TBK1 as a target of Cdon in oligodendrocyte differentiation and myelination." Journal of Neurochemistry **140**(3): 451-462.

Wang, P., H. Zhang, Y. Wang, M. Zhang and Y. Zhou (2020). "Plasma cholesterol in Alzheimer's disease and frontotemporal dementia." Transl Neurosci **11**(1): 116-123.

Ward, M. E., R. Chen, H. Y. Huang, C. Ludwig, M. Telpoukhovskaia, A. Taubes, . . . A. J. Green (2017). "Individuals with progranulin haploinsufficiency exhibit features of neuronal ceroid lipofuscinosis." Sci Transl Med **9**(385).

Warmus, B. A., D. R. Sekar, E. McCutchen, G. D. Schellenberg, R. C. Roberts, L. L. McMahon and E. D. Roberson (2014). "Tau-mediated NMDA receptor impairment underlies dysfunction of a selectively

vulnerable network in a mouse model of frontotemporal dementia." J Neurosci **34**(49): 16482-16495.

Waterham, H. R. and M. S. Ebberink (2012). "Genetics and molecular basis of human peroxisome biogenesis disorders." Biochimica et Biophysica Acta (BBA) - Molecular Basis of Disease **1822**(9): 1430-1441.

Wattenberg, B. W. (2019). "Intra- and intercellular trafficking in sphingolipid metabolism in myelination." Adv Biol Regul **71**: 97-103.

Webster, C. P., E. F. Smith, C. S. Bauer, A. Moller, G. M. Hautbergue, L. Ferraiuolo, . . . K. J. De Vos (2016). "The C9orf72 protein interacts with Rab1a and the ULK1 complex to regulate initiation of autophagy." The EMBO Journal **35**(15): 1656-1676.

Weiss, H., L. Wester-Rosenloef, C. Koch, F. Koch, S. Baltrusch, M. Tiedge and S. Ibrahim (2012). "The Mitochondrial Atp8 Mutation Induces Mitochondrial ROS Generation, Secretory Dysfunction, and β-Cell Mass Adaptation in Conplastic B6-mtFVB Mice." Endocrinology **153**(10): 4666-4676.

Wessel, D. and U. I. Flügge (1984). "A method for the quantitative recovery of protein in dilute solution in the presence of detergents and lipids." Anal Biochem **138**(1): 141-143.

Wilke, C., F. Gillardon, C. Deuschle, M. A. Hobert, I. E. Jansen, F. G. Metzger, . . . M. Synofzik (2017). "Cerebrospinal Fluid Progranulin, but Not Serum Progranulin, Is Reduced in GRN-Negative Frontotemporal Dementia." Neurodegener Dis **17**(2-3): 83-88.

Woollacott, I. O. C., M. Bocchetta, C. H. Sudre, B. H. Ridha, C. Strand, R. Courtney, . . . J. D. Rohrer (2018). "Pathological correlates of white matter hyperintensities in a case of progranulin mutation associated frontotemporal dementia." Neurocase **24**(3): 166-174.

Woolley, J. D., B. K. Khan, N. K. Murthy, B. L. Miller and K. P. Rankin (2011). "The diagnostic challenge of psychiatric symptoms in neurodegenerative disease: rates of and risk factors for prior psychiatric diagnosis in patients with early neurodegenerative disease." J Clin Psychiatry **72**(2): 126-133.

Wu, Y., W. Shao, T. W. Todd, J. Tong, M. Yue, S. Koga, . . . M. Prudencio (2021). "Microglial lysosome dysfunction contributes to white matter pathology and TDP-43 proteinopathy in GRN-associated FTD." Cell Rep **36**(8): 109581.

Xia, Q., H. Wang, Z. Hao, C. Fu, Q. Hu, F. Gao, . . . G. Wang (2016). "TDP-43 loss of function increases TFEB activity and blocks autophagosome-lysosome fusion." Embo j **35**(2): 121-142.

Xu, H., F. R. Boucher, T. T. Nguyen, G. P. Taylor, J. J. Tomlinson, R. A. Ortega, . . . S. A. L. Bennett (2019). "DMS as an orthogonal separation to LC/ESI/MS/MS for quantifying isomeric cerebrosides in plasma and cerebrospinal fluid." Journal of lipid research **60**(1): 200-211.

Yeung, Maggie S. Y., S. Zdunek, O. Bergmann, S. Bernard, M. Salehpour, K. Alkass, . . . J. Frisén (2014). "Dynamics of Oligodendrocyte Generation and Myelination in the Human Brain." Cell **159**(4): 766-774.

Yousef, A., J. L. Robinson, D. J. Irwin, M. D. Byrne, L. K. Kwong, E. B. Lee, . . . J. Q. Trojanowski (2017). "Neuron loss and degeneration in the progression of TDP-43 in frontotemporal lobar degeneration." Acta Neuropathol Commun **5**(1): 68.

Yu, C.-E., T. D. Bird, L. M. Bekris, T. J. Montine, J. B. Leverenz, E. Steinbart, . . . V. M. Van Deerlin (2010). "The Spectrum of Mutations in Progranulin: A Collaborative Study Screening 545 Cases of Neurodegeneration." Archives of Neurology **67**(2): 161-170.

Zhang, J., D. Velmeshev, K. Hashimoto, Y. H. Huang, J. W. Hofmann, X. Shi, . . . E. J. Huang (2020). "Neurotoxic microglia promote TDP-43 proteinopathy in progranulin deficiency." Nature **588**(7838): 459-465.

Zhang, Y., K. Chen, S. A. Sloan, M. L. Bennett, A. R. Scholze, S. O'Keeffe, . . . J. Q. Wu (2014). "An RNA-Sequencing Transcriptome and Splicing Database of Glia, Neurons, and Vascular Cells of the Cerebral Cortex." The Journal of Neuroscience **34**(36): 11929-11947.

Zheng, W.-Q., S. V. Pedersen, K. Thompson, E. Bellacchio, C. E. French, B. Munro, . . . E. Ostergaard (2021). "Elucidating the molecular mechanisms associated with TARS2-related mitochondrial disease." Human Molecular Genetics **31**(4): 523-534.

Zheng, X., L. Boyer, M. Jin, J. Mertens, Y. Kim, L. Ma, . . . T. Hunter (2016). "Metabolic reprogramming during neuronal differentiation from aerobic glycolysis to neuronal oxidative phosphorylation." eLife **5**: e13374.

Zhou, J., G. Gao, J. W. Crabb and G. Serrero (1993). "Purification of an autocrine growth factor homologous with mouse epithelin precursor from a highly tumorigenic cell line." J Biol Chem **268**(15): 10863-10869.

Zhou, L.-Q., M.-H. Dong, Z.-W. Hu, Y. Tang, Y.-H. Chu, M. Chen, . . . D.-S. Tian (2023). "Staged suppression of microglial autophagy facilitates regeneration in CNS demyelination by enhancing the production of linoleic acid." Proceedings of the National Academy of Sciences **120**(1): e2209990120.

Zhou, X., A. M. Nicholson, Y. Ren, M. Brooks, P. Jiang, A. Zuberi, . . . R. Rademakers (2020). "Loss of TMEM106B leads to myelination deficits: implications for frontotemporal dementia treatment strategies." Brain : a journal of neurology **143**(6): 1905-1919.

Zhou, X., L. Sun, F. Bastos de Oliveira, X. Qi, W. J. Brown, M. B. Smolka, . . . F. Hu (2015). "Prosaposin facilitates sortilin-independent lysosomal trafficking of progranulin." The Journal of cell biology **210**(6): 991-1002.

Zhou, X., L. Sun, O. Bracko, J. W. Choi, Y. Jia, A. L. Nana, . . . F. Hu (2017). "Impaired prosaposin lysosomal trafficking in frontotemporal lobar degeneration due to progranulin mutations." Nature Communications **8**(1): 15277.

Zhou, X., L. Sun, O. Bracko, J. W. Choi, Y. Jia, A. L. Nana, . . . F. Hu (2017). "Impaired prosaposin lysosomal trafficking in frontotemporal lobar degeneration due to progranulin mutations." Nat Commun **8**: 15277.

Zhu, J., C. Nathan, W. Jin, D. Sim, G. S. Ashcroft, S. M. Wahl, . . . A. Ding (2002). "Conversion of proepithelin to epithelins: roles of SLPI and elastase in host defense and wound repair." Cell **111**(6): 867-878.